



n. 2 – 2020

Italian Journal of Agrometeorology

Rivista Italiana di Agrometeorologia



SCIENTIFIC DIRECTOR

Simone Orlandini

Department of Agriculture, Food, Environment and Forestry (DAGRI)
University of Florence
Piazzale delle Cascine 18 – 50144, Firenze (FI), Italia
Tel. +39 055 2755755
simone.orlandini@unifi.it

PUBLICATION DIRECTOR

Francesca Ventura

Dipartimento di Scienze e Tecnologie Agro-alimentari
Università di Bologna
Via Fanin, 44 – 40127 Bologna (BO), Italia
Tel. +39 051 20 96 658
francesca.ventura@unibo.it

FIELD EDITORS

CROP PROTECTION

Antonello Cossu

ARPAS - Servizio Valutazione Analisi
Ambientale (Sassari)

Federico Spanna

Phytosanitary sector and technical-scientific
services - Piemonte region (Turin)

CLIMATOLOGY

Emanuele Eccel

Fondazione Edmund Mach di San Michele
all'Adige (Trento)

Valentina Pavan

Arpae – Emilia Romagna (Bologna)

CLIMATE CHANGE

Domenico Ventrella

Environment Research Center Agriculture –
CREA (Bari)

Vittorio Marletto

Arpae – Emilia Romagna (Bologna)

CROP GROWING, PRODUCTION AND AGRO- MANAGEMENT

Roberto Confalonieri

Department of Plant Production -
University of Milano

Anna Dalla Marta

Department of Agriculture, Food,
Environment and Forestry (DAGRI) -
University of Florence

PHENOLOGY

Alessandro Chiaudani

Department of Engineering and Geology –
University of Chieti

Gabriele Cola

Department of Plant Production -
University of Milano

MICRO-METEOROLOGY

Simona Consoli

Department of Agriculture, Food and
Environment (Di3A) - University of Catania

WATER RELATIONS AND IRRIGATION

Marco Napoli

Department of Agriculture, Food,
Environment and Forestry (DAGRI) -
University of Florence

SPATIALIZATION, GIS

Fabio Zottele

Fondazione Edmund Mach di San Michele
all'Adige (TN)

OPERATIVE TECHNIQUES

Luigi Pasotti

Regional Department of Agriculture and
Forests of the Sicily Region

EDITORIAL BOARD

Marco Acutis, University of Milan, Milan (Italy)

Vesselin Alexandrov, National Institute of Meteorology and Hydrology, Sofia (Bulgaria)

Marco Bindi, University of Florence, Florence (Italy)

Stefano Bocchi, University of Milan, Milan (Italy)

Maurizio Borin, University of Padua, Padua (Italy)

Orivaldo Brunini, Center of Ecology and Biophysics - Agronomic Institute, Campinas (Brazil)

Pierluigi Calanca, Agroscope Reckenholz-Tänikon, Zurich (Switzerland)

Raffaele Casa, Tuscia University, Viterbo (Italy)

Francesco Danuso, University of Udine, Udine (Italy)

Josef Eitzinger, University of Boku, Wien (Austria)

Lee Byong-Lyol, Korea Meteorological Administration, Suwon (Republic of Korea)

Vittorio Marletto, ARPA - Emilia Romagna, Bologna (Italy)

Raymond Motha, United States Department of Agriculture, Washington (USA)

Pavol Nejedlik, Slovak Hydrometeorological Institute, Bratislava (Slovakia)

Luigi Perini, CRA – CMA, Rome (Italy)

Laxman Singh Rathore, Agromet Division, India Meteorological Department, New Delhi (India)

Federica Rossi, CNR - IBIMET, Bologna (Italy)

Paola Rossi Pisa, University of Bologna, Bologna (Italy)

Paulo Cesar Sentelhas, Department of Exact Sciences ESALQ - University of São Paulo, Piracicaba, SP, (Brazil)

Donatella Spano, University of Sassari, Sassari (Italy)

Robert Stefanski, WMO, Geneva (Switzerland)

Roger Stone, University of Southern Australia, Toowoomba (Australia)

Italian Journal of Agrometeorology

n. 2 - 2020

Firenze University Press

The *Italian Journal of Agrometeorology (IJAm - Rivista Italiana di Agrometeorologia)* is the official periodical of the Italian Association of Agrometeorology (AIAM) and aims to publish original scientific contributions in English on agrometeorology, as a science that studies the interactions of hydrological and meteorological factors with the agricultural and forest ecosystems, and with agriculture in its broadest sense (including livestock and fisheries).

Italian Association of Agrometeorology (AIAM)

Presidente: Francesca Ventura (francesca.ventura@unibo.it)

Vicepresidente: Federica Rossi

Consiglieri: Filiberto Altobelli, Anna dalla Marta, Emanuele Scalcione, Federico Spanna, Domenico Ventrella

Revisori dei conti: Bruno Di Lena, Chiara Epifani, Marcello Giovanni Onorato

Segreteria: Simone Falzoi, Emanuela Forni, Tiziana La Iacona, Mattia Sanna, Irene Vercellino

e-mail AIAM: segreteria@agrometeorologia.it

Sede legale: via Caproni, 8 - 50144 Firenze

web: www.agrometeorologia.it

e-mail Italian Journal of Agrometeorology: ijagrometeorology@agrometeorologia.it

SUBSCRIPTION INFORMATION

IJAm articles are freely available online, but print editions are available to paying subscribers. Subscription rates are in Eur and are applicable worldwide.

Annual Subscription: € 50,00 Single Issue: € 25,00

CONTACT INFORMATION

Please contact ordini@fupress.com, if you have any questions about your subscription or if you would like to place an order for the print edition. Information on payment methods will be provided after your initial correspondence.

Published by

Firenze University Press – University of Florence, Italy

Via Cittadella, 7 - 50144 Florence - Italy

<http://www.fupress.com/ijam>

Copyright © 2020 **Authors**. The authors retain all rights to the original work without any restrictions.

Open Access. This issue is distributed under the terms of the [Creative Commons Attribution 4.0 International License \(CC-BY-4.0\)](https://creativecommons.org/licenses/by/4.0/) which permits unrestricted use, distribution, and reproduction in any medium, provided you give appropriate credit to the original author(s) and the source, provide a link to the Creative Commons license, and indicate if changes were made. The Creative Commons Public Domain Dedication (CC0 1.0) waiver applies to the data made available in this issue, unless otherwise stated.



Citation: A. Crespi, A. Borghi, A. Facchi, C. Gandolfi, M. Maugeri (2020) Spatio-temporal variability and trends of drought indices over Lombardy plain (northern Italy) from meteorological station records (1951–2017). *Italian Journal of Agrometeorology* (2): 3-18. doi: 10.13128/ijam-1101

Received: September 30, 2020

Accepted: November 14, 2020

Published: January 25, 2021

Copyright: © 2020 A. Crespi, A. Borghi, A. Facchi, C. Gandolfi, M. Maugeri. This is an open access, peer-reviewed article published by Firenze University Press (<http://www.fupress.com/ijam>) and distributed under the terms of the Creative Commons Attribution License, which permits unrestricted use, distribution, and reproduction in any medium, provided the original author and source are credited.

Data Availability Statement: All relevant data are within the paper and its Supporting Information files.

Competing Interests: The Author(s) declare(s) no conflict of interest.

Spatio-temporal variability and trends of drought indices over Lombardy plain (northern Italy) from meteorological station records (1951–2017)

ALICE CRESPI^{1,a,*}, ANNA BORGHI^{1,b}, ARIANNA FACCHI¹, CLAUDIO GANDOLFI¹, MAURIZIO MAUGERI^{2,3}

¹ Department of Agricultural and Environmental Sciences, Università degli Studi di Milano, Milan, 20122, Italy

² Department of Environmental Science and Policy, Università degli Studi di Milano, Milan, 20122, Italy

³ Institute of Atmospheric Sciences and Climate, National Research Council, Bologna, 40129, Italy

^a Now at Institute for Earth Observation, Eurac Research, Bolzano, 39100, Italy

^b Now agronomic consultant, via Costa d'Oro 8, Cernobbio, 22012, Italy

*Corresponding author. E-mail: alice.crespi@eurac.edu

Abstract. A 30-arc second resolution gridded dataset of 1951–2017 monthly series of Standardized Precipitation Index (SPI) and Standardized Precipitation Evapotranspiration Index (SPEI) for a portion of Po Plain in Lombardy region (northern Italy) is presented. The series were derived from an archive of homogenized and quality-checked meteorological station observations covering the study area and its surroundings, which were interpolated onto regular grid by means of an anomaly-based procedure. A significant negative trend in mean regional SPI series was depicted for summer (-0.14 decade⁻¹) while stronger decreases were found for SPEI in spring, summer and year (-0.14 , -0.22 and -0.17 decade⁻¹, respectively). The greatest drying tendencies occur in the southern and western parts of domain where summer index trends reached -0.23 and -0.30 decade⁻¹, respectively. The more negative trends of SPEI than SPI can be probably explained by the increasing role of evapotranspiration over recent decades triggered by arising temperature. The assessment of spatio-temporal variability of drought features (frequency, duration and severity) pointed out increasing tendencies in all cases, especially in the western portion of the region.

Keywords. SPI, SPEI, trend analysis, drought, Po Plain.

INTRODUCTION

Drought is a weather and climate-related natural hazard referring to a temporary scarcity of natural water availability due to a prolonged rainfall deficit, which could affect a wide range of environmental, social and economic systems, such as food production and agriculture (Parsons et al., 2019; Vicente-Serrano

et al., 2012). Several definitions are currently used to classify the different kinds of drought and their impacts; in particular, meteorological droughts refer to the reduction of precipitation with respect to normal conditions over a specific period and region (Spinoni et al., 2014). Although several studies provided evidences that globally land areas in very dry conditions have enlarged over the last decades (Spinoni et al., 2018; Dai et al., 2004) and a general increase of extreme events in the context of global warming is expected (IPCC, 2014), drought behavior exhibits a high variability at both temporal and spatial scales. In Europe spatial differences were clearly depicted with a tendency to wetter conditions in the North-East and to drier regimes in the South, especially in Mediterranean areas, enhanced by lower precipitation together with increasing evapotranspiration fostered by higher temperature (Spinoni et al., 2015; Briffa et al., 2009). However, since drought variations could be even greater at sub-regional and local levels, the reconstruction of the recent climate evolution at high spatial resolution from dense meteorological networks is crucial to analyze local trends and to define water management plans and future adaptation strategies. Moreover, in order to provide a more comprehensive drought characterization and to define its effects on natural and managed systems dependent on water supply, it is necessary to consider not only precipitation, which is the main driver of drought, but also the role of temperature influencing evapotranspiration variability and thus drought severity (Vicente-Serrano et al., 2014). This could be particularly relevant for Mediterranean regions, which are some of the main hotspots in the context of global warming (Founda et al., 2019; Lionello and Scarascia, 2018).

In Italy, recent studies focused on the analysis of drought frequency and intensity variations over several central and southern regions by computing different drought indices from station observations (Vergni and Todisco, 2011; Piccarreta et al., 2004). These studies agreed in depicting a general increase of drought events and their duration over recent decades, even though the intensity of such phenomena depends both on spanned period and temporal resolution, and it is strongly influenced by orographic heterogeneity (Buttafuoco et al., 2015; Di Lena et al., 2014). Less studies dealt with drought characterization for northern Italian regions (Baronetti et al., 2020; Brunetti et al., 2009) and a general positive tendency in drought occurrence was depicted, which became more evident during the most recent decades (Stagge et al., 2017).

The Po river plain is a large alluvial plain in northern Italy characterized by being one of the most important agricultural areas in Europe; consequently, it represents a very interesting study domain, where accurate information about the spatial variability of meteorologi-

cal variables could represent an essential support for the development and implementation of water management adaptation strategies. Agriculture in the Po plain is in fact largely dependent on irrigation and, therefore, it is strongly influenced by droughts.

In this framework, we reconstructed and analyzed the spatio-temporal trend and the variability of droughts over a portion of Po Plain (9°12'-10°30'E and 45°00'-45°45'N), computing the 1951–2017 monthly series of Standardized Precipitation Index (SPI, McKee et al., 1993) and of Standardized Precipitation Evapotranspiration Index (SPEI, Vicente-Serrano et al., 2010) starting from a dense database of historical precipitation and temperature records recovered for the study region and surrounding areas. All the data were checked for quality and homogeneity, and they were interpolated onto a 30-arc second resolution grid covering the study area in order to provide regional SPI and SPEI records and to assess drought indicator variability and hotspot locations at fine scale over the domain. Long and short-term trends in SPI and SPEI records were in fact investigated at both regional and local scales by considering two aggregation intervals (3 and 12 months) and the spatio-temporal evolution of the main features of drought spells, i.e. frequency, intensity and duration, was analyzed throughout the spanned period 1951–2017.

MATERIALS AND METHODS

Study area and meteorological database

The area considered for the present study is located in the middle of northern Italy and it includes a large portion of southern Lombardy and the northernmost part of Emilia-Romagna for a total of about 8500 km² (9°12'-10°30'E and 45°00'-45°45'N, rectangle in Fig. 1). The domain is centered on the lower part of the basin of Adda river, one of the main tributaries of Po river, and is characterized by a flat and homogeneous orography except for the northern part, where the first reliefs of pre-Alps occur.

Despite the presence of large urban centers such as Milan, Brescia and Bergamo, agriculture activities are intensively practiced with about 70% of the surface covered by irrigated crops, mainly maize and pasture. Very high crop productivities are achieved through an extensive development of irrigation, which relies on the water conveyed by a dense channel network and supplied by the main rivers.

The database used to assess the drought variability over the study domain was composed by more than 200 monthly precipitation series and 20 monthly maximum and minimum temperature series. The records were retrieved from the networks of regional services (ARPA

Lombardia, ARPA Emilia-Romagna, ARPA Veneto, ARPA Piemonte), the historical archives of the former Italian Hydrographic Service and several past projects focused on the recovery and homogenization of secular Italian meteorological series, especially RICLIC (<http://www.riclic.unimib.it/>) and NextData (<http://www.nextdataproject.it/?q=en>) projects.

In particular, the precipitation series were extracted from the quality-checked and homogenized database presented by Crespi et al. (2018a) where it was used to reconstruct the secular precipitation record over the upper Adda river basin.

The quality-check procedures included outlier detections and spatial consistency tests, in which each monthly series was reconstructed by means of the surrounding stations and the comparison between simulated and observed values allowed to detect suspicious entries, low-quality sites or periods of station malfunction. The same quality-check procedures were applied to temperature data and whenever the homogenized version was not already available, series homogeneity was controlled by means of a procedure based on the Craddock test (Craddock, 1979). In such method, for each test series several surrounding reference stations were selected and the series of cumulative differences between the test and each reference were computed and used to identify potential breaks. Inhomogeneous periods in the test series were corrected by applying proper correcting factors (Golzio et al., 2018). Relevant breaks were finally identified and the homogenization was performed for 8 minimum and maximum temperature series. After these activities the monthly mean temperature records were obtained as the average of maximum and minimum monthly values. The checked and homogenized dataset of station records was then used to project the meteorological records onto the 30-arc second resolution grid covering the study area.

Even though several series spanned a longer period in the past, the start of study period was set to 1951, when the availability of meteorological records significantly improved and the station distribution over the domain started to be more homogeneous. Although the coverage of temperature series is significantly less dense than that of precipitation data (Fig. 1), this it is not expected to affect result robustness thanks to the greater spatial coherence of temperature (Brunetti et al., 2006), which is particularly favored by the homogeneous orography of the domain. In addition, in the interpolation framework (see the next section for details on the interpolation method) the 20 monthly temperature series were integrated by the 1961–1990 climatological normals, i.e. the 30-year averages, of 125 sites included in the study domain and adjacent areas and retrieved from the database set up by Brunetti et

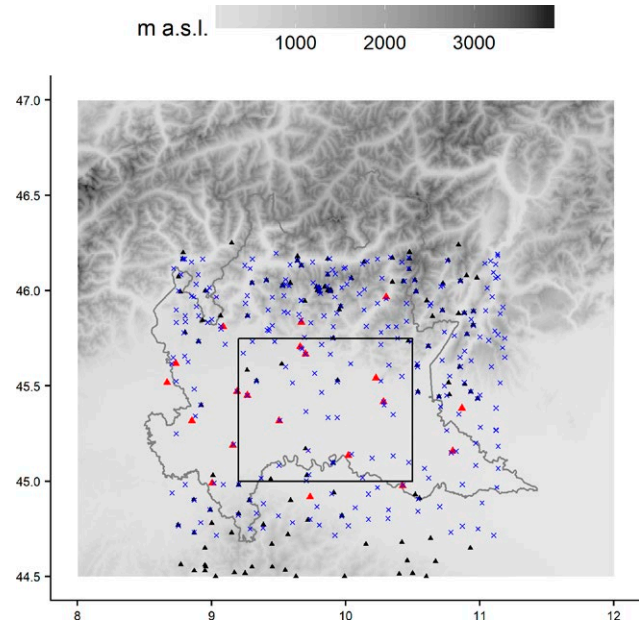


Fig. 1. Study domain (rectangle) and station distribution: blue crosses are precipitation sites, red triangles represent the locations of temperature series, while the black triangles indicate the sites for which 1961–1990 monthly temperature normals were considered.

al. (2014) for the construction of Italian temperature climatologies.

Data interpolation and SPI and SPEI calculation

The gridded datasets of 1951–2017 monthly meteorological records over the study domain were computed by applying the anomaly method (see e.g. New et al., 2001; Brunetti et al., 2012; Isotta et al., 2014). Specifically, the final precipitation and mean temperature grids were obtained by superimposing fields of long-term means of reference, i.e. the 30-year climatologies, and fields of anomalies, i.e. the departures from the reference values. The main advantage of the anomaly method is that it produces fields that are not biased by an uneven station distribution (New et al., 2001; Mitchell and Jones, 2005).

For both temperature and precipitation, 1961–1990 was used as reference period and the monthly normals were computed after filling the missing values in this 30-year interval by means of the procedure described in Crespi et al. (2018b). The normal interpolation over a 30-arc second resolution Digital Elevation Model (DEM, GTOPO30) was then performed by applying a local weighted linear regression of temperature (precipitation) *versus* elevation (Daly et al., 2002; Brunetti et al., 2014; Crespi et al., 2018b). The station weights entering in the fit were locally defined

on a monthly basis accordingly with their distance and orographic similarity to the cell to evaluate. For precipitation only, DEM was smoothed in order to account for the actual spatial scales at which the orography-atmosphere interactions are expected to occur (Foresti et al., 2018).

The station monthly series were then converted into anomalies by the difference (for temperature) and the ratio (for precipitation) from the corresponding normals. The anomalies were interpolated over the same grid by means of a weighted averaging approach with station weights depending on distance and elevation difference from the target cell and their decay was regulated on a yearly basis accordingly with the variation in station density over the study period. In particular, the distance halving coefficient was set year-by-year to the mean radius over the grid including at least three available data. The 1951–2017 monthly series in absolute values were finally computed by adding (multiplying) the gridded temperature (precipitation) anomalies to (times) the gridded climatologies. The accuracy of interpolated data was evaluated by means of the leave-one-out reconstruction of station data and the comparison with corresponding observations in terms of BIAS, Mean Absolute Error (MAE) and Root Mean Square Error (RMSE).

SPI and SPEI were computed both at cell level from the interpolated 1951–2017 meteorological series and at regional level from the areal mean of the gridded temperature and precipitation datasets over the domain. The standardized indices were computed by fitting the observation data with the Gamma probability distribution for SPI and the Log-logistic probability distribution for SPEI over the whole analyzed period (1951–2017). The chosen fitting distributions were proved to be the most suitable for SPI and SPEI computation, respectively, and are the mostly adopted in literature (see e.g. Beguería et al., 2014; Stagge et al. 2015).

While SPI (McKee et al., 1993) takes into account precipitation only, SPEI (Vicente-Serrano et al., 2010) is based on the difference between precipitation and potential evapotranspiration (PET). Several methods can be adopted to evaluate PET, with different requirements in terms of variables that need to be measured. Therefore, the choice largely depends on data availability and, even though more comprehensive methods, like Penman-Monteith's one (Allen et al. 1998), could provide more reliable PET estimation, in this work we applied the Thornthwaite's equation (Thornthwaite, 1948), since it requires only mean temperature values and it is particularly useful for long-term reconstruction if no or very few observations of other variables, such as vapor pressure or wind speed, were available in the past.

Negative SPI and SPEI values for a certain time step indicate drier regimes, i.e. less precipitation and/or greater

deficit, with respect to the mean conditions extracted from the whole period, whereas positive values of the indices highlight wetter conditions than reference mean values.

SPI and SPEI were computed at monthly resolution and for two aggregation intervals (3 and 12 months), in order to highlight the variability of climatic signal in relation to the integration periods and to assess the time scales at which the variations are mostly significant.

The 3 and 12-month aggregation interval records (named thereafter SPI (SPEI) -3 and SPI (SPEI) -12, respectively) were used to define seasonal and annual series. Specifically, seasonal series were defined by considering SPI (SPEI) -3 values in February for winter, May for spring, August for summer and November for autumn, while the annual ones were set up by selecting the SPI (SPEI) -12 values in December for each year.

In this work, long-term trends and significance of time series were evaluated by means of Theil-Sen (TS; Theil, 1950; Sen, 1968) and Mann-Kendall (MK; Kendall, 1975) tests.

RESULTS

The study area is characterized by temperate climatic conditions with the lowest 1961–1990 mean temperature in winter around +3 °C as average and the highest normals in summer when mean temperature values are around +22 °C. The lowest temperatures are depicted over the north-eastern part of the domain where the elevation gradients are higher, while the greatest temperature values characterize the southern part, close to the Po river. As regards the precipitation regime, no relevant seasonal differences occur and, except for winter when the minimum of precipitation is reached (180 mm), the average precipitation is around 250 mm in all seasons. The altitudinal gradient is well depicted also for precipitation distribution: the highest precipitation values occur over the northern part of the domain in correspondence of the beginning of pre-Alpine belt, where total precipitation is in some areas two times greater than the amounts characterizing the plain areas in the central and southern portions of domain. On yearly basis, total precipitation values reach 1500 mm in the North while the plain areas feature minima of less than 800 mm.

The errors on climatological fields were computed by the leave-one-out reconstruction of all station normals within the study area. The monthly mean absolute errors, as average over all stations, range between 7.9 and 14.8 mm for precipitation and between 0.7 and 0.8 °C for temperature.

The assessment of trends and variability in hydrological regime over the study domain was performed for the

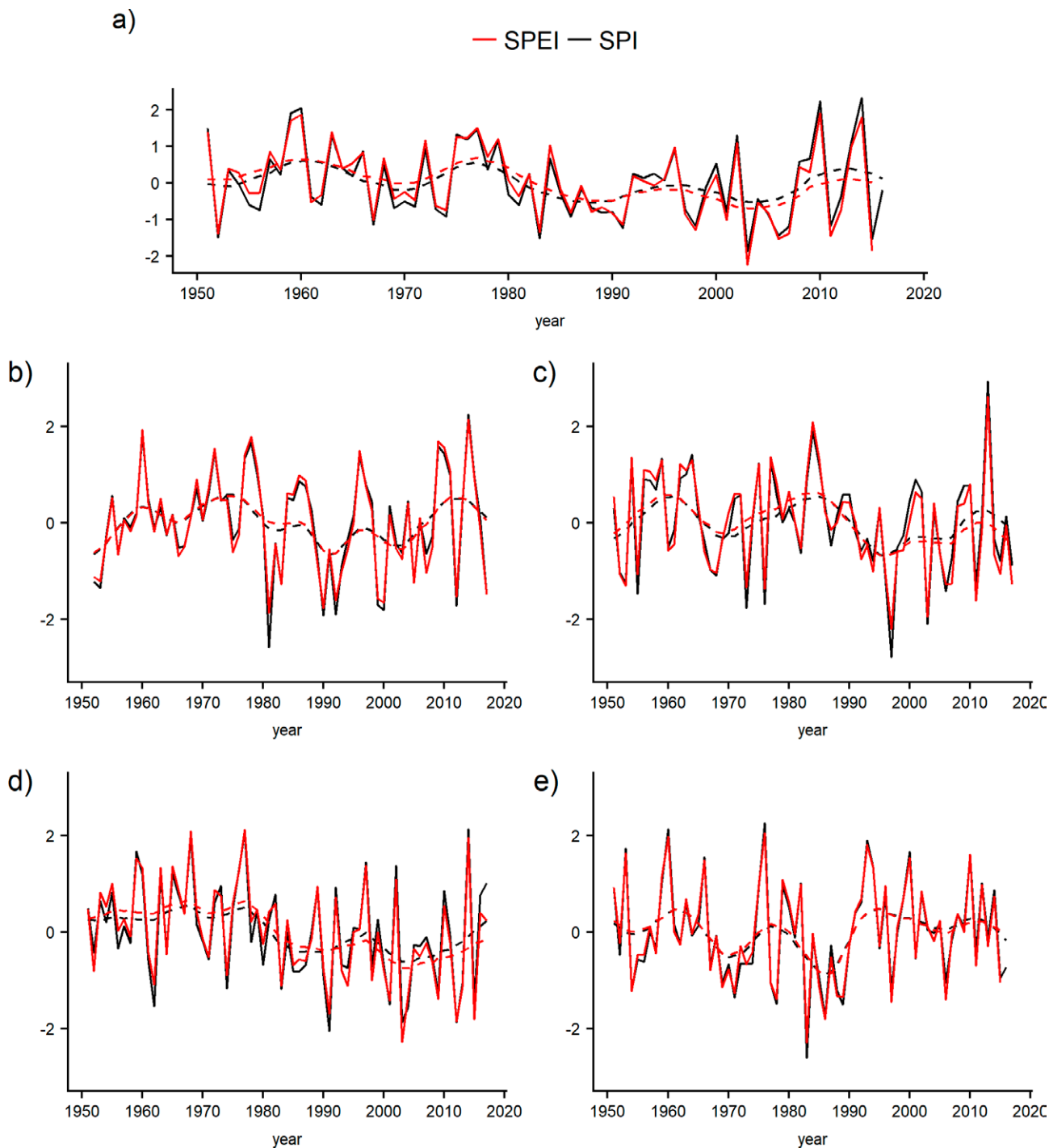


Fig. 2. 1951–2017 a) annual, b) winter, c) spring, d) summer and e) autumn SPI (black line) and SPEI (red line) obtained as average over all the grid cells of the study domain. The dashed lines represent the 11-year centred Gaussian filter with 3-year standard deviation of SPI (in black) and SPEI (in red) series.

1951–2017 period at both seasonal and annual scales. At this aim, the areal 1951–2017 monthly series of precipitation and deficit, i.e. the difference between precipitation

and PET, were defined by averaging the values estimated at all cells of the 30-arc second resolution grid and they were used to reconstruct the corresponding SPI and SPEI series

over the whole spanned period. The series are displayed in Fig. 2. Autumn and annual values were not computed in 2017 for both indices due to the end of precipitation records in October 2017 and in 2016 for SPEI only due to the lack of available temperature observations in November 2016.

In the series of both indices, the driest year was 2003, which was characterized by a dry spell in summer (panels a) and d) in Fig. 2) when exceptional temperature values (mean areal temperature anomaly of $+4.3$ °C in respect with 1961–1990 summer normals) were combined with low precipitation (mean areal precipitation anomaly of 0.5 in respect with 1961–1990 summer normals). The wettest year was 2014 when total precipitation amounts exceeded normals, especially in summer (panels a) and d) in Fig. 2) with a precipitation anomaly of about 1.7 in respect with the corresponding 1961–1990 mean value. High annual index values were also registered in 2010 when the main contribution was provided by winter precipitation (panels a) and b) in Fig 2), which reached a seasonal areal anomaly of 1.7 .

The TS slopes obtained for the 1951–2017 areal SPI and SPEI series at seasonal and annual scales are listed in Tab. 1. As regards SPI, the values experience negative tendencies, i.e. drying trends, in spring, summer and at annual scale, while winter and autumn are characterized by slight index increases, i.e. wetting tendencies. All resulting trends are not statistically significant with MK p-value above 0.05 , except for summer, when the greatest SPI decay occurs and it is around -0.14 decade⁻¹. The trends of SPEI index show similar results, however in this case the TS slopes are more negative in summer, spring and at annual scale and all these three values turned out to be statistically significant. The stronger signal provided by SPEI index could be explained by the increasing role of evapotranspiration driven by a positive and significant mean annual temperature trend of about $+0.3$ °C decade⁻¹ over the period.

In order to further analyze the evolution of drought indices over shorter time scales, the running trend of seasonal and annual SPI and SPEI series was computed. TS

trend and MK test were performed over moving windows of increasing length from a minimum of 20 years to the total length of the series and spanning all the 1951–2017 period. The results of the running trend are reported in Fig. 3 and Fig. 4 for the seasonal SPI and SPEI series, respectively, and Fig. 5 for annual values. The significant long-term trends of seasonal and yearly SPI and SPEI series, i.e. computed over the total length of the series, which were already discussed in Tab. 1, were also confirmed in the running-trend results (Fig. 3, Fig. 4 and Fig. 5). Besides the long-term trends, significant tendencies occurring over shorter time intervals are highlighted. It is interesting to note that SPEI series exhibit more relevant trends than SPI values at both long and short-time scales. In particular, a tendency towards drier conditions over time windows of 20–30 years are pointed out for spring and summer (panels b) and c) in Fig. 4) for intervals starting between 1970 and 1990 and between 1960 and 1980, respectively.

In addition to the regional behavior, the 1951–2017 seasonal and annual trends in SPI and SPEI series were also computed for each cell of the 30-arc second resolution grid in order to assess the spatial distribution of drought variability.

As regards the seasonal analysis, grid cells with significant trends were found out in summer for SPI (panel d) in Fig. 6) and in summer and spring for SPEI (panels c) and d) in Fig. 7).

Spring and summer trends are both negative over the whole domain and statistical significance occurs for all cells for SPEI in summer, while for the SPI gridded dataset no signal is depicted for spring, and in summer the negative trends with MK p-values below 0.05 occur over less than half study region. It is worth noting that both indices suggest a more relevant drying tendency in the southern and the western parts of the domain where SPEI summer trends reach -0.30 decade⁻¹ and SPI ones are slightly lower and around -0.23 decade⁻¹. In winter and autumn trends show MK p-values much greater than 0.05 in all cases, however the spatial patterns of TS slopes are comparable with spring and summer distributions: values are negative in the south-western part of region, even though much less pronounced, while decreasing tendencies occur in the north-eastern portion of the study area.

At annual scale, SPI and SPEI trends are negative over the whole region, with significant slopes located in the western, for SPI, and south-western, for SPEI, portions of the area (panel a) in Fig. 6 and Fig. 7).

As further analysis, SPI-3 and SPEI-3 gridded indices were used to evaluate the spatial distribution and temporal variability of some specific drought indicators. We considered the frequency, duration and severity of drought events, choosing a 3-month temporal aggregation since it

Tab. 1. Trends of SPI and SPEI series over 1951–2017 for winter (DJF), spring (MAM), summer (JJA), autumn (SON) and year. TS slopes are reported only if the trend is statistically significant (MK p-value < 0.05), otherwise trend sign is indicated. Trends are expressed as variation per decade.

	SPI	SPEI
DJF	+	-
MAM	-	-0.14
JJA	-0.14	-0.22
SON	+	+
YEAR	-	-0.17

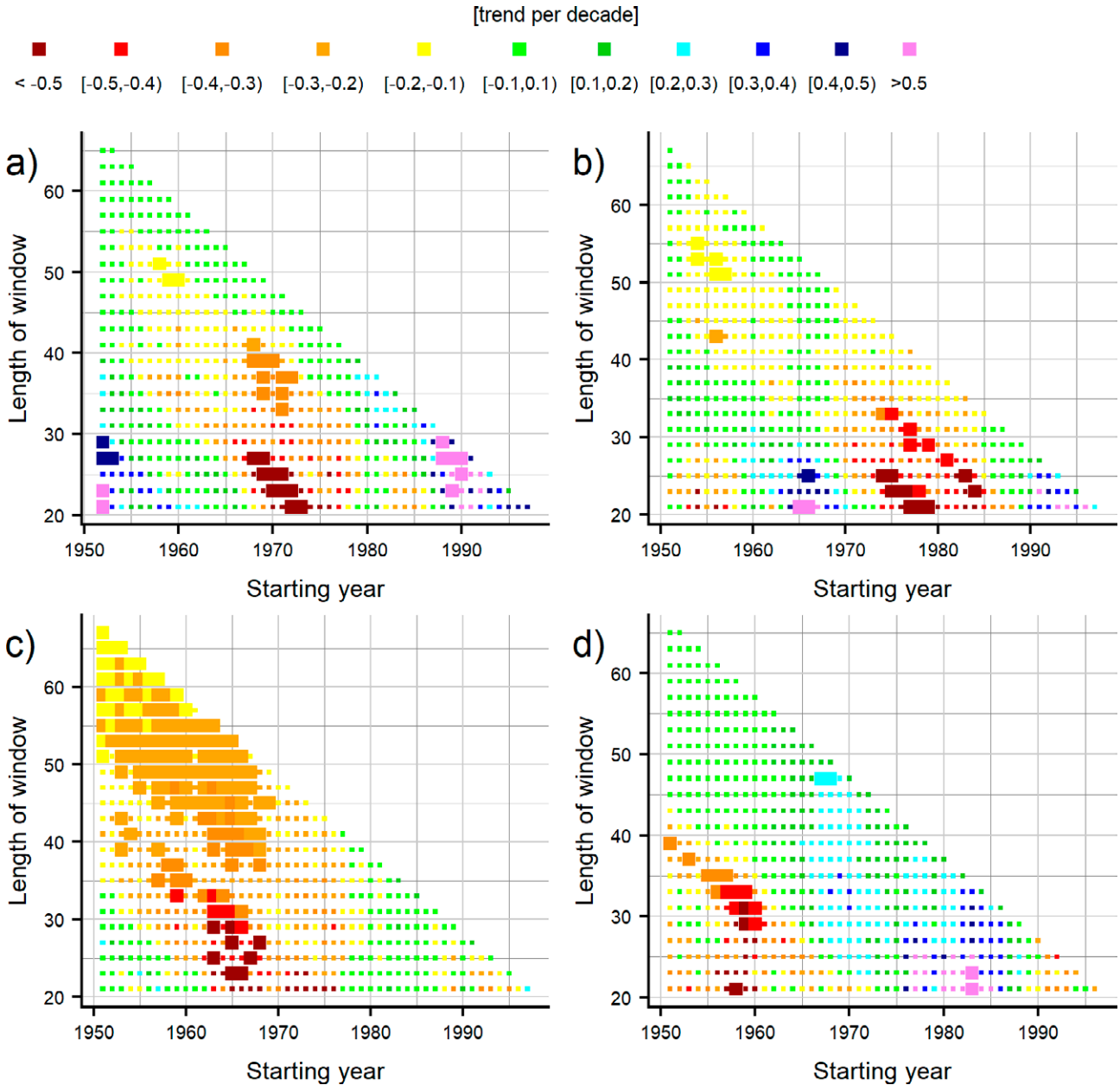


Fig. 3. Running trend analysis on SPI seasonal series: a) winter (DJF), b) spring (MAM), c) summer (JJA), d) autumn (SON). Colors represent the value of the TS slope while pixel thickness depends on the MK trend significance: pixels corresponding to MK p-values below 0.05 are reported with greater size. On the y-axis the length of the window is reported in terms of number of years.

is expected to be a suitable scale to describe drought affecting vegetation and agricultural practices (Bordi et al., 2007). For six subsequent decades from 1951 to 2010, the drought events were identified by following the definition of McKee (1993), i.e. a drought episode starts in the month (included) when the index value falls below -1 and ends in the month (not included) when the value returns positive, for at least two consecutive months. In particular, for each

subperiod we computed the drought frequency (DF) as the total number of identified drought spells in the decade, the total drought duration (TDD) as the total number of months included in the events and the total drought severity (TDS) as the sum (dimensionless) of the absolute values of the integral areas under the index curve from the start to the end month of each drought spell (Spinoni et al., 2015). In the following, only the outcomes from SPEI-3 se-

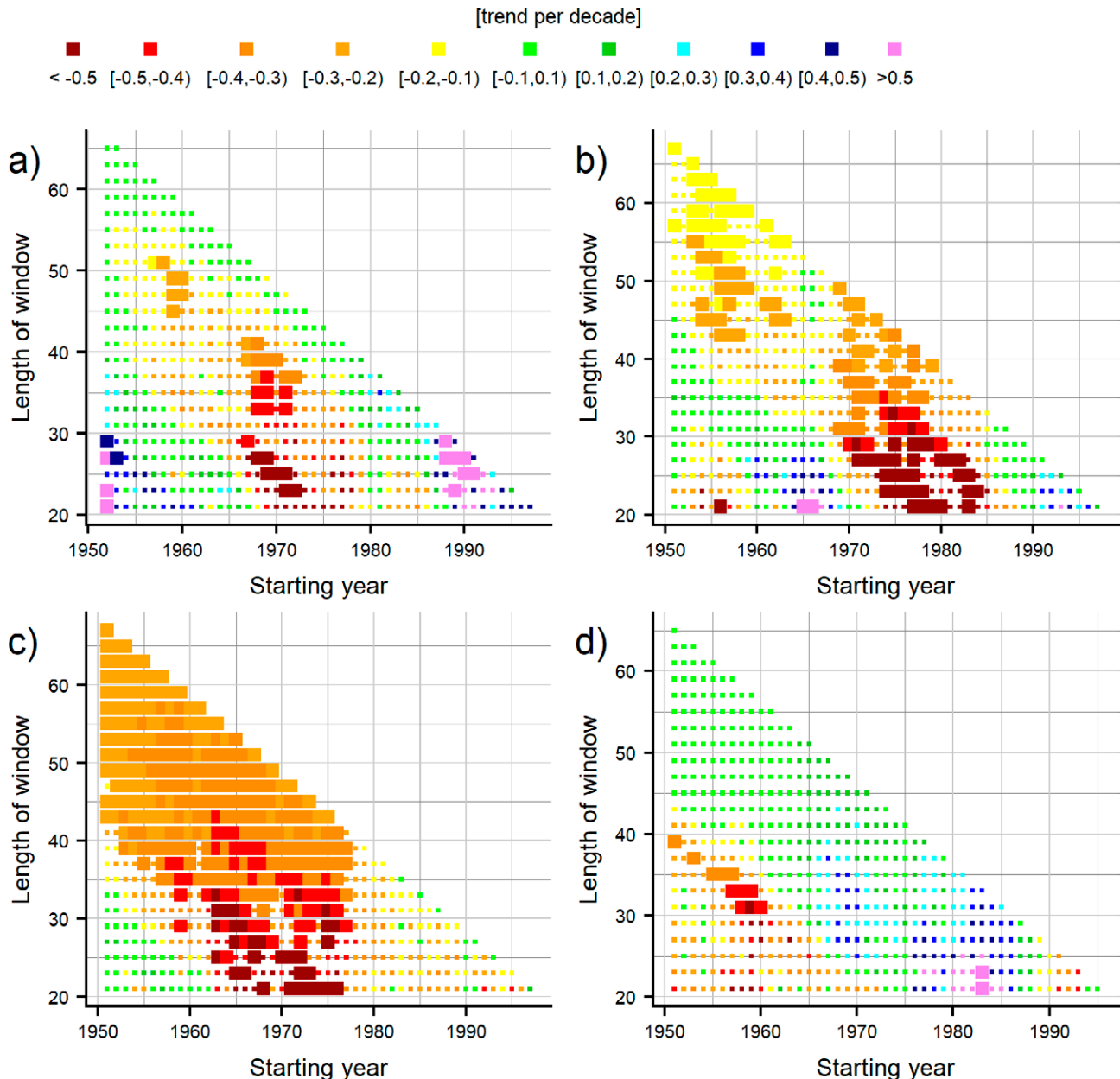


Fig. 4. Running trend analysis on SPEI seasonal series: a) winter (DJF), b) spring (MAM), c) summer (JJA), d) autumn (SON). Colors represent the value of the TS slope while pixel thickness depends on the MK trend significance: pixels corresponding to MK p-values below 0.05 are reported with greater size. On the y-axis the length of the window is reported in terms of number of years.

ries are discussed and shown, since SPI-3 exhibits a similar behavior, but with a weaker signal, as also pointed out by the long-term trend analyses.

The spatial distribution of the gridded indicators over the six subsequent decades (Figs. 8-10) highlights in all cases higher values from the decade 1981–1990 onwards in respect with the previous decades. The total number of drought spells that occurred over each one of the first three

decays was lower than 11 over the whole domain (panels in the top row of Fig. 8), while the number of drought events per decade was in the range of 11–17 in the following 10-year intervals (panels in the bottom row of Fig. 8). A similar increasing behavior was depicted for TDD and TDS: the total number of months experiencing drought conditions and the total severity of the drought events passed, as averages over the study domain, from 32 months and

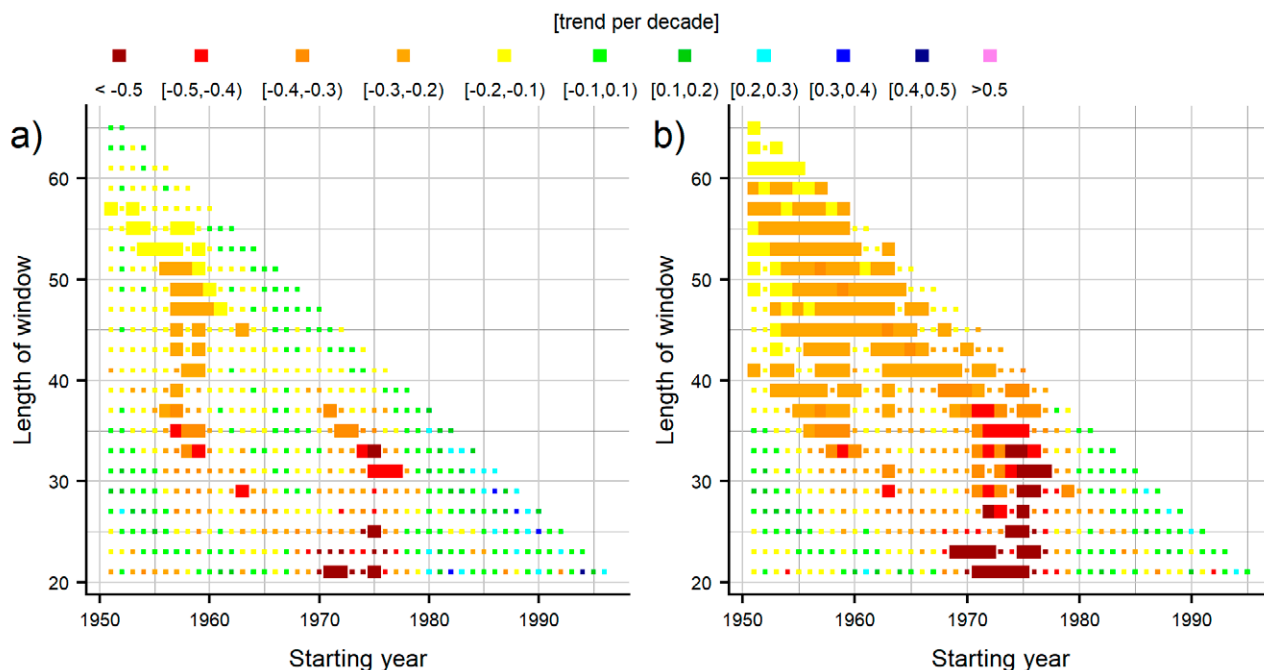


Fig. 5. Running trend analysis on SPI (left panel) and SPEI (right panel) annual series. Colors represent the value of TS slopes while pixel thickness depends on the MK trend significance: pixels corresponding to MK p-values below 0.05 are reported with greater size. On the y-axis the length of the window is reported in terms of years.

29 scores in 1951–1990, respectively, to 71 months and 72 scores in 2001–2010.

The 6-point series of DF, TDD and TDS for each grid cell were then subjected to a linear trend analysis. It is worth to note that this analysis, although the robustness of the results is limited by the small number of values, allows to provide a preliminary description of the inter-decadal variability of drought features as well as of its spatial distribution over the study domain. The spatial variability of the evolution of the three indicators over the domain is reported in Fig. 11, showing the distribution of the linear trends obtained over the 6 decades and their significance.

Despite the high spatial variability of trends as a consequence of the few points entering into the linear fit, the areas with the greatest and significant increase of indicator values are located in the north-western part and in a less extended portion in the eastern domain. These findings are in agreement with the spatial distribution of SPEI-3 trends over the study area even if in this case a more evident signal is depicted for the northernmost parts which turned out to be more influenced by variation in drought features.

CONCLUSIONS

The 1951–2017 monthly series of the two meteorological drought indices SPI and SPEI were computed and

analyzed for a portion of Po plain in northern Italy. The series were extracted from a gridded dataset of monthly precipitation and mean temperature records covering the study area at 30-arc second spatial resolution. The high-resolution fields were based on a quality checked and homogenized archive of long station records located on the domain and surrounding areas which were interpolated onto the grid by means of an anomaly-based method.

The long-term trend analysis on seasonal and annual SPI and SPEI areal series, which were computed by averaging the gridded precipitation and temperature records, pointed out a 5%-significant negative trend in summer for SPI ($-0.14 \text{ decade}^{-1}$) and in spring, summer and year for SPEI (-0.14 , -0.22 and $-0.17 \text{ decade}^{-1}$, respectively). Significant drying tendencies in both indices were depicted also over shorter time windows (20–30 years) starting in 1980 and in 1970 for spring and summer, respectively. In SPEI series the negative tendencies were more evident than in SPI values, probably due to the increasing role of evapotranspiration in recent decades triggered by warming conditions.

The gridded dataset allowed to investigate the long-term spatial variability of the drought indices over the domain. Significant negative trends occurred over the western portion of the study area for summer and annual SPI series and over the south-western parts for spring, sum-

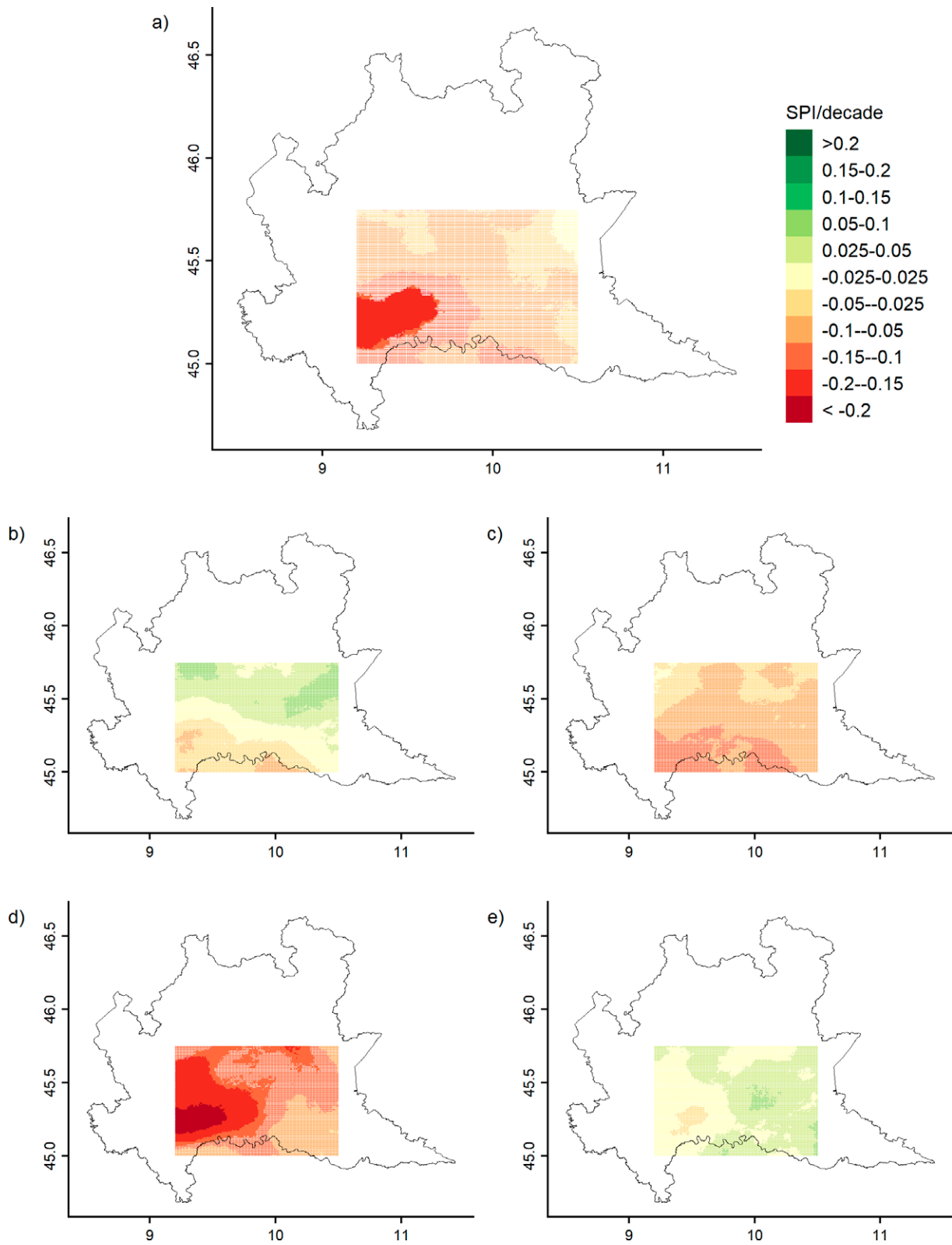


Fig. 6. Spatial distribution of TS trends for annual (a) and seasonal (winter b), spring c), summer d) and autumn e)) SPI series over the domain. Filled areas correspond to trends with MK p-values < 0.05, while dotted areas represent not significant trends. All values are expressed as index variation per decade.

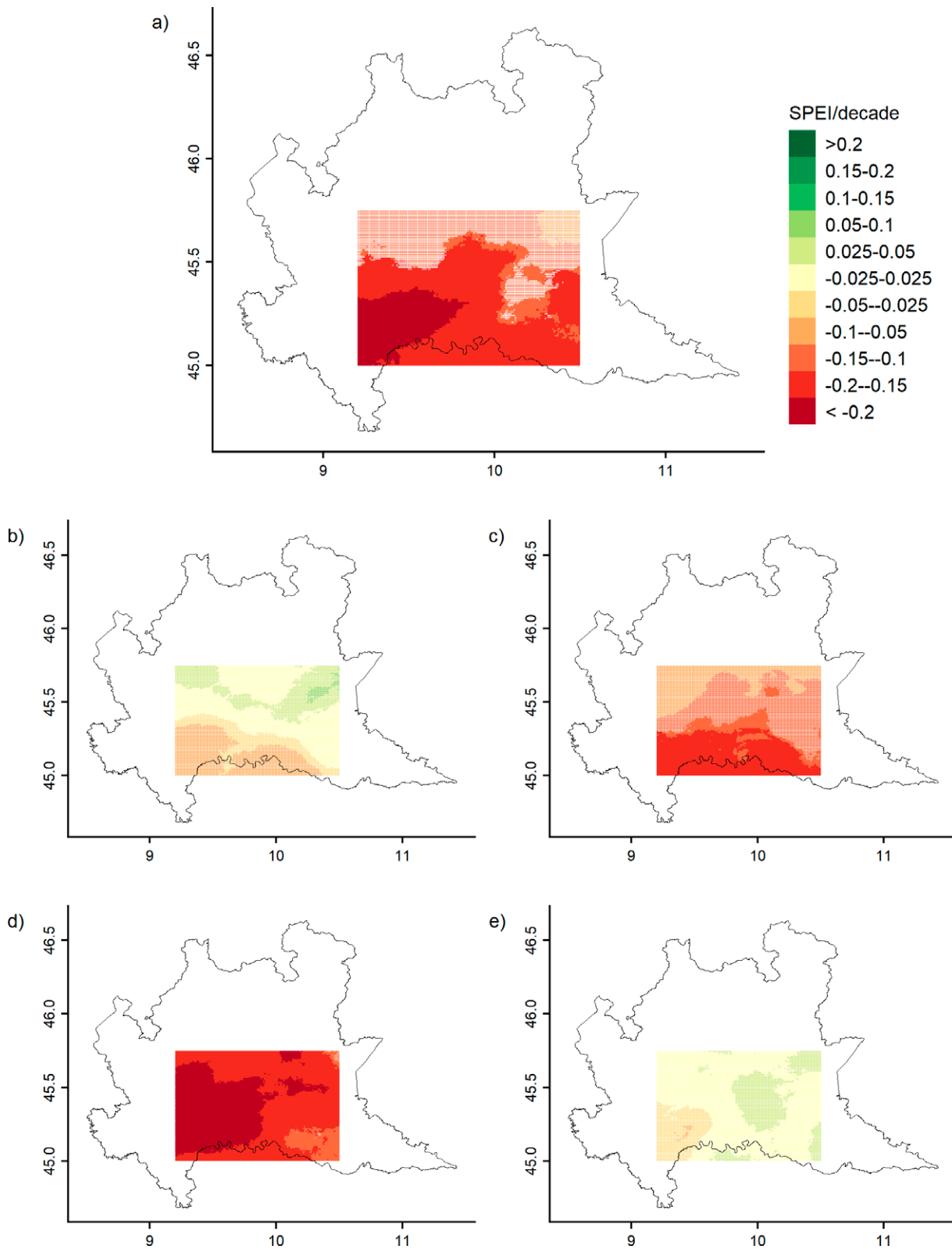


Fig. 7. Spatial distribution of TS trends for annual (a) and seasonal (winter b), spring c), summer d) and autumn e) SPEI series over the domain. Filled areas correspond to trends with MK p-values < 0.05, while dotted areas represent not significant trends. All values are expressed as index variation per decade.

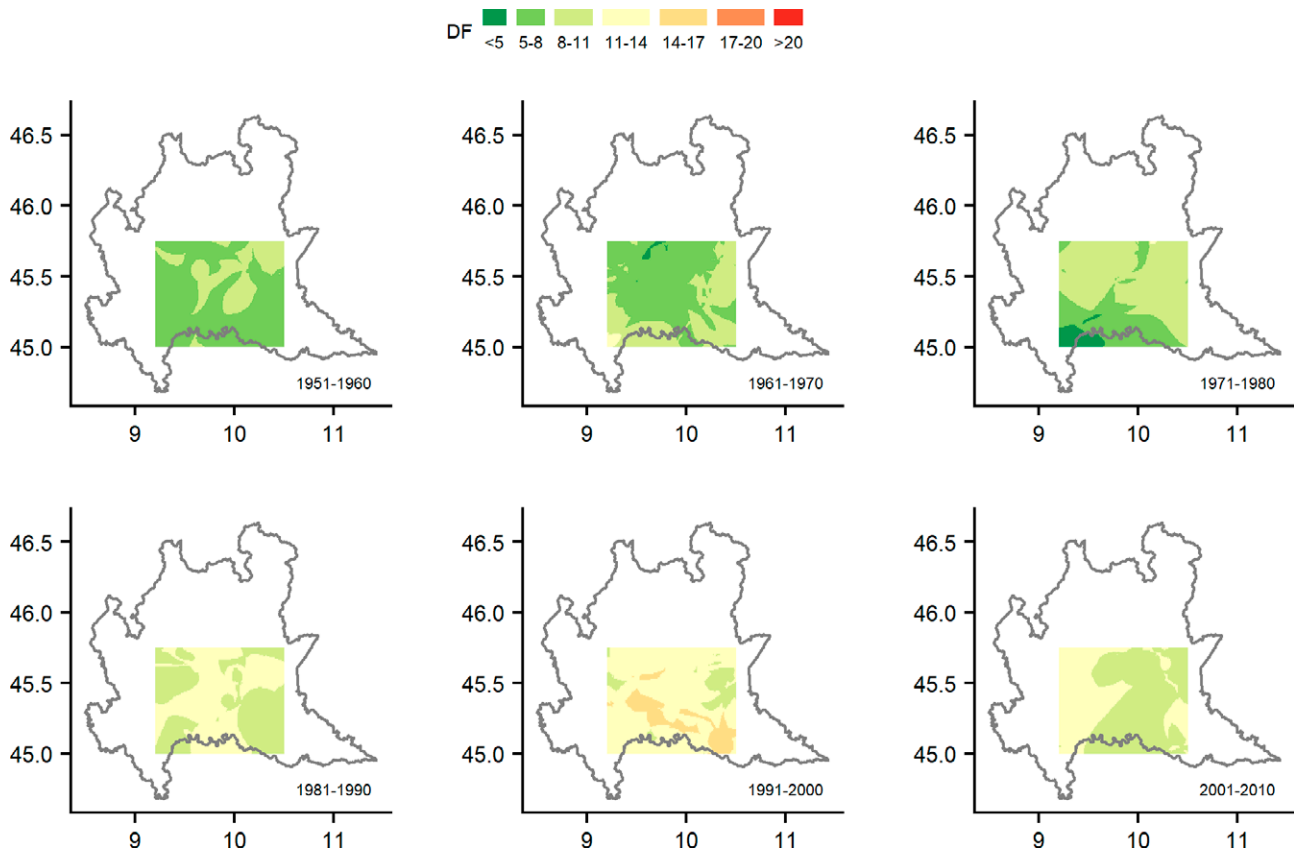


Fig. 8. Spatial distribution of the frequency of drought events (DF) identified in SPEI-3 series over subsequent decades.

mer and annual SPEI series, with the most relevant decrease ($< -0.2 \text{ decade}^{-1}$) in summer for both indices.

The drought spells identified in SPEI-3 over the domain for the whole 67-year period showed an overall intensification in terms of frequency, duration and severity from the 80's onwards. The linear trend analysis on the drought features for subsequent decades partly confirms the outcomes of trend assessment for the seasonal SPEI series, with the western part of the domain mostly affected by variations in drought indices, while the northern portion showed a greater sensitivity to the changes in drought features.

The spatio-temporal variability analysis of the two analyzed drought indices (SPI and SPEI) carried out for the central part of Lombardy plain suggests that the drought risk is expected to increase in the near future as a result of the climate change, leading to a decline in precipitation and an increase in air temperature, and consequently in crop evapotranspiration rates confirming the results of other studies for the same area (e.g. Crespi et al., 2021 and Ranzi et al., 2021). This will have impacts on irrigated agriculture, due to the combined effect of increasing crop water requirements and decreasing summer

flows in the rivers that supply water for irrigation, caused by reduced snow accumulation in winter and anticipated snow melting in spring (see e.g. Jenicek et al., 2018). This mismatch between crop water needs and river flows has already started to manifest itself in the last years increasing the risk of water scarcity (i.e. resources available for irrigation less than irrigation demand) during the months of higher irrigation needs for the majority of crops. This will happen also in geographic areas historically characterized by a good water availability for irrigation such as the Lombardy plain. Further analyses are addressed to forthcoming studies to evaluate more in detail the main factors explaining the spatial variability of drought index trends over the domain, and to extend the high-resolution drought characterization to a larger area in the Po plain. Moreover, the extension of the present study with the analysis of the future drought projections for the region from climate model scenarios would be essential to better evaluate how the drought risk is expected to evolve in the near and far future under climate change and this will be addressed in a forthcoming paper. The availability of detailed information on the drought evolution over northern Italy in the past, present and future could provide relevant

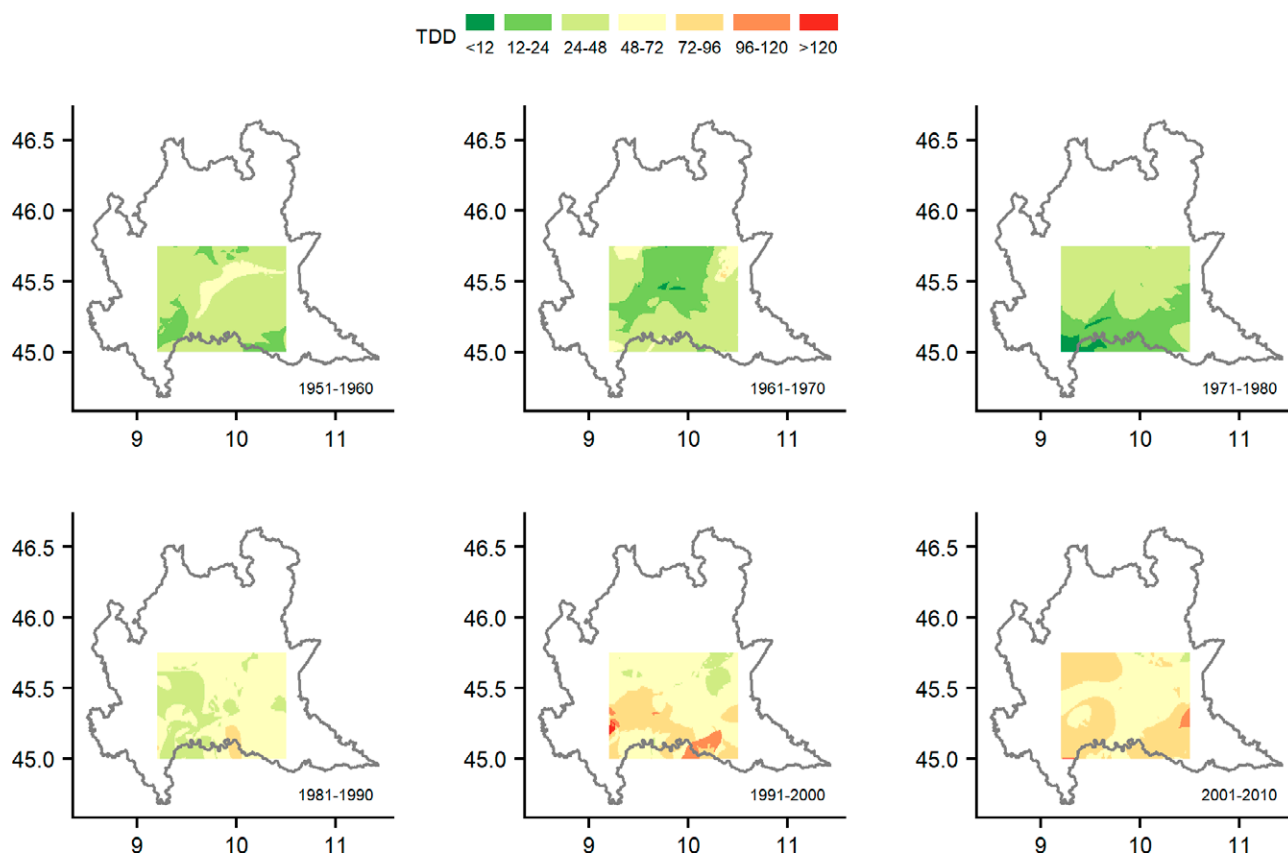


Fig. 9. Spatial distribution of the total month duration of drought events (TDD) identified in SPEI-3 series over subsequent decades.

supporting information to the management of current and future agricultural activities and production.

ACKNOWLEDGEMENTS

The support of Fondazione Cariplo through the So-Watch (Soft path water management adaptation to changing climate) project is gratefully acknowledged.

REFERENCES

- Allen R.G., Pereira L.S., Raes D., Smith M., 1998. Crop evapotranspiration – guidelines for computing crop water requirements. FAO Irrigation and drainage paper 56. Food and Agriculture Organization, Rome.
- Baronetti A., González-Hidalgo J.C., Vicente-Serrano S.M., Acquaotta F., Fratianni S., 2020. A weekly spatio-temporal distribution of drought events over the Po Plain (North Italy) in the last five decades. *International Journal of Climatology*, 40: 4463–4476. <https://doi.org/10.1002/joc.6467>
- Beguiería S., Vicente-Serrano S.M., Reig F., Latorre, B., 2014. Standardized precipitation evapotranspiration index (SPEI) revisited: parameter fitting, evapotranspiration models, tools, datasets and drought monitoring. *International Journal of Climatology*, 34: 3001–3023. <https://doi.org/10.1002/joc.3887>
- Bordi I., Sutera A., 2007. Drought Monitoring and Forecasting at Large Scale. In: Rossi G., Vega T., Bonaccorso B. (eds) *Methods and Tools for Drought Analysis and Management*. Water Science and Technology Library, vol 62. Springer, Dordrecht. https://doi.org/10.1007/978-1-4020-5924-7_1
- Briffa K.R., Van Der Schrier G., Jones P.D., 2009. Wet and dry summers in Europe since 1750: evidence of increasing drought. *International Journal of Climatology*, 29(13): 1894–1905. <https://doi.org/10.1002/joc.1836>
- Brunetti M., Maugeri M., Monti F., Nanni T., 2006. Temperature and precipitation variability in Italy in the last two centuries from homogenised instrumental time series. *International Journal of Climatology*, 26: 345–381. <https://doi.org/10.1002/joc.1251>
- Brunetti M., Lentini G., Maugeri M., Nanni T., Auer I., Böhm R., Schöner W., 2009. Climate variability and

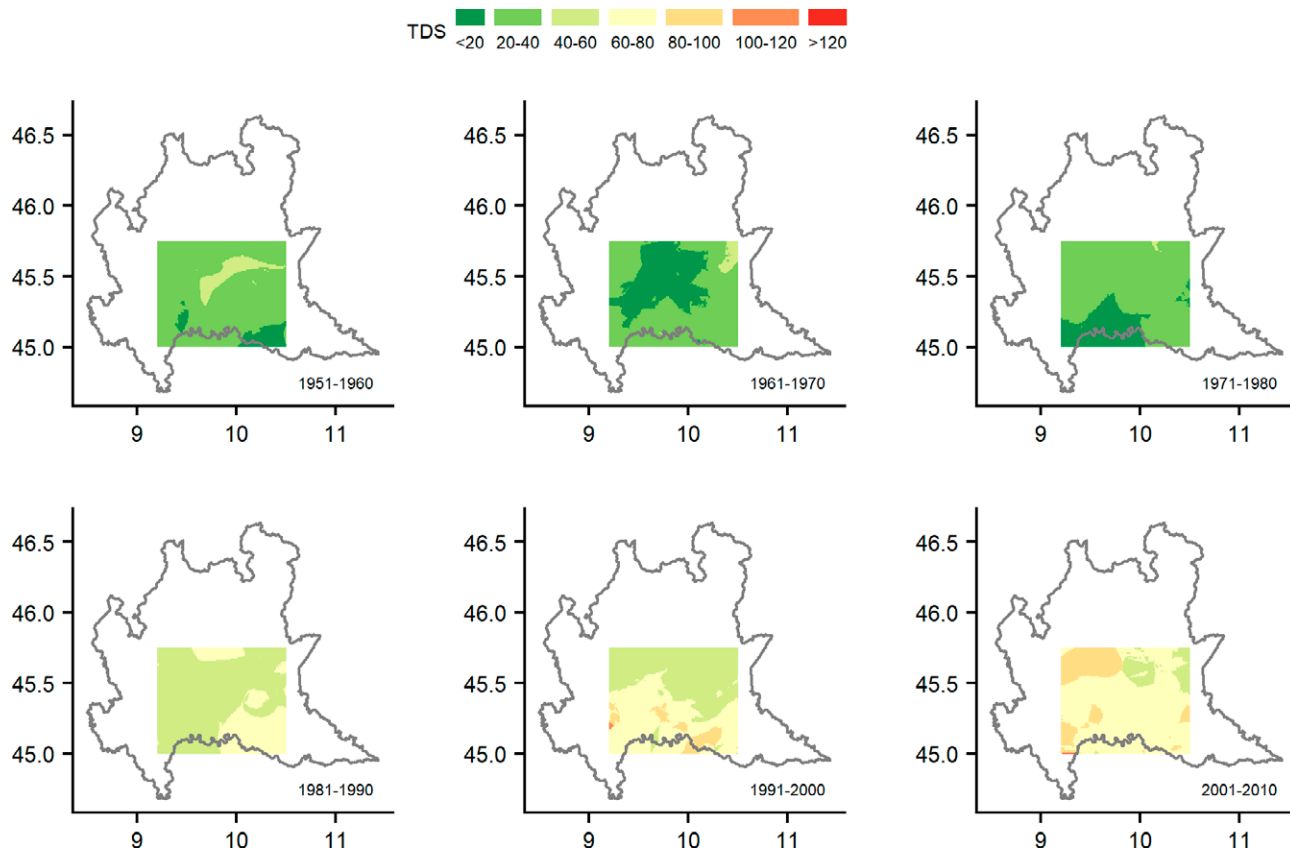


Fig. 10. Spatial distribution of the total severity of drought events (TDS) identified in SPEI-3 series over subsequent decades.

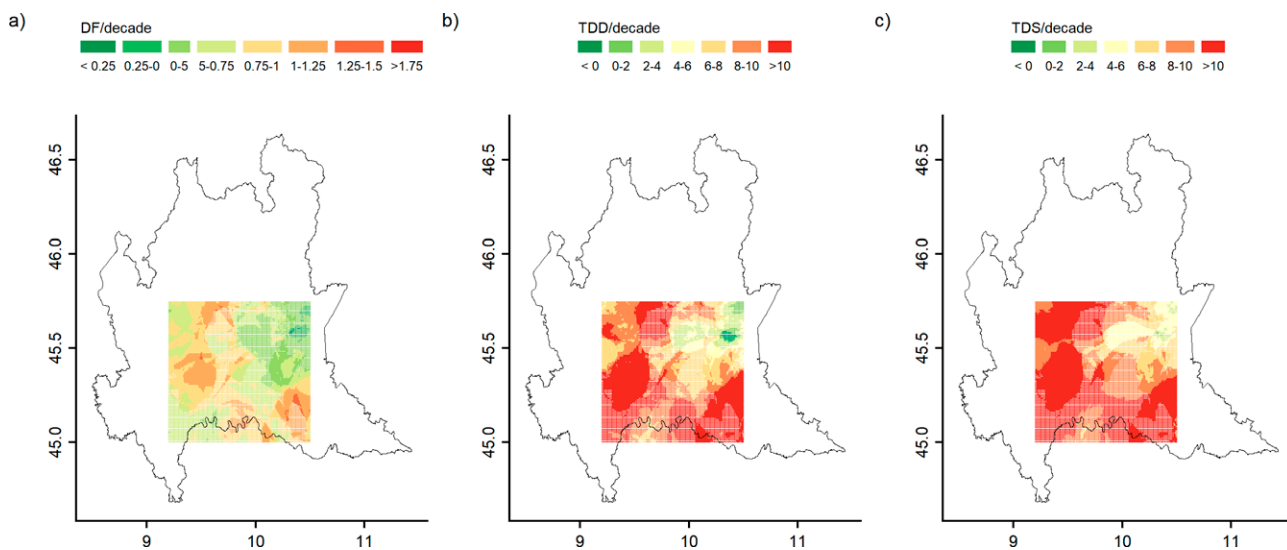


Fig. 11. Distribution of linear trend values of a) DF, b) TDD and c) TDS over 6 subsequent decades from 1951 to 2010 obtained from SPEI-3 series. Filled areas correspond to significant trends (p -value < 0.05), while grid cells corresponding to not significant trends are reported as dotted areas.

- change in the Greater Alpine Region over the last two centuries based on multi-variable analysis. *International Journal of Climatology*, 29: 2197–2225. <https://doi.org/10.1002/joc.1857>
- Brunetti M., Lentini G., Maugeri M., Nanni T., Simolo C., Spinoni J., 2012. Projecting North Eastern Italy temperature and precipitation secular records onto a high-resolution grid. *Physics and Chemistry of the Earth, parts A/B/C*, 40–41: 9–22. <https://doi.org/10.1016/j.pce.2009.12.005>
- Brunetti M., Maugeri M., Nanni T., Simolo C., Spinoni J., 2014. High-resolution temperature climatology for Italy: interpolation method intercomparison. *International Journal of Climatology*, 34: 1278–1296. <https://doi.org/10.1002/joc.3764>
- Buttafuoco G., Caloiero T., Coscarelli R., 2015. Analyses of Drought Events in Calabria (Southern Italy) Using Standardized Precipitation Index. *Water Resource Management*, 29: 557–573. <https://doi.org/10.1007/s11269-014-0842-5>
- Craddock J., 1979. Methods of comparing annual rainfall records for climatic purposes. *Weather*, 34: 332–346. <https://doi.org/10.1002/j.1477-8696.1979.tb03465.x>
- Crespi A., Brunetti M., Maugeri M., Ranzi R., Tomirotti M., 2018a. 1845–2016 gridded dataset of monthly precipitation over the upper Adda river basin: a comparison with runoff series. *Advances in Science and Research*, 15: 173–181. <https://doi.org/10.5194/asr-15-173-2018>
- Crespi A., Brunetti M., Lentini G., Maugeri M., 2018b. 1961–1990 high-resolution monthly precipitation climatologies for Italy. *International Journal of Climatology*, 38: 878–895. <https://doi.org/10.1002/joc.5217>
- Crespi A., Brunetti M., Ranzi R., Tomirotti M., Maugeri M., 2021. A multi-century meteo-hydrological analysis for the Adda river basin (Central Alps). Part I: Gridded monthly precipitation (1800–2016) records. *International Journal of Climatology*, 41: 162–180. <https://doi.org/10.1002/joc.6614>
- Dai A., Trenberth K.E., Qian T., 2004. A global dataset of Palmer Drought Severity Index for 1870–2002: relationship with soil moisture and effects of surface warming. *Journal of Hydrometeorology*, 5(6): 1117–1130. <https://doi.org/10.1175/JHM-386.1>
- Daly C., Gibson W.P., Taylor G.H., Johnson G.L., Pastoris P., 2002. A knowledge-based approach to the statistical mapping of climate. *Climate Research*, 22: 99–113. <https://doi.org/10.3354/cr022099>
- Di Lena B., Vergni L., Antenucci F., Todisco F., Manocchi F., 2014. Analysis of drought in the region of Abruzzo (Central Italy) by the Standardized Precipitation Index. *Theoretical and Applied Climatology*, 115: 41–52. <https://doi.org/10.1007/s00704-013-0876-2>
- Foresti L., Sideris I., Panziera L., Nerini D., Germann U., 2018. A 10-year radar-based analysis of orographic precipitation growth and decay patterns over the Swiss Alpine region. *Quarterly Journal of the Royal Meteorological Society*, 144: 2277–2301. <https://doi.org/10.1002/qj.3364>
- Founda D., Varotsos K.V., Pierros F., Giannakopoulos C., 2019. Observed and projected shifts in hot extremes' season in the Eastern Mediterranean. *Global and Planetary Change*, 175, 190–200. <https://doi.org/10.1016/j.gloplacha.2019.02.012>
- IPCC, 2014. Summary for Policymakers. In: *Climate Change 2014: Mitigation of Climate Change. Contribution of Working Group III to the Fifth Assessment Report of the Intergovernmental Panel on Climate Change* [Edenhofer, O., R. Pichs-Madruga, Y. Sokona, E. Farahani, S. Kadner, K. Seyboth, A. Adler, I. Baum, S. Brunner, P. Eickemeier, B. Kriemann, J. Savolainen, S. Schlömer, C. von Stechow, T. Zwickel and J.C. Minx (eds.)]. Cambridge University Press, Cambridge, United Kingdom and New York, NY, USA. <https://doi.org/10.1017/cbo9781107415416.005>
- Isotta F.A., Frei C., Weilguni V., Perčec Tadić M., Lassègues P., Rudolf B., Pavan V., Cacciamani C., Antolini G., Ratto S.M., Munari M., Micheletti S., Bonati V., Lussana C., Ronchi C., Panettieri E., Mariogo G., Vertaničk G., 2014. The climate of daily precipitation in the Alps: development and analysis of a high-resolution grid dataset from pan-Alpine rain-gauge data. *International Journal of Climatology*, 34: 1657–1675. <https://doi.org/10.1002/joc.3794>
- Kendall M.G., 1975. *Rank Correlation Methods*. Griffin, London.
- Lionello P., Scarascia L., 2018. The relation between climate change in the Mediterranean region and global warming. *Regional Environmental Change*, 18: 1481–1493. <https://doi.org/10.1007/s10113-018-1290-1>
- McKee T.B., Doeskin N.J., Kleist J., 1993. The relationship of drought frequency and duration to time scales. In *Proceedings of the 8th Conference on Applied Climatology*. American Meteorological Society: 179–184.
- Mitchell T.D., Jones P.D., 2005. An improved method of constructing a database of monthly climate observations and associated high resolution grids. *International Journal of Climatology*, 25: 693–712. <https://doi.org/10.1002/joc.1181>
- New M., Todd M., Hulme M., Jones P., 2001. Precipitation measurements and trends in the twentieth century. *International Journal of Climatology*, 21: 1899–1922. <https://doi.org/10.1002/joc.680>
- Parsons D.J., Rey D., Tanguy M., Holman I.P., 2019. Regional variations in the link between drought indi-

- ces and reported agricultural impacts of drought. *Agricultural Systems*, 173:119–129. <https://doi.org/10.1016/j.agsy.2019.02.015>
- Piccarreta M., Capolongo D., Boenzi F., 2004. Trend analysis of precipitation and drought in Basilicata from 1923 to 2000 within a southern Italy context. *International Journal of Climatology*, 24: 907–922. <https://doi.org/10.1002/joc.1038>
- Ranzi R., Michailidi E.M., Tomirotti M., Crespi A., Brunetti M., Maugeri M., 2021. A multi-century meteorological analysis for the Adda river basin (Central Alps). Part II: Daily runoff (1845–2016) at different scales. *International Journal of Climatology*, 41: 181–199. <https://doi.org/10.1002/joc.6678>
- Sen P.K., 1968. Estimates of the regression coefficient based on Kendall's tau. *Journal of the American Statistical Association*, 63(324): 1379–1389. <https://doi.org/10.2307/2285891>
- Spinoni J., Naumann G., Carrao H., Barbosa P., Vogt J., 2014. World drought frequency, duration, and severity for 1951–2010. *International Journal of Climatology*, 34(8): 2792–2804. <https://doi.org/10.1002/joc.3875>
- Spinoni J., Naumann G., Vogt J., 2015. Spatial patterns of European droughts under a moderate emission scenario. *Advances in Science and Research*, 12(1): 179–186. <https://doi.org/10.5194/asr-12-179-2015>
- Spinoni J., Vogt J.V., Naumann G., Barbosa P., Dosio A., 2018. Will drought events become more frequent and severe in Europe?. *International Journal of Climatology*, 38: 1718–1736. <https://doi.org/10.1002/joc.5291>
- Stagge J.H., Kohn I., Tallaksen L.M., Stahl K., 2015. Modeling drought impact occurrence based on meteorological drought indices in Europe. *Journal of Hydrology*, 530: 37–50. <https://doi.org/10.1016/j.jhydrol.2015.09.039>
- Stagge J.H., Kingston D.G., Tallaksen L.M., Hannah D.M., 2017. Observed drought indices show increasing divergence across Europe. *Scientific Reports*, 7: 14045. <https://doi.org/10.1038/s41598-017-14283-2>
- Theil H., 1950. A rank-invariant method of linear and polynomial regression analysis. I. *Proceedings of the Koninklijke Nederlandse Akademie van Wetenschappen A53*: 386–392.
- Thorntwaite C.W., 1948. An approach toward a rational classification of climate. *Geographical Review*, 38: 55–94. <https://doi.org/10.2307/210739>
- Vergni L., Todisco F., 2011. Spatio-Temporal Variability of Precipitation, Temperature and Agricultural Drought Indices in Central Italy. *Agricultural and Forest Meteorology*, 151: 301–313. <https://doi.org/10.1016/j.agrformet.2010.11.005>
- Vicente-Serrano S.M., Beguería S., López-Moreno J.I., 2010. A Multiscalar Drought Index Sensitive to Global Warming: The Standardized Precipitation Evapotranspiration Index. *Journal of Climate*, 23: 1696–1718. <https://doi.org/10.1175/2009JCLI2909.1>
- Vicente-Serrano S.M., Beguería S., Lorenzo-Lacruz J., Camarero J. J., López-Moreno J. I., Azorin-Molina C., Revuelto J., Morán-Tejada E., Sanchez-Lorenzo A., 2012. Performance of Drought Indices for Ecological, Agricultural, and Hydrological Applications. *Earth Interactions*, 16:1–27. <https://doi.org/10.1175/2012EI000434.1>
- Vicente-Serrano S.M., Lopez-Moreno J.I., Beguería S., Lorenzo-Lacruz J., Sanchez-Lorenzo A., García-Ruiz J. M., Azorin-Molina C., Moran-Tejada E., Revuelto J., Trigo R., Coelho F., Espejo F., 2014. Evidence of increasing drought severity caused by temperature rise in southern Europe. *Environmental Research Letters*, 9(4): 044001. <https://doi.org/10.1088/1748-9326/9/4/044001>



Citation: E. Hojjati, G. Mahtabi, F. Taran, O. Kisi (2020) Estimating evaporation from reservoirs using energy budget and empirical methods: Alavian dam reservoir, NW Iran. *Italian Journal of Agrometeorology* (2): 19-34. doi: 10.13128/ijam-1033

Received: July 26, 2020

Accepted: September 19, 2020

Published: January 25, 2021

Copyright: © 2020 E. Hojjati, G. Mahtabi, F. Taran, O. Kisi. This is an open access, peer-reviewed article published by Firenze University Press (<http://www.fupress.com/ijam>) and distributed under the terms of the Creative Commons Attribution License, which permits unrestricted use, distribution, and reproduction in any medium, provided the original author and source are credited.

Data Availability Statement: All relevant data are within the paper and its Supporting Information files.

Competing Interests: The Author(s) declare(s) no conflict of interest.

Estimating evaporation from reservoirs using energy budget and empirical methods: Alavian dam reservoir, NW Iran

ELAHE HOJJATI¹, GHORBAN MAHTABI^{1,*}, FARSHID TARAN², OZGUR KISI³

¹ Department of Water Engineering, University of Zanjan, 45371-38791, Zanjan, Iran

² Department of Water Engineering, University of Tabriz, 51666-16471, Tabriz, Iran

³ Faculty of Natural Sciences and Engineering, Ilia State University, Tbilisi, Georgia

* Corresponding author. E-mail: gmahtabi@znu.ac.ir; ORCID: 0000-0002-3532-8933

Abstract. Accurate estimation of evaporation from open water resources like lakes and dam reservoirs is necessary to proper water balance management, especially in arid and semi-arid regions. A detailed daily evaporation study was conducted on Alavian dam reservoir, located in the northwest of Iran. A two-dimensional hydrodynamic model was used to obtain the distribution of daily water temperature of the reservoir. The water temperature model was calibrated and validated using a three-year observed data set (2013-2016). The Bowen ratio energy budget (BREB) is accepted as a standard approach in estimating evaporation from lakes. To select the best evaporation method(s) over the lake, evaporation rates were determined using 30 empirical methods. These methods were evaluated and ranked with respect to the BREB values. The estimated evaporation values by the BREB approach showed that the monthly mean and the annual evaporation from the Alavian reservoir during 2015-2016 were equal to 4.08 mm day⁻¹ and 1508 mm year⁻¹, respectively. The Rohwer (Dalton) and the deBruin (combination) methods with the RMSEs of 0.71 and 0.79 mm day⁻¹, respectively, provided the best performances. To summarize, the methods depended only on measurement of vapor pressure deficit and wind speed (e.g., Rohwer, deBruin and McMillan) were relatively found to be more cost-effective and more practical alternatives for determining evaporation at the studied area, owing to their high efficiency and simplicity.

Keywords. Alavian reservoir, evaporation, energy budget, empirical methods, temperature simulation.

1. INTRODUCTION

In many arid and semi-arid areas, surface water is an important resource for drinking, agriculture and industry. Since the water demand has increased due to climate change, socioeconomic and environmental conditions, the use of water resources should properly be managed and optimized. Iran is located in an arid and semi-arid region in which many efforts are made to increase the water use efficiency. Evaporation from freshwater lakes or dam reservoirs, as

a main factor in water loss from surface water resources, can play an important role in water resources management in arid and semi-arid regions. In the recent years, climate change has been a big problem for the activities related to agriculture (e.g., change in pattern of rainfall and temperature) which have important effects on the availability of water resources in Iran (Zarghami et al., 2011). In this situation, the evaluation of evaporation from lakes or reservoirs is necessary to manage and control any water loss in the available resources. These issues increase the importance of understanding the evaporation components, as well as the accurate estimation of the evaporation losses. Open-water evaporation is a continuous hydrological process affected by different parameters such as solar radiation, air and water temperature, wind speed, vapor pressure deficit, atmospheric pressure, surface area, water depth and water quality (Brutsaert, 1982). Hence, estimation of evaporation is a very difficult task since it depends on many climatic and geologic parameters.

Different approaches can be utilized to estimate evaporation using meteorological data from free surface resources. They are classified as: (1) water budget, (2) evaporation pans, (3) Bowen ratio energy budget, and (4) empirical methods. The empirical methods can be categorized into five groups: combination, solar radiation-temperature, Dalton (mass-transfer), temperature-day length and temperature (Rosenberry et al., 2007). The Bowen-ratio energy-budget (BREB) approach is one of the most accurate approaches for continuous long-term evaporation monitoring (Harbeck et al., 1958; Omar and El-Bakry, 1981; Lenters et al., 2005). Omar and El-Bakry (1981) evaluated the evaporation rate from Aswan High dam reservoir using the energy-budget and mass transfer methods during 1970-1971 based on measurements over the reservoir. They concluded that the energy budget was the most fundamental method for estimating the evaporation. The effects of errors in the water surface temperature and the vapor pressure on the evaporation calculations were smaller when using the energy budget method. Also, the monthly deviation of evaporation estimated by two methods was 10-14% of actual values. Lenters et al. (2005) presented a comprehensive, 10-years analysis of seasonal, intra-seasonal, and inter-annual variations in lake evaporation for Sparkling Lake, northern Wisconsin (USA). The results of a long-term energy budget method showed that the mean evaporation rate for the lake over the study period was 3.1 mm day^{-1} with a coefficient of variation of 25%.

The BREB, as a standard approach, is commonly used to determine the evaporation losses and the efficacy of different empirical methods with different climatic and physical settings. For instance, Rosenberry et al. (2004) compared evaporation rates calculated by 12 methods with the

energy budget method in Cottonwood Lake in east-central North Dakota, USA. Rosenberry et al. (2007) assessed 15 approaches in Mirror Lake in northeastern USA and then adjusted the methods to better fit the BREB values. Gorjizade et al. (2014) tested eight methods in Dez reservoir in Iran, and concluded that the Priestly-Taylor and the DeBruin-Kejiman approaches performed superior to the other alternatives. The evaluation of 19 methods by Majidi et al. (2015) in Doosti Reservoir in Iran suggested that Jensen-Haise, Makkink, Penman and deBruin were the best approaches considering the BREB values. Antonopoulos et al. (2016) evaluated the Artificial Neural Networks (ANN) and 3 classical empirical methods in Lake Vegoritis, Greece. Hussain (2017) used seven methods to estimate the evaporation from Brullus Lake in the north of Nile Delta in Egypt, recognizing Makkink as the best method followed by DeBruin-Kejiman. Bozorgi et al. (2018) evaluated and ranked 12 methods in Karkheh reservoir in Iran, indicating that Stephens-Stewart, Makkink, Jensen-Haise, and Blaney-Criddle were the best methods, respectively.

In the BREB method, devices and sensors like precision spectral pyranometer are used for accurate measuring of the energy budget fluxes. However, if the access to these devices and sensors is not possible, a number of auxiliary equations can be used to determine the fluxes (Torres and Calera, 2010). The most difficult parameter to estimate is the thermal energy stored in the lake. To compute the energy budget flux, the main parameter to measure is the water temperature profiles. The variations in the water temperature present the changes in the thermal energy of the lake. The flux can be calculated from the outcomes of turbulent diffusion or hydrodynamic models (QUALAKE-DOT or CE-QUAL-W2) which can compute the lake temperature profiles, and therefore the changes in the thermal energy (Antonopoulos and Gianniou, 2016). Up to now, limited studies have been performed to determine the storage heat flux of energy budget using simulation of temperature profile of a lake/reservoir (Gianniou and Antonopoulos, 2007; Antonopoulos et al., 2016). Gianniou and Antonopoulos (2007) determined daily evaporation and energy budget in Lake Vegoritis in Greece for the year 1993. They used the one-dimensional eddy diffusion model (QUALAKE-DOT) to compute the daily water temperature profile of the lake and the thermal energy stored in the lake. Throughout the evaporation calculation, two statistics suggested by Tanner et al. (1987) and Payero et al. (2003) were applied.

The aim of the present study is to (1) estimate the daily evaporation from the Alavian reservoir in Maragheh, Iran, based on the energy budget, and (2) evaluate the suitability of 30 empirical equations. A two-dimensional hydrodynamic model (CE-QUAL-W2) was implemented to

obtain the distribution of water temperature in the reservoir. A comprehensive comparison was made to select the most accurate approaches in estimating the lake evaporation based on the energy budget method.

2. MATERIALS AND METHODS

2.1. Alavian reservoir

Sufi-Chay River is located in Urmia Lake basin in the northwest of Iran. Alavian dam reservoir is constructed on the Sufi-Chay River in East Azerbaijan Province at a distance of 3.5 km from the northwest of Maragheh City with longitude 46°15'E and latitude 37°25'N. The main purpose of the construction of the Alavian dam are to collect and control the Sufi-Chay surface streams and provide drinking water for Maragheh City, compensate for part of agricultural needs of Maragheh-Bonab plain, the industrial areas and the hydroelectric power generation. Fig. 1 illustrates the location of the Alavian dam.

The surface area, surface elevation, and the volume of the lake from October 2015 to September 2016 (the year for this study) are 1.57 km², 1554.51 m and 27.26 mcm, respectively. The maximum depth of the reservoir is 60 m. The climate in the region is semi-arid with 299.4 mm annual mean precipitation. The annual temperature is 13.5 °C in July-September (summer) and January-March (winter). In the results and discussion section, the Alavian dam has been compared with Vegoritits Lake (Gianniou and Antonopoulos 2007) since there are effective similarities between the two lakes. The surface elevation, the surface area, and the volume of the Vegoritits Lake in 1993 (the year of the study) were 513 m, 33.5 km², and 810.4 mcm, respectively. These parameters, as the differences between the two lakes, mainly affect the amount of evaporation, but not the evaporation process. In other words, the more the lake surface area is, the more the evaporation will be. Other parameters like climatic parameters and depth of the lake affect the evaporation process. The maximum depth of the Vegoritits Lake

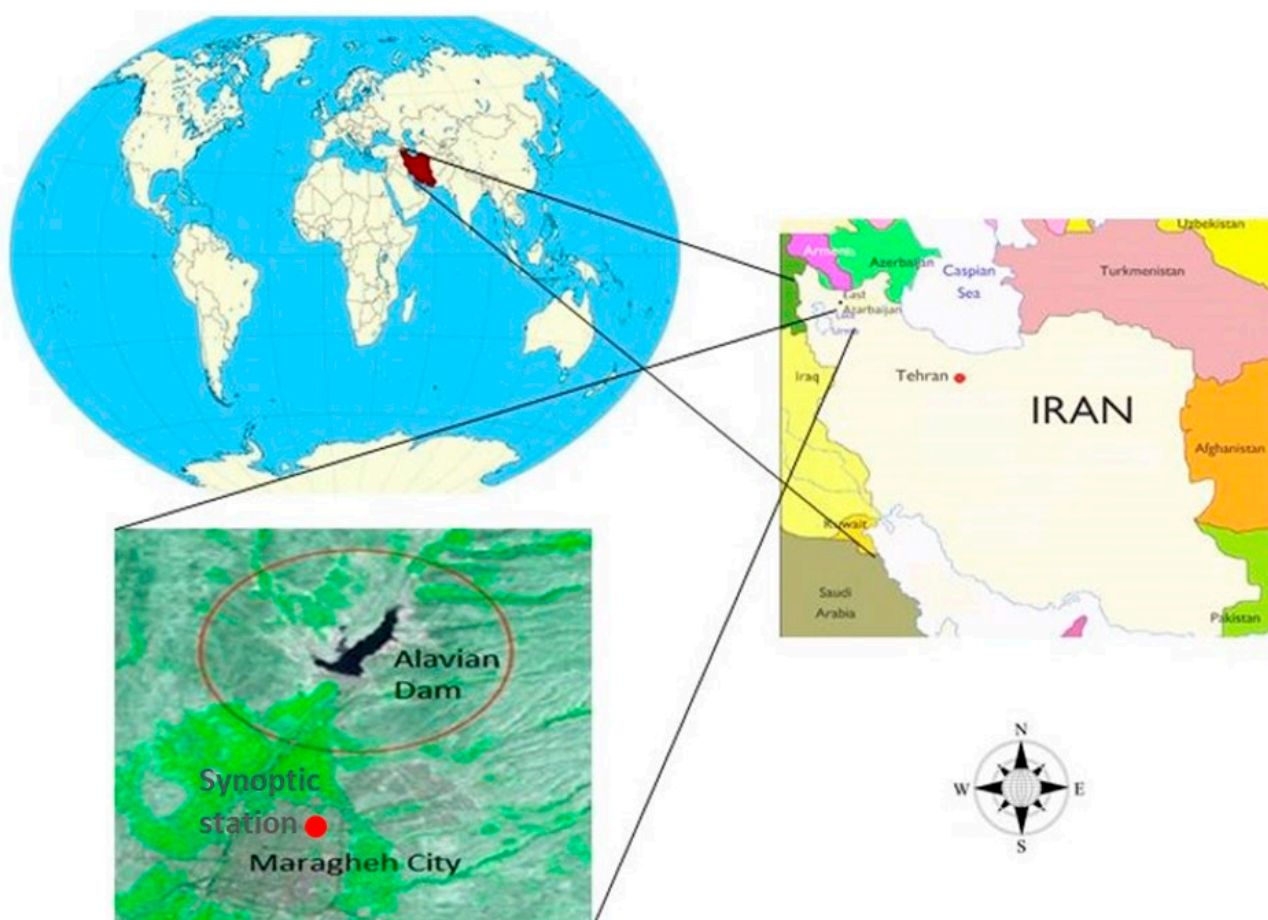


Fig. 1. Location of the Alavian Dam reservoir in East Azerbaijan Province, Iran.

was 48 m (as the similarity between the two lakes). The climate in the Vegoritis area is semi-arid with two-distinguishing warm-dry and cold-wet periods during the year (as similarity). The annual mean temperature was 12.1 °C, with July and January being the warmer and the colder months of the year, respectively (as similarity). These similarities in the evaporation process show that the two lakes could effectively be compared.

2.2. Energy budget method

In order to determine the amount of energy necessary to evaporate water from free surfaces, a Bowen-ratio energy-budget (BREB) approach or, in general, a surface energy budget can be used. That is, in the water system, the energy conservation equation can be applied to determine the evaporation rate (Winter et al., 2003; Lenters et al., 2005; Rosenberry et al., 2007). The BREB is considered as the standard and reference approach in long-term and continuous monitoring and estimating the evaporation from lake surface and requires a large amount of meteorological and hydrological data. The energy budget of a lake can be stated as:

$$Q_s - Q_{sr} + Q_a - Q_{ar} - Q_{bs} - Q_e - Q_h - Q_w + Q_v + Q_b = Q_x \quad (1)$$

where Q_s is the incoming shortwave radiation, Q_{sr} is the reflected shortwave radiation, Q_a is the incoming longwave radiation from the atmosphere, Q_{ar} is the reflected longwave radiation from the atmosphere, Q_{bs} is the emitted longwave atmospheric radiation from the water body, Q_e is the energy used for evaporation, Q_h is the energy conducted from the water body as sensible heat, Q_w is the energy advected from the water body to the atmosphere by the evaporated water, Q_v is the net energy advected into the water body by precipitation, surface water, and ground water, Q_b is the net energy conducted between the lake water and the bottom sediments, and Q_x is the alteration in the energy content of the water body. The unit utilized for the fluxes of Eq. (1) is $W m^{-2}$.

The fluxes Q_e , Q_h , and Q_w , not measured directly, were estimated as functions of the evaporation rate by employing the following equations:

$$Q_e = \rho E L_v \quad (2)$$

$$Q_h = \beta Q_e \quad (3)$$

$$Q_w = \rho c E (T_w - T_b) \quad (4)$$

where ρ is the water density (998 kg m^{-3} at 20 °C), E is the water evaporation (m s^{-1}), L_v is the latent heat of vapori-

zation (J kg^{-1}), β is the Bowen ratio (dimensionless), c is the specific heat capacity of water ($4186 \text{ J kg}^{-1} \text{ }^\circ\text{C}^{-1}$), T_w is the water surface temperature ($^\circ\text{C}$) and T_b is an arbitrary base temperature of 0 °C. When Bowen ratio values (β) are close to -1, extremely inaccurate values for the latent heat flux (Q_e) are estimated. A simple way of facing this problem, as proposed by Tanner et al. (1987), is to reject the data for which $-1.25 < \beta < -0.75$. Furthermore, faulty meteorological data or the fact that they come from different stations could sometimes result in fluxes with the wrong sign (Payero et al., 2003). Valid data should be met the following criteria:

- a) Excluding data when $-1.25 < \beta < -0.75$
- b) $L_v(\Delta e + \gamma \Delta T)(Q_{rm} - Q_x) > 0$ (5)

where $\Delta e = e_{sw} - e_a$, $\Delta T = T_w - T_a$, e_{sw} is the saturation vapor pressure at the water surface temperature (mbar), e_a is the air vapor pressure above water surface (mbar), and T_a is air temperature ($^\circ\text{C}$).

In many cases, especially in large and deep lakes, the fluxes Q_s and Q_b are too small and many researchers agree to omit the fluxes with small values and insignificant effects (Stauffer, 1991; Sacks et al., 1994; dos Reis and Dias, 1998; Winter et al., 2003; Gianniou and Antonopoulos, 2007; Rosenberry et al., 2007). Winter et al. (2003) reported that energy advected to and from the lake by precipitation, surface water, and ground water (Q_v) was found to have little effect on evaporation rates. Net energy gain related to surface water was small since the water temperatures were low when the largest inflows and outflows occurred during spring and the late fall. Net energy gain related to ground-water was small since groundwater inflow was a small part of the water budget and the temperature of groundwater was relatively low (Winter et al., 2003).

Finally, by combining Eqs. 1, 2, 3 and 4, the following equation is obtained:

$$E = \frac{Q_s - Q_{sr} + Q_a - Q_{ar} - Q_{bs} - Q_x}{\rho(L_v(1 + \beta) + cT_w)} = \frac{Q_{rm} - Q_x}{\rho(L_v(1 + \beta) + cT_w)} \quad (6)$$

where E is the water evaporation (m s^{-1}), Q_{rm} is the net radiation (W m^{-2}), and $Q_{rm} = Q_s - Q_{sr} + Q_a - Q_{ar} - Q_{bs}$. In Eq. (6), the fluxes Q_s and Q_a are calculated from meteorological data (Allen et al., 1998; Antonopoulos *et al.*, 2016), and Q_{sr} and Q_{ar} are fixed portions of Q_s and Q_a , respectively (Anderson, 1954; Koberg, 1964). Q_{bs} is computed from the lake surface water temperature by utilizing the law of Stefan-Boltzmann (Rosenberry et al., 2007). The alteration in the energy content of the water body (Q_x) can be calculated by the variation of the lake temperature for each energy-budget period (here the period is a day) (Gianniou

and Antonopoulos, 2007; Duan and Bastiaanssen, 2015), according to the following equation:

$$Q_x = \frac{\rho \cdot c}{A_s} \sum_0^z \frac{\Delta T_{(z,t)}}{\Delta t} A_z \cdot \Delta z \quad (7)$$

where ρ is the water density (kg m^{-3}), c is the specific heat capacity of water ($\text{J kg}^{-1} \text{ }^\circ\text{C}^{-1}$), A_s is the lake surface area (m^2), A_z is the horizontal area as a function of depth (m^2) and $T_{z,t}$ is the water temperature ($^\circ\text{C}$) as a function of depth (z) and time (t). In this study, to determine the water temperature distribution and, as a result, the thermal energy stored in the lake, the mathematical model CE-QUAL-W2 (version 3.7, developed by Edinger and Buchak, 1975) was employed

2.3. Lake water temperature modelling

Many models have been developed in hydrodynamic and water quality simulation of lakes/reservoirs. These models are widely used especially when there are limited water temperature measurements. The CE-QUAL-W2 is a two-dimensional, longitudinal-vertical, laterally averaged model which has been developed since 1975 (Buchak and Edinger, 1984). This model is successfully applied to simulate hydrodynamic, temperature and water quality in lakes/reservoirs in different regions (Kim and Kim, 2006; Gianniou and Antonopoulos, 2007; Norton and Bradford, 2009; Buccola and Stonewall, 2016). The CE-QUAL-W2 model depends on the solution of two-dimensional unsteady hydrodynamic and advection-dispersion equations. The input data required for modeling by CE-QUAL-W2 are: geometric data, meteorological and hydrologic data, shading or vegetation coefficient, wind sheltering coefficient, inflow, outflow, and water temperature distribution. The following data are required to set up the input geometry: topographic map and volume-area-elevation table of the reservoir. The topographic map is utilized to produce bathymetric cross-sections which are inputs of the model. The volume-area-elevation table of project is utilized to compare with the one that is produced by the model (in calibration stage). The meteorological data includes air temperature (TAIR) ($^\circ\text{C}$), dew point temperature (TDEW) ($^\circ\text{C}$), wind direction (PHI) (Radian), wind speed (WIND) (m s^{-1}) and cloud cover (CLOUD) (%). In the present research, these daily data were obtained from the nearest station (with a full data set) to the Alavian dam and introduced to the model (Maragheh synoptic station). The vegetation coefficient and the wind sheltering coefficient were evaluated in the calibration stage (Kim and Kim, 2006). The upstream boundary conditions were introduced to the model using the reservoir inflows (Tazeh-Kand hydromet-

ric station located at the upstream of the Alavian dam) and the inflow temperature (the measured water temperature data). The downstream boundary conditions were determined by the outflows and the water surface level in the reservoir (the operating data of the reservoir).

The parameter set of the CE-QUAL-W2 model was calibrated and validated by utilizing the volume-area-elevation table and the water temperature measurements in the Alavian reservoir during October 2013-September 2016. The constants and coefficients of the model were determined from the literature and modified by using trial and error method during the calibration stage.

After simulating the vertical lake water temperature profiles, the values of thermal energy content of the water body were calculated using Eq. (7) during October 2015-September 2016. Finally, the daily evaporation values for the Alavian reservoir were computed using Eq. (6) for 2015-2016. Throughout the evaporation calculation, the two techniques suggested by Tanner et al. (1987) and Payero et al. (2003) were employed to eliminate the faulty meteorological data or wrong sign of fluxes.

2.4. Evaluation of the empirical methods

To determine the best method(s) for estimating evaporation from the Alavian reservoir, the performance of 30 methods were evaluated by comparing with the BREB approach. In Table 1, the empirical equations used in this research are grouped according to method type. The combination groups are the most data-intensive as they need many energy fluxes and climatic data. The Dalton group requires the measurement of wind velocity and saturated and actual vapor pressures. The solar radiation-temperature group requires the measurement of T_a and Q_s . The last two groups need mean air temperature. The temperature-day length group also requires day length of the studied area.

To discuss the performances of the examined methods, the three MBE (Eq. 8), RMSE (Eq. 9) and NS (Eq. 10) standard statistical indices were used. The MBE (mean bias error), indicates the average of deviations of computational values from observed values, which represents underestimation or overestimation of the model or the equation. The RMSE (root mean square error) shows the average value of errors in the set of predictions, regardless of their direction. The RMSE values closer to zero indicate the better performance of a model or an equation. The NS (Nash-Sutcliffe) is one of the best indicators of performance and accuracy evaluation of a model or an equation. Its larger amount indicates that the model/equation is more accurate (Nash and Sutcliffe, 1970). The NS and the RMSE indices are used to rank the empirical equations.

Tab. 1. The empirical methods or equations used in calculating evaporation from the Alavian reservoir.

Method	Reference	Equation	Developed for
<i>Combination group</i>			
De Bruin–Keijman	deBruin & Keijman (1979)	$E = \alpha \frac{s}{0.85s + 0.63\gamma} \frac{Q_m - Q_s}{L\rho} \times 86.4$	Daily
Brutsaert–Stricker	Brutsaert & Stricker (1979)	$E = (2\alpha - 1) \left(\frac{s}{s + \gamma} \right) \frac{(Q_m - Q_s)}{L\rho} \times 86.4 - \frac{\gamma}{s + \gamma} 0.26(0.5 + 0.54U_2)(e_s - e_a)$	Daily
Priestley–Taylor	Stewart & Rouse (1976)	$E = \alpha \frac{s}{s + \gamma} \frac{Q_m - Q_s}{L\rho} \times 86.4$	Periods of 10 d or greater
Penman	Brutsaert (1982)	$E = \left(\frac{Q_m s}{s + \gamma} + \frac{\gamma e_a}{s + \gamma} \right) / (\rho L)$	Periods greater than 10 d
De Bruin	deBruin (1978)	$E = 1.192 \left(\frac{\alpha}{\alpha - 1} \right) \left(\frac{\gamma}{s + \gamma} \right) \frac{(2.9 + 2.1U_2)(e_s - e_a)}{L\rho} \times 86.4$	Periods of 10 d or greater
<i>Dalton group</i>			
Meyer	Patel & Majmundar (2016)	$E = (1 + \frac{U_9}{16}) \cdot K_M \cdot (e_s - e_a)$	Daily
Marciano	Marciano & Harbeck (1954).	$E = 0.03 U_2 (e_s - e_a)$	Daily
Shahtin	Hajian & Lotfollahi-Yaghin (2015)	$E = (0.116 + 0.017 U_2) (e_s - e_a)$	Daily
Hefner	Marciano & Harbeck (1954).	$E = 0.028 U_2 (e_s - e_a)$	Daily
Box	Shah (2012)	$E = 0.0000778 (e_s - e_a)$	Daily
Leven	Shah (2012)	$E = 0.0000094 (e_s - e_a)^{1.3}$	Daily
Himus-Hinchley	Shah (2012)	$E = 0.0000258 (e_s - e_a)^{1.3}$	Daily
Boelter	Shah (2012)	$E = 0.0000162 (e_s - e_a)^{1.22}$	Daily
Biasin-Krumme	Shah (2012)	$E = -0.059 + 0.000079 (e_s - e_a)$	Daily
Ryan–Harleman	Rasmussen et al. (1995)	$E = \frac{(2.7(T_w - T_a)^{0.333} + 3.1U_2)(e_{sw} - e_a)}{L\rho} \times 86.4$	Daily
Tichomirof	Hajian & Lotfollahi-Yaghin (2015)	$E = (e_s - e_a)(15 + 3U_{10})$	Monthly
Harbeck	Shuttleworth, (1993)	$E = 2.209 A_s^{-0.05} U_2 (e_{sw} - e_a)$	Monthly
Shuttleworth	Shuttleworth, (1993)	$E = 2.209 A_s^{-0.05} U_2 (e_{sw} - e_a)$	Monthly
McMillan	Sweers (1976)	$E = (5 \times 10^6 \times A_s^{-1})^{0.05} (3.6 \times 2.5 U_3) (e_{sw} - e_a)$	Monthly
Rohwer	Patel & Majmundar (2016)	$E = 0.77(1.465 - 0.00073 P_a)(0.44 + 0.073 U_{0.6})(e_s - e_a)$	Monthly
Patel–Majmundar	Patel & Majmundar (2016)	$E = -3.5 - 0.14 T_w + 0.25 T_a + 0.27 U_2 + 0.9(e_s - e_a) + 0.15 S$	Monthly
<i>Solar radiation, temp. group</i>			
Jensen–Haise	McGuinness & Bordne (1972)	$E = (0.014 T_a - 0.37)(Q_s \times 3.523 \times 10^{-2})$	Periods greater than 5 d
Makkink	McGuinness & Bordne (1972)	$E = ((52.6 - \frac{s}{s + \gamma} \frac{Q_s}{L\rho}) - 0.12)$	Monthly
Stephens–Stewart	McGuinness & Bordne (1972)	$E = (0.0082 T_a - 0.19)(Q_s \times 3.495 \times 10^{-1})$	Monthly
<i>Temp., day length group</i>			
Hamon	Hamon (1961)	$E = 0.55 \left(\frac{D}{12} \right)^2 \frac{SVD}{1000} (25.4)$	Daily
Blaney–Criddle	McGuinness & Bordne (1972)	$E = (0.0173 T_a - 0.314) \times T_a \times (D \div D_{1a}) \times 25.4$	Monthly
<i>Temperature group</i>			
Papadakis	McGuinness & Bordne (1972)	$E = 0.5625 (e_{s, \max} \times 10^{-2} - (e_{s, \min} \times 10^{-2} - 2)) \left(\frac{10}{d} \right)$	Monthly
Thornthwaite	Mather (1978)	$E = (1.6 \left(\frac{10 T_a}{I} \right)^{6.75 \times 10^{-7} I^3 - 7.71 \times 10^{-5} I^2 + 1.79 \times 10^{-2} I + 0.49}) \left(\frac{10}{d} \right)$	Monthly
Ivanov	Filimonova & Trubetskova (2005)	$E = 0.0018 (T_a + 25)^2 (100 - RH)$	Monthly
U.S.B.R	Hajian & Lotfollahi-Yaghin (2015)	$E = 0.883 (4.57 T_a + 43.3)$	Monthly

$\alpha = 1.26 =$ constant of Priestley–Taylor approach, dimensionless,

$s =$ slope of the saturated vapor pressure–temperature curve at average air temperature (Pa °C⁻¹),

$\gamma =$ psychrometric “constant” (dependent on atmospheric pressure and temperature) (Pa °C⁻¹),

$Q_m =$ net radiation ($= Q_s - Q_r + Q_a - Q_{ar} - Q_{bs}$) (W m⁻²),

Q_s = incoming shortwave radiation ($W m^{-2}$),
 Q_x = change in heat stored in the water body ($W m^{-2}$),
 L = latent heat of vaporization ($MJ kg^{-1}$),
 ρ = density of water ($998 kg m^{-3}$ at $20^\circ C$),
 $U_{0.6}$ = wind speed at 0.6 m above surface ($km h^{-1}$),
 U_2 = wind speed at 2 m above surface ($km h^{-1}$ for Patel and Majmudar, Shahtin, Hefner and Marciano and $m s^{-1}$ for the other equations),
 U_3 = wind speed at 3 m above surface ($m s^{-1}$),
 U_9 = wind speed at 9 m above surface ($km h^{-1}$),
 U_{10} = wind speed at 10 m above surface ($m s^{-1}$),
 P_a = atmospheric pressure (mm Hg),
 S = duration of sunshine (hr),
 A_s = area of the water surface (m^2),
 K_M = coefficient: 0.36 for large, deep waters and 0.50 for small, shallow waters,
 e_{sw} = saturated vapor pressure at temperature of the water surface (mb),
 e_s = saturated vapor pressure at temperature of the air (mb for Brutsaert–Stricker, Ryan–Harleman and deBruin and mm Hg for the other equations),
 e_a = vapor pressure at temperature and relative humidity of the air (mb for Brutsaert–Stricker, Ryan–Harleman and deBruin and mm Hg for the other equations),
 SVD = saturated vapor density at mean air temperature ($g m^{-3}$),
 T_a = air temperature ($^\circ F$ for the Blaney–Criddle, Jensen–Haise and Stephens–Stewart equations and $^\circ C$ for the other equations),
 T_w = water surface temperature ($^\circ C$),
 D = daylight hours,
 D_{TA} = total annual hours of daylight for specific latitude; for Alavian Lake, $D_{TA} = 4470$,
 $e_{s\ min}$ and $e_{s\ max}$ = saturated vapor pressures at daily minimum and maximum air temperatures (Pa),
 I = annual heat index ($I = \sum_i, i = (T_a/5)^{1.514}$),
 d = number of days in month,
 RH = relative air humidity (%).

$$MBE = \frac{1}{N} \sum_{i=1}^N (E_{i,pre} - E_{i,ref}) \quad (8)$$

$$RMSE = \sqrt{\frac{1}{N} \sum_{i=1}^N (E_{i,pre} - E_{i,ref})^2} \quad (9)$$

$$NS = 1 - \frac{\sum_{i=1}^N (E_{i,pre} - E_{i,ref})^2}{\sum_{i=1}^N (E_{i,ref} - \bar{E}_{i,ref})^2} \quad (10)$$

where $E_{i,ref}$ are the values of reference method (the energy budget evaporation), $E_{i,pre}$ are the calculated values by the other methods, $\bar{E}_{i,ref}$ is the mean values of reference method, and N is the total data pairs.

3. RESULTS AND DISCUSSION

3.1. Water temperature distribution in Alavian dam reservoir

Fig. 2 shows some characteristics of the simulated vertical water temperature profiles versus the measured ones in the Alavian reservoir for different days of the year 2015–2016. The outcomes show that there is a good fit between the measured and simulated water temperature profiles. Based on the simulation results, the values of mean abso-

lute error (MAE) range from 0.68 to 2.2° C for the different water temperature profiles, which seems appropriate regarding the magnitude and the depth of the Alavian reservoir (Kim and kim, 2006; Gianniou and Antonopoulos, 2007). The results indicate that the reservoir has a positive thermal stratification in spring and summer to mid-fall, and a negative thermal stratification in winter.

3.2. Estimation of evaporation

Fig. 3 illustrates the daily and the monthly mean evaporation values derived from the energy budget method in the Alavian reservoir for the one-year period (October 2015 to September 2016). According to this Fig., the daily and the monthly evaporation rates decrease during fall and winter and reach the minimum values in November, January and February. Subsequently, as the temperature increases in the late winter (March) and during the spring, the evaporation rate increases. However, in some days of spring (Fig. 3a), due to the cloudy conditions and precipitation, the evaporation rate reduces sharply. In summer, the evaporation reaches to peak value and the maximum daily evaporation rate becomes about 15.57 $mm day^{-1}$ in April (mean monthly of 10.39 mm). In September, due to the decrease in the air and the water temperature, the evaporation experiences a downward trend again. In general, the mean monthly and the annual evaporation from

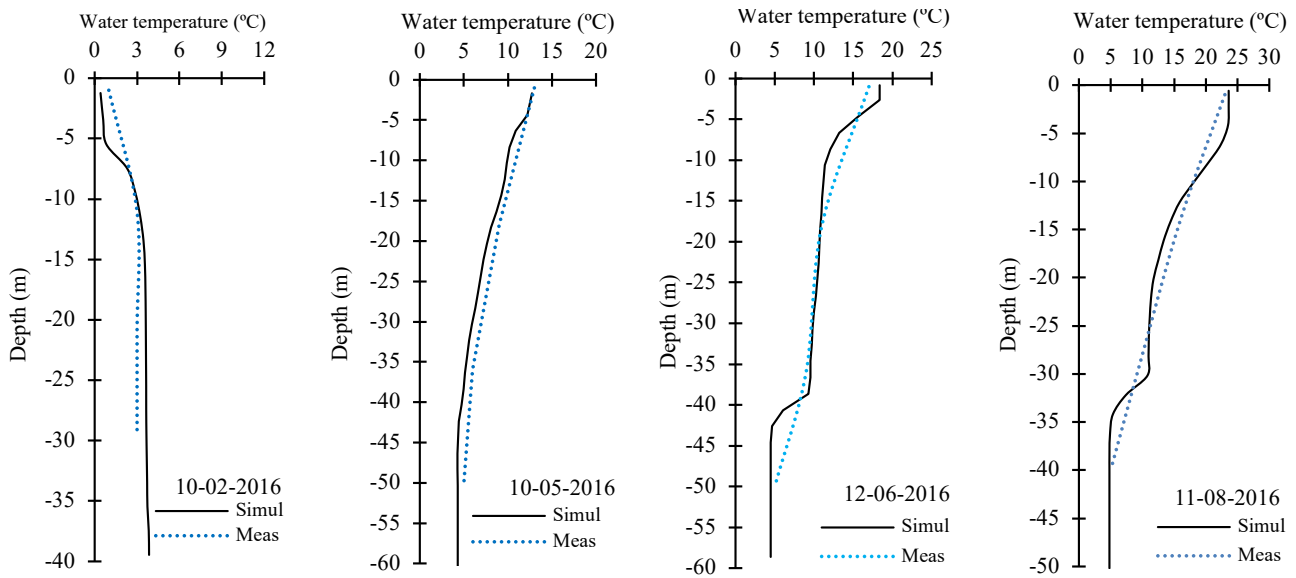


Fig. 2. The simulated (— Simul) and measured (... Meas) temperature profiles in Alavian Reservoir.

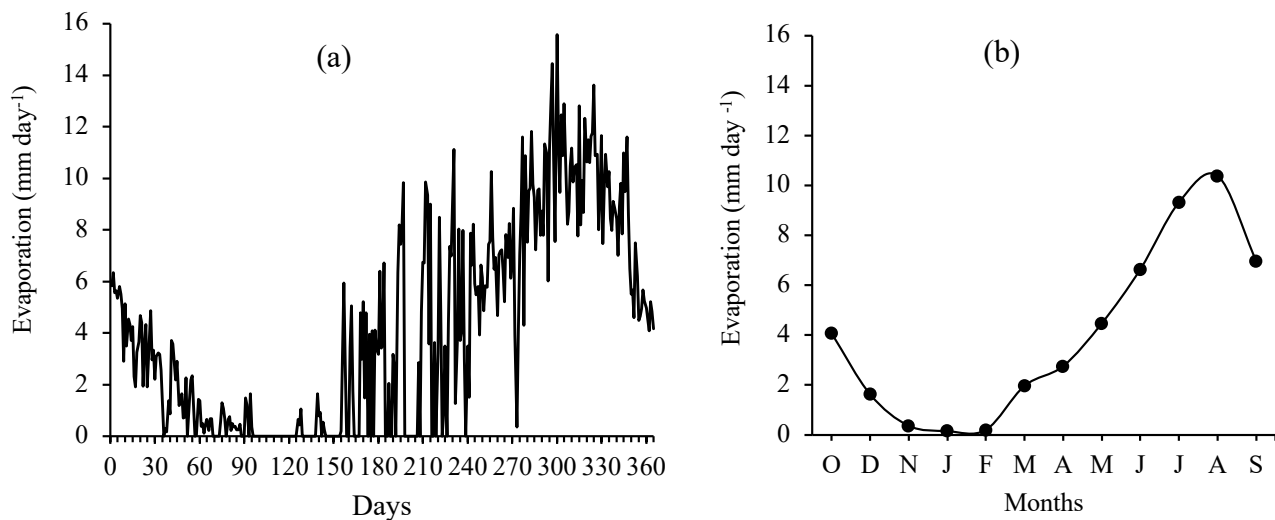


Fig. 3. Daily (a) and monthly (b) estimated evaporation values for Alavian Reservoir during 2015-2016.

the Alavian reservoir during 2015-2016 are equal to 4.08 mm day^{-1} and $1508 \text{ mm year}^{-1}$, respectively. Based on the evaporation values and the surface area of the reservoir, the annual volume of evaporation from the reservoir was obtained equal to 2.8 mcm. Since Maragheh city has a population of nearly 176000 and the daily water usage for human consumption in this city is about 240 liter per day per person, the amount of evaporation over the lake is more than 19% of the annual volume of water consumed in the city (15 mcm). On the other hand, the annual evaporation over the lake is about 6.7% of the annual water volume al-

located from the Alavian reservoir to the agricultural sector (42 mcm). It could be concluded that the importance of evaporation losses over the Alavian reservoir is more in human usage management than the agricultural sector.

Obviously, the results of the daily evaporation are prone to possible errors due to the use of the reconstructed water temperature profiles data. According to the sensitivity analysis performed by Gianniu and Antonopoulos (2007) on the energy budget parameters, a 10% change in the surface water temperature leads to a 16.8% change in the evaporation values of a reservoir. Regarding the good accuracy of the

water temperature simulation, the accuracy of the evaporation values derived from the energy budget method can be confirmed in comparison with the possible errors (Gianniou and Antonopoulos, 2007; Antonopoulos et al., 2016).

3.3. Water temperature and energy budget components of the reservoir

Fig. 4 shows the monthly variation of air (T_a) and lake surface (T_w) temperature for 2015-2016. Based on the results, the mean annual air and water surface temperature are equal to 14.22 and 11.93 °C (with a difference of 2.30 °C), respectively. According to Fig. 4, the monthly air temperature during the year except for November and December is higher than the monthly reservoir surface temperature. In these two months, the air temperature faster decreases than the reservoir surface temperature does (Fig. 4) due to the large water heat capacity (Gianniou and Antonopoulos, 2007). The difference between the air and the surface water temperatures shows an increasing trend during spring and summer and a decreasing trend in fall. The study conducted by Omar and El-Bakry (1981) on evaporation rate from Aswan Reservoir in Egypt also showed that the monthly air temperature throughout the year, except for fall, was higher than the monthly surface water temperature, which is in good agreement with the results of the present study. According to Hasani et al. (2008) on Al-Ghadir reservoir and Majidi et al. (2015) on Doosti reservoir, monthly air temperature is higher than water surface temperature in summer and vice versa during winter. The study carried out by Gianniou and Antonopoulos (2007) on Vegoritis Lake in Greece showed that the air temperature was higher than the surface water temperature during the spring and was lower in other seasons.

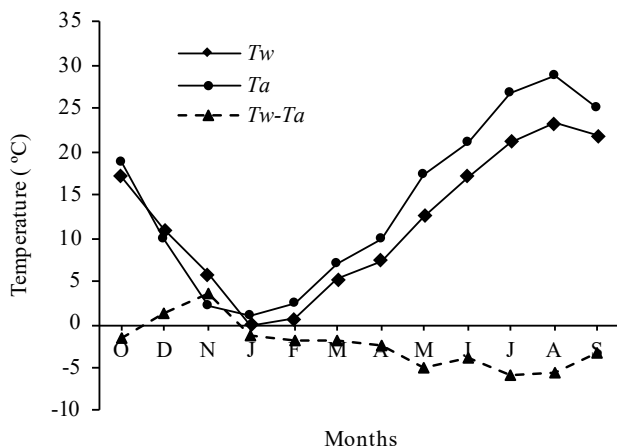


Fig. 4. The Mean monthly variation of air temperature (T_a) and lake surface temperature (T_w) for the Alavian Reservoir.

In Fig. 5a, the mean monthly values of the energy budget components during 2015-2016 are shown. Among the energy budget components, the incoming ($Q_a - Q_{ar}$) and the outgoing (Q_{bs}) long-wave radiations have the largest mean annual rates ($Q_a - Q_{ar} = 304.16 - 9.12 = 295.03 \text{ W m}^{-2}$ and $Q_{bs} = 364.18 \text{ W m}^{-2}$). Accordingly, the mean energy loss is equal to 69.15 W m^{-2} . The energy source, i.e. the net short-wave solar radiation ($Q_{ns} = Q_s - Q_{sr}$), has a mean annual rate of . The short-wave radiation (Q_s) has a characteristic seasonal variation, so that the highest rates happen in the late spring to the mid-summer, and the lowest rates belong to the mid-fall to the early winter. The seasonal variations of the short-wave radiation ($Q_{sr} = 0.07 \times Q_s$), the long-wave atmospheric radiation (Q_a), the reflected atmospheric radiation ($Q_{ar} = 0.03 \times Q_a$) and the reversed radiation (Q_{bs}) are also similar to that of Q_s .

The changes of net radiation (Q_{rn}) are similar to the seasonal variation of its components (Fig. 5b). It has positive mean annual value since the net radiation is the energy source for all biological and physical activities of a lake ecosystem (Gianniou and Antonopoulos, 2007). As shown in Fig. 5b, the variation of $Q_{rn} - Q_x$ (Q_x is the component of the alteration in the thermal content of the reservoir water) has a characteristic seasonal variation, so that its increasing trend begins in the late winter and reaches to the maximum value in the mid-summer, which is also the time of peak evaporation. During this time, the reservoir continuously receives and stores thermal energy through net radiation. Subsequently, the stored energy is released in the form of sensible heat and mostly latent heat in fall and winter, causing a gradual cooling of water at the depth of the reservoir. This energy budget in the reservoir leads to a positive thermal stratification in spring and summer to mid-fall and a negative thermal stratification in winter. The mean annual of Q_x in the Alavian reservoir for the studied year is equal to -12.39 W m^{-2} . Typically, the mean annual of the Q_x flux in a reservoir becomes equal to zero for a few years, and the energy stored in spring and early summer are released in the form of sensible heat and latent heat in the surrounding environment (Gianniou and Antonopoulos, 2007). Therefore, it is described as the phase lag between the occurrence time of the maximum net radiation and evaporation. The comparison between Figs. 3b and 5b shows that the phase lag in the Alavian reservoir is one month. The results obtained by Gianniou and Antonopoulos (2007) on energy budget of Vegoritis Lake in Greece also presented a phase lag of one month.

3.4. Performance and ranking of the methods

Table 2 gives the statistical results of the examined methods in estimating the evaporation rate from the Ala-

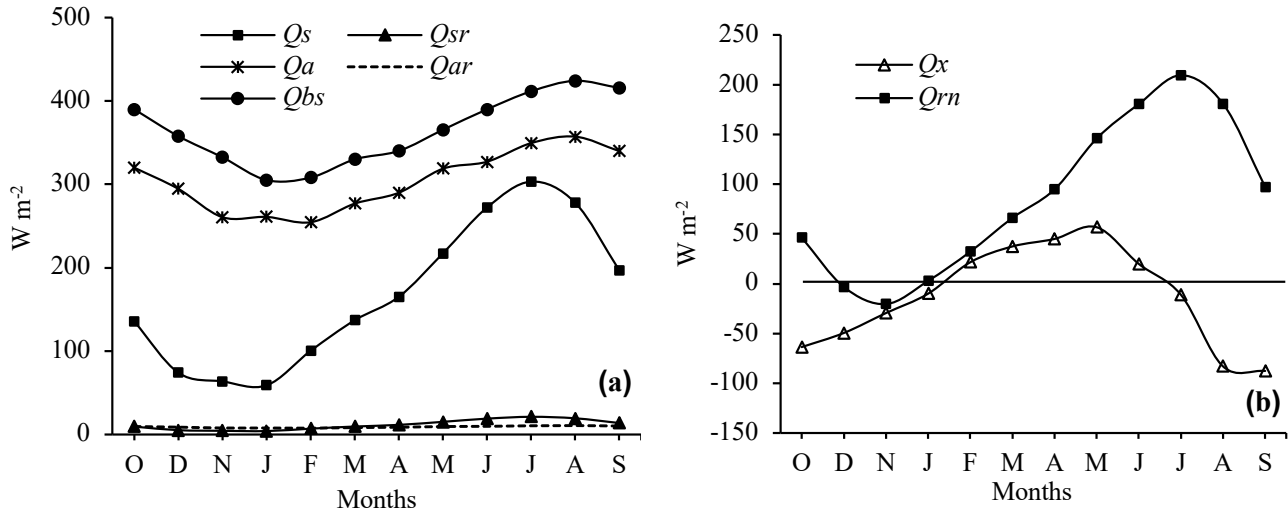


Fig. 5. The Mean monthly variation of the energy budget components for the Alavian Reservoir during the year 2015-2016.

vian reservoir during 2015-2016. In this table, the methods within each group and also between all groups were ranked on the basis of both the RMSE and the NS criteria. Also, the MBA criterion indicates the overestimate or underestimate of the methods.

In the combination group, there was no significant difference in the performances of the methods. However, the deBruin method yielded the best estimates with $NS=0.95$, $RMSE=0.79 \text{ mm day}^{-1}$ and a negligible positive bias ($MBE=0.11 \text{ mm day}^{-1}$). The deBruin is a relatively cost-effective method in comparison with the other methods of this group, due to the necessity for measurement of T_a , e_a , and U , which makes it a good choice to use at the Alavian reservoir. Based on the MBE values, four of the five combination methods had a small overestimate (positive MBE). Rosenbery et al. (2004) and (2007) reported similar results regarding the overestimate of the methods of this group. The overestimations of evaporation were observed during fall and winter and smaller underestimations were observed during spring and summer (Fig. 6). In this group, the highest overestimate and underestimate belonged to the Penman approach with $MBE=0.5 \text{ mm day}^{-1}$ and the Brutsaert-Stricker approach with $MBE=-0.2 \text{ mm day}^{-1}$, respectively.

In the Dalton group, the Rohwer method had the best performance with $NS=0.96$, $RMSE=0.75 \text{ mm day}^{-1}$ and a negligible bias ($MBE=-0.30 \text{ mm day}^{-1}$). This method requires only the measurement of wind velocity, vapor pressure deficit and air pressure. Simplicity and superior performance of the Rohwer method can be the most important advantages of applying this method in the studied area. Also, the McMillan method with the second ranking had a reasonable performance ($NS=0.93$, $RMSE=0.92$

mm day^{-1}) as well as the Rohwer method. In this group, these two methods produced the most accurate evaporation values and could be considered as appropriate methods even by the limited observations of the input data. In contrast, the two methods of Biasin-Krumme with $NS=-0.48$, $RMSE=4.14 \text{ mm day}^{-1}$ and Bax with $NS=-0.47$, $RMSE=4.12 \text{ mm day}^{-1}$ had the worst performances in the estimation of evaporation. The Boelter, Leven and Hefner methods were preceded by the Biasin-Krumme and Bax methods. All the methods require only the measurement of vapor pressure deficit. It was noticed that in these methods, the mass transfer coefficient became more prominent than vapor pressure deficit and calibration of the coefficients gave better results. The Biasin-Krumme with $MBE=-3.22 \text{ mm day}^{-1}$ and the Tichomiroy with $MBE=0.77 \text{ mm day}^{-1}$ had the highest underestimate and overestimate, respectively. In this group, all the methods except Rohwer, McMillan, Meyer, and Tichomiroy had a negative bias (underestimates) that often occurred during all months (Fig. 6). As shown in this group, the monthly-scale methods are more accurate than the daily-scale ones. The better performance of monthly-scale approaches could be attributed to longer time periods due to the reduction of the uncertainty in the evaporation parameters (Majidi et al., 2015). However, different behaviors of Dalton approaches are related to having various coefficients and, due to a disparity in the estimates of the daily-scale Dalton methods, it can be said that the calibration of the mass transfer coefficients for the Alavian reservoir is necessary.

In the radiation-temperature group, the Jensen-Haise method had the best performance with $NS=0.88$, $RMSE=1.17 \text{ mm day}^{-1}$ and a negative bias ($MBE=-0.86 \text{ mm day}^{-1}$). The Jensen-Haise method uses incoming

Tab. 2. The statistical results and ranking of the methods in calculating evaporation from the Alavian reservoir during 2015-2016.

Method	NS	RMSE (mm day ⁻¹)	MBE (mm day ⁻¹)	Rank in group	Overall rank
<i>Combination group</i>					
deBruin-Keijman	0.93	0.90	0.05	2	3
Brutsaert-Stricker	0.91	1.01	-0.20	5	7
Priestley-Taylor	0.93	0.92	0.22	4	6
Penman	0.93	0.91	0.50	3	4
deBruin	0.95	0.79	0.11	1	2
<i>Dalton group</i>					
Meyer	0.78	1.61	0.55	7	14
Marciano	0.20	3.03	-2.48	11	25
Shahtin	0.37	2.70	-2.19	10	23
Hefner	0.13	3.18	-2.60	12	26
Box	-0.47	4.12	-3.20	15	29
Leven	-0.26	3.81	3.03	13	27
Himus-Hinchley	0.81	1.48	-1.18	6	13
Boelter	-0.33	3.93	-3.10	14	28
Biasin-Krumme	-0.48	4.14	-3.22	16	30
Ryan-Harleman	0.71	1.84	-1.40	8	15
Tichomirof	0.87	1.23	0.77	3	10
Harbeck	0.83	1.38	-1.08	4	11
Shuttleworth	0.83	1.42	-1.12	5	12
McMillan	0.93	0.92	0.14	2	5
Rohwer	0.96	0.75	-0.30	1	1
Patel-Majmundar	0.56	2.26	-1.93	9	18
<i>Solar radiation, temp. group</i>					
Jensen-Haise	0.88	1.17	-0.86	1	8
Makkink	0.43	2.57	-1.70	2	20
Stephens-Stewart	0.36	2.71	-2.07	3	24
<i>Temp., day length group</i>					
Hamon	0.43	2.57	-2.02	2	21
Blaney-Criddle	0.87	1.20	-0.74	1	9
<i>Temperature group</i>					
Papadakis	0.69	1.90	-0.93	1	16
Thorntwaite	0.37	2.70	-2.09	4	22
Ivanov	0.65	2.01	1.72	2	17
U.S.B.R	0.49	2.42	-0.95	3	19

short-wave radiation (Q_s) as a substitution for the net radiation (Q_{rn}) and heat storage (Q_x) fluxes. It probably decreases the uncertainty of the fluxes, and therefore the Jensen-Haise method (with periodical time scale) could produce reliable results in comparison with the monthly methods of this group (Majidi et al., 2015). In this group, the evaporation values were underestimated during all months (except for January and February), indicating less amount of evaporation relative to the BREB values (Fig.

6). This underestimation has also been reported in the results of Majidi et al. (2015). The Stephens-Stewart method yielded evaporation rates with a considerable negative bias (MBE=-2.07 mm day⁻¹) which has a good agreement with the results of Rosenberry et al. (2007). The low accuracy of the Stephens-Stewart and the Makkink approaches in comparison with the Jensen-Haise approach is attributed to the coefficients used in the methods.

In the temperature-day length group, the Blaney-Criddle method had a better performance with NS=0.87, RMSE=1.20 mm day⁻¹ and a negative bias (MBE=-0.74 mm day⁻¹). Both the Blaney-Criddle and the Hamon methods provided underestimated results (Fig. 6) which are in agreement with the results of Majidi et al. (2015) and Rosenberry et al. (2007). The Blaney-Criddle (temperature-day length) and the Jensen-Haise (radiation-temperature) methods showed almost similar performances. It can be said that day length is a good indicator of solar radiation, and due to the easy measurement of temperature and day length, the Blaney-Criddle is known as a practical and applicable method with acceptable performance.

In the temperature group, the Papadakis method with NS=0.69, RMSE=1.90 mm day⁻¹ and MBE=-0.93 mm day⁻¹ provided more reliable evaporation estimates than the others. The Papadakis method, followed by the Ivanof method, provided relatively well evaporation estimates. In this group, all methods except the Ivanof produced underestimated results. The underestimations were observed during spring and summer months (Fig. 6). Rosenberry et al. (2004) and Patel and Majmundar (2016) stated that some methods of temperature group (Papadakis and Thornthwaite methods) tend to underestimate evaporation rates.

In general, comparison of the best methods in the five groups showed that the Rohwer equation (Dalton group) with the minimum RMSE (0.71 mm day⁻¹) and the maximum NS (0.96) had the best performance in the estimation of evaporation from the Alavian reservoir. This method requires vapor pressure deficit, wind speed and air pressure. Considering its simplicity and good performance, the Rohwer method surprisingly performed well in comparison with the other methods, specially the combination groups. Patel and Majmundar (2016) analyzed the evaporation estimation methods in the Dharoi Reservoir during a 10-year study period (2001-2010). They concluded that the Rohwer method provided the best estimates compared to other empirical methods. A survey on the overall rank of the methods in the five groups showed that the combination equations had a better performance than the other groups and the Rohwer method followed by the deBruin, deBruin-Keijman and the Penman approaches (combination group), respectively. Numerous researchers such as Abteu (2001), Mosner and Aulenbach (2003), Winter et al.

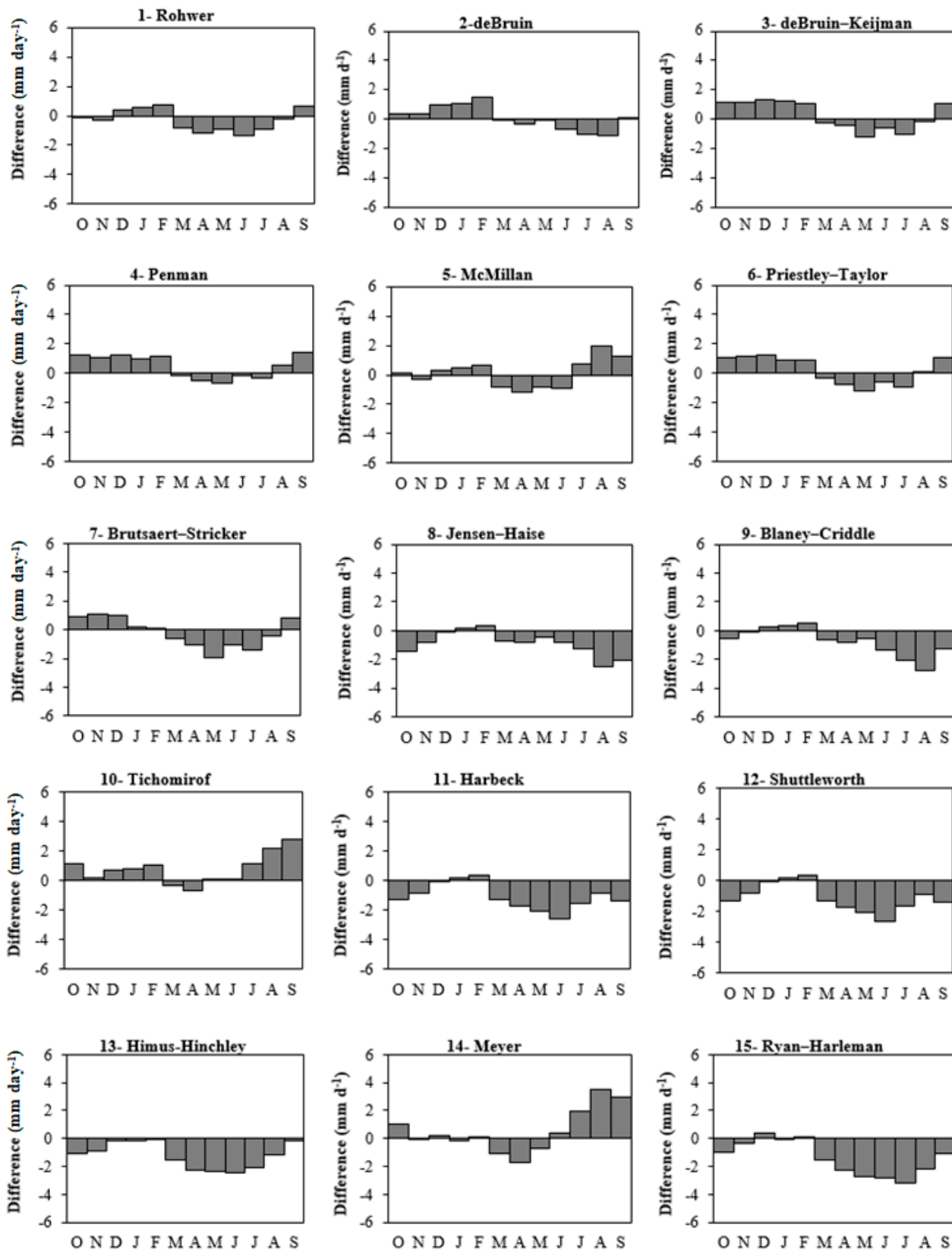


Fig. 6. Differences in calculated evaporations between 30 empirical approaches reported in Table 2 and BREB values, in mm day⁻¹.

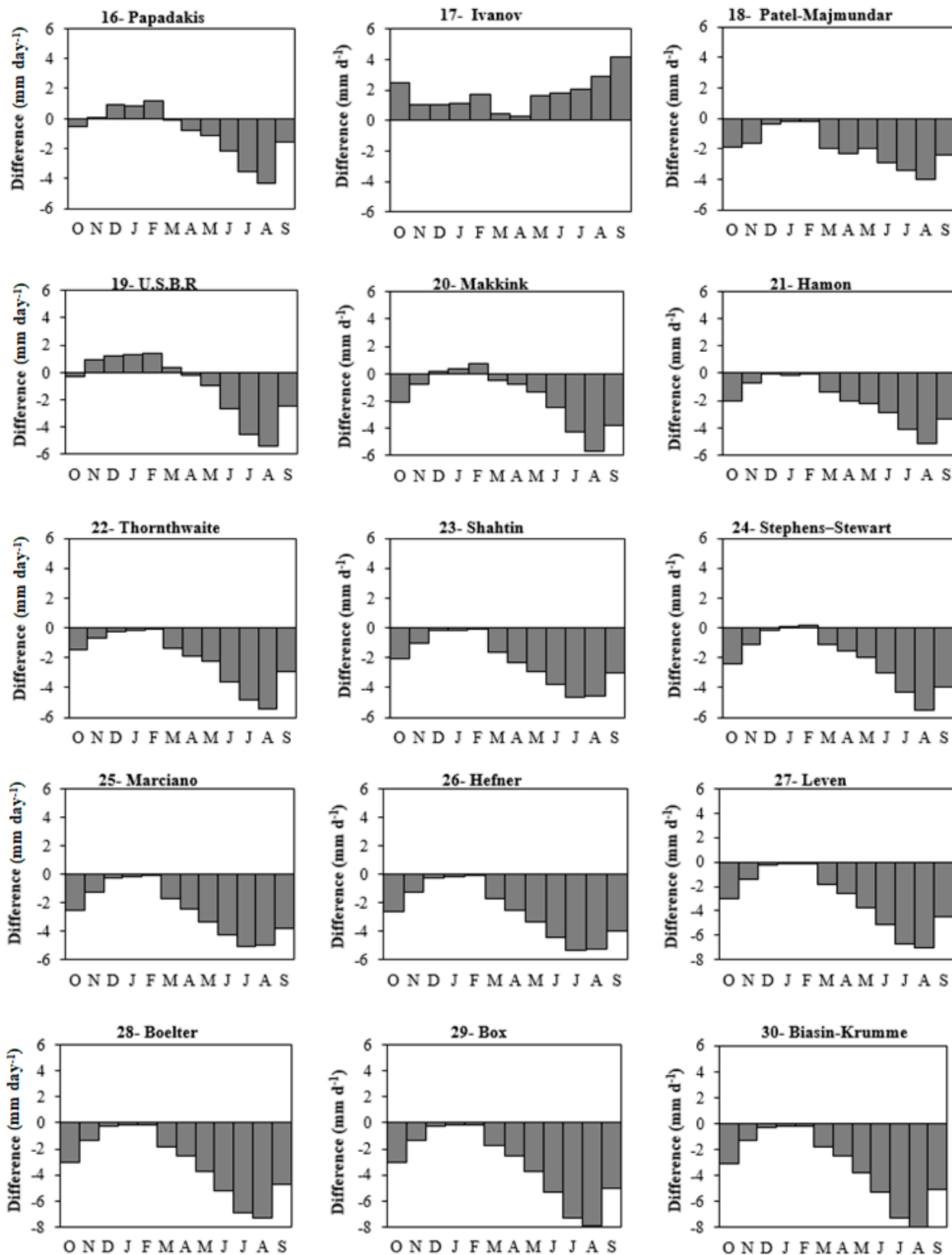


Fig. 6. (continued).

(2003), Rosenberry et al. (2007) Hasani et al. (2008), Yao (2009) and Majidi et al. (2015) have stated the superiority of the deBruin, the Penman and the deBruin–Keijman methods compared to other methods in the calculation of evaporation from a reservoir. The McMillan method, ranked 5th, requires the measurement of wind velocity, vapor pressure deficit and area of the water surface. The Jensen–Haise (radiation-temperature) and Blaney–Cridle (temperature-day length group) methods, ranked as 8th and 9th, had the highest ranks among the evaporation methods, next to the best methods of Dalton and combination groups. Considering the needed column of inputs or data and the efficacy of the examined approaches, it can be said that the Rohwer, the deBruin and the McMillan are the most appropriate methods in estimating the reservoir evaporation in the studied area. Also, among the examined methods, the Biasin-Krumme had the highest error (RMSE=4.41 mm day⁻¹) and the worst performance (NS=-0.48) in estimation of the evaporation. The Box, Boelter and Leven were preceded by the Biasin-Krumme method, respectively.

4. CONCLUSION

In this study, daily evaporation rates from Alavian dam reservoir in northwestern Iran were estimated from October 2015 to September 2016. The two-dimensional temperature stratification prediction model CE-QUAL-W2 was used to simulate the daily lake temperature profile. The simulation model was calibrated and validated using vertical profiles of water temperature data for the year 2013-2016. The thermal energy stored in the reservoir was then calculated by utilizing the distribution of water temperature. Finally, daily evaporation values were calculated by utilizing the BREB method, considering the two criteria suggested by Tanner et al. (1987) and Payero et al. (2003). The estimations by the BREB, as a reference method, were compared to those by 30 empirical methods. The examined methods were evaluated and ranked with respect to the RMSE and NS indices to obtain the best method(s) in the study area.

The results of the lake water temperature model indicated that the reservoir had a positive thermal stratification in spring and summer to mid-fall, and a negative thermal stratification in winter. Monthly air temperature during the year except for the two months of November and December was higher than the monthly reservoir surface temperature. The average value of the evaporation calculated by the energy budget approach for the studied year was equal to 4.08 mm d⁻¹. Performance evaluation of all the methods examined in this study highlighted the su-

periority and efficacy of the Rohwer and the deBruin–Keijman and the deBruin methods in the estimation of evaporation in a semi-arid area. Lack of meteorological data is a main consideration in calculating evaporation rate and selecting an evaporation estimation method. The Rohwer and the deBruin demand less data and require only vapor pressure deficit and wind speed. It is worth noting that these variables in the two methods have an important role in the process of evaporation. Under the limited data condition, the Rohwer and the deBruin methods can be used with acceptable performances. Also, the deBruin–Keijman and Penman methods (combination group) and McMillan (Dalton group) provided the next-best values. In contrast, the estimates obtained by the Biasin-Krumme, Box, Boelter and the Leven methods had the highest difference with the BREB values. In the Dalton group, the results revealed the necessity of calibration and adjustment of some evaporation estimation methods, especially the daily-scale methods. The MBE values showed that the Ivanof and Biasin-Krumme methods had the highest overestimation and underestimation, respectively.

ACKNOWLEDGMENTS

The authors are grateful for the supports and the partial fund provided by the University of Zanjan and for the data and collaborations provided by East Azerbaijan Regional Water Company.

REFERENCES

- Abtew W., 2001. Evaporation estimation for Lake Okeechobee in South Florida. *Journal of Irrigation and Drainage Engineering*, 127: 140-147.
- Allen R., Pereira L., Raes, D., Smith M., 1998. Crop evapotranspiration: guidelines for computing crop water requirements. *FAO Irrigation and Drainage*, Paper 56, FAO, Rome, Italy.
- Anderson E.R., 1954. Energy-budget studies, water-loss investigations: Lake Hefner studies. Paper 269, US Geological Survey Professional.
- Antonopoulos V.Z., Gianniou S.K., Antonopoulos A.V., 2016. Artificial neural networks and empirical equations to estimate daily evaporation: application to lake Vegoritis, Greece. *Hydrological Sciences Journal*, 61 (14): 1-27.
- Bozorgi A., Bozorg-Haddad O., Sima S., Loáiciga H.A., 2018. Comparison of methods to calculate evaporation from reservoirs. *International Journal of River Basin Management*, 17: 1-42.

- Brutsaert W., Stricker H., 1979. An advection–aridity approach to estimate actual regional evapotranspiration. *Water Resource Research*, 15 (2): 44-450.
- Brutsaert W., 1982. *Evaporation into the atmosphere: Theory, history, and applications*. Boston: Kluwer.
- Buchak E.M., Edinger J.E., 1984. *Longitudinal–vertical Hydrodynamics and Transport: Development, Programming and Applications*, Document 84-18-R, Prepared for the U.S. army corps of engineers waterways experiment station, Vicksburg.
- Buccola N.L., Stonewall A.J., 2016. Development of a CE-QUAL-W2 temperature model for Crystal Springs Lake, Portland, Oregon. Open-File Report 2016-1076, U.S. Geological Survey.
- De Bruin H.A.R., 1978. A simple model for shallow lake evaporation. *Journal of Applied Meteorology*, 17: 1132-1134.
- De Bruin H.A.R., Keijman J.Q., 1979. The Priestley–Taylor evaporation model applied to a large shallow lake in the Netherlands. *Journal of Applied Meteorology*, 18: 898-903.
- dos Reis R., Dias N., 1998. Multi-season lake evaporation: energy budget estimates and CRLE model assessment with limited meteorological observations. *Journal of Hydrology*, 208: 135-147.
- Duan Z., Bastiaanssen W.G.M., 2015. A new empirical procedure for estimating intra-annual heat storage changes in lakes and reservoirs: Review and analysis of 22 lakes. *Remote Sensing of Environment*, 156: 143-156.
- Filimonova M., Trubetskova M., 2005. Calculation of evaporation from the Caspian Sea surface. In: *Proceedings of the International Symposium on Stochastic Hydraulics*, Nijmegen, The Netherlands.
- Gianniou S.K., Antonopoulos V.Z., 2007. Evaporation and energy budget in Lake Vegoritis, Greece. *Journal of Hydrology*, 351 (3): 212-223.
- Gorjizade A., Akhond-Ali A.M., Zarei H., Seyyed Kaboli H., 2014. Evaluation of Eight Evaporation Estimation Methods in a Semi-Arid Region (Dez reservoir, Iran). *International journal of Advanced Biological and Biomedical Research*, 2 (5): 1823-1836.
- Harbeck G.E.J., Kohler M.A., Koberg G.E., 1958. *Water-loss investigations: Lake Mead studies*. Professional Paper 298, US Geological Survey.
- Hajian R., Lotfollahi-Yaghin M.A., 2015. Modeling the amount of free water surface evaporation from Mahabad Dam's lake using artificial neural networks and comparing the model with experimental equations. *Journal of Renewable Natural Resources Bhutan*, 3 (5): 196-210.
- Hamon W.R., 1961. Estimating potential evapotranspiration. *J. Hyd. Div.*, 87: 107-120.
- Hassani A., Tajrishi M., Abrishamchi A., 2008. Comparison of Several Evaporation Models Applied to Reservoir of the Saveh Dam, Iran. In: *The 3rd International Conference on Water Resources and Arid Environments and the 1st Arab Water Forum*, Riyadh, Saudi Arabia.
- Hussain M.M.A., 2017. Evaporation and Evaluation of Seven Estimation Methods: Results from Brullus Lake, North of Nile Delta, Egypt. *Atmospheric and Oceanic Sciences*, 2 (3): 66-74.
- Kim Y., Kim B., 2006. Application of a 2-Dimensional Water Quality Model (CE-QUAL-W2) to the Turbidity Interflow in a Deep Reservoir (Lake Soyang, Korea). *Lake and Reservoir Management*, 22 (3): 213-222.
- Koberg G.E., 1964. *Methods to compute long-wave radiation from the atmosphere and reflected solar radiation from a water surface*. Professional Paper 272-F, US Geological Survey.
- Lenters J., Kratz T., Bowser C., 2005. Effects of climate variability on lake evaporation: results from a long-term energy budget study of Sparkling Lake, northern Wisconsin (USA). *Journal of Hydrology*, 308: 168-195.
- Majidi M., Alizadeh A., Farid A., Vazifedoust M., 2015. Estimating Evaporation from Lakes and Reservoirs under Limited Data Condition in a Semi-Arid Region. *Water Resource Management*, 29: 3711-3733.
- Marciano J.J., Harbeck G.E., 1954. *Mass-transfer studies*. In: USGS (Editor), *Water-Loss errors in daily and monthly input data*. *Hydrological Processes*, 11 (11): 1465-1473.
- Mather J.R., 1978. *The Climatic Water Budget in Environmental Analysis*. Lexington: Lexington Books.
- McGuinness J.L., Bordne E.F., 1972. A comparison of lysimeter-derived potential evapotranspiration with computed values. Technical Bulletin 1452, US Department of Agriculture Agricultural Research Service, Washington, DC, USA.
- Mosner M.S., Aulenbach B.T., 2003. Comparison of methods used to estimate lake evaporation for a waterbudget of Lake Semnole, southwestern Georgia and northwestern Florida. In: *Proceedings of the 2003 Georgia Water Resources Conference*, Athens, Georgia, USA.
- Nash J.E., Sutcliffe J.V., 1970. River flow forecasting through conceptual models, part I—a discussion of principles. *Journal of Hydrology*, 10: 282-290.
- Norton E.G., Bradford A., 2009. Comparison of two stream temperature models and evaluation of potential management alternatives for the Speed River, Southern Ontario. *Journal of Environmental Management*, 90: 866-878.

- Omar M.H., El-Bakry M.M., 1981. Estimation of Evaporation from The Lake of the Aswan High Dam (Lake Nasser) Based On Measurements Over the Lake. *Agricultural Meteorology*, 23: 293-308.
- Patel J.A., Majmundar B.P., 2016. Development of evaporation estimation methods for a reservoir in Gujarat, India American Water Works Association, 108 (9): 489-500.
- Payero J., Neale C., Wright J., Allen R., 2003. Guidelines for validating Bowen ratio data. *Transactions of the ASAE*, 46 (4): 1051-1060.
- Rasmussen A.H., Hondzo M., Stefan H.G., 1995. A test of several evaporation equations for water temperature simulations in lakes. *Water Resources Bulletin*, 31 (6): 1023-1028.
- Rosenberry D.O., Stannard D.I., Winter T.C., Martinez M.L., 2004. Comparison of 13 equations for determining evapotranspiration from a prairie wetland, Cottonwood Lake area, North Dakota, USA. *Wetlands*, 24 (3): 483-497.
- Rosenberry D.O., Winter T.C., Buso D.C., Likens G.E., 2007. Comparison of 15 evaporation methods applied to a small mountain lake in the northeastern USA *Journal of Hydrology*, 340, 149-166.
- Sacks L., Lee T., Radell M., 1994. Comparison of energy budget evaporation losses from two morphometrically different Florida seepage lakes. *Journal of Hydrology*, 156: 311-334.
- Shah M.M., 2012. Calculation of evaporation from indoor swimming pools: further development of formulas. *ASHRAE Transactions*, 118 (2): 460-66.
- Shuttleworth W.J., 1993. Evaporation. In: Maidment DR (ed) *Handbook of hydrology*. New York: McGraw-Hill.
- Stauffer R., 1991. Testing lake energy budget models under varying atmospheric stability conditions. *Journal of Hydrology*, 128: 115-135.
- Stewart R.B., Rouse W.R., 1976. A simple method for determining the evaporation from shallow lakes and ponds. *Water Resources Research*, 12 (4): 623-628.
- Sweers H.E., 1976. Anomogram to estimate the heat-exchange coefficient at the air-water interface as a function of wind speed and temperature; a critical survey of some literature. *Journal of Hydrology*, 30: 375-401.
- Tanner B., Greene J., Bingham G., 1987. A Bowen ratio design for long term measurements. In: *Proceedings of the International Winter Meeting of the ASAE*, Hyatt Regency, Chicago, USA.
- Torres E.A., Calera A., 2010. Bare soil evaporation under high evaporation demand: a proposed modification to the FAO-56 model. *Hydrological Sciences Journal*, 55 (3): 303-315.
- Winter T.C., Buso D.C., Rosenberry D.O., Likens G.E., Sturrock A.M.J., Mau D.P., 2003. Evaporation determined by the energy budget method for Mirror Lake, New Hampshire. *Limnology and Oceanography*, 48 (3): 995-1009.
- Yao H., 2009. Long-Term Study of Lake Evaporation and Evaluation of Seven Estimation Methods: Results from Dickie Lake, South-Central Ontario, Canada. *Journal of Water Resource and Protection*, 2: 59-77.
- Zarghami M., Abdi A., Babaeian I., Hassanzadeh Y., Kanani R. 2011. Impacts of climate change on run-offs in East Azerbaijan, Iran. *Global and Planetary Change*, 78: 137-146.



Citation: S. Khajeh Hosseini, F. Fanoodi, S.A. Tabatabaei, R. Yazdani Biouki, J. Masoud Sinaki (2020) Drought stress response of hyssop (*Hyssopus officinalis* L.) as influenced via the anti-transpirants and osmolytes materials. *Italian Journal of Agrometeorology* (2): 35-44. doi: 10.13128/ijam-985

Received: June 27, 2020

Accepted: August 18, 2020

Published: January 25, 2021

Copyright: ©2020 S. Khajeh Hosseini, F. Fanoodi, S.A. Tabatabaei, R. Yazdani Biouki, J. Masoud Sinaki. This is an open access, peer-reviewed article published by Firenze University Press (<http://www.fupress.com/ijam>) and distributed under the terms of the Creative Commons Attribution License, which permits unrestricted use, distribution, and reproduction in any medium, provided the original author and source are credited.

Data Availability Statement: All relevant data are within the paper and its Supporting Information files.

Competing Interests: The Author(s) declare(s) no conflict of interest.

Drought stress response of hyssop (*Hyssopus officinalis* L.) as influenced via the antitranspirants and osmolytes materials

SARAH KHAJEH HOSSEINI¹, FARZAD FANOODI^{2,*}, SAYED ALI TABATABAEI³, ROSTAM YAZDANI BIOUKI⁴, JAFAR MASOUD SINAKI⁵

¹ PhD Student, Department of Agriculture, Damghan Branch, Islamic Azad University, Damghan, Iran

² Department of Agriculture, Damghan Branch, Islamic Azad University, Damghan, Iran

³ Seed and Plant Improvement Research Department, Yazd Agricultural and Natural Resource and Education Center, AREEO, Yazd, Iran

⁴ Assistant Professor, National Salinity Research Center, Agricultural Research, Education and Extension Organization (AREEO), Yazd, Iran

⁵ Department of Agriculture, Damghan Branch, Islamic Azad University, Damghan, Iran

* Corresponding author. E-mail: farzadfanoodi@yahoo.com

Abstract. Drought or insufficient water is considered as one of the most common limiting factors in global agricultural production. This study evaluated the effects of drought stress and foliar application of kaolin, chitosan, and glycine amino acid at different application times in Hyssop (*Hyssopus officinalis* L.) for two-year. The results demonstrated that extreme drought affects the growth and yield parameters of hyssop, such as decrease morphological traits as well as yield components, protein content and increase enzymatic antioxidants. The foliar application, especially with kaolin at flowering, caused the greatest changes in general, greatly enhanced the number of lateral branches, shoot dry weight, protein content by (13.62%), (6.15%), (7%) in the first year, respectively. In addition, chitosan had a beneficial effect on shoot dry weight too. Also, kaolin reduced the effects of oxidative stress in the plant by increasing its antioxidant capacity to. So that the enzymatic antioxidants CAT and POX enhanced by (32.48%), (43.35%) in the first year and by (5.95%), (13.18%) in the next year, respectively.

Keywords. Amino acid, dry matter production, enzymatic antioxidants, transpiration.

INTRODUCTION

Hyssop (*Hyssopus officinalis* L.) belongs to the Lamiaceae family and is considered as a native plant from southern Europe and Near East to the region surrounding the Caspian Sea and cultivated in central and southern European countries including Russia, Spain, France, Yugoslavia, Netherland, Hungary and Italy (Mitic and Dordevic, 2000). The essential oil and extracts isolated from *Hyssopus officinalis* were shown to have biological and pharmacological

activities including anti-bacterial (Michalczyk et al., 2012), antioxidant (Kizil et al., 2010) and antiplatelet (Tognolini et al., 2006). despite hyssop having a slightly bitter taste, it is often used as a minty flavour and condiment in food industries (Fathiazad et al., 2011).

Plants often encounter unfavourable conditions, which interrupts their growth and productivity. Among the various abiotic stresses, drought is considered as the major factor which limits crop productivity worldwide (Tardieu et al., 2014). Also, drought causes the inhibition of shoot growth, adjustment of leaf area, stomatal closure, and reduction of transpiration, inhibition of photosynthesis, shifts in carbon and nitrogen metabolism, synthesis of compatible solutes, and secondary oxidative stress (Xoconostle-Cazares et al., 2011). Further, oxidative stress arises from a significant increase in the concentration of reactive oxygen species (ROS) (Ermak and Davies, 2002). ROS are highly reactive and can alter normal cellular metabolism through oxidative damage to membranes, proteins, and nucleic acids. Further, they cause protein denaturation, DNA mutation (Baby and Jini, 2011). To counter the deleterious effects of ROS, plants have developed the scavenging mechanism of ROS categorized as enzymatic antioxidants, acting as a defence mechanism to regulate the ROS levels (Hossain et al., 2013). The enzymes of the antioxidant system protect cells by eliminating ROS including catalase (CAT), superoxide dismutase (SOD), and numerous peroxidases (POX), among which ascorbate peroxidase (APX) can be mentioned (Jozwiak and Politycka, 2019).

Reduced transpiration rate is considered as one of the effective ways to reduce the unfavourable effects of drought stress in plants (Neyestani and Azimzadeh, 2005). Foliar application of antitranspirants (ATS) is a promising tool for regulating transpiration to maintain a favourable plant water status (Goreta et al., 2007). ATs were classified into three types based on their active role. The first is related to metabolic materials which are chemical compounds which can prevent stomata from opening fully by affecting the guard cells around the stomata pore, leading to a decrease in the loss of water vapour from plant leaves (Anjum et al., 2011); Second, film-forming materials which are emulsions of wax, latex or plastics dry on the foliage to form thin transparent films which hinder the escape of water vapour from the leaves (Faralli et al., 2016) Finally, reflecting materials which reduce the absorption of the radiant energy, as well as leaf temperatures and transpiration rate (Glenn et al., 2003). Reflective materials such as kaolin clay and chitosan can reduce the absorption of radiant energy (heat), lower leaf temperatures, and decrease transpiration (Jifon and Syvertsen, 2003). Kaolin is a white, non-porous, non-swelling, low-abrasive, fine-grained, plate-shaped, and aluminosilicate mineral $[Al_4Si_4O_{10}(OH)_8]$ (Glenn and

Puterka, 2005). Besides, chitosan is produced from chitin, an important component of crustacean shells such as crab, shrimp and crawfish, and is mainly made of (1-4)-2-amino-2-deoxy- β -D-glucan (Ma et al., 2013).

Increasing the synthesis and accumulating osmolytes in plants is regarded as one of the methods which prolong water uptake and reduces osmotic stress due to drought stress (Tang and Newton, 2005). Major osmolytes organic compounds include amino acids, polyols, sugars and methylamines (Pessarakli, 2011). The use of external sources of osmolyte organic compounds in environmental stressors can modulate the destructive effects of stresses on plants (Namvar et al., 2018). Further, glycine amino acid as osmolyte is a soluble nitrogenous compound which is accumulated under stress in plants (Galeshi, 2015; Hussein and Terry, 2002). Glycine is a proteinogenic amino acid and the smallest biological amino acid in the cells with a molar mass of 75 g mol^{-1} . Further, it is a hydrophilic and non-polar amino acid, which can have an acidic or basic reaction in different mediums due to its chemical structure (Souri and Hatamian, 2019).

By considering the above studies, the present research aimed to evaluate the growth, yield changes and antioxidant activities in hyssop (*Hyssopus officinalis* L.) treated with the chitosan, kaolin and glycine amino acid under drought stress condition and different application times.

MATERIALS AND METHODS

Experimental design

The experiment was conducted during a two-year factorial split-plot experiment based on completely randomized block design with three replications at the research field of Yazd Agricultural and Natural Resources Center, Iran (31° N latitude and 54° E longitude 1220 m above sea level) in 2017 and 2018. The presented temperature and rainfall rate of the site during the crop growing periods of the experiments is depicted in Fig 1.

The experimental treatments included irrigation at three levels (25, 50, 75 % of the available water discharge from the soil) as control, mild and intense stress as main treatments and spraying treatments in three levels of water (control), kaolin (2.5%, Sepidan WP 95, Aluminium silicate, LD 50 > 5000 mg.kg^{-1}), chitosan (0.4 g.l^{-1} , Sigma-Aldrich, Medium molecular weight, 75-85% deacetylated chitin, LD 50 > 10.000 mg.kg^{-1}), glycine amino acid (2.5 per thousand, Merck, Molar mass: $75.067 \text{ g.mol}^{-1}$, Density: 1.1607 g.cm^{-3} , LD 50 > 2600 mg.kg^{-1}) and time of spraying (vegetative and flowering, just flowering) were considered as subplots. Soil fertilizers were added to the experimental farmland based on the soil test during farm preparation (Tab. 1). To sup-

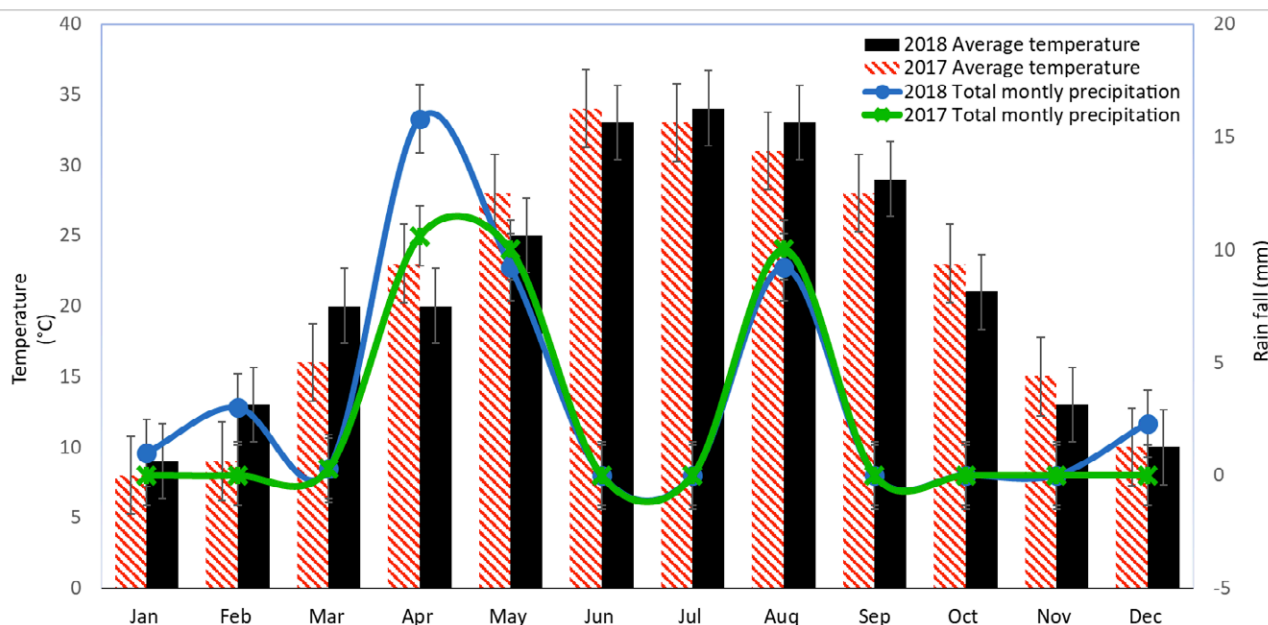


Fig. 1. Meteorological conditions during 2017 and 2018.

ply the needed nitrogen based on the results of soil analysis, urea fertilizer (46% nitrogen) was used in two stages including pre-planting to the soil and mid-vegetative period to the plant at the rate of 100 kilograms per hectare.

Each subplot sizes into the main plot were 3×4 m and consisted of six planting rows. The distance between the plants and rows was 20 and 50 cm, respectively. The distance between the main plot and the blocks was 1.5 and 3 m, respectively. The seeds were sown by hand. All of the plots were regularly irrigated after sowing until seedling establishment. Drought stress after complete plant establishment was increased by irrigation intervals of 7 days (control, 25% of the available water discharge from the soil), 9 days (medium stress, 50% of the available water discharge from the soil), and 11 days (severe stress, 75% of the available water discharge from the soil), which was done based on soil moisture recordings by the TDR model (TRASE System 1). Weeds were controlled by hand during crop growth and development as required. Phonological stages of the hyssop plant were determined based on the 50% of the plants in reaching a specified developmental

stage, and accordingly, the time interval to each stage based on the day after planting was recorded.

Collection of plant samples

Sampling from each experimental unit was performed by considering marginal effects at the end of the flowering stage each year. The number of lateral branches and leaves, as well as leaves and shoot dry weight was determined to evaluate the growth and yield changes. In addition, the water soluble protein content was determined according to Bradford's (1976) to evaluate antioxidant changes. Further, enzymatic antioxidants such as Catalase (CAT), and peroxidase (POX) were measured by using (Dhindsa et al., 1981) and (Mac-Adam et al., 1992), respectively.

Statistical analysis

After checking the data distribution normality (Kolmogorov-Smirnov and Shapiro-Wilk test) assumption,

Tab. 1. The main characteristics of the experimental farm in 0–30 cm soil depth.

Potassium (ppm)	Phosphorous (ppm)	N.Total (%)	Sand (%)	Silt (%)	Clay (%)	Organic Carbon (%)	pH	Electrical conductivity (dS.m ⁻¹)	Soil texture
360	41.6	0.01	76	20	5	0.221	7.67	1.68	Loamy sand

the studied traits were statistically analyzed by ANOVA by using the SAS 9.4 procedure PROC GLM. The mean comparison of data was done by LSD range test at 5% level of significance.

RESULTS

Morphological traits and yield components

Number of the leaves, leaves dry weight

Analysis of variance indicated positive effects of using antitranspirant and osmolytes materials on morphological traits and yield components of hyssop under limited irrigation (Tab. 2). Due to the results of this study, the number

of leaves was significantly affected by antitranspirant and leaves dry weight was significantly affected by osmolytes materials. According to Fig. 2, the highest number of the leaves was observed in the interaction effects of control irrigation with water spraying (4779 per plant) and control irrigation with chitosan spraying (4381 per plant) in the first year and the highest leaves dry weight was observed in the interaction effects of control irrigation and glycin spraying in vegetative and flowering (230.8 g.m⁻²) in the second year (Tab. 3).

Number of lateral branches, Shoot dry weight

Among the materials used, glycin and kaolin had the most influence on the number of lateral branches and

Tab. 2. The results Analysis on hyssop (*Hyssopus officinalis* L.) traits evaluated under, Drought stress (D), Foliar application (F) and Foliar application Time (FT).

Treatment	df	Mean sum of squares							
		Number of leaves		Number of lateral branches		Leaves dry weight		Shoot dry weight	
		2017	2018	2017	2018	2017	2018	2017	2018
R	2	2804010 ^{ns}	3035819 ^{ns}	4051 ^{**}	2452 ^{ns}	410.4 ^{ns}	303.51 ^{ns}	326.9 ^{**}	21.11 ^{ns}
D	2	49883736 ^{**}	21573726 [*]	8372 ^{**}	51646 ^{**}	3757 ^{**}	1249.61 ^{ns}	1522 ^{**}	23867.18 ^{**}
Error a	4	614629	2229893	167.1	766	108.2	930.00	11.70	321.17
FT	1	153735 ^{ns}	4917248 [*]	3472 [*]	6884 [*]	0.125 ^{ns}	2188.90 [*]	48.35 ^{ns}	1326.98 ^{ns}
F	3	112359 ^{ns}	7049457 ^{**}	1124 ^{ns}	16081 ^{**}	1312 ^{**}	2426.48 ^{**}	56.24 ^{ns}	5063.73 ^{**}
D × FT	2	198809 ^{ns}	1542008 ^{ns}	1629 ^{ns}	2865 ^{ns}	25.29 ^{ns}	9699.45 ^{**}	115.5 [*]	1634.31 [*]
D × F	6	647572 ^{**}	4665474 ^{**}	2382 [*]	7607 ^{**}	647.6 ^{**}	7873.52 ^{**}	137.1 ^{**}	1997.43 ^{**}
F × FT	3	59826 ^{ns}	6213617 ^{**}	2683 [*]	2696 ^{ns}	110.1 ^{ns}	10583.34 ^{**}	22.46 ^{ns}	2073.92 ^{**}
FT × F × D	6	222147 ^{ns}	16340720 ^{**}	2800 ^{**}	18355 ^{**}	35.16 ^{ns}	5604.08 ^{**}	47.24 ^{ns}	2112.67 ^{**}
Error b	42	125985	918659	728.8	1449	43.60	384.16	27.21	473.49
C.V		13.70	19.08	18.80	18.57	16.99	21.81	18.68	20.23

Treatment	df	Mean sum of squares					
		Protein		CAT		POX	
		2017	2018	2017	2018	2017	2018
R	2	0.1596 ^{**}	1.1660 ^{**}	0.0824 ^{ns}	0.4777 ^{**}	0.0664 ^{**}	0.0005 [*]
D	2	2.5706 ^{**}	1.4440 ^{**}	2.4956 ^{**}	0.3620 ^{**}	0.0316 ^{**}	0.0151 ^{**}
Error a	4	0.0003	0.0904	0.0004	0.0098	0.0002 ^{ns}	0.0004
FT	1	9.3615 ^{**}	0.0021 ^{ns}	0.0652 ^{**}	0.0791 [*]	0.0739 ^{**}	0.0009 ^{ns}
F	3	17.2600 ^{**}	4.9409 ^{**}	0.2432 ^{**}	0.0217 ^{ns}	2.5934 ^{**}	0.0056 [*]
D × FT	2	0.3773 ^{**}	5.9961 ^{**}	0.105 ^{**}	0.0731 [*]	0.6366 ^{**}	0.0157 ^{**}
D × F	6	20.6942 ^{**}	6.2558 ^{**}	1.0897 ^{**}	0.1052 ^{**}	0.6463 ^{**}	0.0203 ^{**}
F × FT	3	3.2322 ^{**}	0.3547 ^{**}	0.0449 ^{**}	0.0423 ^{ns}	0.6972 ^{**}	0.0046 [*]
FT × F × D	6	6.4904 ^{**}	7.4057 ^{**}	0.1282 ^{**}	0.1314 ^{**}	1.2918 ^{**}	0.0129 ^{**}
Error b	42	0.0002	0.0871	0.0002	0.0208	0.0002	0.0017
C.V		0.14	3.23	2.13	26.54	1.39	17.68

df- degree of freedom; R- Replication; CV – coefficient of variation; ns – not significant; ** – significant at p ≤ 0.01; * - significant at p ≤ 0.05.

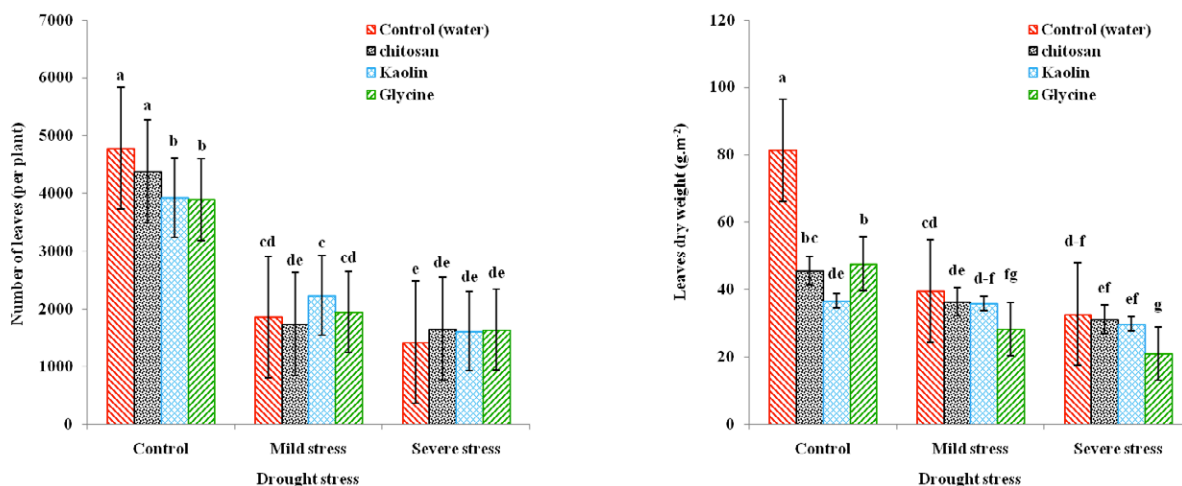


Fig. 2. The effect of drought stress and foliar application on leaves dry weight.

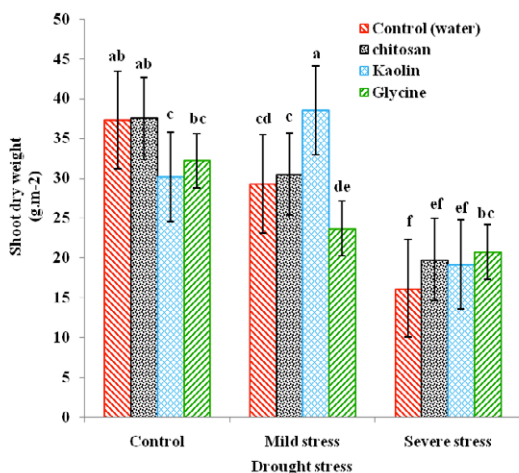


Fig. 3. The effect of drought stress and Foliar application on shoot dry weight.

shoot dry weight compared to control, respectively. The highest number of lateral branches was observed in interaction effects of control irrigation and glycin spraying in vegetative and flowering in 2017 (185 per plant) (Tab. 3) and the highest shoot dry weight was observed in interaction effects of mild stress and kaolin spraying (38.5g.m⁻²) in the first year (Fig. 3).

Protein and enzymatic antioxidants

Analysis of variance indicated the positive effects of using antitranspirant and osmolytes materials on protein content and enzymatic antioxidants of hyssop under limit-

ed irrigation (Tab. 2). The osmolytes materials used caused an increase in protein content in the first year. According to Tab. 3, the highest protein content (12.47%) was observed in the interaction effects of severe stress and glycin spraying at just flowering. The protein content, the CAT and POX activities were also affected by antitranspirants. The highest protein content (12.08%) in 2018 and the highest CAT enzyme activity content (1.593 U. mg protein⁻¹. min⁻¹) in 2018, was observed in interaction effects of severe stress and kaolin spraying at just flowering (Tab. 3). The kaolin affected the POX enzyme activity content too. So that the highest POX activities (2.382 U. mg protein⁻¹. min⁻¹) was obtained in interaction effects of control irrigation and kaolin spraying at vegetative and flowering in the first year (Tab. 3). Among the antitranspirant materials used chitosan showed better results of increasing studied antioxidants traits compared with control too. As the results showed, at the severe stress level, the foliar application of chitosan in just flowering had the highest of activity CAT (0.868 U. mg protein⁻¹. min⁻¹) and POX (0.438 U. mg protein⁻¹. min⁻¹) in the second year (Tab. 3).

DISCUSSION

Grow and yield

Plants are exposed to environmental stresses during their growth. Drought stress is considered as one of the major abiotic stresses leading to a high reduction in plant growth and yield, which can affect the absorption and transfer of nutrients to the plant (Askari et al., 2018). In the present study, the results indicated that the severe drought stress caused a reduction on growing and yielding

Tab. 3. The influence of drought stress (D), foliar application (F) and Foliar application time (FT) on hyssop (*Hyssopus officinalis* L.) traits evaluated.

Treatment			Number of leaves (per plant)		Leaves dry weight (g.m ⁻²)		Number of lateral branches (per plant)		Shoot dry weight (g.m ⁻²)	
D	FT	F	2017	2018	2017	2018	2017	2018	2017	2018
Control	Flowering	Control(water)	NS	2389 ^j	NS	68.5 ^{e-j}	170 ^{ab}	75 ^M	NS	79.0 ^{h-j}
		Chitosan	NS	5330 ^{d-g}	NS	68.3 ^{e-j}	179 ^{ab}	230 ^{b-f}	NS	78.8 ^{h-j}
		Kaolin	NS	4780 ^{e-h}	NS	52.9 ^{h-j}	164 ^{a-c}	160 ^{g-l}	NS	67.38 ^{ij}
		Glycine	NS	5644 ^{d-f}	NS	68.7 ^{e-j}	141 ^{a-e}	225 ^{b-f}	NS	73.3 ^{ij}
	Vegetation and flowering	Control(water)	NS	4753 ^{f-h}	NS	63.9 ^{f-j}	153 ^{a-d}	226 ^{b-f}	NS	73.7 ^{ij}
		Chitosan	NS	4440 ^{f-i}	NS	55.7 ^{g-j}	136 ^{b-f}	154 ^{i-l}	NS	64.2 ^{ij}
		Kaolin	NS	2985 ^{ij}	NS	44.4 ^{ij}	167 ^{a-c}	134 ^{lm}	NS	47.9 ^j
		Glycine	NS	3903 ^{g-j}	NS	230.8 ^a	185 ^a	169 ^{f-l}	NS	84.8 ^{f-i}
Mild stress	Flowering	Control(water)	NS	9829 ^a	NS	183.2 ^b	140 ^{b-e}	281 ^b	NS	161.5 ^{a-c}
		Chitosan	NS	6695 ^{b-d}	NS	143.6 ^c	79 ^g	218 ^{c-h}	NS	156.9 ^{a-c}
		Kaolin	NS	3902 ^{g-j}	NS	64.93 ^{f-j}	163 ^{a-c}	143 ^{j-l}	NS	85.1 ^{f-i}
		Glycine	NS	3974 ^{g-i}	NS	65.8 ^{f-j}	94 ^{fg}	127 ^{lm}	NS	84.5 ^{f-i}
	Vegetation and flowering	Control(water)	NS	3927 ^{g-j}	NS	43.6 ^{ij}	113 ^{d-g}	135 ^{k-m}	NS	143.5 ^{b-d}
		Chitosan	NS	6354 ^{c-e}	NS	75.3 ^{d-i}	181 ^{ab}	202 ^{f-j}	NS	158.4 ^{a-c}
		Kaolin	NS	6742 ^{b-d}	NS	86.9 ^{d-g}	140 ^{b-e}	158 ^{h-l}	NS	98.0 ^{e-i}
		Glycine	NS	7300 ^{cb}	NS	79.4 ^{d-h}	100 ^{e-g}	222 ^{b-g}	NS	116.3 ^{d-g}
Severe stress	Flowering	Control(water)	NS	8009 ^b	NS	147.7 ^c	109 ^{d-g}	410 ^a	NS	183.7 ^a
		Chitosan	NS	4557 ^{f-i}	NS	106.2 ^d	102 ^{e-g}	276 ^{cb}	NS	126.6 ^{c-e}
		Kaolin	NS	3456 ^{j-i}	NS	84.6 ^{d-h}	122 ^{c-g}	188 ^{f-l}	NS	81.5 ^{g-j}
		Glycine	NS	4850 ^{e-h}	NS	90.2 ^{d-f}	144 ^{a-e}	246 ^{b-e}	NS	163.9 ^{ab}
	Vegetation and flowering	Control(water)	NS	4976 ^{e-h}	NS	85.4 ^{d-g}	107 ^{e-g}	265 ^{b-d}	NS	93.3 ^{e-i}
		Chitosan	NS	5303 ^{d-g}	NS	99.6 ^{ed}	160 ^{a-c}	268 ^{cb}	NS	120.3 ^{d-f}
		Kaolin	NS	4107 ^{f-i}	NS	104.7 ^d	152 ^{a-d}	214 ^{c-i}	NS	129.0 ^{b-e}
		Glycine	NS	2353 ^j	NS	42.6 ^j	178 ^{ab}	198 ^{e-k}	NS	109.6 ^{d-h}
LSD (P=0.05)			NS	1579.3	NS	32.296	44.5	62.73	NS	35.855

Different letters indicate significant differences at $\alpha = 0.05$ (LSD test).

Treatment			Protein (%)		CAT (U. mg protein ⁻¹ . min ⁻¹)		POX(U. mg protein ⁻¹ . min ⁻¹)	
D	FT	F	2017	2018	2017	2018	2017	2018
Control	Flowering	Control(water)	11.98 ^c	9.50 ^{ed}	1.276 ^c	0.195 ^{ij}	0.773 ^m	0.145 ^{ij}
		Chitosan	9.73 ^g	10.20 ^{cb}	0.558 ^k	0.490 ^{d-g}	1.265 ^g	0.127 ^{c-h}
		Kaolin	8.24 ⁿ	7.02 ^j	0.963 ^{de}	0.600 ^{b-f}	0.565 ⁿ	0.27 ^{b-e}
		Glycine	9.14 ^j	8.49 ^{gh}	1.493 ^b	0.219 ^{h-j}	0.42 ^q	0.121 ^j
	Vegetation and flowering	Control(water)	11.98 ^c	8.54 ^{gh}	1.276 ^c	0.644 ^{a-f}	0.773 ^m	0.203 ^{e-i}
		Chitosan	7.41 ^p	8.21 ^{hi}	0.800 ^g	0.191 ^j	0.478 ^p	0.205 ^{e-i}
		Kaolin	7.18 ^q	9.47 ^{ed}	0.975 ^d	0.505 ^{d-g}	2.382 ^a	0.267 ^{b-f}
		Glycine	9.40 ^h	9.66 ^{ed}	0.943 ^e	0.429 ^{f-i}	1.105 ⁱ	0.24 ^{c-f}
Mild stress	Flowering	Control(water)	9.29 ⁱ	9.68 ^{ed}	0.4 ^l	0.502 ^{d-g}	1.431 ^f	0.2 ^{f-i}
		Chitosan	10.15 ^e	10.17 ^{cb}	0.556 ^k	0.456 ^{e-h}	0.031 ^r	0.153 ^{j-i}
		Kaolin	9.94 ^f	10.17 ^{cb}	0.057 ^p	0.632 ^{a-f}	1.481 ^e	0.333 ^b
		Glycine	7.41 ^p	9.60 ^{ed}	0.405 ^l	0.335 ^{g-j}	1.505 ^d	0.231 ^{c-g}

Treatment			Protein (%)		CAT (U. mg protein ⁻¹ . min ⁻¹)		POX(U. mg protein ⁻¹ . min ⁻¹)	
D	FT	F	2017	2018	2017	2018	2017	2018
Severe stress	Vegetation and flowering	Control(water)	9.29 ⁱ	8.52 ^{gh}	0.4 ^l	0.755 ^{a-c}	1.431 ^f	0.273 ^{b-d}
		Chitosan	8.47 ^m	7.87 ⁱ	0.337 ^m	0.699 ^{a-d}	0.876 ^k	0.207 ^{d-i}
		Kaolin	8.55 ^l	9.76 ^{cd}	0.242 ^o	0.490 ^{d-g}	0.824 ^l	0.234 ^{c-f}
		Glycine	6.74 ^r	9.24 ^{ef}	0.753 ^h	0.688 ^{a-e}	0.525 ^o	0.202 ^{f-i}
	Flowering	Control(water)	8.70 ^k	8.13 ^{hi}	0.337 ^m	0.703 ^{a-d}	0.958 ^j	0.275 ^{bc}
		Chitosan	8.47 ^m	5.68 ^k	0.884 ^f	0.868 ^a	0.563 ⁿ	0.438 ^a
		Kaolin	7.67 ^o	12.08 ^a	1.593 ^a	0.325 ^{g-j}	1.582 ^c	0.164 ^{g-j}
		Glycine	12.47 ^a	8.73 ^g	0.636 ⁱ	0.794 ^{ab}	1.143 ^h	0.280 ^{bc}
	Vegetation and flowering	Control(water)	8.70 ^k	10.46 ^b	0.337 ^m	0.526 ^{c-g}	0.958 ^j	0.227 ^{c-g}
		Chitosan	12.03 ^b	8.85 ^{gf}	0.600 ^j	0.815 ^{ab}	0.491 ^p	0.253 ^{c-f}
		Kaolin	4.57 ^s	10.17 ^{cb}	1.501 ^b	0.590 ^{b-f}	2.232 ^b	0.225 ^{c-g}
		Glycine	10.22 ^d	8.83 ^{gf}	0.272 ⁿ	0.583 ^{b-f}	0.411 ^q	0.207 ^{d-i}
		LSD (P=0.05)	0.02	0.49	0.026	0.238	0.023	0.608

CAT- Catalase; POX- Peroxidase; Different letters indicate significant differences at $\alpha = 0.05$ (LSD test).

components such as the number of leaves and reciprocally the leaves dry weight, and the number of lateral branches and reciprocally the shoot dry weight. However, the severe stress level had a less negative effect on all of the above traits in the second year compared to the non-stress condition, which is consistent with the other studies (Polanski et al., 2018).

The antitranspirants and osmolytes materials spraying on plant foliage, at different growth stages could reduce the destructive effects of drought stress. In the present study, the foliar application, especially just flowering, had the best result on growth and yield. The foliar application of chitosan and water spraying had the highest number of the leaves at control stress level during the first year. In addition, water spraying caused the highest leaves dry weight in the first year. In general, chitosan may provide some amino compounds required for plant growth, leading to the increasing total nitrogen content in leaves or the higher ability of plants to absorb nitrogen from the soil as chitosan may increase key enzyme activity of nitrogen metabolism, as well as the transportation of nitrogen in the functional leaf. Further, chitosan can increase the availability, uptake and transport of essential nutrients via adjusting cell osmotic pressure, leading to plant growth and development (Abdul Manaim Mohammed et al., 2018). Regarding the second year, water spraying in just flowering had the highest number of the leaves at mild stress level, while the foliar application of glycine spraying in just flowering had the highest leaves dry weight at control stress level. Further more, the water spraying at severe stress level caused the highest number of lateral branches and reciprocally the leaves dry

weight. In addition, the foliar application of glycine had the highest number of lateral branches at control stress level and kaolin spraying had the highest shoot dry weight at mild stress level during the first year. The positive effects of glycine foliar application on growing and yielding hyssop can be related to its ability for inducing osmotic regulation as compatible osmolyte contents in the plant. Generally, osmotic regulation results in expanding the cell, regulating the stomata and photosynthesis, and finally increasing the growth and yield in the plant (Galeshi, 2015). Further, the positive effects of kaolin spraying on growth and yield of hyssop can be attributed to its ability for anti-transpiration. Generally, these substances reduce transpiration in the plant and preserve leaves water potential through improving plant water conditions and dividing cell, which result in producing photosynthetic materials in canopy leading to an increase in the total dry matter accumulation and plant yield (Jan- Mohammadi et al., 2014)

Antioxidant activity


Drought induces oxidative stress in plants by generating reactive oxygen species (ROS) (A. Kasim et al., 2015). which can destroy proteins, lipids, carbohydrates, and nucleic acids (Bian and jiang, 2009). In this regard, the severe drought stress caused a reduction in protein content in the first year, compared to that of the control, which is consistent with the other studies (Rahimi et al., 2019). However, the protein was less affected by drought stress in both control and severe stress during the second year. On the other hand, the highest protein content was observed

in mild stress, which can be related to the synthesis of more specific proteins during stress (Galeshi, 2015). which is consistent with the other studies (Ahrar et al., 2020). Generally, plants should include enzymatic antioxidant systems to protect cells from oxidative damage in order to keep the levels of active oxygen species under control (A. Kasim et al., 2015). Drought stress increased the activity of antioxidant enzymes such as CAT and POX. Based on the results, CAT activity decreased in the first year, while increased in the second year. However, POX increased in both years, which are in line with some other studies (Afsharmohammadian et al., 2016).

The foliar application, especially just flowering, improved the destructive effects of drought on the plant in

Tab. 4. Correlation coefficients among traits of hyssop under different irrigation treatments in 2017.

	1	2	3	4	5	6	7
2	0.73**	1					
3	0.48**	0.24*	1				
4	0.67**	0.57**	0.45**	1			
5	0.17 ^{ns}	0.35**	0.20 ^{ns}	0.16 ^{ns}	1		
6	0.40**	0.38**	0.10 ^{ns}	0.04 ^{ns}	-0.16 ^{ns}	1	
7	0.02 ^{ns}	-0.14 ^{ns}	0.15 ^{ns}	-0.05 ^{ns}	-0.42**	0.15 ^{ns}	1




Red and blue colors show negative and positive, respectively
ns – not significant; ** – significant at $p \leq 0.01$; * - significant at $p \leq 0.05$.

1- The number of leaves; 2- leaves dry weight; 3- Number of lateral branches; 4- Shoot dry weight; 5-Protein content; 6- CAT activity; 7: POX activity.

Tab. 5. Correlation coefficients among traits of hyssop under different irrigation treatments in 2018.

	1	2	3	4	5	6	7
2	0.43**	1					
3	0.65**	0.40**	1				
4	0.49**	0.41**	0.54**	1			
5	0.15 ^{ns}	0.08 ^{ns}	0.25*	0.12 ^{ns}	1		
6	0.26*	0.04 ^{ns}	0.42**	0.37**	0.33**	1	
7	-0.07 ^{ns}	0 ^{ns}	0.17 ^{ns}	0.14 ^{ns}	0.13 ^{ns}	0.48**	1



Red and blue colors show negative and positive, respectively
ns – not significant; ** – significant at $p \leq 0.01$; * - significant at $p \leq 0.05$.

1- The number of leaves; 2- leaves dry weight; 3- Number of lateral branches; 4- Shoot dry weight; 5-Protein content; 6- CAT activity; 7: POX activity.

two crop years. In fact, at severe stress level, the foliar application of glycine had the highest protein content at just flowering in the first year, while kaolin spraying at just flowering had the highest protein content in the second year. In addition, the foliar application of kaolin at severe drought stress in just flowering caused the highest of CAT activity content and spraying at vegetative and flowering at control drought stress caused the highest POX activity content in the first year. Glycine as an osmolyte and kaolin reduce the effects of oxidative stress in the plant by increasing its antioxidant capacity. Further, increased antioxidant activity by spraying kaolin was reported in other studies (Bernardo et al., 2017). Regarding the second year, foliar application of chitosan at severe drought stress in just flowering performed better, leading to the highest CAT and POX activity content. In general, the induction of antioxidant defence in plants by using chitosan can be related to the potential of this substance in neutralizing reactive oxygen species, which may be attributed to its specific structure including large numbers of accessible amine and hydroxyl groups which reacts with reactive oxygen species (Mahdavi et al., 2013). On the other hand, the ability of this substance can play a role in expressing a variety of genes involved in the plant defence response under stress conditions, which ultimately increase the production of secondary metabolites (Howlett, 2006).

CORRELATION BETWEEN TRAITS

In the first year, the calculation of correlation coefficients showed that the highest correlation was related to leaves number and leaves dry weight ($r = 0.73^{**}$). There after, the shoot dry weight had the highest correlation with leaves number ($r = 0.67^{**}$) and leaves dry weight ($r = 0.57^{**}$) (Tab. 4). There was a positive, weak and significant relationship between the antioxidant activity, the growth and yield such as CAT activity with leaves number ($r = 0.40^{**}$) and leaves dry weight ($r = 0.38^{**}$). While the correlation between the antioxidant activity of traits such as POX and protein was negative and significant. So that the amount of protein decreased with increasing POX enzyme. In the second year, the highest correlation was observed between the growth parameters such as the number of lateral branches and number of leaves ($r = 0.65^{**}$) and then between the growth parameters with the yield components such as the number of lateral branches with the shoot dry weight ($r = 0.54^{**}$) (Tab. 5). But there was a weak and significant relationship between the yield and growth as well as between the antioxidant activity and the growth and yield. Also There was a weak and significant relationship between the amount of protein, the CAT

and POX. So on average, it can be concluded that with increasing the growth, the yield will increase and with increasing antioxidant activity in the plant, the growth and yield will decrease.

CONCLUSION

The drought stress caused a reduction on growing and yielding components such as the number of leaves and reciprocally the leaves dry weight, and the number of lateral branches and reciprocally the shoot dry weight. The severe stress had a less negative effect on all of the above traits in the second year compared to the non-stress condition. The drought stress caused a reduction in protein content and CAT activity in the first year while both traits increased in the second year. The POX activity increased in two years too. The foliar application with chitosan, kaolin, and glycine amino acid, especially just flowering, reduced the adverse effects of water stress by improving growth and yield through influencing some traits such as the number of leaves, the leaves dry weight, the number of lateral branches, the shoot dry weight and the antioxidant activity through affecting some traits such as the protein content, activity contents of CAT and POX. Finally, it is recommended to increase plant production and reduce the effects of drought stresses in arid and semi-arid regions due to the beneficial effects of these substances and safety effects on the environment.

REFERENCES

- Abdul Manaim Mohammed sh., Sayed Ahmad H., Ahmad Al-Bouab, A., 2018. Effect of Chitosan, Putrescine and Irrigation Levels on the Drought Tolerance of Sour Orange Seedlings. *Egyptian journal of horticulture*, 45: 257-273.
- Afsharmohammadian M., Ghanati F., Ahmadiani S., Sadrazamani K., 2016. Effect of drought stress on the activity of antioxidant enzymes and soluble sugars content of pennyroyal (*Mentha pulegium* L.). *Nova Biological Reperta*, 3: 228-237.
- Ahrar A., Paknejad F., Tabatabaei S. A., Aghayari F., Soltani E., 2020. Evaluation of forage Amaranth (*Amaranthus hypochondriacus* L.) yield via comparing drought tolerance and susceptibility indices. *Italian Journal of Agrometeorology* 1: 31-40.
- Kasim W., A.M. Hamada E., G. Shams El-Din N., Eskander S., 2015. Influence of seaweed extracts on the growth, some metabolic activities and yield of wheat grown under drought stress. *International Journal of Agronomy and Agricultural Research*, 7: 173-189.
- Anjum S.A., Wang L., Farooq M., Xue L., Ali S., 2011. Fulvic acid application improves the maize performance under well-watered and drought conditions. *Agronomy and Crop Science*, 197:409-417.
- Askari A., Ardakani M. R., Vazan S., Paknejad F., Hosseini Y., 2018. The effect of mycorrhizal symbiosis and seed priming on the amount of chlorophyll index and absorption of nutrients under drought stress in sesame plant under field conditions. *Applied Ecology and Environmental Research*, 16: 335-357.
- Baby J., Jini D., 2011. Development of salt stress-tolerant plants by gene manipulation of antioxidant enzymes. *Asian Journal of Agricultural Research*. 5: 17-27.
- Bernardo S., Dinis L.T., Luzio A., Pinto G., Meijon M., Valledor L., Conde A., Geros H., Correia C.M., Moutinho-Pereira J., 2017. Kaolin particle film application lowers oxidative damage and DNA methylation on grapevine (*Vitis vinifera* L.). *Environmental and Experimental Botany*, 139: 39-47.
- Bian S., Jiang Y., 2009. Reactive Oxygen Species, Antioxidant Enzyme Activities and Gene Expression Patterns in Leaves and Roots of Kentucky Bluegrass in Response to Drought Stress and Recovery. *Scientia Horticulturae*, 120: 264-270.
- Bradford M., 1976. A rapid and sensitive method for quantitation of microgram quantities of protein utilizing the principle of protein-dye binding. *Annual Review of Biochemistry*, 72: 248-254.
- Dhindsa R.H., Plumb-Dhindsa R., Thorpe TA., 1981. Leaf senescence correlated with increased level of membrane permeability lipid peroxidation and decreased level of SOD and CAT. *Journal of Experimental Botany*, 32: 93-101.
- Ermak G., Davies K.J., 2002. Calcium and oxidative stress: from cell signaling to cell death. *Molecular Immunology*, 38: 713-721.
- Faralli M., Ivan G.G., Martin C.H., Roger D.B., Kevinm S.W., Fiona M.K.C., Peter S.K., 2016. Canopy application of film antitranspirants over the reproductive phase enhances yield and yield-related physiological traits of water-stressed oilseed rape (*Brassica napus*). *Crop and Pasture. Science*, 67: 751-765.
- Fathiazad F., Mazandarani M., Hamedeyazdan S., 2011. Phytochemical analysis and antioxidant activity of *Hyssopus officinalis* L. from Iran. *Advanced Pharmaceutical Bulletin*, 1: 63-67.
- Galeshi S., 2015. The Effect of environmental stresses on plants. (Drought, Salinity, Heat and Flooding), Gorgan University of Agricultural Sciences and Natural Resources Publication, 386 pages.

- Glenn D.M., Erez A., Puterka G.J., Gundrum P., 2003. Particle films affect carbon assimilation and yield in Empire' apple. *Journal of the American Society for Horticultural Science*, 128: 356-362.
- Glenn M., Puterka G.J., 2005. Particle films: A new technology for Agriculture. *Horticultural Reviews*, 31: 1-42.
- Goreta S., Leskovar D. I., Jifon J. L., 2007. Gas exchange, water status, and growth of pepper seedlings exposed to transient water deficit stress are differentially altered by antitranspirants. *American Society Horticulture Science*, 132: 603-610.
- Hossain M. A., Mostofa M. G., Fujita M., 2013. Cross protection by cold-shock to salinity and drought stress-induced oxidative stress in mustard (*Brassica campestris* L.) seedlings, *Molecular Plant Breeding*, 4: 50-70.
- Hussein SH., Terry N., 2002. Phytomonitoring the unique colonization of oil-contaminated saline environment by *Limoniastrum monopetalum* L. Boiss in Egypt. *Journal of Environment International*, 28: 127-135.
- Howlett B., 2009. Secondary metabolite toxins and nutrition of plant pathogenic Fungi. *Current Opinion in Plant Biology*, 9: 371-375.
- Jan-Mohammadi M., Mostafavi H., Kazemi H., 2014. Effect of chitosan application on the performance of lentil genotypes under rainfed conditions. *Acta Technologica Agriculture*, 4: 86-90.
- Jifon J.L., Syvertsen J.P., 2003. Kaolin particle film applications can increase photosynthesis and water use efficiency of 'Ruby Red' grapefruit leaves. *Journal of the American Society for Horticultural Science*, 128: 107-112.
- Jozwiak w., Politycka B., 2019. Effect of Selenium on Alleviating Oxidative Stress Caused by a Water Deficit in Cucumber Roots Plants, 8: 1-18.
- Kizil S., Hasimi N., Tolan V., Kilinc E., Karatas H., 2010. Chemical composition, antimicrobial and antioxidant activities of hyssop (*Hyssopus officinalis* L.), Essential Oil. *Notulae Botanicae Horti Agrobotanici Cluj-Napoca*, 38: 99-103.
- Ma Z., Yang L., Yan H., Kennedy J.F., Meng X., 2013. Chitosan and oligochitosan enhance the resistance of peach fruit to brown rot. *Carbohydrate Polymers*, 94: 272-277.
- Mac-Adam J.W., Nelson C.J., Sharp R.E., 1992. Peroxidase activity in the leaf elongation zone of Tall Fescue. *Plant Physiology*, 99: 972-878.
- Mahdavi B., Modarres Sanavy S. A. M., Aghaalikhani M., Sharifi M., 2013. Effect of chitosan on safflower (*Carthamus tinctorius* L.) Seed Germination and antioxidant enzymes activity under water stress. *Journal of Plant Research (Iranian Journal of Biology)*, 26: 352-365.
- Michalczyk M., Macura R., Tesarowicz Z., Banas J., 2012. Effect of adding essential oils of coriander (*Coriandrum sativum* L.) and hyssop (*Hyssopus officinalis* L.) on the shelf life of ground beef. *Meat Science*, 90: 842-850.
- Mitic V., Dordevic S., 2000. Essential oil composition of *Hyssopus officinalis* L. cultivated in Serbia. *Facta Universitatis Series Physics. Chemistry and Technology*, 2: 105-108.
- Namvar A., Hashem H., Seyedsharifi R., 2018. Role of exogenous phytoprotectants in mitigation of adverse effects of abiotic stresses. *Journal of Iranian plant Ecophysiological Research (plant Sciences Research)*, 12: 103-128.
- Neyestani E., Azimzadeh M., 2005. Evaluation of drought tolerance of fifteen lentils (*Lens Culinaris* L.) genotype. *Journal of Agricultural Land and Drought*, 12: 69-77.
- Pessaraki M., 2011. *Handbook of Plant and Crop Stress*, 1245 Pages.
- Polanski Lech G., Khanifar A., Tadeusz W., 2018. Effect of salinity and drought stresses on growth parameters, essential oil constituents and yield in peppermint. *African Journal of Agronomy*, 6: 356-361.
- Rahimi Y., Taleei A., Ranjbar M., 2019. Effect of water stress on Biochemical changes in *Mentha piperita* L. *Iranian Journal of Field Crop Science*, 50: 59-75.
- Souri M.K., Hatamian M., 2019. Aminochelates in plant nutrition: a review. *Journal of Plant Nutrition*, 42: 67-78.
- Tang W., Newton J.R., 2005. Polyamines reduced salt-induced oxidative damage by increasing the activities of antioxidant enzymes and decreasing lipid peroxidation in Virginia pine. *Plant Growth Regul.*, 46: 31-43.
- Tardieu F., Parent B., Caldeira C.F., Welcker C., 2014. Genetic and physiological controls of growth under water deficit. *Plant Physiology*, 164: 1628-1635.
- Tognolini M., Barocelli E., Ballabeni V., Bruni R., Bianchi A., Chiavarini M., Impicciatore M., 2005. Comparative screening of plant essential oils. Phenylpropanoid moiety as basic core for antiplate activity. *Life Sci*, 78: 1419-1432.
- Xoconostle-Cázares B., Ramirez-Ortega F.A., Flores-Elenes L., Ruiz-Medrano R., 2011. Drought tolerance in crop plants. *American Journal of Plant Physiology*, 5: 241-256.



Citation: R.M. Ferrara, N. Martinelli, G. Rana (2020) CO₂ and H₂O fluxes due to green manuring under Mediterranean conditions. *Italian Journal of Agrometeorology* (2): 45-53. doi: 10.13128/ijam-972

Received: June 22, 2020

Accepted: September 13, 2020

Published: January 25, 2021

Copyright: © 2020 R.M. Ferrara, N. Martinelli, G. Rana. This is an open access, peer-reviewed article published by Firenze University Press (<http://www.fupress.com/ijam>) and distributed under the terms of the Creative Commons Attribution License, which permits unrestricted use, distribution, and reproduction in any medium, provided the original author and source are credited.

Data Availability Statement: All relevant data are within the paper and its Supporting Information files.

Competing Interests: The Author(s) declare(s) no conflict of interest.

CO₂ and H₂O fluxes due to green manuring under Mediterranean conditions

ROSSANA MONICA FERRARA, NICOLA MARTINELLI, GIANFRANCO RANA*

CREA, Research Centre for Agriculture and Environment

*Corresponding author. E-mail: gianfranco.rana@crea.gov.it

Abstract. Green manure (GM) is supported by agronomical protocols for improving soil fertility and sustainability of agriculture. The environmental and agronomical efficiency of GM can be evaluated in terms of carbon dioxide (CO₂) and water (H₂O) fluxes. These fluxes were monitored by eddy covariance method, together with meteorological data, before and after faba bean (*Vicia faba* spp. minor L.) GM performed in a semi-arid Mediterranean region. The addition of fresh biomass into the soil increases the microbial activity with a positive priming effect: the addition of ready decomposable carbon to the soil increased CO₂ respiration and surface evaporation. The measured C emitted under CO₂ form during the whole experimental period corresponded to 78% of the C incorporated, while evaporated H₂O in the same period represented 72% of water supplied by encapsulated biomass and precipitations. The cumulated loss of C after GM until the soil preparation of the successive crop was 2957 kgC ha⁻¹, in the same period 200 mmH₂O were lost by soil evaporation.

Keywords. Faba bean (*Vicia faba* spp. minor L.), semi-arid, eddy covariance, surface temperature, aridity index.

1. INTRODUCTION

The green manure (GM) by using a short-season legume crop is a suitable agro-technique because improves soil organic carbon content (C), sustains productivity and represents an important ecosystem service mainly related to the soil nitrogen (N) recycling (Yadav et al., 2000; Tosti and Guiducci, 2010; Couëdel et al., 2018). The practice is suggested by national and international agronomical protocols, such as the developing plan of rural areas of Italian regions (PSR 2014-2020, Measure 10.1.2) which supports the introduction of faba bean or field peas between two cereal crops, and the European EC Regulation No 834/2007 which imposes GM in organic production (EC, 2007). The ploughing of legume cover crops is usually performed between the flowering and the early pod stages, leaving biomass on the surface or/and incorporating it, whole or chopped, into the soil, ensuring N and C gains for the development of the subsequent crop (i.a. Al-luvione et al., 2010). Furthermore, GM increases soil fertility and quality (Zhang and Fang, 2007) and stimulates microbial growth and activity and nutrient mineralization (Eriksen and Gross, 2005). In particular, faba bean (*Vicia faba* L.)

can provide up to 270 kg fixed N ha⁻¹ (Köpke and Nemecek, 2010), including a contribution of 100 kgN ha⁻¹ from the below-ground biomass (Rochester et al., 1998). However, the application of residues with low C:N such as the legume crops increases the rate of biomass decomposition (De Neve and Hofman, 1996), increasing carbon dioxide (CO₂) fluxes (Huang, et al., 2004). Muhammad et al. (2019), by a meta-analysis, showed that residues placed at soil surface will reduce CO₂ emissions compared to their incorporated due to a decreasing in the rate of decomposition. The ending of CO₂ losses due to GM is uncertain: the CO₂ emission process can exhausted in a few days (Alluvione et al., 2010; Heller et al. 2010; Shaaban et al., 2016), in one month (Mancinelli et al., 2013) or it can last until several months (Curtin et al., 2000). Surely, when GM implies crop incorporation into the soil, the starting of CO₂ emissions after GM are due to the tillage operation which causes the sudden physical release of CO₂ entrapped in soil pores from previous microbial activity (Reicosky et al., 1997). The duration of this *degassing*, as defined by Rochette and Angers (Rochette et al., 1999), can be of few hours, depending on soil microclimatic conditions during the time of the year when the tillage is performed (Álvaro-Fuentes et al., 2007; Rochette et al., 1999). Moreover, the CO₂ emissions can be explained by the increased soil organic matter (SOM) decomposition due to the addition to the soil of fresh biomass containing ready decomposable C (Kuzyakov and Domanski, 2000). However, literature reports different outcomes when comparing CO₂ fluxes from bare and GM amended soil, with cases of no differences (Liebig et al., 2010) and others showing an increasing of CO₂ losses by GM (Kallenbach et al., 2010). These differences can be explained taking into account the plant species and critical high emission moments after cover crop residues addition to the soil (Bodner et al., 2018). Mancinelli et al. (2013) demonstrated that when the green matter is incorporated into the soil, the combined effect of temperature and precipitation, given in terms of aridity index, could cause a priming effect of SOM, also promoting soil mineralization processes and increasing CO₂ fluxes.

Finally, considering the impact of water and temperature on soil CO₂ dynamics, it is necessary to evaluate CO₂ fluxes either before or after GM, as well as to study their relationships with H₂O fluxes and temperature regime, in order to understand the effects of GM on the environment in any climatic region (Skinner et al., 2019). The continuous monitoring of CO₂ and H₂O fluxes at hourly scale, together with meteorological variables, immediately before and after GM, gives the chance to identify relationships among CO₂ emissions by GM and the climatic conditions.

The main aim of this study was to verify that GM increased soil CO₂ emissions due to (i) tillage and (ii) input

of organic residues, evaluating the climatic effects on these two sources of CO₂ emissions.

2. MATERIALS AND METHODS

2.1 *The site and the crop*

The trial was carried out on a 2.5 ha field located within the CREA-AA experimental farm sited in southern Italy (Rutigliano-Bari, 41° 01' N, 17° 01' E, altitude 147 m a.s.l.). Faba bean (*Vicia faba spp. minor L.*) was sowed on 19th February 2014 and GM was carried out on 22 May 2014, incorporating crop into the soil at 20 cm depth. Following the usual practice of the area, it could be estimated by eye that almost 70% of the aerial green part of the crop was incorporated into the soil.

The soil was classified as fine, mixed, super-active, thermic Typic Haploxeralfs, clay-loam. Total N and total organic carbon content (TOC) at two depths (0–20 cm and 20–40 cm) were evaluated with mean values equal to 0.92 ± 0.06 gN kg⁻¹ and 10.3 ± 0.12 gC kg⁻¹, respectively.

The climate at the site is classified as semi-arid Mediterranean, with mild winters and warm-dry summers; the mean annual temperature was of 15.7 °C and the mean annual precipitation was of 535 mm year⁻¹ (Campi et al., 2009), mainly concentrated between the autumn and the late winter. The mean annual water deficit (reference evapotranspiration, ET₀ less rain) was 560 mm.

Fresh and dry weight of above and below-ground biomass, together with plant height and double-sided green leaf area (LAI Licor® 300, USA) were measured according to a randomized sampling design. Mean LAI was equal to 6.2 ± 2.2 m² m⁻² and mean height was equal to 81.8 ± 16.6 cm. Above-ground C and N were quantified by TOC Vario Select analyser (Elementar, Germany) and the Kjeldahl method, respectively: the above-ground C and N were 42.2% and 2.7% on a dry weight basis, respectively. The below-ground C and N were equal to 43.2% and 1.6%, respectively. On the basis of the above reported data, the above-ground biomass provided to soil a total estimated supply of 208 kgN ha⁻¹, 3230 kgC ha⁻¹ and 4.6 mmH₂O. The below-ground plant parts contributed with an amount of 22 kgN ha⁻¹, 590 kgC ha⁻¹ and 1.5 mmH₂O, respectively. The C:N ratio was equal to 15.5 and 27.3 for the aboveground and the belowground biomasses, respectively.

2.2 *CO₂ and H₂O fluxes*

CO₂ and H₂O fluxes were measured by eddy covariance (EC) method, a micrometeorological technique

based on the covariance between the instantaneous vertical wind speed (w) and the concentration of the scalar (Lee et al., 2004).

The EC CO₂ and H₂O fluxes were measured in 2014 from March 7th until September 17th: see Rana et al. (2018) for all details about the trial and eddy covariance data analysis carried out by EddyPro[®] software (<http://www.licor.com/eddypro>). In this study the period from May 15th (one week before GM) until September 17th (last day before new soil managements for the following crop) was analysed.

The EC tower were equipped with a three-dimensional sonic anemometer (USA-1, Metek GmbH, Germany) for measuring wind components and sonic temperature, and a fast-responding open-path infrared gas analyser LI-7500 (IRGA, LI-7500, Li-COR Inc., Lincoln NE, USA) for detecting atmospheric CO₂ and H₂O concentrations. These sensors were placed at the centre of the plot at 1.2 m above the top of the canopy, adjusted to follow its growth for the entire growing season, while, after GM, the measurement height was at 1.10 m above soil surface. Data were sampled at 10 Hz by an Industrial Computer (Advantech, USA) running a resident software (MeteoFlux, Servizi Territorio, S.n.c., Cinisello Balsamo, Italy) and recorded at hourly time step.

The Mauder and Foken (2004) and Kormann and Meixner (2001) approaches were followed for performing quality check and footprint analysis, respectively.

2.3 Ancillary measurements and aridity index

Air temperature (T_{air}), relative humidity, precipitation and incident global radiation (R_g) were continuously measured at hourly time step by standard sensors placed on a grass meadow close to the experimental field. The soil-crop surface temperature T_{surf} was measured by four infrared radiometers (IRR-P, Apogee Instruments Inc., Utah, USA) at the centre of the plot, close to the EC tower, positioned 1 m above the crop, at an angle of 60° on the horizontal and pointing toward each of the four cardinal points. Data were collected until 1st July by a CR10X (Campbell Scientific Inc., USA) at a frequency of 0.1 Hz and stored for as hourly averages; on 2nd July a serious failure interrupted the acquisition of T_{surf} values.

The aridity index, AI , firstly introduced by De Martonne (1926) and widely used to link climatic characteristics and agricultural features (see for example Francaviglia et al., 2017; Emadolin and Reinsch, 2018), was calculated at monthly scale as:

$$AI = \frac{P_i}{T_i + 10}$$

where P_i = monthly precipitation, T_i = monthly mean air temperature. Following Mancinelli et al. (2013), the aridity index can be used to assess temporary variations of crop water conditions during crop growing season and can be related to CO₂ flux to verify the relationships between climatic factors and soil respiration.

3. RESULTS AND DISCUSSION

3.1 Meteorological conditions

The weather conditions recorded during the experimental period (T_{air} , R_g , vapour pressure deficit VPD , rain) are reported in Table 1 at monthly scale. In the whole period T_{air} , VPD and R_g followed the typical seasonal patterns for this Mediterranean area, with low values of VPD and R_g recorded during rainy and cloudy days. The precipitation throughout the experimental trial was negligible in the first days after crop incorporation until 14 June, when a huge precipitation event (30.6 mm) occurred; June and July were particularly rainy for this area (see Tab. 1) with precipitations concentrated in few stormy events.

T_{surf} followed T_{air} pattern even if about 10 °C above it during the hottest hours of the day and with similar values during the night-(data not shown).

Tab. 1. Weather variables at monthly scale: air temperature (T_{air}), global radiation (R_g), vapour pressure deficit (VPD), rain: all values are mean, except rain, which is expressed as sum.

Month	T_{air} (°C)	R_g (MJm ⁻² d ⁻¹)	VPD (kPa)	Rain (mm)
May	17.2	20.4	1.4	17.1
June	21.3	24.4	1.8	108.1
July	22.8	21.7	1.8	107.5
August	24.1	21.3	2.0	8.5
September	20.2	15.1	0.8	30.8

Tab. 2. Footprint dimensions during daytime and night-time, calculated with the Kormann and Meixner (2001) footprint approach. Length is the length of the footprint, width is the width of the ellipse at the centre of length.

	Daytime		Night time	
	Length (m)	Half width (m)	Length (m)	Half width (m)
Mean	75.22	9.89	109.99	13.38
Max	203.84	24.40	547.53	53.85

3.2 Footprint analysis

The analysis of the source area is summarised in Tab. 2. The mean peak emitting point of the flux footprint was estimated to be around 12 m away from the mast, while on average 90% contribution to total fluxes during the daytime was provided by an area extending 134.4 m upwind.

3.3 CO₂ and H₂O fluxes

On the experimental period (15 May - 17 September) 56, 32, and 12 % of data were flagged 0 (best quality fluxes), 1 (fluxes suitable for general analysis) and 2 (discarded fluxes), respectively (Kormann and Meixner, 2001).

Fig. 1 shows CO₂ and H₂O fluxes at hourly scale from one week before GM until the end of the monitoring period. Before GM, daily trends of CO₂ fluxes followed the typical pattern of an active green crop with negative daytime photosynthesis values and night-time positive ecosystem respiration values. In the days following the GM, the CO₂ fluxes became positive during daytime, following a typical bell shape pattern; in particular, only soil respiration was detected until the soil remained bare. During the first 6 days immediately after GM the increasing observed in CO₂ emissions was due to the effect of tillage performed for incorporating the faba bean, after that the pattern of CO₂ flux was gently decreasing until the end of the considered period of measurements. During the last three days of monitoring, the CO₂ fluxes showed the pattern of an active green crop since the emerging of weeds started. It is also clear that the CO₂ emissions increased after any effective

rain event, mainly due to the restart of decomposition of encapsulated biomass of remaining residue (Muhammad et al., 2019; Curtin et al., 2000), this behaviour was also observed in other studies (Álvaro-Fuentes et al., 2007), and can be explained by the physical release of the CO₂ entrapped in soil pores due to water filling and by the subsequent stimulation of soil microbial activity.

To further investigate the effect of ploughing on CO₂ emissions a zoom on the period immediately before and after GM until the first effective rain (13 June) is reported in Fig. 2, where the components of ecosystem respiration were obtained by the partitioning method applied to the eddy covariance data (Rana et al., 2018). In particular, considering the short-term effect of tillage, few days after GM, CO₂ emission was the result of the above-mentioned *degassing* and the stimulated soil microbial activity by the addition of fresh biomass. The soil respiration increased from 1.76 $\mu\text{molm}^{-2}\text{s}^{-1}$ (mean over the week before tillage) to 5.46 $\mu\text{molm}^{-2}\text{s}^{-1}$ (mean over 6 days after GM).

In order to take into account the effect of water on CO₂ fluxes, hourly fluxes of H₂O were also analysed. Before the GM the water (see Fig. 1) showed the typical daily patterns and absolute values of the actual evapotranspiration of a well-watered crop under Mediterranean climate (Katerji and Rana, 2006). With the termination of the crop by the GM, the H₂O flux decreased due to plant transpiration suppression and only evaporation process occurring. This clear trend did not occur after the first rain effective event on 13th June, in fact after this day the H₂O evaporation from bare soil was addressed by the soil water content following the water supply. Other details, including the overall trends of CO₂ and H₂O fluxes for this crop along the growing season since plants' emergence, are reported

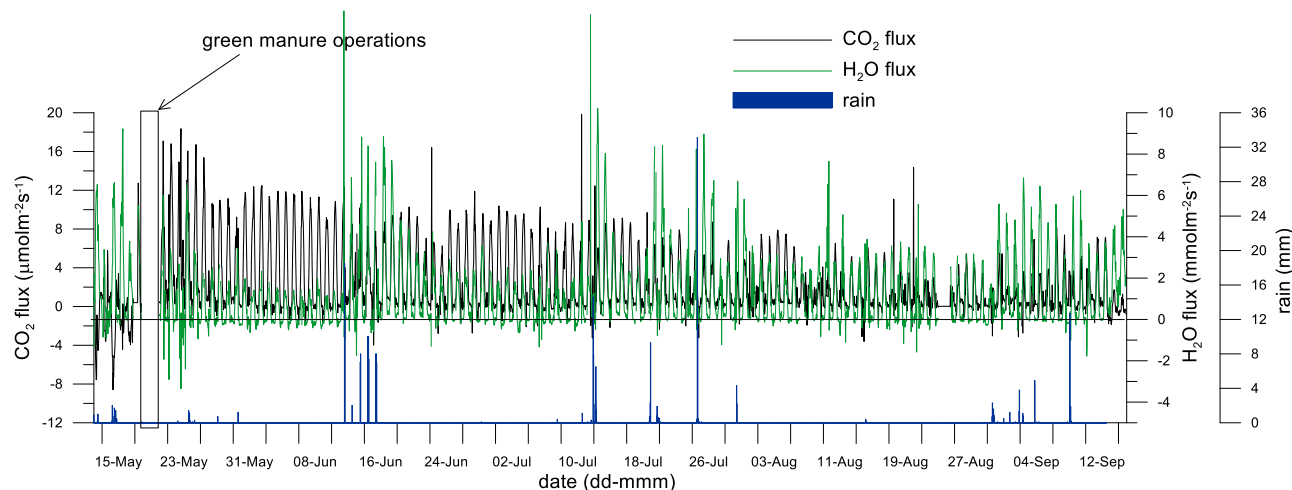


Fig. 1. Time trends of hourly CO₂ and H₂O fluxes during the trial. The rainfall and the time interval of harrowing operation for green manure are also indicated.

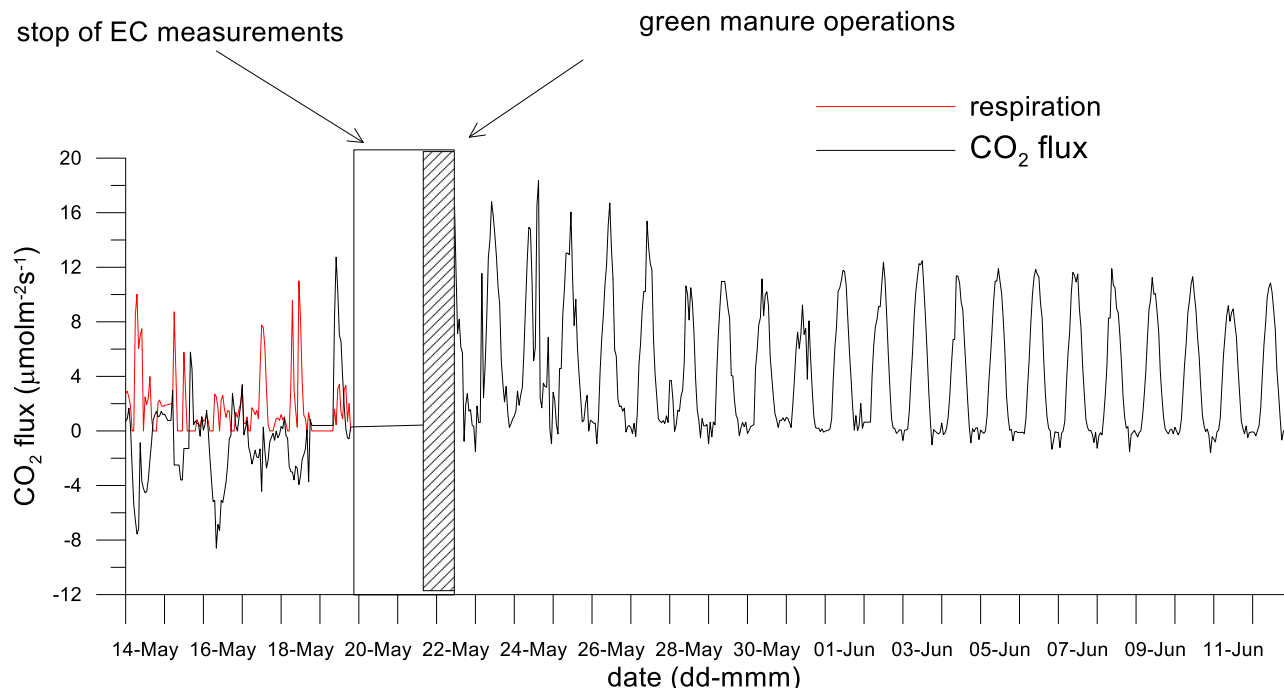


Fig. 2. Zoom of soil respiration from one week before green manure (GM) until the day of first effective rain event (13th June).

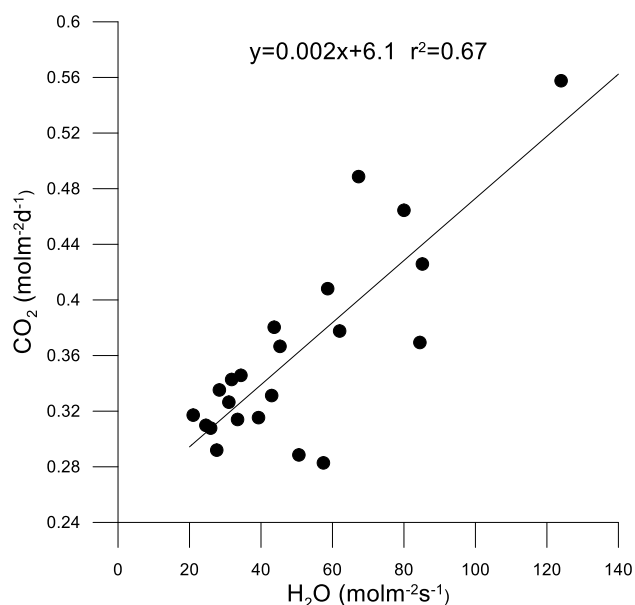


Fig. 3. Daily values of CO₂ vs H₂O fluxes in the first days after green manure until 13th June.

in Rana et al. (2018).

Since both CO₂ and H₂O fluxes decreased in absolute values starting from the first day after GM until 13th June, a possible relationship between these two variables was inves-

tigated. Actually, the comparison between total daily values of CO₂ and H₂O fluxes (Fig. 3) confirmed a correlation between them due to the analogy in the mechanisms of transport toward the atmosphere of these gases of non-stomatal origin in the absence of rain (Scanlon and Sahu, 2008).

3.4 Soil Surface Temperature effect on H₂O and CO₂ fluxes

Considering the widely demonstrated relationship between surface temperature and the soil surface evaporation (Kalma et al., 2008; Qiu and Ben-Asher, 2010), the linkage between these variables was investigated at daily scale, always taking into account the period from one week before GM until 13th June. Fig. 4 showed a clear decreasing of H₂O fluxes with the increasing of surface temperature. In particular, two periods can be distinguished: the first one before GM, when the green crop was active, and the second one; after GM, when plants were dead and encapsulated into the soil.

Then, considering that CO₂ emissions were strongly related to soil surface evaporation (see Fig. 3), which depends on surface temperature (see Fig. 4), the relationship between CO₂ emissions and the mean daily surface temperature was further investigated. The daily trend of CO₂ flux until 13th June is shown in Fig. 5: it is clear that the CO₂ flux sudden increased after GM for tillage effect. Moreover, CO₂ emissions further increased after rainy days

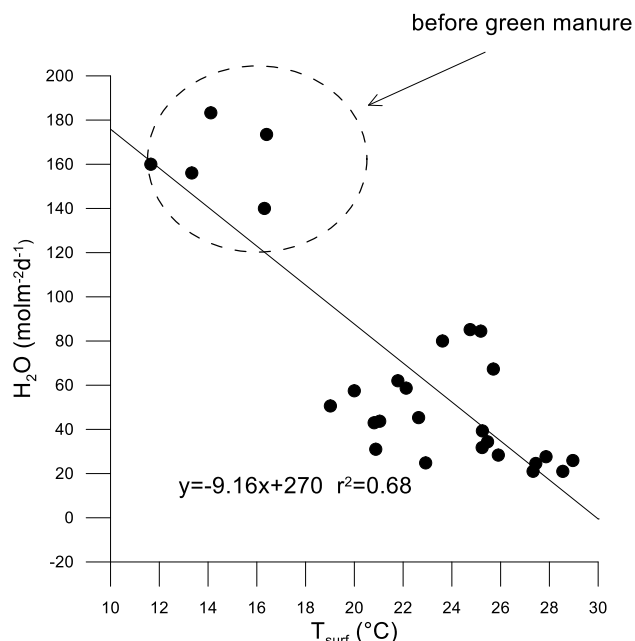


Fig. 4. Daily H_2O fluxes vs surface temperature (T_{surf}) for the period 15 May - 13 June.

on 26th and 30th May and 1st June. One week before GM the daily CO_2 balance was still negative, and the actively growing crop performed as a CO_2 sink. Just after the GM incorporation, the soil became a net source of CO_2 , reaching a maximum 2 days after the GM (24 May, around $0.5 \text{ mol m}^{-2} \text{ d}^{-1}$) and slowly decreasing for several days until it

became almost constant during the last displayed thirteen days. These results are supported by other authors: Mancinelli et al. (2013) reported analogous trends for the peaks of CO_2 emitted immediately after green manuring due to the addition of fresh biomass containing ready decomposable C, which enhances SOM decomposition (Kuzayakov and Domanski, 2000). This positive priming effect results in soil organic matter mineralization and subsequent CO_2 efflux toward atmosphere.

The relationship between CO_2 emissions as daily mean of fluxes ($\mu\text{molm}^{-2}\text{s}^{-1}$) and T_{surf} is displayed in Fig. 6 by considering all available T_{surf} data (from May 23th until July 1st). In the first two weeks after incorporation (red symbols) CO_2 emissions were strongly related to T_{surf} while during the last monitored weeks (white symbols) T_{surf} increasing was not related to any increasing in CO_2 emissions. This latter lack of relationship between T_{surf} and CO_2 fluxes could be explained considering that in this stage CO_2 fluxes likely came from layers of soil below the soil surface where surface temperature did not have effect. This behaviour is similarly to the results reported by Rochette et al. (2000) and Bol et al. (2003) for CO_2 emissions following slurry-C incorporation in grassland. These authors highlighted a two-stage decomposition process: (i) rapid increase in emitted CO_2 due to the decomposition of the labile and easily available fraction of C contained in the biomass, (ii) slow decrease due to decomposition of less available recalcitrant C material. In the present study, the advantage is the chance to follow at hourly scale in continuous the dynamics of these CO_2

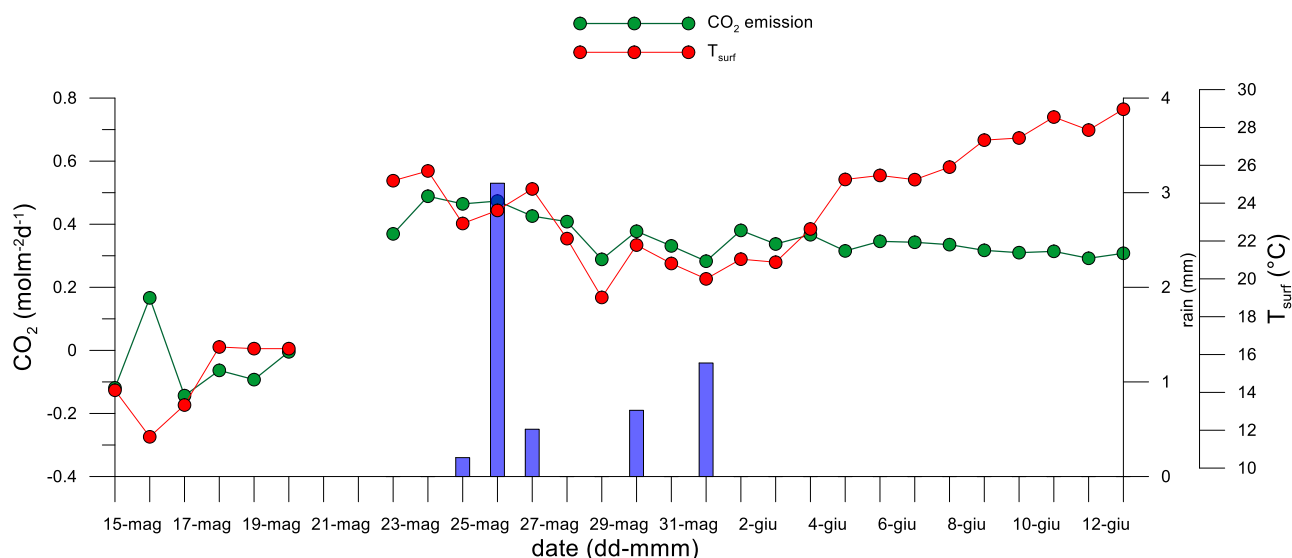


Fig. 5. Daily rain, CO_2 fluxes and surface temperature (T_{surf}) from one week before green manure (GM) until the first effective rain (13th June).

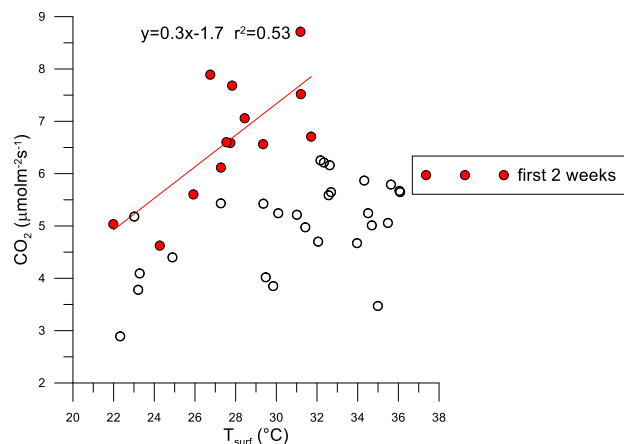


Fig. 6. Relationship between CO₂ emissions as means of hourly fluxes at daily scale and mean daily surface temperature.

releases coming from two different sources, highlighting also the effect of tillage.

The strong relationship between surface temperature and CO₂ flux during the first two weeks after GM could suggest that the majority of CO₂ production occurred in plants residue likely before it was completely dry. Parkin and Kasper (2003), in residue covered no-till field crops (corn and soybean) in Iowa (USA), and Rana et al. (2016), in a bioenergetic crop in semi-arid climate in Italy, found similar relations between CO₂ flux and soil surface temperature.

3.5 CO₂ fluxes and the Aridity Index

Fig. 7 displays the cumulated monthly soil CO₂ fluxes (in mol m⁻²) in function of the monthly values of AI: the greatest values of CO₂ corresponds to the highest value of AI. This result is in agreement with Mancinelli et al. (2013): under Mediterranean conditions, high AI value at the time of green manuring may promote the start of soil mineralization processes which may result in a priming effect of native SOM. Thereafter, the decreasing in AI corresponds in a decreasing of CO₂ fluxes. In order to develop a finding useful for agronomical purpose, a linear relationship between CO₂ flux and AI at monthly scale was investigated (see small upper panel in Fig. 7), founding $CO_2 = 0.07 AI + 0.06$ with high value of r^2 (0.68).

4. CONCLUSIONS

Eddy covariance measurements of CO₂ and H₂O fluxes before and after the GM of faba were performed in a typical dry environment of the Mediterranean basin. During the trial, the starting of increased soil metabolic activ-

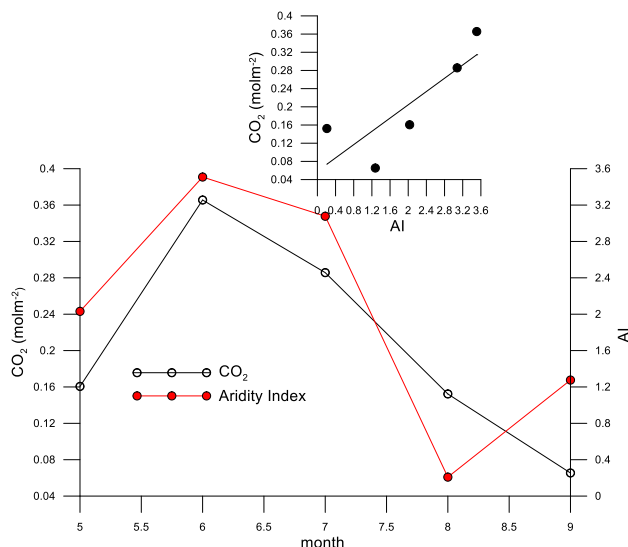


Fig. 7. Monthly patterns of Aridity Index and CO₂ flux in the experimental period; in the small upper panel the relationship between these variable is illustrated ($CO_2 = 0.07 AI + 0.06$ $r^2 = 0.68$).

ity and respiration due to GM was monitored in terms of increasing in CO₂ emissions, highlighting the *degassing* effect due to tillage and the emissions due to decomposition of new fresh biomass following GM: this latter CO₂ emissions was not affected by the surface temperature.

Furthermore, the addition to the soil of fresh biomass containing ready decomposable C increased CO₂ respiration and surface evaporation. The measured C emitted under CO₂ form during the whole experimental period correspond to 78% of the C incorporated, and evaporated H₂O in the same period represents 72% of water supplied by encapsulated biomass and precipitations.

The cumulated loss of C after the GM until the soil preparation of the successive crop was 2957 kgC ha⁻¹; in the same period, 200 mmH₂O were lost by soil evaporation. This value of emitted C after GM is comparable to those found by Hoyle et al. (2011) which report between 50% and 75% of the C in plant residues can be lost as CO₂ by microbes during the first year of decomposition.

ACKNOWLEDGEMENTS

The authors dedicate this study to the memory of Dr Domenico Palumbo.

The work was funding by Italian Project "Biodati" funded by the Italian Ministry of Agricultural, Food and Forestry Policies and Tourism. The data analysis and paper writing were fully supported by the AgriDigit-Agro-modelli project (DM n. 36502 20/12/2018), funded by the

Italian Ministry of Agricultural, Food and Forestry Policies and Tourism.

The authors would like to thank the colleagues from CREA-AA of Bari for their support: in particular, we wish to thank Dr Angelo D. Palumbo for agronomic management of the trial, Dr Carolina Vitti and Mr Marcello Mastangelo for soil and plant laboratory analysis.

REFERENCES

- Alluvione, F. Bertora, C. Zavattaro, L. Grignani, C., 2010. Nitrous Oxide and Carbon Dioxide Emissions Following Green Manure and Compost Fertilization in Corn. *Soil Sci. Soc. Am. J.*, 74(2), 384–395.
- Álvaro-Fuentes, J. Cantero-Martínez, C. López, M.V. Arrúe, J.L., 2007. Soil carbon dioxide fluxes following tillage in semiarid Mediterranean agroecosystems. *Soil Till. Res.*, 96, 331–341
- Bodner, G. Mentler, A. Klik, A. Kaul, A.-P. Zechmeister-Boltenstern, S., 2018. Do cover crops enhance soil greenhouse gas losses during high emission moments under temperate Central Europe conditions? *J. Land Manage. Food Environ.*, 68, pp. 171–187
- Bol, R. Moering, J. Kuzyakov, Y. Amelung, W., 2003. Quantification of priming and CO₂ respiration sources following slurry-C incorporation into two grassland soils with different C content. *Rapid Commun. Mass Spectrom.*, 17, 2585–2590, DOI: 10.1002/rcm.1184.
- Campi, P. Palumbo, A.D. Mastrorilli, M., 2009. Effects of tree windbreak on microclimate and wheat productivity in a Mediterranean environment. *Eur. J. Agron.*, 30, 220–227.
- Couëdel, A. Alletto, L. Tribouillois, H. Justes, E., 2018. Cover crop crucifer-legume mixtures provide effective nitrate catch crop and nitrogen green manure ecosystem services agriculture. *Ecosyst. Environ.*, 254, 50–59.
- Curtin, D. Wang, H. Selles, F. Zentner, R.P. Biederbeck, V.O. Campbell, C.A., 2000. Legume green manure as partial fallow replacement in semiarid Saskatchewan: effect on carbon fluxes. *Can. J. Soil Sci.*, 80, 499–505.
- De Martonne, E., 1926. L'indice d'aridité Bulletin de l'Association des Géographes Français 9, 3–5.
- De Neve, S. Hofman, G., 1996. Modelling N mineralization of vegetable crop residues during laboratory incubations. *Soil Biol Biochem*, 28, 1451–1457.
- EC, European Commission, 2007. Council Regulation (EC) No 834/ 2007 of 28 June 2007 on organic production and labelling of organic products and repealing Regulation (EEC) No 2092/91. Official Journal of the European Union L 189: 1–23.
- Emadodin, I., Reinsch, T., 2018. Assessing the impact of land use change on aridification in semiarid land. *Land Degrad Dev*, 29, 3423–3431.
- Eriksen, J. Gross, L., 2005. Sulphur mineralization-immobilization turnover in soil amended with plant residues. *Soil Biol. Biochem.*, 37, 2216–2224.
- Francaviglia, R., Di Bene, C., Farina, R., Salvati, L., 2017. Soil organic carbon sequestration and tillage systems in the Mediterranean Basin: a data mining approach. *Nutr Cycl Agroecosyst*, 107, 125–137.
- Heller, H. Bar-Tal, A. Tamir, G. Bloom, P. Venterea, R.T. Chen, D. et al., 2010. Effects of manure and cultivation on carbon dioxide and nitrous oxide emissions from a corn field under Mediterranean conditions. *J Environ Qual*, 39, 437–48.
- Hoyle, F.C., Baldock, J.A., Murphy, D.V., 2011. Soil organic carbon—role in Australian farming systems. In: Tow P, Cooper I, Partridge I, Birch C (eds) Rainfed farming systems. Springer, Netherlands, pp. 339–361
- Huang, Y. Zou, J. Zheng, X. Wang, Y., Xu, X., 2004. Nitrous oxide emissions as influenced by amendment of plant residues with different C:N ratio. *Soil Biol Biochem*, 36, 973–981. <https://doi.org/10.1016/j.soilbio.2004.02.009>
- Kallenbach, C.M. Rolston, D.E Horwath, W.R., 2010. Cover cropping affects soil N₂O and CO₂ emissions differently depending on type of irrigation. *Agriculture, Ecosystems and Environment*, 137, 251–260.
- Kalma, J.D., McVicar, T.R., McCabe, M.F., 2008. Estimating land surface evaporation: a review of methods using remotely sensed surface temperature data. *Surv Geophys*, 29, 421–469.
- Katerji, N. Rana, G., 2006. Modelling evapotranspiration of six irrigated crops under Mediterranean climate conditions. *Agricultural and Forest Meteorology*, 138, 142–155.
- Köpke, A., Nemecek, T., 2010. Ecological services of faba bean. *Field Crops Res*, 115, 217–233.
- Kormann, R. Meixner, F.X., 2001. An analytical footprint model for nonneutral stratification. *Boundary-Layer Meteorol.*, 99, 207–224.
- Kuzyakov, Y Domanski, G., 2000. Carbon input by plants into the soil. Review. *Journal of Plant Nutrition and Soil Science*, 163, 421–431.
- Lee, X. Massman, W. Law, B.E., 2004. Handbook of micrometeorology: a guide for surface flux measurement and analysis. In: Atmospheric and Oceanographic Sciences Library. Kluwer Academic Publishers, Dordrecht, The Netherlands, pp. 250.
- Liebig, M.A. Tanaka, D.L. Gross, J.R., 2010. Fallow effects on soil carbon and greenhouse gas flux in Central North Dakota. *Soil Science Society of America Journal*, 74, 358–365.

- Mancinelli, R. Marinari, S. Di Felice, V. Savin, M.C. Campiglia, E., 2013. Soil property, CO₂ emission and aridity index as agroecological indicators to assess the mineralization of cover crop green manure in a Mediterranean environment. *Ecological Indicator*, 34, 31–40.
- Mauder, M. Foken, T., 2004. Documentation and Instruction Manual of the Eddy Covariance Software Package TK2, vol. 26. Universität Bayreuth, Abt. Mikrometeorologie, Arbeitsergebnisse, 44 pp., ISSN 1614-8916.
- Muhammad, I. Sainju, U. Zhao, F. Khan, A. Ghimire, R. Fu, X. et al., 2019. Regulation of soil CO₂ and N₂O emissions by cover crops: a meta-analysis. *Soil Till. Res.*, 192, 103–112.
- Parkin, T.B. Kaspar, T.C., 2003. Temperature Controls on Diurnal Carbon Dioxide Flux: Implications for Estimating Soil Carbon Loss. *Soil Sci. Soc. Am. J.*, 67, 1763–1772.
- Qiu, G.Y. Ben-Asher, J., 2010. Experimental Determination of Soil Evaporation Stages with Soil Surface Temperature. *Soil Sci. Soc. Am. J.*, 74, 13–22, doi:10.2136/sssaj2008.0135
- Rana G. Ferrara R.M. Vitale D. D'Andrea L. Palumbo A.D., 2016. Carbon assimilation and water use efficiency of a perennial bioenergy crop (*Cynara cardunculus* L.) in Mediterranean environment. *Agricultural and Forest Meteorology*, 217, 137–150.
- Rana. G. Palatella, L. Scanlon. T.M. Martinelli, N. Ferrara, R.M., 2018. CO₂ and H₂O flux partitioning in a Mediterranean cropping system. *Agricultural and Forest Meteorology*, 260–261, 118–130.
- Reicosky, D.C. Dugas, W.A. Torbert, H.A., 1997. Tillage-induced soil carbon dioxide loss from different cropping systems. *Soil Till. Res.*, 41, 105–118
- Rochester, I.J. Peoples, M.B. Constable, G.A. Gault, R.R., 1998. Faba beans and other legumes add nitrogen to irrigated cotton cropping systems. *Aust. J. Exp. Agric.*, 38 (3), 253–260.
- Rochette, P. Angers, D.A., Côté, D., 2000. Soil Carbon and Nitrogen Dynamics Following Application of Pig Slurry for the 19th Consecutive Year I. Carbon Dioxide Fluxes and Microbial Biomass Carbon. *Soil Sci. Soc. Am. J.*, 64, 1389–1395, doi:10.2136/sssaj2000.6441389x
- Rochette, P. Angers, D.A., 1999. Soil surface carbon dioxide fluxes induced by spring, summer, and fall moldboard plowing in a sandy loam. *Soil Sci. Soc. Am. J.*, 63, 621–628
- Scanlon, T.M. Sahu, P., 2008. On the correlation structure of water vapor and carbon dioxide in the atmospheric surface layer: a basis for flux partitioning. *Water Resour. Res.*, 44, W10418.
- Shaaban, M. Peng, Q. Hu, R. Lin, S. Zhao, J., 2016. Soil Nitrous oxide and Carbon dioxide emissions following incorporation of above- and below-ground biomass of green bean. *Int. J. Environ. Sci. Technol.*, 13, 179–186. <https://doi.org/10.1007/s13762-015-0843-9>
- Skinner, C. Gattinger, A. Krauss, M. Krause, H.-M. Mayer, J. van der Heijden, M.G.A. Mäde, P., 2019. The impact of long-term organic farming on soil-derived greenhouse gas emissions. *Sci Rep*, 9, 1702, <https://doi.org/10.1038/s41598-018-38207-w>.
- Tosti, G. Guiducci, M., 2010. Durum wheat-faba bean temporary intercropping: Effects on nitrogen supply and wheat quality. *Eur. J. Agron.*, 33, 157–165.
- Yadav, R.L. Dwivedi, B.S. Pandey, P.S., 2000. Rice-wheat cropping system: assessment of sustainability under green manuring and chemical fertilizer inputs. *Field Crops Res*, 65, 15–30.
- Zhang, M.K., Fang, L., 2007. Effect of tillage, fertilizer and green manure cropping on soil quality at an abandoned brick making site. *Soil Till Res*, 93, 87–93.



Citation: A. Laaboudi, A. Slama (2020) Using Neuro-fuzzy and linear models to estimate reference Evapotranspiration in South region of Algeria (A comparative study). *Italian Journal of Agrometeorology* (2): 55-64. doi: 10.13128/ijam-971

Received: June 18, 2020

Accepted: July 26, 2020

Published: January 25, 2021

Copyright: ©2020 A. Laaboudi, A. Slama. This is an open access, peer-reviewed article published by Firenze University Press (<http://www.fupress.com/ijam>) and distributed under the terms of the Creative Commons Attribution License, which permits unrestricted use, distribution, and reproduction in any medium, provided the original author and source are credited.

Data Availability Statement: All relevant data are within the paper and its Supporting Information files.

Competing Interests: The Author(s) declare(s) no conflict of interest.

Using Neuro-fuzzy and linear models to estimate reference Evapotranspiration in South region of Algeria (A comparative study)

ABDELKADER LAABOUDI^{1*}, ABDELJALIL SLAMA²

¹ National Institute of research in agronomy of Algeria. Experimental station of Adrar, Algeria

² Laboratory of Mathematics, Modeling and Applications (LAMMA), University of Adrar, Algeria

*Corresponding author. E-mail: Laaboudiaek@yahoo.fr

Abstract. In order to estimate daily reference evapotranspiration (ET_o) in arid region of Algeria, Adaptive Neuro-Fuzzy Inference System (ANFIS) and regression methods as Robust Regression (RR), Bayesian Regression (BR) and Multiple Linear Regression (MLR) techniques were used to develop models based on four explanatory climatic factors: temperature, relative humidity, wind speed and sunshine duration. These factors have been used as inputs, and ET_o values computed by the Penman-Monteith formula have been used as outputs. Determination coefficient (R²), root mean square error (RMSE), Mean absolute error (MAE), mean absolute relative error (MARE) and Nash-Sutcliffe efficiency coefficient (NSE) were used to evaluate the performance of models developed with different input configurations. We concluded that RR, BR and MLR models were able to successfully estimate ET_o, but ANFIS technique seems to be more powerful. Thus, the obtained results by the best ANFIS model, during the test phase are: 0.98, 0.27 (mm/day)², 0.36 (mm/day) and 5.52 % respectively for R, MAE, RMSE and MARE.

Keywords. Reference evapotranspiration, arid regions, Adaptive Neuro-Fuzzy Inference System, robust regression, Bayesian regression, Penman-Monteith formula.

1. INTRODUCTION

Evapotranspiration (ET) is an important factor in climatological, hydrological and agricultural management. So its estimate is of vital importance for irrigation scheduling, water resources planning and management, and for drought forecasting (e.g. Abyaneh et al., 2010, Meng et al., 2018, Lee et al. 2012). Thus, the evapotranspiration is used to compute many Drought Indices as Reconnaissance Drought Index (RDI) (Tsakiris et al., 2007), the water surplus variability index (WSVI) (Gocic and Trajkovic, 2014) and standardized precipitation evapotranspiration index (SPEI) (Vicente-Serrano et al., 2010). To

estimate reference evapotranspiration (ET_o), the Penman-Monteith (PM) equation has been recommended as the standardized equation, but it has high requirements of climatic data (Peng et al. 2017, Wable et al. 2019). However, in developing countries, application of this equation for ET_o estimation has certain limitations due to unavailability of specific data requirements (Naidu and Majhi, 2019).

According to Tabari et al. (2012), Practitioners and researchers need to be provided with guidance on the choice of the most appropriate ET_o method to be adopted when weather data are insufficient to apply the Penman-Monteith method. In this context, some researchers was evaluated the reliability of simplified pan-based approaches for estimating ET_o directly that do not require the data of meteorological parameters (Trajkovic et al., 2010). Others have used the modeling approaches (Keshtegar et al., 2018). In this direction we have decided to use modeling techniques to estimate ET_o based on a daily time step. Thus, Adaptive neuro-fuzzy inference system (ANFIS), robust regression (RR), Bayesian regression (BR) and multiple linear regression (MLR) models were developed and compared to each other.

Multiple Linear Regression method is one of the most widely known modeling techniques. It was used for reference evapotranspiration modeling either alone (Yirga, 2019) or for a comparison (Khoshravesh et al., 2015; 2016; Ozgur et al., 2017) and to examine the relationship between weather parameters and Carbone monoxide (CO) concentration (Ve and Jo, 2016). However, this method is extremely sensitive to deviations from the model assumptions as a normal distribution assumed for the error terms (Stahel, 1997). Consequently, robust regression estimators can be a powerful tool for outlier detection in complicated data sets. For this reason, robust regression model can be the best alternative for multiple linear regression model (Marona et al., 2006).

Bayesian linear regression is an extension of linear regression for modeling and predicting some complex phenomena. It has numerous advantages over classical methods. One of the main advantage of Bayesian predictions over maximum likelihood methods of estimation is an overall increase in accuracy with high levels of reliability on a fraction of the test sample (Braga et al., 2005).

Adaptive Neuro-Fuzzy Inference System (ANFIS) technique which is introduced first by Jange (1993) is a multilayer feed-forward network. It uses neural network training algorithms and fuzzy logic to create an input-output correlation for fuzzy decision rules that perform well on any given task. According to Karimaldini et al. (2012), while neural networks are good at recognizing patterns, they are not good at explaining how they reach to decisions because this technique is, in fact, a black-box for its

user. Fuzzy logic systems are good at explaining their decisions, but they cannot learn and adjust themselves to a new environment. These limitations have been solved with ANFIS technique.

The present study aims to: (1) Investigate the potential of using robust regression, Bayesian regression and ANFIS models to estimate reference evapotranspiration, (2) choose the best approach for users in arid region conditions and (3) to adapt the best models to the climatic conditions in south region of Algeria.

2. MATERIALS AND METHODS

Our study was carried out in the region of Adrar, located in the south-west of Algeria. Latitude: 27°49'N and Longitude: 00°18'E (Fig. 1).

2.1 Climate characteristics

Adrar region is characterized by its extreme meteorological parameters. Its climate is dry throughout the year and is characterized by the extended thermal amplitudes during the year, the month and even the day. The absolute



Fig. 1- Sketch of the investigation area.

maximum temperature reaches 49.5°C in summer (July and August), while, ice and frost are the rare phenomena.

2.2 Description of data and availability

For estimating reference evapotranspiration, the ANFIS, RR BR and MLR models were trained. The entire database (the overall size is, $n = 1825$) was splitting into two datasets, 80% were used in training phase and 20 % remaining were used in test phase.

In the present investigation, daily data (temperature, relative humidity, wind speed and sunshine duration) consist of daily series values recorded throughout the period of 1825 days (From January 2013 to December 2017). The registration of these meteorological statements was performed by the meteorological station located within the experimental site. Using these observed climatic data, daily values of ETo were computed initially using the Penman-Monteith (Eq. 1). These computed ETo values were used to train the ANFIS models.

2.3 Estimation of reference evapotranspiration

The Penman-Montheith equation used for estimating reference evapotranspiration is written as bellow (Allen et al., 1998):

$$ETo = \frac{0.408\Delta(R_n - G) + \gamma \frac{900}{T+273} u_2 (e_s - e_a)}{\Delta + \gamma(1+0.34u_2)} \quad (1)$$

Where ETo is the reference evapotranspiration (mm day^{-1}), R_n is the net radiation at the crop surface ($\text{MJ m}^{-2} \text{day}^{-1}$), G is the soil heat flux density ($\text{MJ m}^{-2} \text{day}^{-1}$), T is the mean of daily air temperature at 2 m height ($^{\circ}\text{C}$), u_2 is the wind speed at 2 m height (m s^{-1}), e_s is the saturation vapor pressure (kPa), e_a is the actual vapor pressure (kPa), $(e_s - e_a)$ is the saturation vapor pressure deficit (kPa), Δ is the slope vapor pressure curve ($\text{kPa } ^{\circ}\text{C}^{-1}$), γ is the psychometric constant ($\text{kPa } ^{\circ}\text{C}^{-1}$).

The parameters air temperature, relative humidity, wind speed and sunshine duration: were taken directly from the meteorological station and were used to estimate other parameters. According to Doorenbos and Pruitt (1977), net radiation and the saturation vapor pressure deficit can be estimated by air temperature and sunshine duration. Net radiation is the difference between the net short wave radiation (R_{ns}), and the outgoing net long wave radiation (R_{nl}).

$$R_n = R_{ns} - R_{nl} \quad (2)$$

if

$$R_{ns} = (1-\alpha)(0.25+0.50\frac{n}{N})Ra \quad (3)$$

and

$$R_{nl} = f(t).f(ea).f(n/N) \quad (4)$$

$$R_n = (1-\alpha)(0.25+0.50\frac{n}{N})Ra - f(t).f(ea).f(n/N) \quad (5)$$

2.4 Statistics of meteorological variables

The statistical features of meteorological variables and evapotranspiration in training and test subsets (Tab. 1) indicate that the data structures of these subsets have the same characteristics.

It can be noted that the variability range of meteorological parameters in the study area was very large. For instance, the daily values of temperature ranged between 7.10 $^{\circ}\text{C}$ and 42 $^{\circ}\text{C}$: relative humidity ranged between 17.50 % and 95 %, wind speed ranged between 0.00 and 4.27 ms^{-1} and sunshine duration ranged between 0.00 to 12.35 hours per day. Hence, any model developed on this data set should have a wide application in all regions that have meteorological parameters in the range the of the study area. The standard deviation values indicated that the variability of meteorological variable values is very important.

The correlations of all input variables are presented in (Tab. 2). This table shows that the linear correlations between ETo and two independent variables: temperature, and relative humidity are very high. Their values are 0.85 and -0.86 respectively Hence, any model that uses these explanatory climatic parameters should be able to estimate the ETo satisfactorily.

Tab. 1. Statistics of meteorological variables in training, test and validation data subsets. T temperature, RH Relative humidity, U_2 Wind speed and n sunshine duration.

Phases	Statistic parameters	T ($^{\circ}\text{C}$)	RH (%)	U_2 (ms^{-1})	n (h.day $^{-1}$)
Training	Min	7.10	17.50	0.00	0.00
	Max	42.00	95.00	4.27	12.35
	Mean	25.92	41.60	1.62	9.14
	Std	9.02	14.03	0.72	2.74
Testing	Min	10.75	23.50	0.28	0.00
	Max	42.25	90.00	4.18	12.35
	Mean	26.34	46.71	1.48	8.81
	Std	8.97	16.38	0.61	2.26

Tab. 2. Correlation matrix between input and output variables.

	Temperature	Humidity	Wind speed	Sunshine duration	ETo
Temperature	1.00				
Humidity	-0.81	1.00			
Wind speed	0.07	0.03	1.00		
Sunshine duration	0.28	-0.39	0.05	1.00	
ETo	0.86	-0.85	0.31	0.57	1.00

The temperature and humidity are also highly correlated. Therefore, a combination of these two factors may provide a good estimate of reference evapotranspiration. It should be noted that all these correlations between variables are linear type but the ETo is universally considered a nonlinear process dependent on interacting meteorological variables (Laaboudi et al., 2012; Fang et al., 2018).

2.5 Adaptive neuro-fuzzy inference system (ANFIS)

An adaptive network, as its name implies, is a network structure consisting of nodes and directional links through which the nodes are connected. Moreover, parts or all of the nodes are adaptive, which means each output of these nodes depends on the parameters pertaining to this node and the learning rule specifies how these parameters should be changed to minimize a prescribed error measure (Jange, 1993). In ANFIS, fuzzy rule bases are combined with neural networks to train the system using experimental data and obtain appropriate membership functions for process prediction and control. The inference system has two input variables x and y as each variable has two fuzzy subsets. A typical rule set with two fuzzy if then rule set for a first order Sugeno fuzzy model can be defined as Eq. 6 and 7:

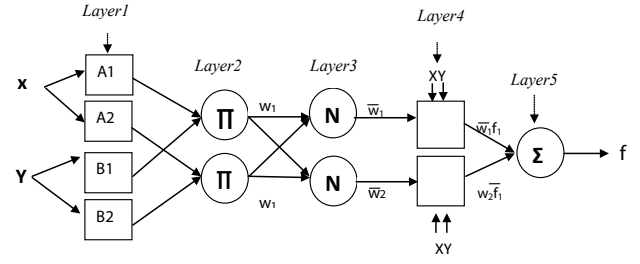
$$\text{Rule 1: If } x \text{ is } A_1 \text{ and } y \text{ is } B_1 \text{ Then } f_1 = p_1x + q_1y + r_1 \quad (6)$$

$$\text{Rule 2: If } x \text{ is } A_2 \text{ and } y \text{ is } B_2 \text{ Then } f_2 = p_2x + q_2y + r_2 \quad (7)$$

Where A_1, A_2 and B_1, B_2 are the membership functions (MFs) for inputs x and y respectively, p_1, q_1, r_1 and p_2, q_2, r_2 are the parameters of the output function. f_1 and f_2 are constant output respectively for rule 1 and rule 2 in ANFIS for the first-order Sugeno inference system.

The general architecture of ANFIS consists of five layers, namely, a fuzzy layer, a product layer, a normalized layer, a defuzzy layer and a total output layer.

The membership function (MF) of each input was tuned using the hybrid method consisting of back propa-

**Fig. 2.** ANFIS architecture with 5 layers. and are the membership functions (MFs) for inputs x and y respectively.

gation for the parameters associated with the input membership function and the least square estimation for the parameters associated with the output membership functions. The architecture of the ANFIS is shown in Fig. 2.

2.6 Multiple Linear Regression (MLR)

Multiple linear regression (MLR) is a statistical approach to modeling the linear relationship between a response (dependent) variable and one or more explanatory (independent) variables.

Given an independent and identically distributed (i.i.d) observations (x_i, y_i) , $i = 1, \dots, n$, in order to understand how the response y_i 's are related to the covariates x_i 's, we traditionally assume the following linear regression model:

$$y_i = x_i^T \theta + \varepsilon_i, \quad (8)$$

Where θ is an unknown $p \times 1$ vector, and the ε_i 's are i.i.d and independent of x_i with $E(\varepsilon_i | x_i) = 0$.

The most commonly used estimate for θ is the ordinary least-square (OLS) estimate that minimizes the sum of squared residuals

$$\sum_{i=1}^n (y_i - x_i^T \theta)^2. \quad (9)$$

2.7 Robust regression (RR)

It is well known that the OLS estimate is extremely sensitive to the outliers. A single outlier can have large effect on the OLS estimate (Yu and Yao, 2017). Thus robust regression analysis provides an alternative to a least squares regression model when fundamental assumptions are unfulfilled by the nature of the data, such as if the distribution of errors is asymmetric or prone to outliers.

The Statistics Toolbox function "robustfit" is useful in these cases. The function implements a robust fitting

method that is less sensitive than OLS to large changes in small parts of the data (Matlab Statistics Toolbox 2010).

Robust regression works by assigning a weight to each data point. Weighting is done automatically and iteratively using a process called *iteratively reweighted least squares*. In the first iteration, each point is assigned equal weight and model coefficients are estimated using ordinary least squares. At subsequent iterations, weights are recomputed so that points farther from model predictions in the previous iteration are given lower weight. Model coefficients are then recomputed using weighted least squares. The process continues until the values of the coefficient estimates converge within a specified tolerance (Matlab Statistics Toolbox 2010). For more details on robust regression, see Fox and Weisberg (2002) and Yu and Yao (2017).

2.8 Bayesian Regression (BR)

Suppose that we are interested in estimating a parameter θ from the data $y = (y_1, y_2, \dots, y_n)$ using a statistical model described by a density $l(y|\theta)$, called the likelihood function or likelihood. Bayesian philosophy states that θ can be considered as random variable with probability distribution $\pi(\theta)$, which is known as the prior distribution, or just the prior. The prior distribution expresses our beliefs about the parameter before examining the data. Given the observed data y , update of beliefs about θ by combining information from the prior distribution and the data by the use of Bayes' theorem, and so the calculation of the posterior distribution, $\pi(\theta|y)$. For the prior distribution we have considered a Jeffrey non-informative prior based on the Fisher information (see Bernard et al. 2000 and Ghosh et al. 2007).

Consider a standard linear regression problem given in (12) and consider $\varepsilon_i, i=1, \dots, n$ are independent and identically normally distributed random variables $N(0, \sigma^2)$, $\sigma > 0$.

The likelihood function $l(y|\theta, \sigma)$ is given by

$$l(y|\theta, \sigma) \propto \sigma^{-n} \exp\left(-\frac{1}{2\sigma^2} \sum_{i=1}^n (y_i - x_i^T \theta)^2\right). \quad (10)$$

With Jeffrey's non-informative prior for (θ, σ) given by

$$\pi(\theta, \sigma) \propto \frac{1}{\sigma}. \quad (11)$$

The posterior distribution of θ , obtained by combination of (10) and (11) is given by:

$$\pi((\theta, \sigma)|y) \propto \sigma^{-n-1} \exp\left(-\frac{1}{2\sigma^2} \sum_{i=1}^n (y_i - x_i^T \theta)^2\right). \quad (12)$$

The posterior distribution (12) is used to estimate the vector parameter (θ, σ) .

The performances of linear regression and ANFIS models were evaluated to compare their predictive accuracies based on the following statistical criteria:

- The coefficient of determination (R^2) is the square of correlation coefficient (r) between the observed and estimated data values of the dependent variable. The coefficient r is expressed as:

$$r = \frac{\sum_{i=1}^n (Y_{obs} - \bar{Y}_{obs})(Y_{sim} - \bar{Y}_{sim})}{\sqrt{\sum_{i=1}^n (Y_{obs} - \bar{Y}_{obs})^2 \sum_{i=1}^n (Y_{sim} - \bar{Y}_{sim})^2}} \quad (13)$$

- The root mean squared error (RMSE):

$$RMSE = \sqrt{\frac{\sum_{i=1}^n (Y_{obs} - Y_{sim})^2}{n}} \quad (14)$$

- The mean absolute error (MAE):

$$MAE = \frac{1}{n} \sum_{i=1}^n |Y_{obs} - Y_{sim}| \quad (15)$$

- The mean absolute relative error (MARE):

$$MARE = \frac{1}{n} \sum_{i=1}^n \frac{|Y_{obs} - Y_{sim}|}{|Y_{obs}|} \times 100 \quad (16)$$

- The Nash- Sutcliffe efficiency (NSE) coefficient, It is calculated as follows:

$$NSE = 1 - \frac{\sum_{i=1}^n (Y_{sim} - Y_{obs})^2}{\sum_{i=1}^n (Y_{sim} - \bar{Y}_{obs})^2} \quad (17)$$

Where,

NSE: Nash-Sutcliffe efficiency; \bar{Y}_{obs} : Average of observations; Y_{sim} is a simulated variable, Y_{obs} the observed variable, \bar{Y}_{sim} the average of simulated variable, \bar{Y}_{obs} the average of observed variable, n a number of observations.

The NSE coefficient is the Nash-Sutcliffe efficiency coefficient, proposed by Nash and Sutcliffe (1970), It is used to evaluate the predictive power of the model (Latrech et al., 2019).

The Matlab software was used for the implementation and application of ANFIS approach and regression methods (BR, RR MLR). Two phases were employed in ANFIS modeling: training and testing phases.

3. RESULTS AND DISCUSSIONS

For estimating reference evapotranspiration, the ANFIS, RR, BR and MLR models were trained. The results ob-

Tab. 3. Comparison of the models in terms of R, E, RMSE, MAE and MARE

Modeling methods	Datasets	R ²	NSE	RMSE (mm/day)	MAE (mm/day)	MARE (%)
Robust regression	Dataset1	0.951	0.950	0.6045	0.4584	9.6774
	Dataset2	0.966	0.966	0.4622	0.3744	9.0191
Linear Multiple Regression	Dataset1	0.951	0.949	0.5967	0.4665	9.5345
	Dataset2	0.966	0.965	0.4631	0.3756	8.9746
Bayesian regression	Dataset1	0.951	0.949	0.5967	0.4668	11.7285
	Dataset2	0.966	0.965	0.4617	0.3757	8.970
ANFIS (Tr. P) (T.P)	Dataset1	0.982	0.981	0.3660	0.2506	4.7574
	Dataset2	0.984	0.980	0.3579	0.2709	5.5199

Tr.P: Training phase, T.P: test phase.

tained from evaluating performance of these models: in terms of statistical criteria are given in Tab. 3.

As it can be seen in (Tab. 3), the ANFIS model represented more consistent estimates. The ANFIS model has the smallest MAE, RMSE and the highest R² and NSE in the Training and testing phase. In testing phase, the ANFIS model has the smallest RMSE (0.3579), MAE (0.2709) and MARE (5.5199) and the highest R² (0.984) and NSE (0.981). The performance of the ANFIS model on the testing dataset showed that the ANFIS model can be used to provide accurate and reliable reference evapotranspiration (ET_o) prediction. The models RR, BR and MLR are almost similar one to each other. Moreover, from this table, it is evident that all performance criteria illustrate a reasonably good performance for all models. This is meant that all models could provide a good estimation of reference evapotranspiration. Nevertheless, if we deal with each method separately, we find slight differences between them: according to the size of the samples, its dispersion and the number of inputs.

3.1 Adaptive Neuro-Fuzzy Inference System

For the ANFIS approach the model developed in this study provided consistent RMSE, MAE and MARE values during training and testing phases when compared to other models. To find out the best model in among the all ANFIS models 50 and 100 epochs, 2 and 3 number of membership functions were tried for each model (Tab. 4).

While in training phase there were slight differences in terms of RMSE according to number of membership functions (MF), in testing phase, all models with the same number of MF are similar one to each other in terms of RMSE. Thus, their values are 0.358 mm/day for 2 MF and 0.475 mm/day for 3 MF respectively.

Increasing number of MF more than 2 MF, enhances the model performance in training phase but contrary in

testing phase. Thus, it can be seen (Tab.4) that the model 4 (2, gebellmf, linear) and model 5 (2, gauss2mf, linear) perform well, as they have high coefficients of determination R² (0.964 and 0.984) and the lowest values of RMSE =0.366 and 0.358 in training and testing phase respectively. These models perform better than model 7 (3, gauss2mf, linear) and model 8 (3, gauss2mf, linear) in testing phase. The given coefficient of determination values are higher than values of R² = 0.67 obtained by Areerachakul (2012) and R² 0.943 obtained by Pour-Ali Baba et al. (2015) but they are much closer to R² = 0,986 obtained by Kumar et al. (2012).

Regarding RMSE values obtained by this study, they were higher than RMSE = 0.265 mmday⁻¹ obtained by Shamshirband et al. (2016) but they were lower than RMSE = 0.753 and 0.821 mmday⁻¹ obtained by Patil et al. (2017) in training and test periods respectively.

3.2 Linear regression models

To study the performance of linear regression models: RR, BR and MLR models were evaluated together and compared one to each other.

Tab. 4. R and RMSE (mm.day⁻¹) values of the ANFIS models in training and testing phases.

Model N°	MF	number of MF	Training phase		Testing phase	
			R ²	RMSE	R ²	RMSE
Model 1	Trimf	2	0.953	0.414	0.984	0.358
Model 2	Trapmf	2	0.964	0.371	0.984	0.358
Model 3	Psigmf	2	0.964	0.367	0.984	0.358
Model 4	Gbellmf	2	0.964	0.366	0.984	0.358
Model 5	gauss2mf	2	0.964	0.366	0.984	0.358
Model 6	Gbellmf	3	0.972	0.323	0.974	0.475
Model 7	Trapmf	3	0.968	0.341	0.974	0.475
Model 8	gauss2mf	3	0.972	0.328	0.974	0.475

Although limitations of MLR, this technique is widely used at present, it has been used by Tabari et al. (2012) who have reported that MLR model provided good agreement with the ETo obtained by the PM method. They have got a $R^2 = 0.96$ with the best MLR model which was much closer to $R^2 = 0.966$ obtained by the present study. These values were higher than the best value ($R^2 = 0.82$) obtained by Saylan et al. (2019).

Khoshravesh et al. (2016) who have used the multivariate fractional polynomial (MFP), robust regression and Bayesian regression to estimate the monthly ETo, their results showed that the accuracy of MFP model was greater than the other models. RR and BR models gave the same results in terms of R^2 and RMSE in different locations. The higher value of R^2 , which was 0.97, it was closer to $R^2 = 0.9662$ obtained in this study.

3.2.1 Coefficients of regression estimation

The regression coefficients are the least squares estimates of the parameters. Their values indicate how much change in Y occurs for a one-unit change in X when the remaining X 's are held constant. These coefficients are the values of $\beta_0, \beta_1, \dots, \beta_p$. They are illustrated in Tab. 5.

It is clear that there were differences between these coefficients from one method to another. Robust regression has

Tab. 5. Regression coefficients according to each linear modeling method.

Inputs	β_i	LMR	RR	BR
Contant	β_0	0.957	0.823	1.028
Temperature	β_1	0.131	0.131	0.130
Relative humidity	β_2	-0.057	-0.056	-0.058
Wind speed	β_3	0.013	0.014	0.013
Sunshine duration	β_4	0.277	0.282	0.275

Tab. 6. Comparison between MLR, RR and BR in terms of MARE according to the sample size (number of observations).

Model N°	Sample size (n)	Robust Regression	Multiple linear Regression	Bayesian Regression
Model 9	30	2.214	2.239	2.220
Model 10	50	4.072	4.544	4.520
Model 11	100	8.798	8.829	8.802
Model 12	150	8.827	8.851	8.822
Model 13	200	8.042	7.996	7.979
Model 14	300	7.108	7.076	7.047
Model 15	375	9.019	8.975	8.970

provided much better regression coefficient estimates when outliers are present in the data. Thus, as can be seen from Tab. 6, models 9, 10, and 11, MARE values given by RR were slightly less than those given by MLR and BR methods. Contrary, models 13, 14 and 15, MARE values were slightly high.

This indicates that robust regression models were affected by the sample size. Consequently, with small samples, RR method performed more accurate models than MLR and BR techniques. However, BR models become more accurate than RR and MLR methods in case of larger samples. Similar result was shown by Grzenda (2015).

Contrary, models 13, 14 and 15 performed by LMR were slightly better than those performed by RR. They were very closer to models 13, 14 and 15 performed by BR. Consequently, RR method was more effectiveness for the small sample sizes and BR method was effectiveness with larger sample sizes.

Another parameter that could affect the model accuracies was the number and nature of the inputs. Thus, according to the MARE values (Tab. 7), there were differences between the different methods, Sometimes RR models are better than LMR models (16, 17, 18, 19 and 21). May be these models were affected by outlier effect and RR has overcome this problem.

With non-informative prior, BR method was always much closer to LMR method.

Fig. 3 shows Scatter plots of observed versus simulated values of reference evapotranspiration (ETo) for the ANFIS, RR, BR and MLR models in the testing phase database. This figure has confirmed that the used regression models were closer each other but ANFIS model was closest to ETo. In this context, Ladlani et al. (2014) have proved that ANFIS model was more accurate than MLR model.

Fig. 4 demonstrates the observed values of ETo compared with the estimated values from different approach-

Tab. 7. Comparison between MLR, RR and BR in terms of MARE according to the number of inputs. T temperature, Hr: Relative humidity, U_2 Wind speed and n sunshine duration.

Model N°	Input combinaisons	RR	LMR	BR
Model 16	T	19.35	19.52	18.34
Model 17	T+n	15.73	16.08	23.35
Model 18	T+ U_2	15.73	16.08	18.03
Model 19	T+Hr	15.74	16.08	15.99
Model 20	T+Hr + U_2	13.91	13.96	13.75
Model 21	T+Hr + n	12.71	13.08	13.11
Model 22	T+ U_2 + n	12.27	12.46	12.48
Model 23	Hr + U_2 + n	15.36	15.19	15.19
Model 24	T+Hr + U_2 +n	9.02	8.97	8.97

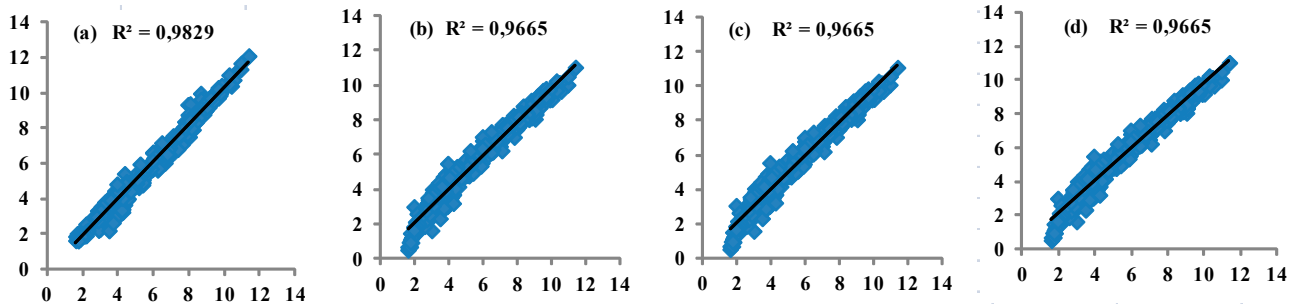


Fig. 3. Scatters plots of observed ET0 (mm/day) and simulated ET0 (mm/day) obtained by different approaches in (test phase database) a: ANFIS; b Bayesian regression; c: Robust regression ; d: Multiple regression. Observed ET0 (ET0o), Simulated ET by ANFIS (ET0a), Simulated ET by RR (ET0r), Simulated ET by MLR (ET0m), ET0 Simulated ET by BR (ET0b).

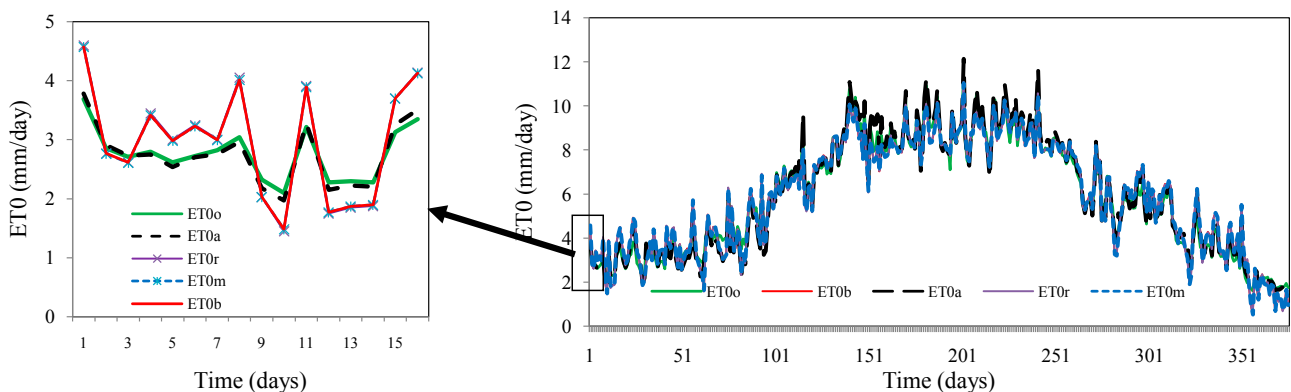


Fig. 4. Graphical comparison of observed ET0 and simulated ET0 obtained by the two approaches in testing phase ; Observed ET0 (ET0o), Simulated ET by ANFIS (ET0a), Simulated ET by RR (ET0r), Simulated ET by MLR (ET0m), ET0 Simulated ET by BR (ET0b).

es. The graph has illustrated that predicted values from the ANFIS were closer to the observed values than those obtained from linear regression techniques.

In fact, according to the works of Yaseen et al. (2016), in some cases, the ANFIS models were the best predictors, in other cases, Bayesian models were the best. Thus, the ANFIS spatial model structure was the best predictor of flow and Bayesian temporal model structures performed better than the ANFIS spatial model structure. In our case ANFIS model performances were always better than Bayesian model performances this is probably due to the consideration of the non-informative prior.

If we focus on the 16 first values of different series obtained by the different methods we clearly see that the series of simulated values by ANFIS was very close to the values of the observed series of ET0. The other series of values simulated by the other methods were somewhat distant from the observed series of the ET0 but they were very close one to each other and they hid one behind the other.

Overall, the ANFIS models provided the best ET0 estimates than statistical models. For practical uses, the

ANFIS model with the RMSE values less than 0.3 mm/day and MARE values less than 6 % had good accuracy in ET0 modeling and can be used where climatic data are limited. This is especially true in some regions of developing countries where reliable weather data sets required for FAO -56 formula are always not available.

As a whole, the findings of this study revealed that the ANFIS models can be employed successfully in reference evapotranspiration estimation. The main disadvantage of this approach is the complexity of implementation with additional of inputs or membership functions, this task required more time and the results could be very poor.

4. CONCLUSION

In this study we have analyzed and compared adaptive neuro fuzzy inference system (ANFIS) and linear regression models to well estimate reference evapotranspiration when climatic data sets are not enough available. Results showed that the best ANFIS model compared with linear

regression models were approximately similar and they were very satisfactory. But in terms of accuracy, ANFIS model seems to be the most reliable. The results were quite encouraging and suggest the usefulness of ANFIS-based modeling techniques for accurate prediction of evapotranspiration as an alternative to statistical approaches. Because the advantage of the ANFIS method lies in the possibility of having improvements in the performance criteria by modifying the membership functions, ANFIS have become powerful tools for modeling in many varied fields of research.

Another advantage may be behind its powerful in modeling is its nonlinear feature, because evapotranspiration process is a nonlinear phenomena. Using linear regression methods in the modeling could result in satisfactory findings, however the ANFIS method has justified its superiority in the power of prediction. Indeed, the designed ANFIS model showed higher performance than other models because the simulated series matches the observed series perfectly.

For the other class of extended linear models (splines, thin-plate, additive,) and the Bayesian regression models with informative prior distribution can be considered in future work.

ACKNOWLEDGEMENT

The authors would like to extend their gratitude to the many people who helped to bring this research project to fruition. Thanks are also to the anonymous reviewers for their careful reading, their useful comments and suggestions which have helped to improve the quality of the paper.

REFERENCES

- Abyaneh H. Z., Nia A. M., Varkeshi M. B., Marofi S., Kisi O. 2011. Performance evaluation of ANN and ANFIS models for estimating garlic crop evapotranspiration. *Journal of irrigation and drainage engineering*, 137(5): 280-286.
- Allen R.G., Pereira L.S., Raes D., Smith M. 1998. Crop evapotranspiration (guidelines for computing irrigation crop water requirement). Irrigation and drainage paper no. 56. Food and Agriculture Organization. Rome.
- Areerachakul S. 2012. Comparison of ANFIS and ANN for Estimation of Biochemical Oxygen Demand Parameter in Surface Water. *International Journal of Chemical and Biological Engineering*, 6: 286-290.
- Bernard M. and Smith A. F. 2000. *Bayesian Theory*. Hoboken, NJ, USA: Wiley.
- Braga J., Heuze Y., Chabadel O., Sonan. N. K., Gueramy A. 2005. Non-adult dental age assessment: correspondence analysis and linear regression versus Bayesian predictions. *Int J Legal Med*. 119: 260-274 DOI 10.1007/s00414-004-0494-8
- Demelash N. 2013. Deficit irrigation scheduling for potato production in North Gondar, Ethiopia. *African Journal of Agricultural Research*, 8(11): 1144-1154.
- Doorenbos J., Pruitt W.O. 1977. Guidelines for predicting crop water requirements. Irrigation and drainage.pap. 24. Food and Agriculture Organization, Rome.
- Fang W., Huang S., Huang Q., Huang G., Meng E., Luan J. 2018. Reference evapotranspiration forecasting based on local meteorological and global climate information screened by partial mutual information. *Journal of Hydrology*, 561: 764-779.
- Fox J., and Weisberg S. 2002. Robust regression. *An R and S-Plus companion to applied regression*, 91.
- Ghosh J. K., Delampady M., Samanta T. 2007. An introduction to Bayesian analysis: theory and methods. Springer Science & Business Media.
- Gocic M. and Trajkovic S. 2014. Drought characterisation based on water surplus variability index. *Water resources management*, 28(10), 3179-3191.
- Grzenda W. 2015. The advantages of Bayesian methods over Classical methods in the context of credible Intervals. *Information systems in management*, 4(1): 53-63.
- Hunsaker D.J., Fitzgerald G.J, French A.N., Clarke T.R., Ottman M., Jand P.J. 2007. Wheat irrigation management using multispectral crop coefficients: II. Irrigation scheduling performance. grain yield and water use efficiency. *Am Soc Agric Biol Eng*, 50(6): 2035-2050.
- Jange J. 1993. ANFIS: Adaptive-network-based fuzzy inference system." *IEEE transactions on systems, man. and cybernetics*, 23(3): 665-685.
- Karimaldini F., Teang Shui L., Ahmed Mohamed T., Abdollahi M., Khalili N. 2012. Daily evapotranspiration modeling from limited weather data by using neuro-fuzzy computing technique. *Journal of irrigation and drainage engineering*, 138(1): 21-34.
- Keshtegar B., Kisi O., Arab H. G., Zounemat-Kermani M. 2018. Subset modeling basis ANFIS for prediction of the reference evapotranspiration. *Water resources management*, 32(3): 1101-1116.
- Khoshravesh M., Sefidkouhi M.A.G., Valipour M. 2015. Estimation of reference evapotranspiration using multivariate fractional polynomial, Bayesian regression, and robust regression models in three arid environments. *Appl Water Sci.*, 7(4): 1911-1922.

- Kumar P., Kumar D., Jaipaul Tiwari A.K. 2012. Evaporation Estimation Using Artificial Neural Networks and Adaptive Neuro-Fuzzy Inference System Techniques. *Pakistan Journal of Meteorology*, 8 (16): 81-88.
- Laaboudi A., Mouhouche B., Draoui B. 2012. Neural network approach to reference evapotranspiration modeling from limited climatic data in arid regions. *International journal of biometeorology*, 56(5): 831-841.
- Ladlani I., Houichi L., Djemil L., Heddami S., Belouz K. 2016. Estimation of Daily Reference Evapotranspiration (ETO) in the North of Algeria Using Adaptive Neuro-Fuzzy Inference System (ANFIS) and Multiple Linear Regression (MLR) Models: A Comparative Study. *Arab J Sci Eng*, 39(8).
- Latrech B., Ghazouani H., Lasram A., M'hamdi B. D., Mansour M., Boujelben A. 2019. Assessment of different methods for simulating actual evapotranspiration in a semi-arid environment. *Italian Journal of Agrometeorology*, (2): 21-34.
- Lee K. H., Cho H. Y. 2012. Simple method for estimating pan coefficients: Conversion of pan evaporation to reference evapotranspiration. *Journal of irrigation and drainage engineering*, 138(1): 98-103.
- Malamos N., Barouchas P.E., Tsirogiannis I.L., Liopatsakalidia A., Koromilasc Th. 2015. Estimation of monthly FAO Penman-Monteith evapotranspiration in GIS environment, through a geometry independent algorithm. *Agriculture and Agricultural Science Procedia*, 4 2015: 290-299
- Meng Li., Ronghao Chu., Abu Reza Md Towfiqul Islam, Shuanghe, Shen. 2018. Reference Evapotranspiration Variation Analysis and Its Approaches Evaluation of 13 Empirical Models in Sub-Humid and Humid Regions: A Case Study of the Huai River Basin, Eastern China. *Water*, 10(4): 493-502
- Naidu D. and Majhi B. 2019. Reference evapotranspiration modeling using radial basis function neural network in different agro-climatic zones of Chhattisgarh. *Journal of Agrometeorology*, 21(3): 316-326.
- Patil A. P. and Deka P.C. 2017. Performance evaluation of hybrid Wavelet-ANN and Wavelet-ANFIS models for estimating evapotranspiration in arid regions of India. *Neural Computing and Applications*, 28(2): 275-285.
- Peng L., Li Y., Feng H. 2017. The best alternative for estimating reference crop evapotranspiration in different sub-regions of mainland China. *Scientific reports*, 7(1): 1-19.
- Pour-Ali Baba A., Shiri J., Kisi O., Fard A. F., Kim S., Amini R. 2015. Estimating daily reference evapotranspiration using available and estimated climatic data by adaptive neuro-fuzzy inference system (ANFIS) and artificial neural network (ANN). *Hydrology Research*, 44(1): 131-146.
- Saylan L., Kimura R., Altınbaş N., Çaldağ B., Bakanoğulları F. 2019. Modeling of Surface Conductance over Sunn Hemp by Artificial Neural Network. *Italian Journal of Agrometeorology*, (3): 37-48.
- Shamshirband S., Amirmojahedi M., Gocić M., Akib S., Petković D., Piri J., Trajkovic S. 2016. Estimation of reference evapotranspiration using neural networks and cuckoo search algorithm. *Journal of Irrigation and Drainage Engineering*, 142(2): 04015044.
- Stahel W. 1997. "Robust alternatives to least squares," *Adv. Math. Tools in Metrol. III, Ser. Adv. Math. for Appl. Sci.*, World Scientific Publishing Company, 45: 118-133.
- Tabari H., Kisi O., Ezani A., Talaei, P. H. 2012. SVM, ANFIS, regression and climate based models for reference evapotranspiration modeling using limited climatic data in a semi-arid highland environment. *Journal of Hydrology*, 444: 78-89.
- Trajkovic S., and Kolakovic S. 2010. Comparison of simplified pan-based equations for estimating reference evapotranspiration. *Journal of irrigation and drainage engineering*, 136(2): 137-140.
- Tsakiris G., Pangalou D., Vangelis H. 2007. Regional drought assessment based on the Reconnaissance Drought Index (RDI). *Water resources management*, 21(5): 821-833.
- Vicente-Serrano S. M., Beguería S., López-Moreno J. I. 2010. A multiscalar drought index sensitive to global warming: the standardized precipitation evapotranspiration index. *Journal of climate*, 23(7): 1696-1718.
- Wable P.S., Jha M.K., Gorantiwar S.D. 2019. Assessing suitability of temperature-based reference evapotranspiration methods for semi-arid basin of Maharashtra. *Journal of Agrometeorology*, 21(3): 351-356.
- Yaseen A H., Amir P.N., Zhen Z., Subhasis G., Sean A.W. 2016. Bayesian Regression and Neuro-Fuzzy Methods Reliability Assessment for Estimating Streamflow. *Water*, 8, 287 pp. 15.
- Yirga S. A. 2019. Modelling reference evapotranspiration for Megecha catchment by multiple linear regression. *Modeling Earth Systems and Environment*, 5(2): 471-477.



Citation: Ö. Baydaroğlu Yeşilköy, K. Koçak, L. Şaylan (2020) Prediction of commonly used drought indices using support vector regression powered by chaotic approach. *Italian Journal of Agrometeorology* (2): 65-76. doi: 10.13128/ijam-970

Received: June 18, 2020

Accepted: October 17, 2020

Published: January 25, 2021

Copyright: © 2020 Ö. Baydaroğlu Yeşilköy, K. Koçak, L. Şaylan. This is an open access, peer-reviewed article published by Firenze University Press (<http://www.fupress.com/ijam>) and distributed under the terms of the Creative Commons Attribution License, which permits unrestricted use, distribution, and reproduction in any medium, provided the original author and source are credited.

Data Availability Statement: All relevant data are within the paper and its Supporting Information files.

Competing Interests: The Author(s) declare(s) no conflict of interest.

Prediction of commonly used drought indices using support vector regression powered by chaotic approach

ÖZLEM BAYDAROĞLU YEŞİLKÖY^{1,*}, KASIM KOÇAK², LEVENT ŞAYLAN²

¹ Altınbaş University, School of Engineering and Natural Sciences, Department of Civil Engineering, İstanbul/Turkey

² İstanbul Technical University, Faculty of Aeronautics and Astronautics, Department of Meteorological Engineering, İstanbul/Turkey

*Corresponding author. E-mails: ozlembaydaroglu@gmail.com, kkocak@itu.edu.tr; saylan@itu.edu.tr

Abstract. An effective water resources management requires accurate predictions of possible risks. Drought is one of the most devastating phenomena that has a certain risk of occurrence. Understanding the variability of the drought indices is of great importance in determining the spatiotemporal behavior of the drought phenomenon. Moreover, determination of the variability and short-term prediction of the drought indices enables us to take necessary steps in hydrological and agricultural issues. In this study, drought indices have been predicted via Support Vector Regression, SVR. This method originated from a linear regression method in a high dimensional feature space. SVR necessitates a special input matrix. In this study, this matrix has been constructed on the basis of Chaotic Approach, CA. Commonly used drought indices are used in the prediction stage. These indices consist of monthly Palmer Drought Severity Index, PDSI, Palmer Hydrological Drought Index, PHDI, Palmer Z-Index, ZNDX, Modified Palmer Drought Severity Index, PMDI, and Standard Precipitation Index, SPI. One-step ahead prediction has been realized for a 36-month period. Most results show that predictions of the drought indices using SVR are quite promising.

Keywords. Drought indices, prediction, phase space reconstruction, machine learning.

1. INTRODUCTION

It is a well-known fact that drought is one of the most important natural disasters in the world. Severity and duration of droughts in different regions of the world are expected to increase in the future due to climate change. Most countries will be affected by drought at different levels depending on the risk factors they have (Carrao et al., 2016). Drought is a natural disaster with the power to produce significant social and economic consequences. For this reason, better management of water resources will gain more importance in the future. In drought studies, the first step is the determination of drought's level

and its variation and predicting the future value of the drought indices. Drought indices are used for determination and classification of the drought (Yihdego et al., 2019; Hao et al., 2016).

In literature, there are some studies about prediction of the drought indices. Liu et al. (2009) have implemented the Markov Chain Model to predict the PDSI. They constructed a one-step prediction model which produces different prediction accuracy such as 96.68%, 64.45%, 52.6% and 0.40% for normal, slight, moderate, and severe drought conditions, respectively. Mehta et al. (2014) have used the Model for Interdisciplinary Research on Climate 5 (MIROC5) and Statistical Forecast System (SPS) in order to predict the Self-Calibrating Palmer Drought Severity Index (SC-PDSI). Although correlation coefficients and root mean square errors are big enough with regard to the time period and grid spacing, the accuracy of the prediction is within the acceptable limits. Cutore et al. (2009) employed neural networks and climate indices so as to predict the Palmer Indices. They found that the North Atlantic Oscillation (NAO) series are uncorrelated with the Palmer Indices for winter months while the European Blocking (EB) are correlated with the Palmer Indices both for winter and autumn months. Belayneh et al. (2014) have used a wavelet-neural network and wavelet-support vector regression approaches to predict long-term SPI series. The best prediction result is produced from the coupled wavelet neural network.

The SVR which is an advanced, state-of-the-art prediction method can be seen as a specific implementation of Support Vector Machines (SVMs) to the regression problem (Vapnik, 1995; Cortes and Vapnik, 1995). The SVM is a kind of statistical learning machine which is widely used in an area of classification (Vapnik and Lerner, 1963; Vapnik and Chervonenkis, 1964). SVR transforms input space which is formed from the observations into high dimensional feature space by way of a kernel function and performs a linear regression in this space.

There are many applications of SVR about prediction of many variables. Yu et al. (2006) have used SVR for real-time flood stage prediction. This study has demonstrated that a SVR has strong prediction performance. Santamaria-Bonfil et al. (2016) have developed a method based on the SVR to predict wind speeds for wind farms. They showed that the SVR is more appropriate for short term wind speed and wind power values prediction than persistence and autoregressive models. SVR has been employed to predict hourly O₃ concentrations by Ortiz-Garcia et al. (2010) with accurate prediction results. Baydaroğlu and Koçak (2014) have used SVR algorithm to predict evaporation values. The results show that SVR-based predictions are very successful with high determination coefficients as

83% and 97% for univariate and multivariate time series embeddings, respectively. Moreover, river flow prediction using hybrid models of the SVR with Wavelet Transform (WT), Singular Spectrum Analysis (SSA) and CA is realized by Baydaroğlu et al. (2017). The SVR-WT combination has resulted in the highest coefficient of determination and the lowest mean absolute error. Granata et al. (2016) have applied SVR for a simulation of rainfall-runoff processes in two experimental basins and compared with EPA's stormwater management model. The hydrograph shape and the time to peak are correctly modelled by these approaches. It can be said that the SVR shows considerable potential for applications to the problems of urban hydrology.

The main idea behind this study is to predict drought indices consisting of many nonlinear variables with high accuracy. Prediction of drought indices enables decision makers to monitor all components of hydrologic cycle, gain simple information about different kinds of droughts which are complex phenomena, determine economic impacts, risks and changes on agricultural productivity, plan irrigation facilities and water distribution. In the prediction part of the study, SVR has been employed. It requires a special input data format. Chaotic Approach (CA) is utilized in order to prepare the input data set for SVR. For this purpose, a phase space is reconstructed by using Embedding Theorem (Takens, 1981). According to this theorem, time delays and embedding dimensions are determined from the time series in question. In this study, False Nearest Neighbour (FNN) (Kennel et al., 1992) and Mutual Information Function (MIF) (Fraser and Swinney, 1986) have been implemented to determine the embedding dimension and the time delay, respectively.

In the organization of this paper, Section 2 introduces the methods and material used in the study, Section 3 discusses the results obtained in the study.

2. MATERIAL AND METHODS

The following are employed in this study: (1) Determining the optimum embedding dimensions and time delays (2) A phase space is constructed with these embedding parameters in order to prepare input matrix for SVR (3) Prediction of the drought indices using SVR.

FNN algorithm is based on the definition of true and false neighboring points in a phase space. Percentages of the false neighboring points in a successively higher dimensional phase space provide to develop this algorithm to choose an optimum embedding dimension. The Mutual Information Function (MIF) can be considered as a nonlinear counterpart of the Autocorrelation Function (ACF).

2.1. Data

The American Meteorological Society (1997) categorizes droughts as meteorological or climatological, agricultural, hydrological and socioeconomic droughts. Wilhite and Glantz (1985) are expressed numerically some indices based on historical climate records such as temperature and precipitation.

In this study, US Palmer Drought Severity Index (PDSI), Palmer Hydrological Drought Index (PHDI), Palmer Z-Index (ZNDX), Modified Palmer Drought Severity Index (PMDI) and Standard Precipitation Index (SPI) are considered. These indices were calculated from monthly data between June 1929 and December 2015 provided by National Oceanic and Atmospheric Administration (NOAA) (downloaded from <https://www7.ncdc.noaa.gov/CDO/CDODivisionalSelect.jsp>)

The PDSI is widely and operationally used for determination of drought status (Palmer, 1965). This index is based on a soil moisture balance between supply and demand. In other words, it is a function of precipitation, temperature, and available water content of the soil (Palmer, 1965; Alley, 1984). It is generated indicating the severity of wet or dry spells. This index is above +4 and below -4. Negative values indicate dry spells while positive values denote wet spells.

The PHDI is a monthly hydrological drought index used to assess long-term moisture supply and indicates the severity of a wet or dry spell like the PDSI. This index considers the information about precipitation as inflow, outflow and storage. Increased irrigation, new reservoirs, and added industrial water use are not typically included in the computation of this index. The index generally ranges from -6 to +6. The major disadvantage of this index is that it does not take the long-term precipitation trend in consideration (Karl and Knight, 1985).

The ZNDX essentially measures the moisture anomaly. It specifies a deviation from the normal monthly PDSI. This index can respond to a month of above-normal precipitation, even during periods of drought.

The PMDI is derived from the PDSI having the difference with respect to transition periods between dry and wet spells. The PMDI is based on a weighting factor for wet and dry indices (Heddingshaus and Sabol, 1991). An index value is selected as the PDSI drought index. This selection is realized by the program regarding probabilities (see <https://www7.ncdc.noaa.gov/CDO/CDODivisionalSelect.jsp>).

The Surface Water Supply Index (SWSI) is calculated by using the components of precipitation, snowpack (in winter), stream flow (in summer) and reservoir storage inputs. Monthly data are used for the computation of the SWSI. McKee et al. (1993) stated that the SPI is another

well-known and frequently used meteorological drought index in application. This index is a transformation of the probability of observing a given amount of precipitation in given months (see <https://www7.ncdc.noaa.gov/CDO/CDODivisionalSelect.jsp>).

The Global Historical Climatology Network (GHCN) Daily dataset is the source of station data. GHCN-Daily contains several major observing networks in North America. The primary network is the National Weather Service (NWS) Cooperative Observing (COOP) program. These data update every day from a variety of data streams with quality checks. Moreover the data are reconstructed each weekend from its data source components (see detail <https://www.ncdc.noaa.gov/data-access/land-based-station-data/land-based-datasets/global-historical-climatology-network-ghcn>).

Drought indices used in the study are given in the Figures 1 (a) to (k). These figures clearly reveal the erratic behavior of the drought indices.

2.2. Phase Space Reconstruction

Prediction of drought indices by way of SVR requires a special set of input data matrix. In this study, chaos theory is utilized to construct the input data matrix. The phase spaces of drought indices have been reconstructed using the most appropriate embedding parameters.

To estimate optimum embedding dimensions, a method proposed by Cao (1997) has been applied to all series. For this purpose, nonlinearTseries package in R-Studio has been used (Cao, 1997; Arya and Mount, 1993; Arya et al., 1998). Embedding dimension values are determined from the points which $E1(d)$ and $E2(d)$ stay constant together.

To reconstruct the phase space we need the proper time delays. In the application, this parameter is extracted from both autocorrelation and mutual information functions (MIF). In this study, we have chosen the MIF to decide the proper time delay because of its flexibility in measuring both linear and nonlinear inner-dependences in a given series. To estimate optimum time delay, the fractal package in R-Studio has been used (Kantz and Schreiber, 1997; Bassingthwaight et al., 1994; Fraser and Swinney, 1986; Casdagli et al., 1991).

The details of phase space reconstruction from a univariate or single variable time series is given in Packard et al. (1980). A phase space can be reconstructed by using delay coordinate method. Coordinates of the phase space are spanned by the variables which are necessary to specify the time evolution of the system (Koçak et al., 2004). With regard to Embedding Theorem (Takens, 1981), a phase space can be constructed from a one-dimensional

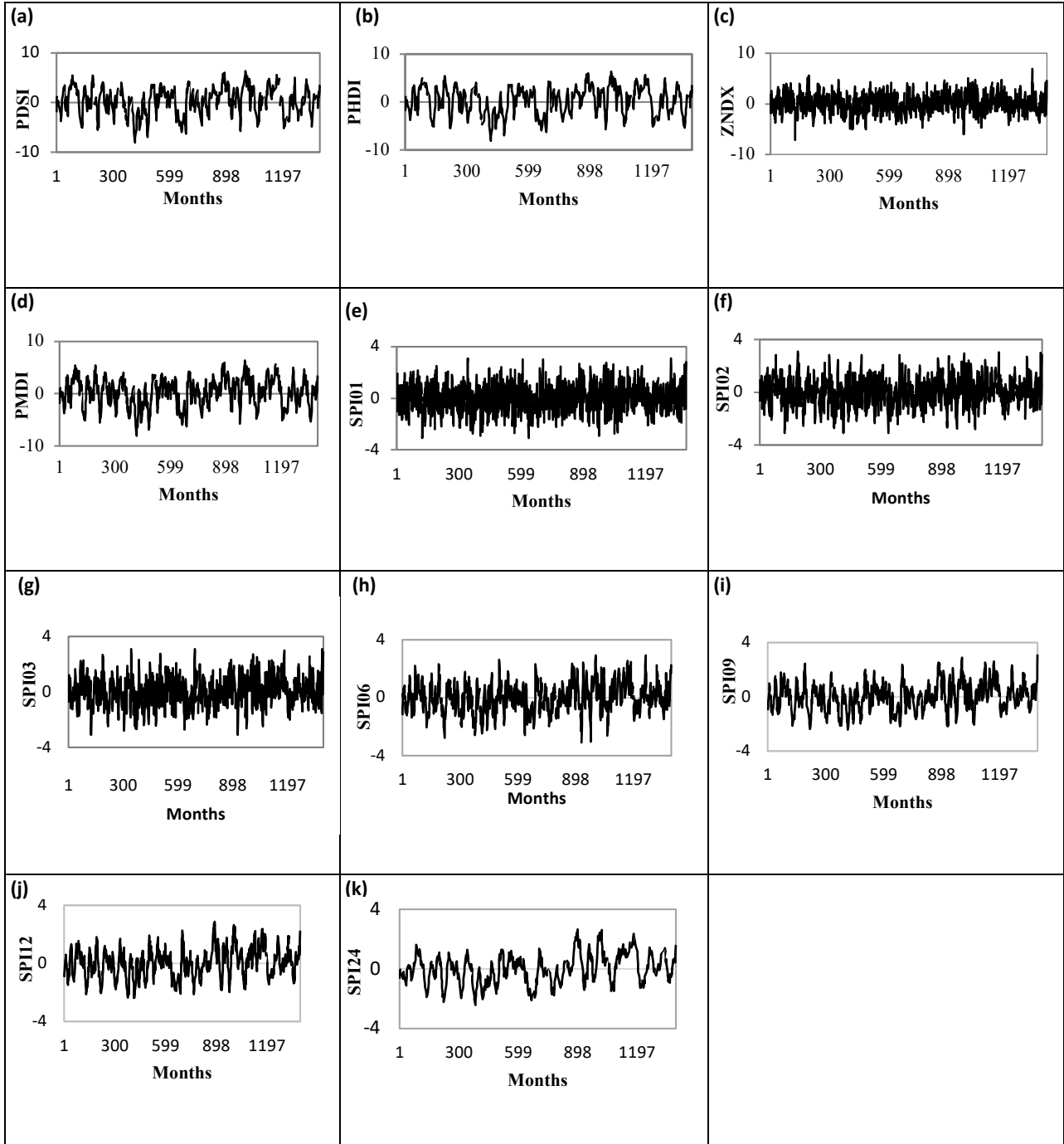


Fig. 1. Monthly (a) PDSI (b) PHDI (c) ZNDX (d) PMDI (e) 1-month SPI (f) 2-month SPI (g) 3-month SPI (h) 6-month SPI (i) 9-month SPI (j) 12-month SPI (k) 24-month SPI.

series. Let's consider a time series $x_i \in \mathbb{R}$, $i=1,2,\dots,N$, then the reconstruction procedure for the purpose of prediction is given as

$$X_i = (x_i, x_{i-\tau}, \dots, x_{i-(d-1)\tau}) \in \mathbb{R}^d, i=1,2,\dots,N-(d-1)\tau \quad (1)$$

where X_i is an d -dimensional phase space vector, τ is a time delay and m is an embedding dimension.

In the d -dimensional space, phase space vectors describe an object which is topologically equivalent to the attractor of the physical system (Porporato and Ridolfi, 1997).

2.2.1. False Nearest Neighbor (FNN) Method

To reconstruct a phase space, embedding dimensions and time delays should be determined from a given time series. In literature, there are some methods like False Nearest Neighbor (Kennel et al., 1992) and Grassberger-Procaccia (GP) methods (Grassberger and Procaccia, 1983).

In this study, another algorithm proposed by Cao (1997) has been implemented to determine the minimum embedding dimension. For a time series x_1, x_2, \dots, x_N , the time delay vectors reconstructed,

$$X_i(d) = (x_i, x_{i+\tau}, \dots, x_{i+(d-1)\tau}), \quad i=1, 2, \dots, N-(d-1)\tau \quad (2)$$

Similar to FNN algorithm,

$$a(i, d) = \frac{\|x_{i(d+1)} - x_{n(i,d)(d+1)}\|}{\|x_{i(d)} - x_{n(i,d)(d)}\|}, \quad i = 1, 2, \dots, N - d\tau \quad (3)$$

where $\| \cdot \|$ is some measurement of Euclidean distance and the maximum norm of the distance

$$\|X_k(d) - X_l(d)\| = \max_{0 \leq j \leq d-1} |x_{k+j\tau} - x_{l+j\tau}| \quad (4)$$

$X_i(d+1)$ is the i th reconstructed vector with embedding dimension $d+1$, i.e., $X_i(d+1) = (x_i, x_{i+\tau}, \dots, x_{i+d\tau})$; $n(i, d)$, ($1 \leq n(i, d) \leq N - d\tau$), is an integer such that $x_{n(i,d)(d)}$ is the nearest neighbour of $x_i(d)$ in the d -dimensional reconstructed phase space in the sense of distance $\| \cdot \|$.

The threshold value should be determined by the derivative of the underlying signal, therefore, for different phase point i , $a(i, d)$ should have different threshold values. Also, different time series may have different threshold values. For this problem, Cao (1997) defines the mean value of all $a(i, d)$'s

$$E(d) = \frac{1}{N-d\tau} \sum_{i=1}^{N-d\tau} a(i, d) \quad (5)$$

To investigate its variation from d to $d+1$

$$E1(d) = \frac{E(d+1)}{E(d)} \quad (6)$$

$E1(d)$ stops changing when d is greater than some value d_0 if the time series comes from an attractor. Then, the d_0+1 is the minimum embedding dimension.

Another quantity which is useful to distinguish deterministic signals from stochastic signals can be developed by using $E^*(d)$

$$E^*(d) = \frac{1}{N-d\tau} \sum_{i=1}^{N-d\tau} |x_{i+d\tau} - x_{n(i,d)+d\tau}| \quad (7)$$

$$\text{Finally, } E2(d) = \frac{E^*(d+1)}{E^*(d)} \quad (8)$$

For time series data from a random set of numbers, $E1(d)$, in principle, will never attain a saturation value as d increases. In practical computations, it is difficult to resolve whether the $E1(d)$ is slowly increasing or has stopped changing if d is sufficiently large. Because available observed data samples are limited, it may happen that $E1(d)$ stops changing at some d although the time series is random. To solve this problem, $E2(d)$ can be considered. For random data, because the future values are independent of the past values, $E2(d)$ will be equal to 1 for any d in this case. However, for deterministic data, $E2(d)$ is certainly related to d , as a result, it cannot be a constant for all d ; in other words, there must exist some d 's such that $E2(d) \neq 1$.

2.2.2. Mutual Information Function (MIF)

Another important embedding parameter for reconstructing a phase space is a time delay. Various methods such as Mutual Information Function (MIF) (Fraser and Swinney, 1986), autocorrelation function, Cross Autocorrelation (CAC) (Palit et al., 2013), C-C Method (Kim et al., 1999) based on correlation integral can be used to determine proper time delay. MIF which is a nonlinear counterpart of autocorrelation function is the most commonly used approach in nonlinear time series analysis. The time corresponding to the first minimum of the MIF gives the optimum value for the time delay.

2.2.3. Support Vector Regression

Vapnik and Lerner (1963) and Vapnik and Chervonenkis (1964) have developed SVM algorithm. SVM is a state-of-the-art method which provides a good generalization capability to dynamics of a given process thanks to Structural Risk Minimization (SRM) approach. SVR, an application of SVM to the regression problem, is based on the computation of a linear regression function in a multidimensional feature space.

For a set of k examples $[(x_1, y_1), (x_2, y_2), \dots, (x_k, y_k)]$, each generated from an unknown probability distribution $P(x, y)$ where x_i are the input vectors and y_i are the corresponding output values ($i=1, 2, \dots, k$), the best approximate function of the possible smallest risk can be given as (Liong and Sivapragasam, 2002; Yu et al., 2006),

$$R(\alpha) = \int (y - f(x, \alpha))^2 dP(x, y) \quad (9)$$

where $f(x, \alpha)$ is a class of functions and α is the parameter of this function.

$R(\alpha)$ cannot be calculated because $P(x,y)$ is unknown. For this reason, an induction principle for risk minimization should be taken into consideration. The approach which replaces the probable smallest risk $R(\alpha)$ by the empirical risk $R_{emp}(\alpha)$ is given by

$$R_{emp}(\alpha) = \frac{1}{k} \sum_{i=1}^k (y - f(x, \alpha))^2 \quad (10)$$

This approach is named Empirical Risk Minimization (ERM) induction principle. However, ERM does not guarantee a small $R(\alpha)$ if the number of training data is limited. Therefore, SRM principle based on statistical learning theory has been developed by Vapnik (1999).

The SRM principle theoretically minimizes $R(\alpha)$ based on the simultaneous minimization of both the empirical risk and the confidence interval Ω (Yu et al., 2006). The bound on $R(\alpha)$ is given by

$$R(\alpha) \leq R_{emp}(\alpha) + \Omega\left(\frac{k}{h}\right) \quad (11)$$

where the parameter h is called the VC-dimension (Vapnik, 1995) of a set of functions. It can be seen as the capacity or the complexity of a set of functions.

The learning machine is given a training data set $\{x_i, y_i\}$, $i=1, \dots, k$, $y_i \in \mathbb{R}, x_i \in \mathbb{R}^D$. The regression function assumed for this data set is a linear regression on the hyperplane

$$y_i = wx_i + b \quad (12)$$

where w is the weight vector, y_i is the element of $\{+1, -1\}$ and b is the bias or deviation. In case of real observations, most of the processes exhibit nonlinearity. Therefore, linear approaches may not be practical and effective. When considering nonlinearity, the input data, x , in the input space is mapped to high dimensional feature space using nonlinear function $\phi(x)$ and the decision function is given by

$$f(w, b) = w \cdot \phi(x) + b \quad (13)$$

If data are not separated linearly, then slack variables are inserted to the optimization problem. Then the regression problem can be converted into the following convex optimization problem (Yu et al., 2006).

$$\min_{w, b, \xi^+, \xi^-} \frac{1}{2} w^2 + C(\xi^+ + \xi^-) \quad (14)$$

subject to $y_i - (w \cdot \phi(x_i) + b) \leq \varepsilon + \xi^+$; $(w \cdot \phi(x_i) + b) - y_i \leq \varepsilon + \xi^-$; $\xi^+, \xi^- \geq 0$, $i=1, 2, \dots, k$

where ξ^+ and ξ^- are slack variables that indicate the upper and lower training errors subject to an error tolerance ε . C is the penalty factor which is a balance between the training error and model complexity. To find Lagrange multipliers α_i^+ and α_i^- which are necessary to solve convex optimization problem, the following function is maximized

$$L_D = \sum_{i=1}^k (\alpha_i^+ - \alpha_i^-) y_i - \varepsilon \sum_{i=1}^k (\alpha_i^+ - \alpha_i^-) - \frac{1}{2} \sum_{i,j} (\alpha_i^+ - \alpha_i^-) (\alpha_j^+ - \alpha_j^-) \phi(x_i) \cdot \phi(x_j) \quad (15)$$

subject to $\sum_{i=1}^k (\alpha_i^+ - \alpha_i^-) = 0$; $0 \leq \alpha_i^+ \leq C$, $i=1, 2, \dots, k$; $0 \leq \alpha_i^- \leq C$, $i=1, 2, \dots, k$

In Eq. (15), $\phi(x_i) \cdot \phi(x_j)$ is a kernel function, $K(x_i, x_j)$. There are various kernel functions such as linear, polynomial, radial basis and sigmoid. The application of SVR requires the selection of an appropriate kernel function. Radial Basis Function (RBF) is the most commonly used kernel function because of its flexibility in applications (see Baydaroğlu and Koçak, 2014; Baydaroğlu et al., 2017; Yu and Liong, 2007; Belayneh et al., 2014; Ortiz-Garcia et al., 2010). Besides, it has a strong learning ability and is able to reduce computational complexity of the training process and improve the generalization performance of SVR (Li and Xu, 2005). In the study, RBF has been chosen as the kernel function

$$K(x_i, x_j) = e^{-\frac{\|x_i - x_j\|^2}{2g^2}} \quad (16)$$

where g is the width of radial basis function. The final decision function of nonlinear SVR can be given by

$$f(x_i) = \sum_{i=1}^k (\alpha_i^+ - \alpha_i^-) K(x_i, x_k) + b \quad (17)$$

where x_k is a new entry for the estimation.

2.3. Prediction

In general, prediction from a time series can be performed by using three different approaches. These are one-step prediction, direct multi-step prediction and indirect multi-step prediction (Wang et al, 2010). Let η shows the prediction horizon or predefined time interval used for how far ahead the model predicts the future. Then the abovementioned prediction methods can be expressed as given below.

- a. One-step prediction ($\eta=1$)
 $X(t+1) = F(X(t))$ (18)
- b. Direct multi-step prediction ($\eta > 1$)

The prediction value of $t + \eta$ can be estimated according to the historical measurement data, and the prediction equation is

$$X(t + \eta) = F[X(t)] \tag{19}$$

c. Indirect multi-step prediction ($\eta > 1$)

Using iteration method to process one-step prediction model, and the prediction equation is

$$X(t + \eta) = F\{F\{\dots F[X(t)]\}\} \tag{20}$$

In application, one-step prediction is the most frequently used method due to its simplicity and its high accuracy. Thus, throughout this study, one-step prediction was preferred to other prediction approaches and run for 36 months (three years). This time period is enough to evaluate the accuracy of the prediction method.

2.4. Performance Criteria

In this study, Mean Absolute Error (MAE) (Willmott and Matsuura, 2005), Relative Error (RE) (Golub and Charles, 1996) and coefficient of determination (R^2) (Steel and Torrie, 1960) are calculated to estimate the prediction performance.

Let N , x_i , y_i , \bar{x} , \bar{y} denote the total number of observations, observed values, forecasts, the arithmetic means of the observed and forecasted values, respectively.

$$MAE = \frac{1}{N} \sum |y_i - x_i| \tag{21}$$

$$RE = \frac{|y_i - x_i|}{x_i} \tag{22}$$

$$R^2 = \frac{\{\sum(x_i - \bar{x})(y_i - \bar{y})\}^2}{\sum(x_i - \bar{x})^2 \sum(y_i - \bar{y})^2} \tag{23}$$

3. RESULTS

The recent studies on climate change indicate that drought will be one of the most important challenges in the future. To facilitate the drought related analysis, some drought indices have been developed to judge numerically whether current conditions fall within the drought limits or not. Thus, predictions of drought indices will enable us to take some necessary precautions to mitigate the possible effects of drought related damages.

All drought indices have been predicted for a 36-month prediction period by way of one-step ahead prediction. Prediction of drought indices is a very com-

Tab. 1. Optimum time delays and embedding dimensions for drought indices.

Drought Indices	Time Delays	Embedding Dimensions	Drought Indices	Time Delays	Embedding Dimensions
PDSI	17	9	SP02	2	10
PHDI	17	9	SP03	2	9
ZNDX	17	9	SP06	6	10
PMDI	2	10	SP12	14	8
SP01	2	10	SP24	20	8

Tab. 2. SVR parameters used in the predictions of the drought indices.

SVR Parameters	C	ϵ	g
PDSI	0.3536	0.0044	0.0060
PHDI	8.0000	0.0229	0.7711
ZNDX	197.4029	0.0001	0.5452
PMDI	1.8340	0.0499	1.6818
SP01	256.0000	0.0004	0.0482
SP02	98.7015	0.0031	0.4585
SP03	256.0000	0.1294	0.1621
SP06	1.4142	0.1187	1.0000
SP09	279.1699	0.1996	0.0078
SP12	256.0000	0.1088	0.0060
SP24	58.6883	0.0593	0.3855

plicated task since this kind of data show quite high variability. Therefore, SVR that is a state-of-the-art method when comparing other counterparts is chosen to predict drought indices.

To prepare an input matrix for SVR, optimum embedding parameters have been estimated as seen in Tab. (1).

After the proper determination of embedding parameters phase spaces for the drought indices can be reconstructed. Then by using these phases, the input data matrix can be formed properly. In this case, any input data matrix consists of two parts. One is a training data set and the other is a test data set. In addition, the input data set also includes the target data column. This column indicates the next or future values of the predicted variable.

From embedding parameters given in Tab. 1, phase spaces are reconstructed.

Tab. 2 shows the SVR parameters used in the predictions of drought indices. As mentioned before, the parameter C given in the second column of the table controls the trade-off between the slack variable penalty and the size of the margin. SVR uses a more sophisticated penalty function than the SVM, not allocating a penalty if the predicted value is less than a distance ϵ away from the actual value.

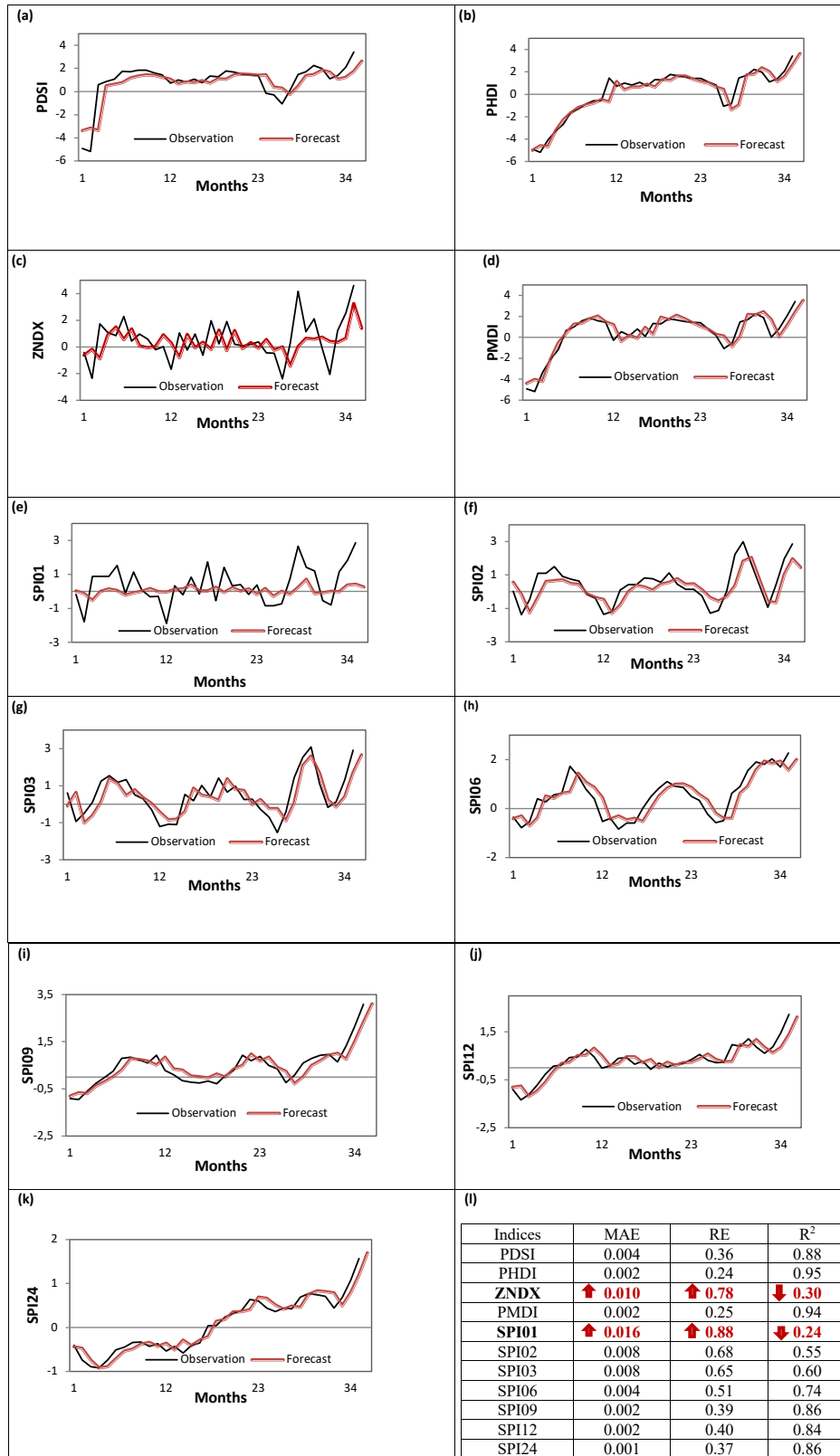


Fig. 2. Prediction results of (a) PDSI (b) PHDI (c) ZNDX (d) PMDI (e) SPI01 (f) SPI02 (g) SPI03 (h) SPI06 (i) SPI09 (j) SPI12 (k) SPI24 (l) Prediction performance of the drought indices.

The last parameter, g , is the width of the Gaussian kernel function. These parameters are calculated for their valid ranges which are determined by using a Fortran code and optimum values of parameters given in Tab. 2 are used for the implementation of SVR.

The application of SVR requires the selection of an appropriate kernel function. In the study, RBF has been chosen as the kernel function. RBF is the most commonly used kernel function because of its flexibility in applications (see Baydaroglu and Koçak, 2014; Baydaroglu et al., 2017; Yu and Liang, 2007; Belayneh et al., 2014; Ortiz-Garcia et al., 2010). Besides, it has a strong learning ability and is able to reduce computational complexity of the training process and improve the generalization performance of SVR (Li and Xu, 2005).

Predictions of the last 36-month period of the drought indices are given in Fig. 2(a) to (k). In this fig., normalized prediction and indices values have been used. Besides, statistics of the performance criteria of the predictions can be seen in Fig. 2(l).

As stated before, drought is the most devastating natural phenomenon that causes serious loss of life and property. Therefore, prediction of drought occurrence is extremely important for decision makers. In the current literature, there are various drought indices and each one is developed for different purposes. Instead of focusing on a specific drought index, most of the well-known drought indices are considered in the prediction process

The importance of drought indices' prediction originates from the cruciality of drought prediction. Calculation of drought indices consists of many meteorological and hydrologic parameters. Therefore, prediction of these indices has a complex and difficult challenge. Since accurate drought prediction enables people to take necessary precautions for agricultural sustainability, disaster management and plan water management, agricultural activities, a hybrid prediction method based on SVR powered by Chaos Theory has been used in this study. It is a well-known fact that there is an inverse relationship between variability and prediction accuracy. Although drought indices have high variability, high generalization capability of SVR leads to predictions with high accuracy.

Fig. 2 (l) shows prediction performance criteria, MAE, RE, R^2 . High MAE and RE values and low R^2 values indicate medium and low prediction accuracy and vice versa.

If $RE=0$, prediction is perfect while $RE=1$ means that only the average value is predicted. From Fig. 2 (l), it is seen that ZNDX and SP01 have the highest relative errors. Namely, these indices have been predicted on their average levels. Similarly, it can be easily seen that ZNDX and SPI01 are indices which are difficult to predict as seen similarly on MAEs and R^2 values of ZNDX and SPI01.

Willmott and Matsuura (2005) indicate that MAE is a good natural measure of average error. Fig. 2 (l) shows that maximum MAE values of all indices belong to ZNDX and SPI01. Moreover, ZNDX and SPI01 have the smallest R^2 values.

As a result, PDSI, PHDI, PMDI, SP09, SP12 and SP24 can be predicted with high accuracy when considering all performance criteria. These indicators show that all Palmer drought indices can be predicted accurately using SVR.

In summary, the results show that the proposed hybrid method can accurately predict drought indices but ZNDX and SPI01. The low predictability of these indices is quite understandable. Because ZNDX is limited to just one month, it is a short-term drought measure without memory from previous months (see <https://www.cisa.sc.edu/atlas/glossary.html>). Similarly, it may be difficult to obtain the required number of data for high prediction accuracy of SPI01 since it shows the anomalies of the observed total precipitation for a month. Obviously, prediction errors decrease as the numbers of the month increase for SPIs. Predictions for Palmer Indices and long-term SPIs are very promising.

4. CONCLUSION

One of the most important features that distinguish the drought phenomenon from other natural disasters is of its slowly developing feature over time. The second important feature of drought events is that once it has started, its devastating effects continue for a relatively long period of time. Drought has the ability to deeply affect all sectors and leaves permanent marks on the life of society. For this reason, it is a natural disaster that deserves further study. There are many drought indices which are widely used in the monitoring of drought events. Therefore, in order to minimize the negative effects of drought events, it is of vital importance to realize accurate predictions of drought indices.

SVMs were developed on the basis of statistical learning. It had outstanding advantages in theory and it realized the nonlinear mapping of the high-dimensional space by kernel function, and it was used to solve nonlinear classification and regression estimation problems (Li et al., 2019). On the other hand, Chaos Theory has made a great success in many fields of pure and applied sciences, especially in atmospheric sciences, climatology, economy, fluid mechanics, hydrology, medical sciences, etc. In this study, the two state of the art techniques were applied to the prediction of drought indices.

SVR is a product of SVM developed to be applied to the regression problems. In SVR, the most important

step of the application is to form the input matrix. In the current literature, there is no standard procedure in the construction of input matrix. CA enables the scientists to use a standard method to construct the input matrices which plays an important role in the success of the SVR method.

In the application stage, the above mentioned methods were applied to five frequently used drought indices for prediction purposes. Except for ZNDX and SPI01, which fluctuate almost randomly, the results are very encouraging. The results show clearly that the proposed hybrid method produces very accurate one-step predictions of drought indices. The proposed method has the ability to produce the prediction higher than one-step. Undoubtedly, such predictions will provide significant flexibility to the decision makers in terms of taking the necessary measures on time.

ACKNOWLEDGEMENT

This article was presented in American Meteorological Society (AMS)-27th Conference on Weather Analysis and Forecasting in Chicago, July 2nd, 2015.

REFERENCES

- Alley, W. M., (1984). The Palmer Drought Severity Index: Limitations and Assumptions. *Journal of Climate and Applied Meteorology* 23:1100–1109. doi: 10.1175/1520-0450(1984)023<1100:TPDSIL>2.0.CO;2
- American Meteorological Society, (1997) Meteorological Drought-Policy statement. *Bulletin of the American Meteorological Society* 78: 847-849.
- Arya, S., Mount, D. M., (1993). Approximate nearest neighbor searching. *Proc. 4th Ann. ACM-SIAM Symposium on Discrete Algorithms (SODA'93)* 271-280.
- Arya, S., Mount, D.M., Netanyahu, N. S., Silverman, R., Wu, A. Y., (1998). An optimal algorithm for approximate nearest neighbor searching fixed dimensions. *Journal of the ACM* 45 891-923. doi: 10.1145/293347.293348
- Bassingthwaighte, J. B., & Raymond, G. M. (1994). Evaluating rescaled range analysis for time series. *Annals of biomedical engineering*, 22(4), 432-444.
- Baydaroğlu, Ö., Koçak, K., (2014). SVR-based prediction of evaporation combined with chaotic approach. *Journal of Hydrology* 508 356-363. doi: 10.1016/j.hydrol.2013.11.008
- Baydaroğlu, Ö., Koçak, K., Duran, K. (2017). River flow prediction using hybrid models of support vector regression with the wavelet transform, singular spectrum analysis and chaotic approach. *Meteorology and Atmospheric Physics* 1-11. doi: 10.1007/s00703-017-0518-9
- Belayneh, A., Adamowski, J., Khalil, B., Ozga-Zielinski, B., (2014). Long-term SPI Drought forecasting in the Awash River Basin in Ethiopia using wavelet neural network and wavelet support vector regression model. *Journal of Hydrology* 508 418-429. doi: 10.1016/j.hydrol.2013.10.052
- Cao, L., (1997). Practical method for determining the minimum embedding dimension of a scalar time series. *Physica D: Nonlinear Phenomena* 110 1 pp. 43-50. doi: 10.1016/S0167-2789(97)00118-8
- Carrão, H., Naumann, G., & Barbosa, P., (2016). Mapping global patterns of drought risk: An empirical framework based on sub-national estimates of hazard, exposure and vulnerability. *Global Environmental Change*, 39, 108-124.
- Casdagli, M. (1989). Nonlinear prediction of chaotic time series. *Physica D: Nonlinear Phenomena*, 35(3), 335-356.
- Cortes, C., Vapnik, V., (1995). Support vector networks. *Machine Learning* vol. 20 pp. 273-297. doi: 10.1007/BF00994018
- Cutore, P., Di Mauro, G., Cancelliere, A., (2009). Forecasting Palmer Index using neural networks and climate indexes. *Journal of Hydrologic Engineering* Vol. 14 No.6. doi: 10.1061/(ASCE)HE.1943-5584.0000028#sthash.7USLO2fj.dpuf
- Fraser, A. M., Swinney, H. L., (1986). Independent coordinates for strange attractors from mutual information. *Phys. Rev. A* Vol. 33 Number 2. doi: 10.1103/PhysRevA.33.1134
- Golub, G., Charles, F. V. L., (1996). *Matrix Computations-Third Edition*. Baltimore. The John Hopkins University Press. P.53. ISBN 0-8018-5413-X
- Granata, F., Gargano, R., De Marinis, G., (2016). Support vector regression for rainfall-runoff modeling in urban drainage: A comparison with the epa's storm water management model. *Water* 8(3) 69. doi: 10.3390/w8030069
- Grassberger, P., Procaccia, I., (1983). Estimation of the Kolmogorov entropy from a chaotic signal. *Physical Review A* 28(4): 2591-2593. doi: 10.1103/PhysRevA.28.2591
- Hao, Z., Hao, F., Singh, V. P., Xia, Y., Ouyang, W., & Shen, X., (2016). A theoretical drought classification method for the multivariate drought index based on distribution properties of standardized drought indices. *Advances in water resources*, 92, 240-247.

- Heddinghaus, T. R., & Sabol, P. (1991, September). A review of the Palmer Drought Severity Index and where do we go from here. In *Proc. 7th Conf. on Applied Climatology* (pp. 242-246). Boston, MA: American Meteorological Society
- Kantz, H., & Schreiber, T. (1997). *Nonlinear time series analysis*. Cambridge University press.
- Karl, T. R., Knight, R. W., (1985). Atlas of Monthly Palmer Hydrological Drought Indices (1931–1983) for the Contiguous United States. Historical Climatology Series 3–7 National Climatic Data Center Asheville North Carolina.
- Kennel, M. B., Brown, R., Abarbanel, H. D. I., (1992). Determining embedding dimension for phase-space reconstruction using a geometrical construction. *Phys. Rev. A* 45 3403-3411. doi: 10.1103/PhysRevA.45.3403
- Kim, H. S., Eykholt, R., Salas, J. D., (1999). Nonlinear dynamics, delay times and embedding windows. *Physica D* 127 48-60. doi: 10.1016/S0167-2789(98)00240-1
- Koçak, K., Şaylan, L., Eitzinger, J., (2004). Nonlinear prediction of near-surface temperature via univariate and multivariate time series embedding. *Ecological Modelling* 1-7. doi: 10.1016/S0304-3800(03)00249-7
- Li, X., Luo, A., Li, J., & Li, Y. (2019). Air pollutant concentration forecast based on support vector regression and quantum-behaved particle swarm optimization. *Environmental Modeling & Assessment*, 24(2), 205-222.
- Li, P. C., Xu, S. H., (2005). Support vector machine and kernel function characteristic analysis in pattern recognition. *Computer Engineering and Design* vol. 26 pp. 302-304.
- Liong, S., Sivapragasam, C., (2002). Flood stage forecasting with support vector machines. *Journal of the American Water Resources Association* Vol.38 No.1. doi: 10.1111/j.1752-1688.2002.tb01544.x
- Liu, X., Ren, L., Yuan, F., Yang, B., (2009). Meteorological drought forecasting using Markov Chain Model. 2009 International Conference on Environmental Science and Information Application Technology. doi: 10.1109/ESIAT.2009.19
- McKee, T. B., Doesken, N. J., Kleist, J., (1993). The Relationship of Drought Frequency and Duration to Time Scales. *Proceedings of the Eighth Conference on Applied Climatology* American Meteorological Society: Boston: 179–184.
- Mehta, V. M., Wang, H., Mendoza, K., Rosenberg, N. J., (2014). Predictability and prediction of decadal hydrological cycles: A case study in Southern Africa. *Weather and Climate Extremes* 3 47-53. doi: 10.1016/j.wace.2014.04.002
- Ortiz-Garcia, E. G., Salcedo-Sanz, S., Perez-Bellido, A. M., Portilla-Figueraz, J. A., Prieto, L., (2010). Prediction on hourly O₃ concentrations using support vector regression algorithms. *Atmospheric Environment* 44 4481-4488. doi: 10.1016/j.atmosenv.2010.07.024
- Packard, N. H., Crutchfield, J. P., Farmer, J. D., Shaw, R. S., (1980). Geometry from a time series. *Physical Review Letters* 45 (9). doi: 10.1103/PhysRevLett.45.712
- Palit, S. K., Mukherjee, S., Bhattacharya, D. K., (2013). A high dimensional delay selection for the reconstruction of proper phase space with cross auto-correlation. *Neurocomputing* 113 49-57. doi: 10.1016/j.neucom.2013.01.034
- Palmer, W. C., (1965). *Meteorological Drought*. Res. Paper No.45 58pp. Dept. of Commerce Washington D.C.
- Porporato, A., Ridolfi, L., (1997). Nonlinear Analysis of near-wall turbulence time series. *Applied Scientific Research* 57: 235-261. doi: 10.1007/BF02506062
- Santamaria-Bonfil, G., Reyes-Ballesteros, A., Gershenson, C., (2016). Wind speed forecasting for wind farms: A method based on support vector regression. *Renewable Energy* 85 790-809. doi: 10.1016/j.renene.2015.07.004
- Steel, R. G. D., Torrie, J. H., (1960). *Principles and Procedures of Statistics with Special Reference to the Biological Sciences*. McGraw Hill.
- Takens, F., (1981). Detecting strange attractors in turbulence. In: Rand, DA Young, LS (Eds.) *Lecture Notes in Math*. Springer-verlag pp. 366-381.
- Vapnik, V., Lerner, A., (1963). Pattern recognition using generalized portrait method. *Automation and Remote Control* 24: 774-780.
- Vapnik, V., Chervonenkis, A., (1964). A note on one class of perceptrons. *Automation and Remote Control* vol. 25.
- Vapnik, V. N., (1995). *The nature of statistical learning theory*. Springer New York.
- Vapnik, V. N., (1999). An overview of statistical learning theory. *Neural Networks IEEE Transactions on* Vol.10 No.5 988-999. doi: 10.1109/72.788640
- Wang Y, Wu D.L., Guo C.X., Wu Q.H., Qian W.Z. and Yang J., (2010). Short-term wind speed prediction using support vector regression. *IEEE PES General Meeting, Providence, RI*, pp. 1-6, doi: 10.1109/PES.2010.5589418.
- Wilhite, D. A., Glantz, M. H., (1985). Understanding the drought phenomenon: The role of definitions. *Water International* 10 (3): 111–120. doi: 10.1080/02508068508686328
- Willmott, C. J., & Matsuura, K. (2005). Advantages of the mean absolute error (MAE) over the root mean

- square error (RMSE) in assessing average model performance. *Climate research*, 30(1), 79-82.
- Yihdego, Y., Vaheddoost, B., & Al-Weshah, R. A. (2019). Drought indices and indicators revisited. *Arabian Journal of Geosciences*, 12(3), 69.
- Yu, P., Chen, S., Chang, I., (2006). Support vector regression for real time flood stage forecasting. *Journal of Hydrology* 328 704-716. doi: 10.1016/j.jhydrol.2006.01.021
- Yu, X., Liang, S., (2007). Forecasting of hydrologic time series with ridge regression in feature space. *Journal of Hydrology* 332 290-302.
- <ftp://ftp.ncdc.noaa.gov/pub/data/cirs/climdiv/drought-readme.txt> (accessed in May, 2014)
- <https://www.cisa.sc.edu/atlas/glossary.html> (accessed in October, 2020)
- <https://cran.r-project.org/web/packages/nonlinearTseries/nonlinearTseries.pdf>
- <https://cran.r-project.org/web/packages/fractal/index.html>
- <https://www.ncdc.noaa.gov/data-access/land-based-station-data/land-based-datasets/global-historical-climatology-network-ghcn> (accessed in October, 2020)



Citation: I. Mubarak, M. Janat (2020) Quinoa response to different transplanting dates and nitrogen fertilization levels in an arid environment. *Italian Journal of Agrometeorology* (2): 77-89. doi: 10.13128/ijam-962

Received: June 8, 2020

Accepted: September 26, 2020

Published: January 25, 2021

Copyright: © 2020 I. Mubarak, M. Janat. This is an open access, peer-reviewed article published by Firenze University Press (<http://www.fupress.com/ijam>) and distributed under the terms of the Creative Commons Attribution License, which permits unrestricted use, distribution, and reproduction in any medium, provided the original author and source are credited.

Data Availability Statement: All relevant data are within the paper and its Supporting Information files.

Competing Interests: The Author(s) declare(s) no conflict of interest.

Quinoa response to different transplanting dates and nitrogen fertilization levels in an arid environment

IBRAHIM MUBARAK*, MUSSADDAK JANAT

Atomic Energy Commission of Syria

*Corresponding author. E-mail: ascientific10@aec.org.sy

Abstract. Quinoa is recognized as a water-stress tolerant crop. Nevertheless, few findings are presently available on fully-irrigated quinoa growth and productivity grown in arid Mediterranean area. Field experiments conducted in Syria for two growing seasons (2017/18 and 2018/19) determined the response of quinoa crop (ICBA-Q5 cultivar) to five different transplanting dates (TD) (December, January, February, March, and April) and four nitrogen fertilizer levels (0, 90, 180 and 270 kg N ha⁻¹). Main findings showed that quinoa had a good adaptation (up to 5.30 and 15.9 t ha⁻¹ of seed and dry matter yields, respectively) to very low N-inputs, with a high capacity to evapotranspire (ETc), resulting in high crop coefficient (kc). ETc and kc varied in the range of 590-1136 mm and 0.37-2.05 among the TDs, respectively. Moreover, quinoa growth and productivity were highly affected by TDs, and varied from year to year, influenced mainly by temperature. Emphasis in future experiments should probably be given to TD in December, which exhibited a high degree of consistency over years with high crop performance, and to TDs in January and February, which performed extremely well in the first year.

Keywords. Agro-meteorology, water productivity, irrigation water use efficiency, quinoa seed yield potentials, arid Mediterranean area.

1. INTRODUCTION

Quinoa (*Chenopodium quinoa* Willd.) is a well-known highly nutritional crop due to the high-quality proteins contained in its seeds (Repo-Carrasco et al., 2003). The whole plant of quinoa can also be used as livestock feed (Blanco Callisaya, 2015). Moreover, quinoa is recognized as a resilient crop to abiotic stresses, such as salinity (Hinojosa et al., 2018), drought (Fuentes and Bhargava, 2011), heat (Alvar-Beltrán et al., 2020) and frost (Jacobsen et al., 2003), and there is a wider global interest in its cultivation (Choukr-Allah et al., 2016). Thanks to its exceptional features, the Food and Agriculture Organization of the United Nations (FAO) considered quinoa as one of the most important crops, playing a crucial role on ensuring food security (FAO and CIRAD, 2015).

Quinoa crop performed well under deficit irrigation without detriments to yield (Geerts et al., 2008a, b; Razzaghi et al., 2011, 2012; Pulvento et al., 2012;

Alvar-Beltrán et al., 2019). However, very little information is available on growth and seed and biomass productivity potentials of quinoa crop grown under full irrigation in hot and dry environment (Al-Naggar et al., 2017; Ahmadi et al., 2019). Under such climate conditions, Ahmadi et al. (2019) indicated that quinoa showed very high crop evapotranspiration (1448-1687 mm) and transpiration (777-1228 mm) rates for different plant density rates. They reported that quinoa has a specific physiological system (relatively high stomata conductance and sizes) transpiring continually and allowing better leaf cooling under hot climate conditions, resulting in high water consumption. However, Alvar-Beltrán et al. (2019) showed crop evapotranspiration rates of 400-500 mm under full irrigation in Burkina Faso for short-cycle quinoa cultivars (about 3 months). This indicates that quinoa crop water needs may vary under full irrigation according to the agro-climatic context.

Moreover, many findings indicated that quinoa seed yields increased with increasing nitrogen applications. Different N-fertilizer needs of quinoa crop were reported: 120 kg N ha⁻¹ (Schulte auf'm Erley et al., 2005), 240 kg N ha⁻¹ (Hirich, 2014), 350 kg N ha⁻¹ (Ahmadi et al., 2019), 360 kg N ha⁻¹ (Shams, 2017; Shoman, 2018), 570 kg N ha⁻¹ (Rao and Shahid, 2012), and 200 mg N per kg of soil (equivalent to 780 kg N ha⁻¹ for 30-cm soil profile with a supposed density of 1.35 g cm⁻³) (Lavini et al., 2014). The obtained N-requirements were very high and pose the question on the eco-environmental impacts of quinoa crop fertilization. On the other hand, there is another contradictory trend indicating that N-fertilizer had no critical role on quinoa crop growth or seed production. For instance, Alvar-Beltrán et al. (2019) found a high performance of quinoa under very low nitrogen applications (25 kg N ha⁻¹). Moreale (1993) also showed that the N-uptake of quinoa crop was of 25 kg N per ton of seed production. Hence, selecting the optimal nitrogen application rate for quinoa is a continuous need in ever changing agro-pedo-climatic conditions.

In the context of semi-arid and arid Mediterranean region, where water scarcity is a constraint to agricultural production, scientists considered quinoa as an alternative crop to sustain seed crop production (Rao and Shahid, 2012; Benlhabib et al., 2015; Dost, 2015; Choukr-Allah et al., 2016). Several studies were carried out in the northern Mediterranean countries (e.g. in Italy (Pulvento et al., 2015), in Turkey (Yazar et al., 2015) and in Greece (Noulas et al., 2015)), as well in most of the MENA (Middle East and North Africa) countries (Choukr-Allah et al., 2016). However, to the best of our knowledge, very limited attempts related to quinoa cultivation in Syria were conducted (Lavini et al., 2014; Jbawi et al., 2018). Almost no research findings based on multi-year field experiments are presently available on quinoa cultivation, adaptation and productivity

in Syria, and therefore, important scientific outcomes are much needed. Therefore, the objectives of this two-year field experiment were (i) to determine crop water and N-fertilizer requirements and crop coefficient for quinoa crop, (ii) to determine the suitable transplanting date for quinoa crop under arid Mediterranean climate in Syria and (iii) to determine potential seed and dry matter yields, water productivity and irrigation water-use efficiency under full irrigation.

2. MATERIALS AND METHODS

2.1. Study site, soil and agricultural practices

Field experiments were conducted during two consecutive growing seasons 2017/18 and 2018/19 at the Agricultural Experiment Station, Deir Al-Hajar, Damascus Countryside in Syria (33°20'N, 36°26'E, 600 m a.s.l.). The arid Mediterranean climate type dominates the study area with a yearly potential evapotranspiration (ET₀) exceeds 2000 mm, and with a yearly precipitation of about 120 mm. The main climate data which were collected during both tested growing seasons (maximum and minimum air temperatures and precipitation) and those estimated based on the procedures of Allen et al. (1998) are displayed in Tables (1 and 2) and Figures (1 and 2).

The soil was classified as a clay loam texture, containing 29.5% clay, 42.7% silt, 27.8% sand, with a bulk density of 1.35 g cm⁻³. Some chemical and physical soil properties were: pH 8.0; ECe 0.19 ds m⁻¹; organic matter <1%; available P 5.7 ppm; NO₃⁻ 10.9 ppm; NH₄⁺ 19.8 ppm. Volumetric soil water contents at field capacity and permanent wilting point were 0.36 and 0.18 m³ m⁻³, respectively. Irrigation water properties were of pH 8.4; ECe 0.46 ds m⁻¹; NO₃⁻ 1.05 ppm; NH₄⁺ 1.99 ppm.

The quinoa seeds of Q5 cultivar (with long cycle of around 150 days) used in this study were obtained from ICBA (the International Centre for Biosaline Agriculture). Due to the difficulties encountered in seed germination in the field, quinoa seedlings, which were produced indoor at room temperature (20-25 °C), were used instead of direct sowing. Seedlings were transplanted 15-20 days after sowing, with seedling density of 8 plants m⁻². Five different transplanting dates separated with one month were tested in each year: TD-Dec (mid-December), TD-Jan (mid-January), TD-Feb (mid-February), TD-Mar (mid-March) and TD-Apr (mid-April). At each planting date, four N-fertilizer levels were evaluated: 0 (N0), 90 (N90), 180 (N180) and 270 (N270) kg N ha⁻¹. N-fertilizer as urea (N: 46%) was broadcasted in 2, 4, and 6 equally split applications, for N90, N180 and N270, respectively, with two-week intervals. The 1st application of urea was at transplanting. Experiments were arranged in a split-plot design involving

Tab. 1. The main climate data for the experimental station during both growing seasons 2017/18 and 2018/19.

Parameter	Growing season	Dec.	Jan.	Feb.	Mar.	Apr.	May	Jun.	Jul.	Aug.
Mean temperature (°C)	2017/18	11.2	8.7	12.3	16.1	18.6	23.5	26.4	28.3	28.7
	2018/19	10.2	7.9	10.0	11.9	15.1	24.6	27.8	28.3	29.0
Maximum temperature (°C)	2017/18	18.9	14.2	18.8	24.3	27.2	31.5	34.6	36.9	37.1
	2018/19	14.8	13.2	15.1	18.3	22.2	34.2	36.6	37.3	38.0
Minimum temperature (°C)	2017/18	3.6	3.3	5.7	7.9	10.0	15.6	18.2	19.8	20.2
	2018/19	5.6	2.6	4.8	5.5	8.1	15.0	19.0	19.4	20.1
Precipitation (mm)	2017/18	0.0	34.0	30.3	1.0	14.0	9.9	6.4	0.0	0.0
	2018/19	35.8	48.0	32.5	17.4	11.6	0.0	0.0	0.0	0.0
Reference evapotranspiration, ET ₀ (mm day ⁻¹)	2017/18	3.31	2.56	3.56	5.18	6.33	7.35	8.15	8.66	8.26
	2018/19	2.40	2.44	2.87	3.92	5.11	8.43	8.79	8.86	8.59

Tab. 2. Agro-climate parameters during the growing period of each transplanting date for both seasons 2017/18 and 2018/19.

Treat.	Trans-planting date	Harvesting date	Flowering date	Growing period (days)	I (mm)	P (mm)	ΔS (mm)	ETc (mm)	kc (-)	Tmean (°C)	VPD (kPa)	Rn (mm)	ET0 (mm)	α (-)
TD-Dec	10/12/2017	22/04/2018	14/02/2018	133	540	66.7	32.6	639.3	1.16	1757.8	127.6	361.2	549.5	1.77
TD-Jan	14/01/2018	04/06/2018	25/03/2018	141	800	84.0	-18.3	865.7	1.15	2350.9	173.0	565.9	755.9	1.53
TD-Feb	15/02/2018	24/06/2018	20/04/2018	129	956	54.2	-37.5	972.7	1.18	2553.0	191.7	634.1	827.6	1.53
TD-Mar	18/03/2018	15/07/2018	16/05/2018	119	1083	31.3	-11.4	1102.4	1.22	2712.5	214.1	679.6	903.4	1.62
TD-Apr	15/04/2018	06/08/2018	10/06/2018	113	1010	28.9	15.0	1053.9	1.13	2850.8	226.4	689.8	936.7	1.53
TD-Dec	16/12/2018	01/06/2019	09/03/2019	167	450	138.9	-0.7	588.2	0.80	2256.3	165.9	574.8	739.7	1.02
TD-Jan	16/01/2019	01/07/2019	09/04/2019	166	804	80.5	-2.4	882.1	0.93	2825.3	222.0	733.7	948.8	1.20
TD-Feb	11/02/2019	09/07/2019	26/04/2019	148	930	41.2	61.2	1032.4	1.08	2820.0	226.1	741.6	957.5	1.39
TD-Mar	17/03/2019	21/07/2019	19/05/2019	126	1010	26.4	100.2	1136.6	1.19	2808.5	231.4	724.0	958.8	1.57
TD-Apr	14/04/2019	22/08/2019	18/06/2019	130	1005	9.4	36.6	1051.0	0.93	3339.4	285.5	806.4	1131.8	1.30

I=total irrigation water amount; P=total precipitation; ΔS= the change in soil water storage; ETc=seasonal crop evapotranspiration; kc=the average of crop coefficient computed as $kc=ETc/ET_0$; Tmean=cumulative mean temperature; VPD=cumulative vapour pressure deficit; Rn=cumulative net radiation (converted from MJ m⁻² into mm); ET0=cumulative reference evapotranspiration; α=the advection correction factor computed as $\alpha=ETc/Rn$.

five transplanting dates as main-plots and four N-fertilizer levels as sub-plots, with three replicates.

The field was conventionally prepared before transplanting. In each transplanting date, 12 plots (4 N-levels with 3 replicates) were prepared with 3×4 m² per plot, each surrounded by dikes from all sides. Enough spacing (about 1.5 m) was maintained between plots to minimize water and N-fertilizer intervention. Weeds were removed by hand three times within 10–50 days after transplanting during the growing season.

2.2. Irrigation management and crop evapotranspiration

During the growing season full irrigation was applied to all quinoa plots. Irrigation water was delivered through a

polyethylene pipe of 25 mm diameter to each plot, in order to enhance irrigation practices; and volumes of applied water were measured by flow meters. Irrigation was scheduled once a week based on the soil water content measurements just before each irrigation event. Monitoring the soil water content was done using *in-situ* calibrated neutron probe, which ensured that the soil moisture depleted in the previous week was precisely replenished. For irrigation scheduling purposes, the depths of active roots were 0.30 m from the beginning until peak flowering, and then 0.60 m until termination. The amount of irrigation water applied per irrigation event (I, mm) was estimated as follows:

$$I = 1000 \times (\theta_{fc} - \theta_{ob}) \times Z_r \quad (1)$$

where θ_{fc} is the volumetric soil water content at field capac-

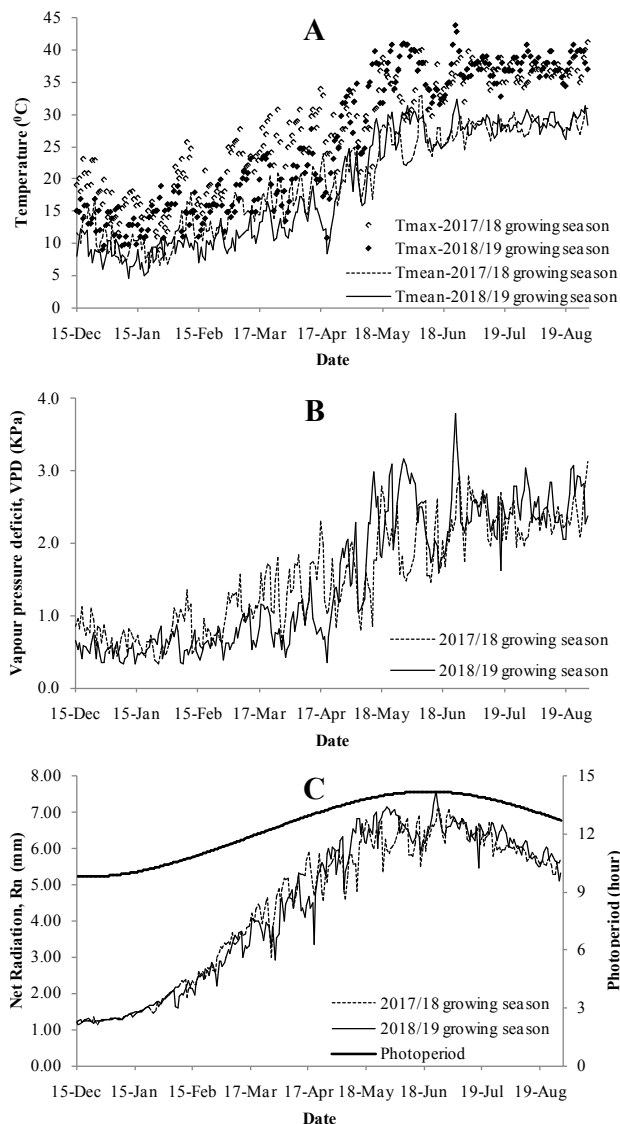


Fig. 1. Variations of (A) mean and max air temperatures, (B) vapor pressure deficit and (C) net radiation and photoperiod during both growing seasons.

ity ($=0.36 \text{ m}^3 \text{ m}^{-3}$), θ_{ob} is the volumetric soil water content observed just before irrigation event ($\text{m}^3 \text{ m}^{-3}$), Z_r is the soil depth (active root depth) to be considered (m). To convert this amount into m^3 per plot, it was multiplied by the plot area (m^2) and then divided by 1000.

Quinoa crop evapotranspiration (ET_c) was estimated using the water balance equation:

$$ET_c = I + P - D_p - R_o \pm \Delta S \quad (2)$$

where I is the amount of irrigation water applied (mm), P is the precipitation (mm), D_p is the deep percolation (mm),

and R_o is the amount of runoff (mm), ΔS is the change in soil water storage in the specified soil profile (mm), as measured by the neutron probe. Since the amount of irrigation was controlled, runoff was assumed to be zero. Observing soil water content showed that the deep percolation below 0.60 m in depth was negligible. The daily crop evapotranspiration (mm day^{-1}) was estimated by dividing the ET_c calculated using Eq. (2) by the days between two successive irrigations (7 days). The seasonal ET_c was the summation of the daily ET_c , which represented the total crop water requirements for each planting set. The daily reference evapotranspiration (ET_0) was calculated by FAO Penman-Monteith equation (Allen et al., 1998). Crop coefficient (k_c) for quinoa was calculated by dividing ET_c by ET_0 as:

$$k_c = \frac{ET_c}{ET_0} \quad (3)$$

2.3. Seed yield, dry matter and crop water productivities

Quinoa plants were harvested when seeds were ripened and dry. Representative 1-m^2 area (8 plants) was selected from each experimental unit (a total of 60 units = 5 TDs \times 4 N-levels \times 3 replicates). The heads of selected plants were cut off and the seeds were separated and weighted to estimate quinoa seed yield (QSY). The empty heads (after seed separation) and the aboveground vegetative parts of selected plants were gathered, and then oven dried at 70°C until constant weight for dry matter yield (DMY) determination. Weights of grains and vegetative parts of selected plants were converted into ton per hectare (t ha^{-1}). The harvest index (HI) was calculated by dividing the seed yield (QSY) by the total plant biomass (the sum of QSY and DMY). The weights of thousand seeds (manually counted) were also recorded (W1000). Both crop water productivity (WP, kg per m^{-3}) and irrigation water use efficiency (IWUE, kg per m^{-3}) were determined using equations (4) and (5), respectively.

$$WP = \frac{QSY}{ET_c} \quad (4)$$

$$IWUE = \frac{QSY}{I} \quad (5)$$

2.4. Statistical analysis

All measured variables (QSY, DMY, HI, W1000, WP and IWUE) were subjected to a two-way analysis of variance using the DSAASTAT add-in version 2011 (Onofri, 2007). A combined analysis of data over both years was performed to identify transplanting date and N-level

managements whose average effect over years is stable and high (Gomez and Gomez, 1984). As both tested factors are quantitative, trend comparison (regression analysis) was conducted to test the functional relationship between measured variable and tested factors. The coefficient of determination of regression function and its significance were presented.

3. RESULTS

3.1. Climate data, crop evapotranspiration and crop coefficient

Mean and max air temperature (T_{mean} and T_{max}), vapour pressure deficit (VPD), reference evapotranspiration (ET_0) variations over both growing seasons are shown in Figures 1A, 1B and 2A, respectively. In general, these parameters decreased from December to mid-January, to gradually increase up to the end of June before they reached a plateau for the rest of growing season. Comparing of both growing seasons reveals two distinguished parts: from December to April, and from May to the end of August. In the 1st part, the four parameters T_{mean} , T_{max} , VPD and ET_0 in the 2017/18 season were 20, 23, 25 and 37% higher than those in the 2018/19, respectively. While in the 2nd part they were about 3, 4, 7 and 11% lower. Starting from the flowering stage till the maturity, the critical 35 °C threshold was exceeded 0, 7, 14, 31 and 39 times for TD-Dec, TD-Jan, TD-Feb, TD-Mar and TD-Apr in the 2017/18 season, but 15, 33, 41, 45 and 56 times in the 2018/19 season, respectively.

Figure 1C shows variations of both net radiation (R_n , converted from MJ m^{-2} to mm) and photoperiod parameters over both growing seasons. Due to the latitude of the experimental site, the photoperiodicity and R_n varied strongly during growing cycle. The values of R_n from December to

April in the 2017/18 season were higher than those in the 2018/19 season; after that, they were somewhat lesser.

Rainfall distribution patterns during both studied years are illustrated in Figure 2B. The 2018/19 recorded 145.3 mm (21% more than the annual precipitation), almost uniformly distributed from December to mid-April. However, the cumulative precipitation in the 2017/18 was 95.6 mm (20% less than the annual record), with no rain in December or from the end of February to the last third of April. However, cumulative precipitation (P) recorded within each transplanting date were presented in Table 2.

The total values of T_{mean} , VPD, ET_0 and R_n which quinoa plants were exposed to during the growing cycle of each transplanting date, were also presented in Table 2. Minimum values were observed for quinoa transplanted in TD-Dec, and then they increased as the transplanting date delayed. During the 2018/19 season the total values of the accumulated climatic parameters were much higher than those accumulated during the 2017/18 season, due to the prolongation in growing periods for all TDs as mentioned below. For instance, cumulative ET_0 for TD-Dec, TD-Jan, TD-Feb, TD-Mar and TD-Apr in the 2018/19 season were 35, 26, 16, 6 and 21% higher than those in the 2017/18 season.

The differences in climatic parameters within a growing season influenced the lengths of growing periods, so that they decreased after January (Table 2). The growing period lengths were also affected by the differences between both growing seasons, so that they prolonged for all TDs in the 2018/19 season compared with those in the 2017/18 season. This prolongation was obvious for the earlier transplanting dates in December, January and February.

The soil water balance components (I , P and ΔS) and seasonal ET_c for each transplanting date are shown in Table 2. Minimum ET_c was observed for quinoa transplanted in TD-Dec (639 and 588 mm in the 2017/18 and the 2018/19 seasons, respectively), and then increased as the transplant-

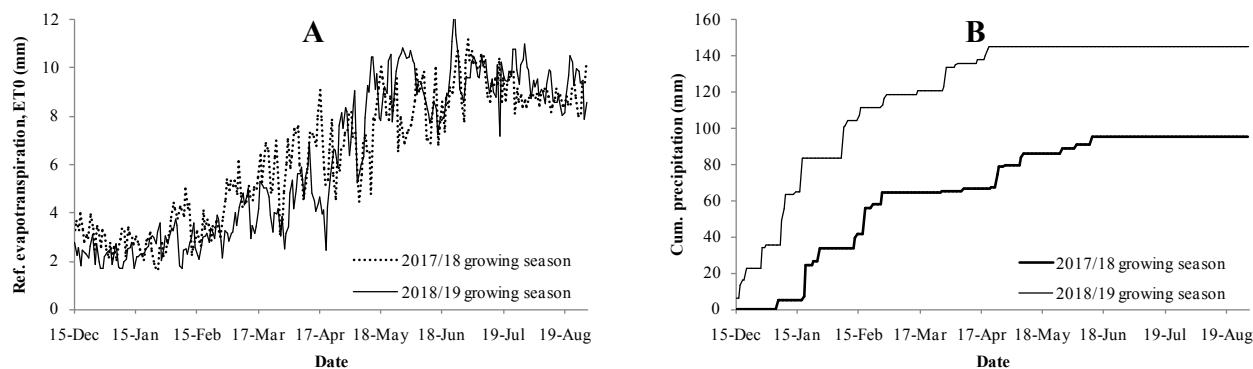


Fig. 2. Variations of (A) reference evapotranspiration and (B) cumulative precipitation during both growing seasons.

Tab. 3. Analysis of variance of the combined data of quinoa crop responses as affected by transplanting date, N-fertilizer level and year (significance of *F*-test).

Source of variance	df	QSY	DMY	HI	W1000	WP	IWUE
Year (Y)	1	b	b	b	b	b	b
Rep. within Y	4						
Transplanting date (TD)	4	ns	ns	ns	ns	ns	ns
N-fertilizer level (N)	3	ns	*	ns	ns	ns	ns
Y × TD	4	**	**	**	**	**	**
Y × N	3	ns	ns	ns	ns	ns	ns
TD × N	12	ns	ns	ns	ns	ns	ns
Y × TD × N	12	ns	ns	ns	ns	ns	ns
Pooled error	60						
Total	119						

^b = Repls. within year d.f. is not adequate for valid test of significance.

* = significant at 5% level; ** = significant at 1% level; ns = non-significant at 5% level,

df = degree of freedom; QSY = quinoa seed yield; DMY = dry matter yield; HI = harvest index; W1000 = weight of 1000 seeds; WP = water productivity and IWUE = irrigation water use efficiency.

ing date delayed (Table 2). These results reveal the effects of transplanting date on crop water requirements.

Crop coefficient (kc) of quinoa was nearly weekly calculated using Eq. (3) (data not shown). Its minimum values varied between 0.53 and 0.62 in the 2017/18 growing season and between 0.37 and 0.56 in the 2018/19 season. Whereas its maximum values varied between 1.83 and 2.05 in the 2017/18 growing season, and between 1.23 and 1.93 in the 2018/19 season. However, the kc values presented in Table 2, were determined for the whole growing period for each TD using the seasonal ET_c and the cumulative ET₀ as inputs for Eq. (3). The time-averaged kc values varied among TDs and from year to year. It was higher in the 2017/18 season compared with the 2018/19 season, for all TDs.

3.2. Nitrogen fertilizer impact

Except for DMY, the combined analysis over years indicated that the main effect of N-fertilizer level and the interaction effects involving N-level were not statistically significant (Table 3). However, only the main effect of N-fertilizer on DMY was significant at the 5% level, but with a very high *p*-value (*p*=0.04). Trend analysis demonstrated that the relationship between DMY and N-fertilizer level was cubic (equation not presented) with significant values of R-square at the 5% level. DMY peaked at N90 (7.92 t ha⁻¹) and bottomed out at N270 (6.49 t ha⁻¹). However, although the trend analysis indicated that the maximal DM

yield could be mathematically obtained at 90 kg N ha⁻¹, the increase in DMY between 0 and 90 kg N ha⁻¹, following the regression equation, is very small (less than 7%). Although no statistical significant differences were found to the increasing N-fertilizer level, adding 90 kg N ha⁻¹ (N90) showed superiority over the other tested levels for W1000 (2.16 g), WP (0.20 kg m⁻³) and IWUE (0.22 kg m⁻³). While QSY and HI reached their maximum averaged values under N180 (1.71 t ha⁻¹ and 20.6%, respectively). The averaged values of QSY over both growing seasons were 1.37, 1.62, 1.71 and 1.57 t ha⁻¹ under N0, N90, N180, and N270, respectively; while the averaged values of DMY over both growing seasons were 6.99, 7.92, 7.03 and 6.49 t ha⁻¹ under N0, N90, N180, and N270, respectively.

3.3. Transplanting date impact

As mentioned above, irrigation water amounts and seasonal crop evapotranspiration (ET_c) for the studied TDs are shown in Table 2 for both growing seasons. The seasonal ET_c differed slightly from the applied irrigation water amounts, due to the different precipitations. However, irrigation water amount followed the same tendency as the seasonal ET_c, where it increased considerably as the transplanting date delayed. Compared with the irrigation amount applied to plants transplanted in December (TD-Dec), irrigation water amount increased by 260, 416, 543 and 470 mm in the 2017/18 season, and by 354, 480, 560 and 555 mm in the 2018/19 season, for TD-Jan, TD-Feb, TD-Mar and TD-Apr, respectively. This indicates the role of transplanting date on irrigation water requirements of quinoa crop.

Figure 3 shows the evolutions over time of both water productivity (WP) and irrigation water use efficiency (IWUE) for both growing seasons. In the 2017/18, both parameters reached high points for TD-Jan, and bottomed out for TD-Mar and TD-Apr. However, in the 2nd season TD-Dec rivalled both TD-Jan and TD-Feb with very high values of both WP and IWUE, and they both decreased as TD delayed. Trend analysis indicated that the relationships between WP and IWUE and transplanting date for each growing season were cubic in the 2017/18 growing season and quadratic in the 2018/19 season (equations not presented) with significant values of R-square at the 1% level.

The combined analysis over years indicated that the main effects of TD were not significant. However, only the year × transplanting date interaction effect was detected to be highly significant with *p*<0.01 (Table 3). Therefore, the response of quinoa crop to transplanting date varied from year to year.

The QSY data of different transplanting dates was compared under both growing seasons (Fig. 4A). In the

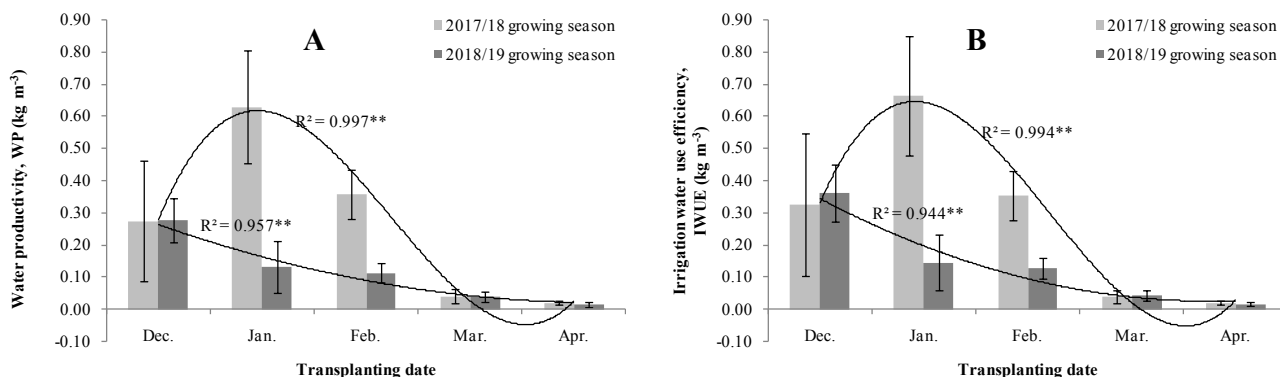


Fig. 3. Variations of (A) water productivity and (B) irrigation water use efficiency during both growing seasons. Error bars represent the standard deviations. R-square represents the coefficient of determination of regression equations fitted but not showed. ** = significant at the 1% level.

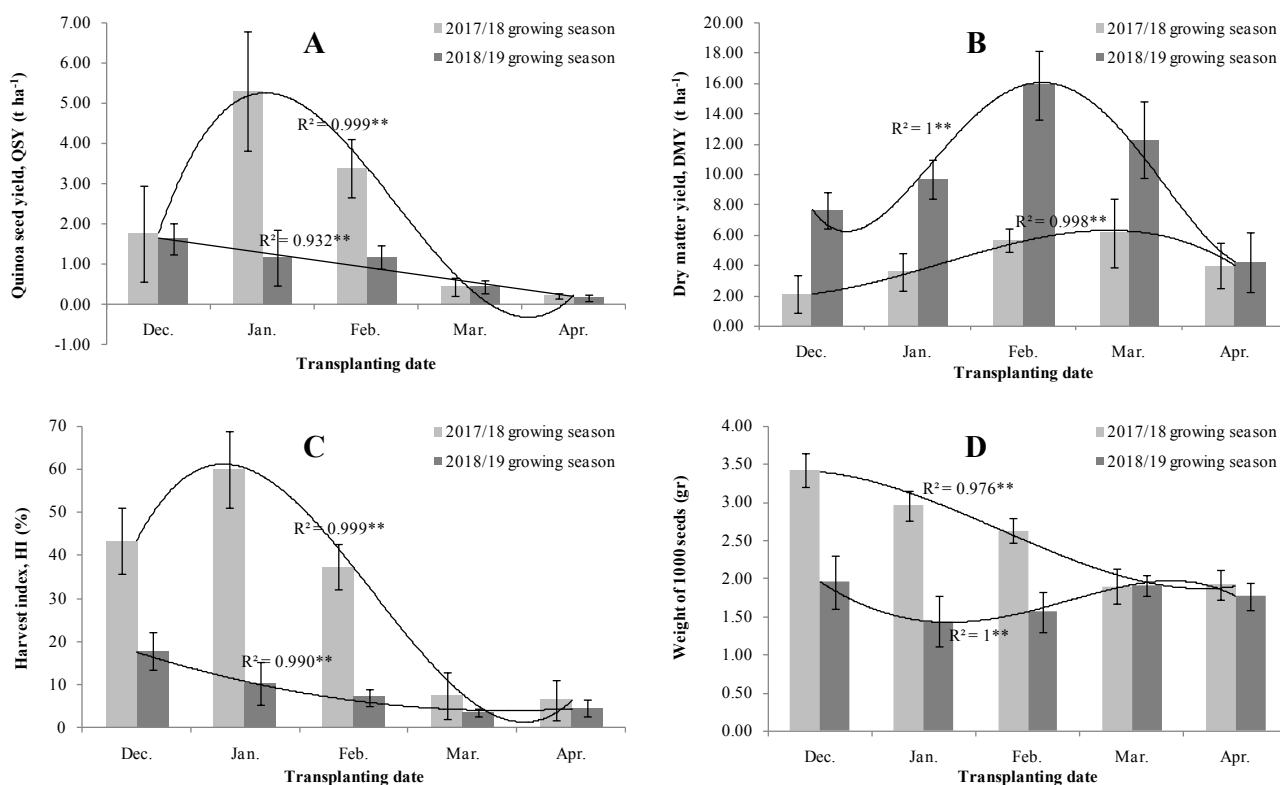


Fig. 4. Variations of (A) quinoa seed yield, (B) dry matter yield, (C) harvest index and (D) weight of 1000 seeds during both growing seasons. Error bars represent the standard deviations. R-square represents the coefficient of determination of regression equations fitted but not showed. ** = significant at the 1% level.

2017/18 growing season, QSY peaked in TD-Jan and bot-tomed out in TD-Mar and TD-Apr. While in the 2018/19 growing season, QSY decreased as transplanting date de-layed. However, quinoa plants transplanted in December, March and April showed somewhat similar seed produc-tions when both growing seasons were compared, while

plants transplanted in January and February produced seeds much higher in the 2017/18 growing season than their homologues in the 2018/19 season. This difference in QSY evolutions could explain the nature of the year × transplanting date interaction. Trend analysis indicated that the relationships between QSY and transplanting date

were cubic in the 2017/18 growing season and linear in the 2018/19 season (equations not presented) with significant values of R-square at the 1% level (Fig. 4A).

The variations over both growing seasons in dry matter yield could also explain the nature of the interaction effects of year \times transplanting date on DMY (Fig. 4B). Dry matter yield varied between 2.10 and 6.14 t ha⁻¹ in the 2017/18 growing season, and between 4.21 and 15.88 t ha⁻¹ in the 2018/19 growing season. DMY reached a peak with plants for TD-Mar in the 1st season, while it peaked with plants transplanted for TD-Feb in the 2nd season. Moreover, DMYs of the 2018/19 growing season were found to be much higher than those of the 2017/18 season for all TDs. Trend analysis indicated that the relationships between DMY and transplanting date were quartic in the 2017/18 growing season and cubic in the 2018/19 season (equations not presented) with significant values of R-square at the 1% level (Fig. 4B).

The values of harvest index (HI) varied between 6.5 and 59.9% and between 5.5 and 17.7% in the 2017/18 and 2018/19 growing seasons, respectively (Fig. 4C). In the 1st growing season, HI peaked for TD-Jan and bottomed out for TD-Mar and TD-Apr. While it dropped as transplanting date delayed in the 2nd growing season. However, its values were much higher in the 1st growing season than their homologues in the 2nd season for all TDs. Its different evolutions over time among TDs and from year to year could explain the nature of the year \times transplanting date interaction effects on HI. Trend analysis indicated that the relationships between HI and transplanting date were cubic in the 2017/18 growing season and quadratic in the 2018/19 season (equations not presented) with significant values of R-square at the 1% level (Fig. 4C).

The weight of 1000 seeds (W1000) significantly varied over time for both growing seasons (Fig. 4D). It dropped as the transplanting date delayed in the 2017/18 season. However, it decreased from TD-Dec to TD-Jan, then it recover after that in the 2018/19 season. Quinoa seeds of TD-Dec, TD-Jan and TD-Feb in the 2017/18 season were much heavier than those of the 2018/19 season, while both TD-Mar and TD-Apr produced seeds with somewhat similar weights in both seasons. Trend analysis showed that the relationships between W1000 and transplanting date were quartic in the 2017/18 growing season and cubic in the 2018/19 season (equations not presented) with significant values of R-square at the 1% level (Fig. 4D).

4. DISCUSSION

Unlike the common idea that quinoa crop needs large quantity of N-fertilizer (Rao and Shahid, 2012; Hirich,

2014; Lavini et al., 2014; Shams, 2017; Shoman, 2018; Ahmadi et al., 2019), this study revealed contrasting findings under full irrigation conditions in an arid environment. Our findings showed that quinoa crop has a very good adaptation to low fertility soil, i.e., <1% organic matter and very low N-requirements. Either the nitrogen quantities initially found in both soil (about 43.5 kg N ha⁻¹) and irrigation water (about 1.06 kg N per 1000 m³) were satisfactory to meet the crop N-requirements, and no extra N-fertilizer amount was required, or the quinoa crop N-requirements exceed the range of N-levels tested herein (> 270 kg N ha⁻¹) to probably have significant impacts. Our results are in agreement with those of Alvar-Beltrán et al. (2019) who found that quinoa crop can be highly performing under very low nitrogen applications (25 kg N ha⁻¹). Moreover, these results are in accordance with those of Moreale (1993) who showed that the N-uptake of quinoa crop was of 25 kg N per ton of seed production, indicating that N-fertilizer had no critical role on quinoa crop growth or seeds produced. The combined effect of both full irrigation (high level of soil water content) and high temperature could cause ammonia volatilization and hydrolysis, especially under high N-fertilizer levels (Alvar-Beltrán et al., 2019). On the other hand, our findings are not in harmony with those of other studies showing quinoa yield enhancement with increasing N-fertilizer applications. The optimal N-fertilization needs of quinoa crop obtained by those studies were of about 360 kg N ha⁻¹ (Shams, 2017; Shoman, 2018), 570 kg N ha⁻¹ (Rao and Shahid, 2012), and 200 mg N per kg of soil (Lavini et al., 2014). These various values could be attributed to the growing region, soil type and quinoa cultivar tested. However, these very huge N-requirements pose the question on the eco-environmental impacts of quinoa crop fertilization.

Variations over time in quinoa crop response could be attributed to climatic fluctuation condition, which caused variation among TDs from year to year. Temperature, photoperiod, hydric status and radiation are the main factors affecting both growth and productivity of quinoa crop (Hirich et al., 2014; Bertero, 2015; Hinojosa et al., 2018; Hinojosa et al., 2019a, b; Alvar-Beltrán et al., 2019; Alvar-Beltrán et al., 2020). Quinoa crop tolerates a wide range of temperatures (from -8 to 35 °C) depending on genotype characteristics and phenological stage (Jacobsen et al., 2005). Temperature has the highest relative impact on the duration of development, which was reported to be longer in colder environments and shorter in high temperature environments (Bertero, 2015). In this study, the low temperature in January and February slowed down quinoa plant growth and increased the lengths of growing period. This was intensified during the 2nd season (2018/19) which was colder for the period from December to April,

as compared with the 1st season (2017/18). In addition, more net radiation and daylight hours led to more quinoa leaf elongation and growth, and therefore, reduced growing period as in late-date TDs (TD-Mar and TD-Apr). In other words, increasing solar radiations and photoperiod was found to shorten the growing cycle of quinoa crop under the context of the study. Our results are in agreement with similar investigations which found that growing period was strongly depended on the year (Jacobsen, 2003) and on TD within a year (Hirich et al., 2014). A negative relationship between both solar radiation and time-averaged photoperiod and the length of growing period was also reported by Hirich et al. (2014) in south Morocco. Temperature and photoperiod both interact to determine the growing length of crop under field conditions by controlling the rate of leaf appearance (Bertero et al., 1999). This could explain genotype×environment interaction patterns for quinoa crop yield (Bertero, 2001 and 2015). Moreover, photoperiod sensitivity is manifested from the early stages of development up to advanced stages of grain filling; but plants grown under short days before flowering present less inhibition for photoperiod during seed filling than those from long days (Bertero, 2015). Dry matter productivity of quinoa was increased as daylight hours were low and temperatures were cool during early development period and warmer after that. Prolonged growing periods before seed initiation resulted in active plant's growth and high plant biomass production, as found in the 2nd season.

In the 1st season, plants for TD-Jan and TD-Feb were grown most of the time within mean temperatures closer to the optimal growing temperatures of quinoa (15-25 °C, according to Garcia et al., 2015), resulting in higher seed yields. However, plants in the 2nd season were exposed to a heat stress starting from flowering, resulting in yield depletion. In fact, high-temperature stress negatively affected pollination process, and therefore, high seed abortion (Hinojosa et al., 2018; Alvar-Beltrán et al., 2019; Alvar-Beltrán et al., 2020). The translocation of the nutrients manufactured in leaves to storage organs maybe also affected. This led to considerable decreases in seed yields associated with considerable increases in dry matter yields, which was reflected by low harvest index. Many investigations demonstrated that quinoa plants would become fruitless at high temperatures above 34 °C at flowering (Lesjak and Caldeini, 2017), 35 °C during flowering and seed set (Hirich et al., 2014; Breidy, 2015; CNRADA, 2015; Djamal, 2015; Hassan, 2015; Saeed, 2015; Bazile et al., 2016; Eisa et al., 2017), but above 39 °C as found by Alvar-Beltrán et al. (2019). Alvar-Beltrán et al. (2020) concluded that most of the seed yield losses occurred between 34 and 38 °C, and considered that 38 °C is the highest temperature threshold at flowering. However, inflorescences were observed

to be either lacked seeds or contained empty seeds when the temperature pass 35 °C (Walters et al., 2016). Herein, starting from the flowering stage, the critical 35 or 39 °C thresholds were passed in the 2nd season many times much more than in the 1st season, for all TDs. In fact, pollen vitality is strongly related to its humidity, which in its turn is related to the vapour pressure deficit (VPD). The last was highest at high temperatures (Fig 1). This could reduce the pollen viability and might lead to pollen dehydration (Hatfield and Prueger, 2015, Alvar-Beltrán et al., 2019).

According to the economic yields and upon comparison of the mean difference between both growing seasons for each variable, two groups of transplanting dates can be identified. The first one is composed of TD-Dec, TD-Mar and TD-Apr, which gave similar QSYs, WPs and IWUEs in both growing seasons, but with an obvious better preference in TD-Dec. The second one is composed of TD-Jan and TD-Feb, which performed better in the 1st growing season than the 2nd season. Even though it is evident that a consistently optimal transplanting date cannot be specified in this experiment, emphasis in future investigations should probably be given to TD-Dec, which exhibited a high degree of consistency over both growing seasons with high mean values of HI, W1000, WP and IWUE, and to TD-Jan and TD-Feb which, also showed very high mean values of all variables (QSY, DMY, HI, W1000, WP and IWUE) over growing seasons, and performed extremely well in the first growing season.

It is worth noting that both the maximum and time-averaged values of *kc* found herein are higher than the common maximum values for quinoa crop reported in its natural distribution region (1.00 as found by Garcia et al., 2003), and in a temperate and humid environment (1.22 as found by Razzaghi et al., 2012), but less-than or somewhat equal to those found in a very hot and dry climate in Iran, as reported by Ahmadi et al. (2019). The last observed high single crop coefficients (*kc*) for the same quinoa cultivar tested herein (ICBA-Q5 cultivar) which varied from nearly 1 to 2.4 during the growing period. The very high values of *kc* found under high evaporative demand (Fig. 2A) reveal the outstanding of quinoa plant. This could be explained by its physiological properties such as large rooting system that facilitate water uptake (Ahmadi et al., 2019) and high number of stomata and stomatal size and conductance that facilitate transpiration (Kaushal et al., 2016; Yang et al., 2016; Becker et al., 2017; Hinojosa et al., 2019a, b). Moreover, another reason for the high *kc* values for quinoa crop could be strongly associated with the climatic conditions. The values of advection correction factor, which is estimated as the ratio between crop evapotranspiration and net radiation ($\alpha = ET_c/R_n$) according to Ahmadi et al. (2019), are presented in Table 2 for each TD for both growing sea-

sons. Advection factor values varied between 1.53 and 1.77 in the 2017/18 growing season and between 1.02 and 1.57 in the 2018/19 season. These values, which are higher than unity (1.00), reflect that there was regional advection effect of sensible heat flux during the growing periods of all TD tested, which was due to the horizontal transfer of sensible heat from hot and dry air from outside the area toward quinoa plants, thereby increasing transpiration and evaporation rates (ETc), which increased kc (Ahmadi et al., 2019). These results indicate that quinoa crop in order to survive, consumes high amounts of water when grown under full watering conditions in arid environment.

Our results of seed yield were similar to those published in other works for the ICBA-Q5 quinoa cultivar: 2.86-3.65 t ha⁻¹ under different planting density in Iran (Ahmadi et al., 2019); 3.90 t ha⁻¹ in Morrcoo (Hirich, 2016); from 0.40 t ha⁻¹ in Kyrgyzstan to 5.57 t ha⁻¹ in Uzbekistan (Choukr-Allah et al., 2016); about 2 to 10 t ha⁻¹ in five different locations in United Arab Emirates (Rao, 2016); 4.62 t ha⁻¹ at ICBA Research Station in United Arab Emirates (Rao and Shahid, 2012). Similarly, DMY results were in agreement with those reported earlier (Sells, 1989; Stolen and Hansen, 1993; Rao and Shahid, 2012). The maximum value of dry matter yield obtained in our study (15.9 t ha⁻¹) was similar to that found by Rao and Shahid (2012) for the ICBA-Q5 cultivar (14.9 t ha⁻¹). Moreover, HI results were comparable with those documented earlier (Hirich et al., 2014; Hassan, 2015; Alvar-Beltrán et al., 2019). Finally, the obtained values of QSY and DMY (5.30 and 15.9 t ha⁻¹, respectively) reveal that quinoa crop has high potentials in seed and/or forage production in this area and in other areas with similar climatic contexts.

5. CONCLUSIONS

Unlike the common idea that quinoa crop needs huge quantity of nitrogen fertilizer, our study revealed contrasting findings under full irrigation conditions in an arid environment. Our findings showed that quinoa crop had a very good adaptation to low fertility soil with very low N-requirements. Quinoa crop showed a very high crop evapotranspiration resulting in high crop coefficient that was higher than the common values. One main reason is the advection effect of sensible heat flux during the growing periods, considerably increased evapotranspiration.

It was demonstrated that quinoa crop growth and productivity were highly affected by transplanting dates and varied from year to year, influenced by climate conditions, mainly by maximum and mean temperatures. Emphasis in future work should probably be given to transplanting date in December, which demonstrated a high degree of

consistency over years with high mean values of harvest index, weight of 1000 seeds, water productivity and irrigation water use efficiency. Furthermore, transplanting dates in January and February should be considered, which showed very high mean values of seed and dry matter yields and water use efficiencies over years and performed very well in the first year.

In this study, seed and dry matter yield potentials of quinoa crop (ICBA-Q5 cultivar) were investigated under full irrigation in an arid environment. However, as full irrigation may not be an eco-environmental option in water-scarce zones, further studies are needed to assess the quinoa crop response to water-saving irrigations such as drip irrigation method under partial root zone drying and regulated deficit irrigations. Moreover, adapting economically sound and scientifically proven agronomic and irrigation practices, such as mulching, increasing irrigation interval to deepen rooting system, short-cycle cultivars and/or earliness of planting date, etc... is recommended to substantially reduce soil evaporation, and therefore, seasonal water requirements of quinoa crop and increasing water use efficiency in the arid Mediterranean area. Due to the scant information in Syria, further studies are also needed in order to provide further information on quinoa crop cultivation, adaptation and productivity in the country's different agro-pedo-climatic zones.

ACKNOWLEDGEMENTS

We would like to thank the Atomic Energy Commission of Syria (AECS) for encouragement. We would also like to thank the International Centre for Biosaline Agriculture (ICBA) for providing the quinoa seeds. We are grateful to the Editor-in-chief and both reviewers for their time and very constructive and valuable comments and suggestions that have been considered in this improved manuscript.

REFERENCES

- Ahmadi S.H., Solgi S., Sepaskhah A.R., 2019. Quinoa: A super or pseudo-super crop? Evidences from evapotranspiration, root growth, crop coefficients, and water productivity in a hot and semi-arid area under three planting densities. *Agric. Water Manag.* 225, <https://doi.org/10.1016/j.agwat.2019.105784>
- Allen R.G., Pereira L.S., Raes D., Smith M., 1998. *Crop Evapotranspiration: Guidelines for Computing Crop Requirements, Irrigation and Drainage Paper No. 56.* FAO.

- Al-Naggar A.M., Abd El-Salam R.M., Badran A., El-Moghazi M., 2017. Genotype and drought effects on morphological, physiological and yield traits of quinoa (*Chenopodium quinoa* Willd.). *Asian J. Adv. Agric. Res.* 3, 1–15.
- Alvar-Beltrán J., Saturnin C., Dao A., Dalla Marta A., Sanou J., Orlandini S., 2019. Effect of drought and nitrogen fertilisation on quinoa (*Chenopodium quinoa* Willd.) under field conditions in Burkina Faso. *Ital. J. Agrometeorol.* 1, 33–43.
- Alvar-Beltrán J., Verdi L., Marta A.D., Dao A., Vivoli R., Sanou J., Orlandini S., 2020. The effect of heat stress on quinoa (cv. Titicaca) under controlled climatic conditions. *The J. Agric. Sci.* 1–7. <https://doi.org/10.1017/S0021859620000556>
- Bazile D., Jacobsen S. E., Verniau A., 2016. The global expansion of quinoa: Trends and limits. *Front. Plant Sci.* 7, 622.
- Becker V.I., Goessling J.W., Duarte B., Caçador I., Liu, F., Rosenqvist E., Jacobsen S.-E., 2017. Combined effects of soil salinity and high temperature on photosynthesis and growth of quinoa plants (*Chenopodium quinoa*). *Funct. Plant Biol.* 44, 665–678.
- Benhabib O., Jacobsen S.E., Jellen R., Maughan J., Choukr-Allah R., Oussible M., 2015. Status of quinoa production and research in Morocco. Chapter 6.1.5. In *FAO & CIRAD. State of the Art Report on Quinoa Around the World in 2013*, p. 478–491. Rome.
- Bertero H.D., King R.W., Hall A.J., 1999. Photoperiod-sensitive development phases in quinoa (*Chenopodium quinoa* Willd.). *Field Crop Res.* 60, 231–243.
- Bertero H., 2001. Effects of photoperiod, temperature and radiation on the rate of leaf appearance in quinoa (*Chenopodium quinoa* Willd.) under field conditions. *Ann. Bot.* 87, 495–502.
- Bertero H.D., 2015. Environmental control of development. Chapter 2.1. In *FAO & CIRAD. State of the Art Report on Quinoa Around the World in 2013*, p. 120–130. Rome.
- Blanco Callisaya J.A., 2015. Fodder and Animal Feed. Chapter 3.2. In *FAO & CIRAD. State of the Art Report on Quinoa Around the World in 2013*, p. 250–266. Rome.
- Breidy J., 2015. In final report on quinoa evaluation trials in Lebanon. (Rome: FAO)
- Centre National de Recherche Agronomique et de Développement Agricole (CNRADA), 2015. In Mauritania final evaluation report on quinoa. Rome: FAO
- Choukr-Allah R., Rao N.K., Hirich A., Shahid M., Alshankiti A., Toderich K., Gill S., Butt K., 2016. Quinoa for Marginal Environments: Toward Future Food and Nutritional Security in MENA and Central Asia Regions. *Front. Plant Sci.* 7, 346. doi: 10.3389/fpls.2016.00346
- Djamal S., 2015. In technical assistance for the introduction of quinoa and appropriation/ institutionalization of its production in Algeria-Second Evaluation Report. Rome: FAO
- Dost M., 2015. Field evaluation results across locations and identification of suitable QUINOA varieties, in *Wrap up Workshop of Regional Quinoa Project (TCP/RAB/3403-FAO)*. Rome: FAO.
- Eisa S.S., Eid M.A., Abd E.S., Hussin S.A., Abdel-Ati A.A., El-Bordeny N.E., Ali S.H., Al-Sayed H.M. A., Lotfy M.E., Masoud A.M., et al., 2017. *Chenopodium quinoa* Willd. A new cash crop halophyte for saline regions of Egypt. *Aust. J. Crop Sci.* 11, 343–351.
- FAO and CIRAD, 2015. State of the art report of quinoa in the world in 2013, by D. Bazile, D. Bertero and C. Nieto, eds. Rome.
- Fuentes F., Bhargava A., 2011. Morphological analysis of quinoa germplasm grown under lowland desert conditions. *J. Agron. Crop Sci.* 197, 124–134.
- Garcia M., Raes D., Jacobsen S.E., 2003. Evapotranspiration analysis and irrigation requirements of quinoa (*Chenopodium quinoa*) in the Bolivian highlands. *Agric. Water Manag.* 60, 119–134.
- Garcia M., Condori B., Castillo C.D., 2015. Agroecological and agronomic cultural practices of quinoa in South America. In *Matanguihan J. and Murphy K.S. (eds). Quinoa: Improvement and Sustainable Production*. New Jersey, USA: Wiley-Blackwell, pp. 25–46.
- Geerts S., Raes D., Garcia M., Vacher J., Mamani R., Mendoza J., Huanca R., Morales B., Miranda R., Cusicanqui J., Taboada C., 2008a. Introducing deficit irrigation to stabilize yields of quinoa (*Chenopodium quinoa* Willd.). *Eur. J. Agron.* 28, 427–436.
- Geerts S., Raes D., Garcia M., Condori O., Mamani J., Miranda R., Cusicanqui J., Taboada C., Vacher J., 2008b. Could deficit irrigation be a sustainable practice for quinoa (*Chenopodium quinoa* Willd.) in the Southern Bolivian Altiplano? *Agric. Water Manag.* 95, 909–917.
- Gomez K.A., Gomez A.A., 1984. *Statistical Procedures for Agricultural Research*, second ed. John Wiley & Sons, New York. 680 pp.
- Hassan L., 2015. Iraq final evaluation report on quinoa. Rome: FAO
- Hatfield J.L., Prueger J.H., 2015. Temperature extremes: Effect on plant growth and development. *Weather. Clim. Extremes.* 10, 4–10.
- Hinojosa L., González J., Barrios-Masias F., Fuentes F., Murphy K., 2018. Quinoa abiotic stress responses:

- a review. *Plants* 7(4), 106, <https://doi.org/10.3390/plants7040106>
- Hinojosa L., Matanguihan J.B., Murphy K.M., 2019a. Effect of high temperature on pollen morphology, plant growth and seed yield in quinoa (*Chenopodium quinoa* Willd.). *J. Agron. Crop Sci.* 205, 33–45.
- Hinojosa L., Kumar N., Gill K.S., Murphy K.M., 2019b. Spectral reflectance indices and physiological parameters in quinoa under contrasting irrigation regimes. *Crop Sci.* 59, 1927–1944.
- Hirich A., 2014. Effects of Deficit Irrigation using Treated Waste water and Irrigation with Saline Water on Legumes, Corn and Quinoa Crops. Ph.D., thesis, Hassan II Institute of Agronomy and Veterinary Medicine, Morocco.
- Hirich A., Choukr-Allah R., Jacobsen S.E., 2014. Quinoa in Morocco- Effect of sowing dates on development and yield. *J. Agron. Crop Sci.* 200, 371–377.
- Hirich A., 2016. Phenotyping the combined effect of heat and water stress on quinoa introduction, in International Quinoa Conference: Quinoa for Future Food and Nutrition Security in Marginal Environments. Dubai, United Arab Emirates. pp. 6–8.
- Jacobsen S.E., 2003. The worldwide potential for quinoa (*Chenopodium quinoa* Willd.). *Food Rev. Int.* 19, 167–177. doi:10.1081/FRI-120018883
- Jacobsen S.E., Mujica A., Jensen C.R., 2003. The resistance of Quinoa (*Chenopodium quinoa* Willd.) to adverse abiotic factors. *Food Rev. Int.* 19, 99–109. doi:10.1081/FRI-120018872
- Jacobsen S.E., Monteros C., Christiansen J.L., Bravo L.A., Corcuera L.J., Mujica A., 2005. Plant responses of quinoa (*Chenopodium quinoa* Willd.) to frost at various phenological stages. *Eur. J. Agron.* 22, 131–139.
- Jbawi E.A., Danoura R., Yaacoub A., 2018. Effect of deficit irrigation and manure fertilizer on improving growth and yield of quinoa in Syria. *Open Acc. J. Agric. Res. OAJAR-100007*.
- Kaushal N., Bhandari K., Siddique K.H.M., Nayyar H., 2016. Food crops face rising temperatures: an overview of responses, adaptive mechanisms, and approaches to improve heat tolerance. *Cogent Food Agric.* 2, 1–42.
- Lavini A., Pulvento C., D'Andria R., Riccardi M., Choukr-Allah R., Belhabib O., et al., 2014. Quinoa's potential in the Mediterranean region. *J. Agron. Crop Sci.* 200, 344–360. doi:10.1111/jac.12069
- Lesjak J., Calderini D.F., 2017. Increased night temperature negatively affects grain yield, biomass and grain number in Chilean quinoa. *Front. Plant Sci.* 8, 352.
- Moreale A., 1993. In *The quinoa project*: Wageningen University. <http://edepot.wur.nl/354101> (accessed 06 February 2020).
- Noulas C., Karyotis T., Iliadis C., 2015. Greece. Chapter 6.1.6. In *FAO & CIRAD. State of the Art Report on Quinoa Around the World in 2013*, p. 492–510. Rome.
- Onofri A., 2007. Routine statistical analyses of field experiments by using an Excel extension. National Conference Italian Biometric Society. Proc. 6th (Pisa). In: “La statistica nelle scienze della vita e dell'ambiente”; 20–22, 93–96.
- Pulvento C., Riccardi M., Lavini A., Iafelice G., Marconi E., d'Andria R., 2012. Yield and quality characteristics of quinoa grown in open field under different saline and non-saline irrigation regimes. *J. Agron. Crop Sci.* 198, 254–263.
- Pulvento C., Riccardi M., Biondi S., Orsini F., Jacobsen S.-E., Ragab R., D'Andria R., Lavini A., 2015. Quinoa in Italy: research and perspectives. Chapter 6.1.3. In *FAO & CIRAD. State of the Art Report on Quinoa Around the World in 2013*, p. 454–465. Rome.
- Rao N.K., 2016. Quinoa: a future-proof crop for climate smart agriculture, in *Global Forum for Innovations in Agriculture*, Choukr-Allah, R., (Ed) (Abu Dhabi).
- Rao N.K., Shahid M., 2012. Quinoa– a promising new crop for the Arabian Peninsula. *American-Eurasian J. Agric. Environ. Sci.* 12, 1350–1355.
- Razzaghi F., Ahmadi S.H., Adolf V.I., Jensen C.R., Jacobsen S.E., Andersen M.N., 2011. Water relations and transpiration of Quinoa (*Chenopodium quinoa* Willd.) under salinity and soil drying. *J. Agron. Crop Sci.* 197, 348–360.
- Razzaghi F., Plauborg F., Jacobsen S.E., Jensen C.R., Andersen M.N., 2012. Effect of nitrogen and water availability of three soil types on yield, radiation use efficiency and evapotranspiration in field-grown quinoa. *Agric. Water Manag.* 109, 20–29.
- Repo-Carrasco R., Espinoza C., Jacobsen S.E., 2003. Nutritional value and use of the Andean crops quinoa (*Chenopodium quinoa*) and Kañiwa (*Chenopodium pallidicaule*). *Food Rev. Int.* 19, 179–189. doi:10.1081/FRI-120018884
- Saeed A.L., 2015. In *Yemen progress report on quinoa*. Rome: FAO
- Schulte auf'm Erley G., Kaul H.P., Kruse M., Aufhammer W., 2005. Yield and nitrogen utilization efficiency of the pseudocereals amaranth, quinoa, and buckwheat under differing nitrogen fertilization. *Eur. J. Agron.* 22, 95–100.
- Sells J.E., 1989. *Combimble alternative crops*. AFRC Institute of Engineering Research, Bedford, UK.
- Shams A., 2017. Response of quinoa to nitrogen fertilizer rates under Egyptian soils conditions. Proc. 13th international Conf. Agron., Fac. of Agric., Benha Univ., Egypt, 9–10.

- Shoman H.A., 2018. Effect of Sowing Dates and Nitrogen on Productivity of Quinoa (*Chenopodium quinoa* Willd.) at Desert Areas. *J. Plant Production, Mansoura Univ.* 9(4), 327–332.
- Stolen O., Hansen G., 1993. Introduction of New Crops in Denmark, in: Anthony, K.R.M., Meadley, J., Robbelen, G. (Eds.), *New Crops for Temperate Regions*. Chapman and Hall, London, pp. 45–53.
- Walters H., Carpenter-Boggs L., Desta K., Yan L., Matanguihan J., Murphy K., 2016. Effect of irrigation, intercrop, and cultivar on agronomic and nutritional characteristics of quinoa. *Agroecol. Sustain. Food Syst.* 40, 783–803.
- Yang A., Akhtar S.S., Amjad M., Iqbal S., Jacobsen S.E., 2016. Growth and physiological responses of quinoa to drought and temperature stress. *J. Agron. Crop Sci.* 202, 445–453.
- Yazar A., Incekaya C., Sezen M.S., Tekin S., 2015. Quinoa Experimentation and Production in Turkey. Chapter 6.1.4. In *FAO & CIRAD. State of the Art Report on Quinoa Around the World in 2013*, p. 466–477. Rome.



Citation: M. Topuz, H. Feidas, M. Karabulut (2020) Trend analysis of precipitation data in Turkey and relations to atmospheric circulation: (1955-2013). *Italian Journal of Agrometeorology* (2): 91-107. doi: 10.13128/ijam-887

Received: March 24, 2020

Accepted: August 27, 2020

Published: January 25, 2021

Copyright: © 2020 M. Topuz, H. Feidas, M. Karabulut. This is an open access, peer-reviewed article published by Firenze University Press (<http://www.fupress.com/ijam>) and distributed under the terms of the Creative Commons Attribution License, which permits unrestricted use, distribution, and reproduction in any medium, provided the original author and source are credited.

Data Availability Statement: All relevant data are within the paper and its Supporting Information files.

Competing Interests: The Author(s) declare(s) no conflict of interest.

Trend analysis of precipitation data in Turkey and relations to atmospheric circulation: (1955-2013)

MUHAMMET TOPUZ^{1,*}, HARALAMBOS FEIDAS², MURAT KARABULUT³

¹ Hatay Mustafa Kemal University, Faculty of Arts and Sciences, Geography Department Hatay 31040, Turkey

² Aristotle University of Thessaloniki, School of Geology, Department of Meteorology and Climatology, Thessaloniki, 54124, Greece

³ Kahramanmaraş Sutcu Imam University, Faculty of Arts and Sciences, Geography Department Kahramanmaraş 46100, Turkey

*Corresponding author. E-mail: ksutopuz@gmail.com

Abstract. Climate change is expected to significantly affect the precipitation regime of the Mediterranean basin where Turkey is located. This study investigates the trends of seasonal and annual precipitation time series of 29 rain gauge stations of the Turkish State Meteorological Service (TSMS) for the period 1955–2013, using two statistical tests based on a simple linear regression model and the well-known Mann-Kendall test. The non-parametric Sen's slope estimator was used to estimate the slope of the trend. The results of the trend analysis at the national scale for the entire period 1955–2013 revealed a clear significant upward trend of 5.5%/decade only for autumn precipitation. No significant trend was found in the annual and other seasonal time series. The investigation of abrupt precipitation changes in the series averaged over Turkey resulted in a distinct significant upward trend in autumn precipitation starting in 1984 and a downward trend in winter precipitation initiating in 1971, which, however, seems to start reversing after 1996. The influence of atmospheric circulation on the precipitation variability in Turkey was assessed using five atmospheric circulation indices: North Atlantic Oscillation Index (NAOI), Mediterranean Oscillation Index (MOI), Mediterranean Circulation Index (MCI), Eastern Mediterranean Pattern Index (EMPI) and North-Sea Caspian Pattern Index (NCPI). The analysis of the circulation indices revealed an important link between precipitation variability in Turkey and some atmospheric teleconnection patterns, expressed mainly by the indices of NAOI and MCI.

Keywords. Trend analysis, precipitation, Turkey, atmospheric circulation.

1. INTRODUCTION

Precipitation is a highly variable climatological element both in space and time (Karabulut and Cosun, 2009). This variability results from changes in atmospheric circulation and complex topographic characteristics and affects many aspects of human life e.g. water resources, aridity and desertification

conditions, agriculture (Sarış et al., 2010). The global mean precipitation is likely to increase due to increases in the atmospheric moisture-holding capacity associated with global warming (IPCC, 2007). However, future changes in precipitation will not be uniform. An increase in annual mean precipitation is likely by the end of the 21st century over the high latitudes, the equatorial Pacific and in many mid-latitude wet regions, while a decrease is expected in many mid-latitude and subtropical dry regions (IPCC, 2014). Observations indicate an area-averaged precipitation increase since 1951 over the mid-latitude land areas of the Northern Hemisphere (IPCC, 2014).

The Mediterranean basin is deemed vulnerable to climate changes, due to the diverse topography and its position at the interface between the temperate climate of southern Europe and the arid climate of North Africa (Giorgi and Lionello, 2008). The winter precipitation in the Mediterranean region has experienced an overall decreasing trend during the last few decades (Philandras et al., 2011; Norrant and Douguédroit 2006; Piervitali et al., 1997; Palutikof et al., 1996). The eastern Mediterranean has tended towards drying conditions since the mid 20th century (Feidas et al., 2007; Tomozeiu et al., 2005; Alexandrov et al., 2004).

Turkey exhibits spatial differences in precipitation between the southern coasts and the northern and western regions (Tayanç et al., 2009; Partal and Kahya 2006) and between coastal and mountainous regions (Türkeş 1996; Xoplaki et al., 2000; Kadioglu 2000). Toros et al (1994) used seasonal and annual precipitation data of 68 stations in the west part of Anatolia in Turkey for the period 1930-1992 to show a decline in precipitation after 1982 that was attributed only to a fluctuation in precipitation. Kadioglu (1993) analyzed monthly precipitation data of 18 Turkish stations for the period 1929-1990 and found an overall decrease in winter precipitation and an increase in spring precipitation. Türkeş (1996) have conducted a spatio-temporal analysis of annual precipitation variability using monthly precipitation series from 91 stations in Turkey, during the period 1930–1993. They found a slight decrease in area-averaged annual precipitation series averaged over Turkey. Kadioglu (2000) has found a decrease in winter precipitation for Anatolia and Black Sea region and an increase for Mediterranean coastal regions for the period 1931-1990. Partal and Kahya (2006) applied a trend analysis to long precipitation time series (1929-1993) of 96 stations in Turkey and found a significant decreasing trend in the annual rainfall for southern and western Turkey as well as a the Black Sea coast. In another study, Türkeş et al., (2007), detected downward trends in annual and winter rainfall totals and a general upward trend in the spring, summer and autumn rainfall for the period 1930-2002.

There are many reports on the subject published by public authorities. Toros (2012) examined expected spatio-temporal changes in precipitation time series of 165 Turkish stations for the period 1961 to 2008 in order to assess the impact of climate change on precipitation over Turkey. He found a significant decreasing trend at the 35, 13 and 12% of the stations in the winter, annual and rainy period precipitation totals, respectively, with some oscillations during the examined period (decrease during 1968–1973 and 1998–2008 and increase, during 1973–1981 and 1989–1998). In contrast, a significant increase was detected at the 19, 3 and 4% of the stations in the autumn, rainy period and annual precipitation, respectively. It was concluded that climate dynamics such as the effect of NAO on the tracks of the Mediterranean storms are among the main causes of the precipitation variability in Turkey.

According to Efe et al. (2015), trend analysis of the annual total precipitation for the period 1950-2013 showed a general increasing tendency in precipitation on the coastline, mainly in the regions of Marmara and Black Sea. In contrast, a decreasing trend was found in annual total precipitation inland that could be a sign of evolving drought conditions.

Sensoy et al. (2013), found decreasing trends during the period 1960-2010 for annual precipitation totals in the northern Turkey, whereas Mediterranean Sea, Aegean Sea and south-eastern Anatolia regions presented decreasing trends. On the other hand, the number of days with heavy precipitation shows an upward trend in most of the stations with the exception of the Southeastern Anatolia and Aegean Sea regions.

Atmospheric circulation is a significant contributor to the precipitation variability in Mediterranean. Many studies have detected an important link between Mediterranean precipitation and various large and regional-scale circulation patterns such a North Atlantic Oscillation (NAO), Mediterranean Circulation (MC), North Sea – Caspian Pattern (NCP) and Mediterranean Oscillation (MO) (Greatbach 2000; Cullen et al., 2000; Visbeck et al., 2000; Trigo et al., 2002; Erlat 2002; Karabork et al., 2002; Xoplaki 2002; Krichak and Alpert 2005; Türkeş and Erlat 2005; Turp 2006; Bachmann 2007; Feidas et al., 2007; Lopez-Moreno et al., 2011; Karakoç and Tagil 2014). The variability of winter precipitation in Turkey (especially in the northern Marmara, northwestern Mediterranean and Central Anatolia) was found to be strictly related to the variability of NAO indices (Türkeş and Erlat 2005, 2006).

This study aims primarily at investigating recent trends in the mean seasonal and annual precipitation observations in Turkey for the longest length of historical homogenous precipitation data available for analysis (1955–2013), using two statistical tests. Another objective

is to examine any likely link between precipitation variability in Turkey and atmospheric circulation using five atmospheric circulation indices.

2. STUDY AREA AND DATA ANALYSIS

Turkey has a 1650 km length from the west to the east covering an area from 36° N to 42° N latitude and from 26° E to 45° E longitude. According to first Turkish Geography Association (in Turkish Synonym TCK), the country is divided based on First Turkish Geography Congress (6-21 June 1941) into seven geographic regions: Mediterranean, Black Sea, Aegean, Central, East and South-East Anatolia regions (MEB, 1941). Turkey is considered as a large peninsula because it is surrounded by water (Mediterranean Sea, Aegean Sea and Black Sea). While northeast of Turkey receives large precipitation amounts due to the characteristics of the Black Sea coast, the western, eastern and southern regions get less precipitation. Precipitation is irregularly distributed in mountainous regions. Maximum precipitation occurs in winter, early spring late and autumn due to the depression and frontal activity during this period. The average annual total precipitation ranges from 350-500 mm over central and south eastern Anatolia to 800 mm over the Eastern Anatolia and more than 1000 mm along the western Mediterranean basin (Türkeş 1996 and 2003; Kadioglu 2000; Ozfidaner 2007).

2.1 Precipitation data

In this study, monthly precipitation records from 29 stations of the Turkish State Meteorological Service (TSMS) covering a period of 59 years (1955-2013) were used (Table 1, Figure 1). Observations have been made using mainly pluviometer-type stations. Rain gauges are bucket type and are of 0.2mm accuracy (Irvem and Ozbuldu, 2019). Based on the station history files, not any significant relocation and systematic and countrywide rain gauge change has been made during the study period (Türkeş 1996).

The choice of these stations was made based on the data length and completeness. Missing monthly values in the precipitation series were few, less than 3 per cent of the total size of the dataset, and were filled out with estimates from surrounding stations according to the normal ratio method (Sing 1992; Türkeş 1998; Feidas et al., 2007). The normal ratio method has a long history and high capability in estimating missing values in rainfall time series. Therefore, due to its simplicity, it is the most commonly used method in imputing missing rainfall records from surrounding stations (Burhanuddin et al., 2017). The

Tab. 1. Metadata of the selected stations.

Station WMO Number	Station Name	Latitude (N)	Longitude (E)	Altitude (m)	Data Length (Years)
17292	Mugla	37.17	28.22	646	59
17370	Iskenderun	36.35	36.10	2	59
17250	Nigde	37.28	34.41	1211	59
17261	Gaziantep	37.40	37.29	854	59
17270	SanliUrfa	37.90	38.47	547	59
17210	Siirt	37.55	41.56	896	59
17220	Izmir	38.23	27.40	20	59
17240	Isparta	37.47	30.34	997	59
17172	Van	38.29	43.23	1670	59
17180	Dikili	39.40	26.53	7	59
17184	Akhisar	38.48	27.50	79	59
17188	Usak	38.68	29.47	929	59
17190	Afyonkarahisar	38.44	30.34	1034	59
17196	Kayseri	38.43	35.29	1092	59
17130	Ankara	39.59	32.41	879	59
17160	Kirsehir	39.90	34.10	1007	59
17084	Corum	40.32	34.56	776	59
17090	Sivas	39.45	37.10	1285	59
17112	Canakkale	40.80	26.23	5	59
17050	Edirne	41.40	26.33	51	59
17056	Tekirdag	40.59	27.29	4	59
17059	Kumkoy	41.25	29.04	38	59
17070	Bolu	40.44	31.36	737	59
17074	Kastamonu	41.22	33.46	800	59
17022	Zonguldak	41.27	31.47	154	59
17024	Inebolu	41.58	33.45	66	59
17030	Samsun	41.21	36.14	4	59
17034	Giresun	40.55	38.23	38	59
17040	Rize	41.20	40.30	8	59

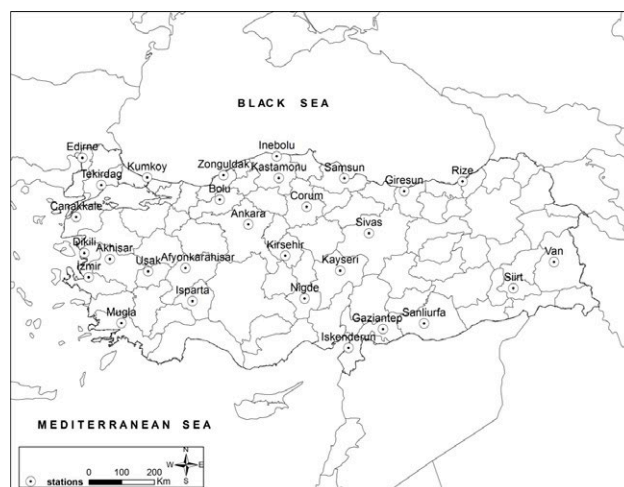


Fig. 1. The locations of the 29 Turkish stations used in the study.

choice of the adjacent reference stations was made based on the highest correlation coefficients (above 0.65 at 95% level of significance), between the station with the missing value and the nearby reference stations.

In order to retain the rainy season as one continuous period, annual precipitation totals were calculated based on a water year, defined as the twelve-month period from September 1 of one given year through August 31 of the next year. Both, annual and winter precipitation was attributed to the year in which January belonged. Finally, precipitation data was expressed as percentage of normal precipitation based on data from 1961 to 1990 period.

The homogeneity of the precipitation records were checked by applying four absolute test methods to the seasonal and annual precipitation series: the Buishand range test, the Bartlett short-cut test, the Levene test and the Von Neumann ratio test (Buishand 1982; Mitchell et al., 1966; Levene 1960; Von Neumann 1941). Although relative tests with respect to homogeneous neighboring stations are deemed to be much more efficient than absolute tests that relies only on a single station climate series (Peterson et al., 1998), these tests are not considered suitable for the precipitation records of this study due to the low correlation of precipitation data of neighboring stations and the sparse station network. The null hypothesis states that precipitation data of a time series are random variables identically and independently distributed whereas the alternative hypothesis assumes that the series is not randomly distributed with the exception of the Buishand range test in which the alternative hypothesis assumes the presence of a step-wise shift in the mean (called as a break). The Buishand test has the advantage of being able to locate the year of a likely break (Feidas et al., 2007).

The next step is to apply the Schönwiese and Rapp (1997) classification in which a data series is labelled 'suspect' when more than two tests reject the null hypothesis at the 5% significance level. A 'suspect' series is considered inhomogeneous and is not used in the trend analysis. According to the results of the homogeneity tests, all the precipitation series of the 29 stations were characterized as homogeneous.

The existence of possible trends in the seasonal and annual precipitation time series was investigated using two statistical tests: a simple parametric linear regression model and the non-parametric Mann-Kendall statistic test (Sneyers, 1990). Linear trends are considered to be significant at the 95% confidence level when found as such by both statistics t and $u(d_n)$.

In the first test, the null hypothesis that the slope b of the regression line is zero is rejected using the value of the t -test statistic $t = \hat{b} / s_1(\hat{b})$, where $s_1(\hat{b})$ is the standard error of slope b . The second test is considered the most suit-

able not only for trend analysis of climate data but also for detecting a climatic discontinuity in the data series (Goossens and Berger, 1986). The null hypothesis of zero slope b of the regression line is rejected when the final (for $i = n$) absolute value $u(d_n)$ of the statistic series $u(d_i)$ is greater than 1.96 at 95% level of confidence, where n is the data series size. The plot of all $u(d_i)$ and its retrograde series $u'(d_i)$, for $1 \leq i \leq n$, is marked as C_1 and C_2 , respectively. The intersection of curves C_1 and C_2 denotes the starting year of the trend or climate change.

The non-parametric Sen's slope estimator (Sen, 1968) was used to estimate the slope b (mm/year) of the trend line, given that precipitation amounts are typically not normally distributed. It is a robust non-parametric method that is insensitive to outliers and it does not draw from any probability distribution. The method estimates the slope by choosing the median of the slopes of all lines through pairs of points. The upper (b_u) and lower (b_l) limits for the slope are also computed at the 95% confidence level.

The Sen's slope b was expressed as well as %/decade by computing the average decadal percent change. A log-level regression $\ln(y) = a + bt$ was run between precipitation values (y) and time (t) in tin years intervals to estimate the average decadal percent change as $\exp(b) - 1$, where b is the regression coefficient of the equation $\ln(y) = a + b \times t$ (Clegg et al., 2009).

2.2 Circulation indices

In order to assess the relation of precipitation in Turkey with large-scale and regional atmospheric circulation, five circulation indices were used:

(a) the North Atlantic Oscillation Index (NAOI), which uses the surface pressure difference between stations in the subtropical high of Azores and the subpolar Icelandic low pressure system (Walker 1924; Walker and Bliss 1932; Rogers and van Loon 1979),

(b) the Mediterranean Oscillation Index (MOI), calculated as the difference of standardized anomalies of the 500 hPa geopotential height field between western and eastern parts (usually the stations of Algiers and Cairo) of the Mediterranean basin (Conte et al., 1989; Colacino and Conte 1993; Kutiel et al., 1996; Douguedroit 1998; Maheras et al., 1999; Maheras and Kutiel 1999; Piervitali et al., 1999; Criado-Aldeanueva and Soto-Navarro 2013),

(c) the Mediterranean Circulation Index (MCI), expressed as the standardized mean sea level pressure difference between two stations (Marseille and Jerusalem) located in the northwestern and southeastern Mediterranean (Brunetti et al., 2002),

(d) the Eastern Mediterranean Pattern Index (EMPI), which is a seesaw pattern between the eastern Mediterra-

nean basin and northeastern Atlantic ocean at the 500 hPa surface (Hatzaki et al., 2007), and

(e) the North-Sea Caspian Pattern Index (NCPI), expressed as the normalized difference between averages of the 500 hPa geopotential height of two areas located at the North Sea (0°E, 55°N and 10°E, 55°N) and North Caspian Sea (50°E, 45°N and 60°E, 45°N) (Kutiel and Benaroch 2002).

Monthly values of NAOI for the period of interest (1955–2013) were acquired from the database of the National Center of Atmospheric Research (NCAR) whereas the other five indices were calculated using the gridded reanalysis dataset of the National Center for Environmental Prediction (NCEP) of NCAR. The relationship of the precipitation variability in Turkey with atmospheric circulation was assessed based on the Pearson correlation coefficients between the data series of the teleconnection indices and the precipitation averaged over Turkey.

3. RESULTS AND DISCUSSION

3.1 Precipitation trends

Trend analysis of precipitation time series in Turkey was performed by applying the two statistical tests (a parametric regression-based model and the non-parametric Mann-Kendall test) to the seasonal and annual precipitation series of the 29 Turkish stations for the period 1955–2013.

The non-parametric Sen's slope estimator (Sen, 1968) was applied to estimate the magnitude of the linear trends expressed with the slope b of the regression line. Table 2 presents the values of the slope b in mm/year, the lower b_l and upper b_u slope limits at the 95% confidence level and the statistics t and $u(d_n)$ for the seasonal and annual precipitation series. Linear trends (b) are deemed to be significant at the 95% confidence level when found as such by both statistics t and $u(d_n)$. These significant cases are indicated in Table 2 with boldface characters. The Sen's slope b expressed as well as %/decade along with its upper (b_u) and lower (b_l) limits at the 95% confidence level is presented in Table 3.

Seasonal and annual precipitation time series, trend line and its lower and upper limits at the 95% confidence level were plotted and analyzed for each of the 29 stations. Figure 2 presents an example with the graphs for Sivas station.

The spatial distribution of the sign and statistical significance of the Sen's slope b estimates of the trend line for the seasonal and annual precipitation time series of the 29 stations is presented in Figure 3. Squares indicate positive values and circles denote negative slope values. Figure 3 and Table 2 and 3 combined can be used to locate positive or negative trends of the stations' time series and assess their spatial distribution.

On an individual station level, significant trends are found mainly in autumn and annual time series. Prevalent increasing trends were observed for the autumn time series with 9 out of 29 statistically significant stations, located mainly in central Anatolia. The average percent decadal change ranges from 8.6% to 14.7% per decade (Table 3). Only three stations (Gaziantep, Sivas and Kastamonu) were found to have small but statistically significant (upward) trends in the annual time series in the range 3.8–4.9%. Only one station exhibited statistically significant trend in winter (Isparta) and summer (Samsun) but with opposite signs (downward and upward, respectively) and magnitudes (-6.5% and 11.9% per decade, respectively).

Concerning the neighboring of different sign of changes (positive and negative), this exists only in no statistically significant cases. Moreover, the large geomorphic diversity of landscapes in Turkey can explain such spatial differences in the start and the sign of a change, even if trends are not statistically significant.

In order to have a representation of the country as a whole, precipitation series of the 29 Turkish stations were spatially averaged to estimate precipitation trends at the national scale. Precipitation was expressed as percentage of the normal based on data of the 1961 - 1990 period to facilitate merging and prevent any trend from being prevailed by highly variable time series (Feidas et al., 2007). The results of the trend analysis for these area averaged time series are presented in Table 2 (last row) and plotted in Figure 4. Table 2 and Figure 4 indicate that only autumn precipitation spatially averaged over Turkey present a distinct significant upward trend of 5.5%/decade. No clear significant trend was detected in the annual and other seasonal series.

The $u(d_i)$ and $u'(d_i)$ statistics of the sequential Mann-Kendall test were plotted for the precipitation series of each station and the regional mean series for Turkey, in order to locate the beginning of a trend or change based on the intersection of the curves C_1 and C_2 . Plots for Sivas station and Turkey as a whole are given in Figure 5 and 6, respectively. This graphical analysis was performed on the full range of the 29 stations to locate any likely trend statistically significant at the 95% confidence level and the time of an abrupt precipitation change. The increasing (+) and decreasing (-) trends and the approximate year of the initiation of the trend for the seasonal and annual series are provided in Table 4. The second year in some stations indicates a not statistically significant new change in the trend. The asterisk connotes the absence of a statistically significant trend for the period 1955-2013.

Table 4 shows a clear evidence of trends only for winter and autumn precipitation series. More precisely, a downward trend for winter series initiated during the

Tab. 2. Trend analysis results of the application of the two statistical tests on the seasonal and annual precipitation series over the period 1955-2013^a (Statistically significant cases at the 95% confidence level, provided by both tests, are indicated with boldface characters).

Station	Winter				Spring				Summer				Autumn				Annual			
	b	b_l	b_u	t	$u(d_{it})$	b	b_l	b_u	t	$u(d_{it})$	b	b_l	b_u	t	$u(d_{it})$	b	b_l	b_u	t	$u(d_{it})$
Iskenderun	0.60	-1.29	2.26	0.30	0.67	-0.65	-1.93	0.45	-1.22	-1.07	0.66	0.12	1.16	1.92	2.30	0.83	-0.20	1.94	1.14	1.57
Kumkoy	0.80	-0.76	2.20	0.35	0.92	-0.05	-0.76	0.78	-0.19	-0.14	0.03	-0.70	0.85	0.39	0.06	2.00	0.70	3.19	2.60	2.48
Mugla	-2.65	-6.61	0.94	-1.43	-1.56	0.46	-0.95	1.95	0.48	0.67	0.13	-0.20	0.54	1.07	0.84	1.24	-0.17	2.48	1.82	1.70
Izmir	-0.02	-2.16	2.15	-0.21	-0.02	0.28	-0.69	1.23	0.74	0.62	-0.04	-0.15	0.06	-0.12	-0.95	1.43	0.16	2.64	2.83	2.38
Dikili	-1.21	-3.27	0.67	-1.59	-1.37	-0.10	-0.88	0.74	0.28	-0.27	0.07	-0.09	0.23	1.17	0.87	0.33	-0.64	1.32	0.70	0.66
Gaziantep	0.55	-0.93	2.08	0.93	0.49	0.19	-0.98	1.36	0.25	0.32	0.01	-0.10	0.15	0.88	0.26	1.12	0.36	1.99	2.38	2.37
Sanliurfa	-0.97	-2.25	0.23	-1.40	-1.50	-0.37	-1.50	0.51	-0.99	-0.92	0.00	-0.01	0.06	0.70	0.75	0.36	-0.20	1.04	1.08	1.05
Siirt	-0.02	-1.60	1.43	-0.47	-0.06	-0.64	-1.78	0.99	-0.81	-0.56	0.08	-0.06	0.22	1.17	0.90	0.07	-0.89	1.06	0.29	0.10
Isparta	-1.43	-2.98	-0.16	-2.24	-2.28	-0.01	-0.87	0.84	-0.14	-0.03	0.20	-0.37	0.73	0.46	0.73	0.27	-0.41	0.83	1.19	0.97
Afyonkarahisar	0.18	-0.50	0.91	0.88	0.35	-0.17	-0.85	0.54	-0.54	-0.52	-0.11	-0.67	0.45	-0.39	-0.27	0.48	-0.08	0.99	1.37	1.67
Usak	-0.20	-1.54	1.17	-0.25	-0.23	0.23	-0.59	1.02	0.78	0.71	-0.02	-0.48	0.46	-0.28	-0.14	0.77	0.14	1.29	1.48	2.07
Akhisar	-1.04	-2.55	0.64	-1.61	-1.27	-0.07	-0.84	0.71	-0.13	-0.11	-0.12	-0.35	0.12	-0.68	-0.92	0.84	-0.14	1.80	3.17	3.00
Nigde	0.03	-0.56	0.64	0.28	0.03	-0.22	-0.93	0.51	-0.63	-0.57	0.21	-0.10	0.53	1.32	1.26	0.82	0.40	1.23	4.34	3.85
Kayseri	-0.02	-0.55	0.49	0.41	-0.02	0.32	-0.31	1.02	1.02	0.87	-0.08	-0.58	0.44	-0.03	-0.23	0.56	0.09	1.08	2.04	2.30
Ankara	-0.23	-0.92	0.54	-0.99	-0.47	0.07	-0.57	0.76	0.33	0.12	-0.09	-0.62	0.42	-0.31	-0.44	0.40	-0.22	1.01	1.16	1.23
Kirsehir	-0.60	-1.30	0.10	-1.39	-1.52	-0.17	-0.91	0.60	-0.12	-0.46	-0.02	-0.53	0.44	-0.07	-0.15	0.86	0.36	1.50	3.05	2.90
Corum	-0.13	-0.89	0.61	-0.64	-0.30	0.08	-0.66	0.64	0.10	0.32	0.31	-0.51	1.08	1.03	0.77	0.87	0.31	1.43	2.34	3.03
Sivas	0.26	-0.33	0.92	0.84	0.94	0.52	-0.14	1.18	1.42	1.48	0.08	-0.36	0.55	0.13	0.35	1.10	0.55	1.63	3.81	3.63
Van	0.25	-0.38	0.78	0.82	0.84	-0.10	-0.74	0.55	-0.31	-0.37	0.02	-0.25	0.30	0.19	0.12	0.21	-0.39	0.92	0.26	0.65
Canakkale	-0.78	-2.88	0.86	-1.06	-1.22	-0.16	-0.91	0.62	-0.12	-0.37	0.01	-0.45	0.41	-0.83	0.05	-0.30	-1.34	0.86	-0.05	-0.47
Edirne	-0.30	-1.62	1.10	0.01	-0.48	-0.54	-1.19	0.23	-1.01	-1.34	-0.30	-1.01	0.62	-0.70	-0.52	0.29	-0.62	1.35	0.93	0.70
Tekirdag	-0.40	-1.79	0.84	-0.44	-0.69	-0.24	-1.02	0.51	-0.62	-0.50	-0.27	-0.74	0.30	-0.62	-0.97	0.71	-0.67	1.97	1.04	0.99
Bolu	-0.16	-0.98	0.48	-0.83	-0.83	0.42	-0.39	1.10	1.05	1.04	0.09	-0.75	-0.92	0.16	0.19	0.32	-0.23	0.93	0.76	1.16
Kastamonu	0.23	-0.40	0.85	0.73	0.76	0.46	-0.38	1.21	1.08	1.09	0.51	-0.59	1.56	1.52	0.83	0.54	-0.04	1.13	1.37	1.81
Zonguldak	-0.54	-1.65	0.74	-0.94	-0.85	-0.65	-1.47	0.44	-1.01	-1.01	-0.42	-1.74	1.30	0.23	-0.49	1.76	0.05	3.40	1.76	2.02
Inebolu	-0.01	-1.29	1.51	-0.10	-0.03	0.27	-0.73	1.16	0.49	0.57	0.08	-0.94	1.20	0.36	0.18	0.70	-0.50	2.21	2.01	1.11
Samsun	-0.38	-1.42	0.59	-0.96	-0.79	-0.21	-0.96	0.59	-0.48	-0.49	1.18	0.18	2.00	2.59	2.24	0.70	-0.53	1.75	0.36	0.98
Giresun	-0.28	-1.74	0.86	-1.01	-0.44	-0.11	-1.03	0.83	-0.42	-0.29	0.50	-1.21	1.76	0.91	0.50	1.32	-0.57	3.19	2.15	1.43
Rize	-0.53	-2.44	1.43	-0.55	-0.69	-0.86	-2.00	0.27	-1.36	-1.54	0.52	-1.56	2.04	0.52	0.48	1.99	-0.43	5.04	1.47	1.64
Turkey	-0.28	-1.12	0.61	-0.80	-0.46	-0.08	-0.51	0.40	-0.24	-0.37	0.15	-0.20	0.49	1.00	0.83	0.94	0.45	1.36	3.35	3.38

^a b (mm/year) is the Sen's slope estimates of the trend line, b_l and b_u are the lower and upper slope limits at the 95% confidence level, t is the statistic of the linear regression model and $u(d_{it})$ is the final value (for $i = n$) of the Mann-Kendall statistic.

Tab. 3. Sen's slope estimates (b) for the trend of seasonal and annual precipitation series over the period 1955-2013, expressed as average percent change per decade. b_l and b_u denotes the lower and upper slope limits at the 95% confidence level (Statistically significant cases, provided by both tests, are indicated with boldface characters).

Station	Winter			Spring			Summer			Autumn			Annual		
	b (%)	b_l (%)	b_u (%)	b (%)	b_l (%)	b_u (%)	b (%)	b_l (%)	b_u (%)	b (%)	b_l (%)	b_u (%)	b (%)	b_l (%)	b_u (%)
Iskenderun	2.3	-4.6	9.6	-2.9	-8.6	2.2	17.8	2.7	43.8	4.5	-1.0	11.4	2.5	-1.0	6.2
Kumkoy	2.8	-2.5	8.2	-0.3	-4.9	5.4	0.4	-8.8	11.6	8.9	3.1	15.0	3.2	-0.4	6.7
Mugla	-4.0	-9.6	1.5	2.2	-4.2	9.4	5.7	-6.7	28.1	6.1	-0.7	12.7	-0.4	-4.4	3.2
Izmir	0.0	-5.7	6.4	2.1	-4.5	9.6	-6.3	-27.7	8.5	10.4	1.1	20.9	2.6	-1.2	6.5
Dikili	-3.8	-9.6	2.2	-0.8	-6.1	5.8	7.5	-7.7	29.7	2.6	-4.7	10.3	-1.9	-5.9	2.0
Gaziantep	2.1	-3.1	8.3	1.3	-6.4	10.1	1.3	-10.0	22.3	12.6	3.9	25.8	4.0	0.2	7.8
Sanliurfa	-4.1	-9.0	1.0	-3.2	-11.4	4.7	1.5	-8.7	56.3	5.8	-2.9	18.2	-1.7	-5.3	1.6
Siirt	-0.1	-5.9	5.5	-1.4	-6.4	4.0	8.2	-5.6	37.3	0.7	-7.6	10.2	-0.3	-3.8	3.8
Isparta	-6.5	-12.8	-0.8	-0.1	-5.4	5.6	4.6	-6.5	18.1	3.1	-4.5	10.7	-1.8	-5.7	1.7
Afyonkarahisar	1.5	-4.0	8.1	-1.2	-5.9	4.2	-1.7	-9.8	8.5	6.5	-0.9	14.9	1.8	-1.1	5.3
Usak	-1.0	-7.3	5.7	1.5	-3.7	7.0	-0.4	-9.2	10.6	7.7	1.4	13.9	1.7	-1.7	4.7
Akhisar	-3.7	-8.9	2.4	-0.5	-5.7	5.4	-6.3	-19.0	7.1	8.9	3.1	15.0	-0.5	-3.9	2.8
Nigde	0.3	-5.3	6.7	-1.7	-6.4	4.5	6.5	-3.3	22.2	14.5	7.0	24.5	1.8	-1.6	5.3
Kayseri	-0.2	-4.8	4.9	2.3	-2.2	7.2	-1.6	-10.4	9.3	8.6	1.3	19.3	2.6	-0.4	6.2
Ankara	-1.9	-6.9	4.8	0.5	-4.0	5.8	-1.7	-10.6	8.9	5.8	-2.7	14.6	1.2	-2.0	4.6
Kirsehir	-4.5	-9.6	0.8	-1.5	-7.1	5.3	-0.5	-11.8	12.8	13.2	5.4	27.6	0.5	-2.6	4.4
Corum	-1.1	-7.4	5.7	0.5	-4.2	4.7	4.1	-7.1	14.9	11.4	3.9	21.0	2.4	-0.3	5.8
Sivas	2.1	-2.5	7.9	3.4	-0.8	8.2	1.6	-7.1	14.2	14.7	7.2	25.1	4.9	1.5	7.8
Van	2.6	-3.8	8.6	-0.6	-4.8	4.0	0.7	-10.3	14.1	1.8	-3.4	8.9	1.5	-1.9	5.2
Canakkale	-2.8	-9.8	3.5	-1.2	-6.5	4.7	0.4	-11.3	15.7	-2.0	-7.6	5.8	-1.5	-5.3	2.2
Edirne	-1.7	-8.6	6.6	-3.6	-7.5	1.6	-3.3	-10.5	7.0	2.0	-4.0	10.1	-1.3	-4.5	2.7
Tekirdag	-2.0	-8.1	4.5	-1.8	-6.8	4.1	-4.5	-11.4	5.5	4.5	-3.7	14.8	-0.5	-4.2	3.3
Bolu	-1.0	-5.5	3.0	2.7	-2.3	7.4	0.8	-6.9	9.6	2.9	-2.0	8.7	0.7	-2.1	3.9
Kastamonu	2.8	-4.0	10.7	3.0	-2.4	8.4	4.3	-4.8	13.5	6.4	-0.5	15.4	3.8	0.4	7.4
Zonguldak	-1.3	-4.0	2.0	-3.0	-6.5	2.1	-2.3	-8.5	7.0	4.6	0.2	9.7	0.4	-1.8	2.9
Inebolu	0.0	-3.8	4.8	1.6	-3.9	7.4	0.7	-7.1	10.1	2.0	-1.3	6.7	2.2	-0.6	4.8
Samsun	-1.9	-6.7	3.2	-1.2	-5.6	3.7	11.9	1.7	20.8	3.4	-2.6	9.3	2.4	-0.9	5.3
Giresun	-0.8	-4.8	2.7	-0.5	-4.3	3.8	2.1	-5.1	7.9	3.2	-1.3	8.1	3.2	-1.3	8.1
Rize	-0.8	-3.6	2.3	-2.5	-5.6	0.8	1.2	-3.3	4.7	2.7	-0.5	7.1	1.2	-1.0	3.6
Turkey	-1.1	-4.3	2.5	-0.5	-2.9	2.4	2.1	-2.4	6.2	5.5	2.6	8.1	1.3	-0.5	2.9

decade of 1970s in almost one third of the stations. There are only two neighboring stations (Zonguldak and Samsun) whose downward trend began earlier, during 1960s. On the contrary, an upward trend dominates almost the half of the stations for autumn but with approximate years of the initiation ranging from early 1960s to early 1980s. There is only a small number of stations presenting a statistically significant trend for summer (one station) and spring season (four stations). There is not any clear signal for annual series, with only one third of the stations showing a statistically significant trend starting during 1960s but with opposite signs. In particular, five stations located in western Turkey show positive trends starting between 1960 and 1970 whereas five stations

situated in northern and central Turkey exhibit negative trends beginning during the period 1957-1972. It should be noted that the detection of the beginning of a change in the time series is indicative and approximate as it is based on the graphical analysis of the Mann-Kendall rank statistics.

The graphical analysis of the Mann-Kendall statistics implemented to the regional mean precipitation series for the area of Turkey (see last row of Table 4 and Figure 6) supports the previous findings. In particular, autumn shows an upward trend starting in 1984, whereas winter exhibits a downward trend initiating in 1971 which, however, seems to start reversing after 1996. No trend has been found for annual and other seasonal precipitation series.

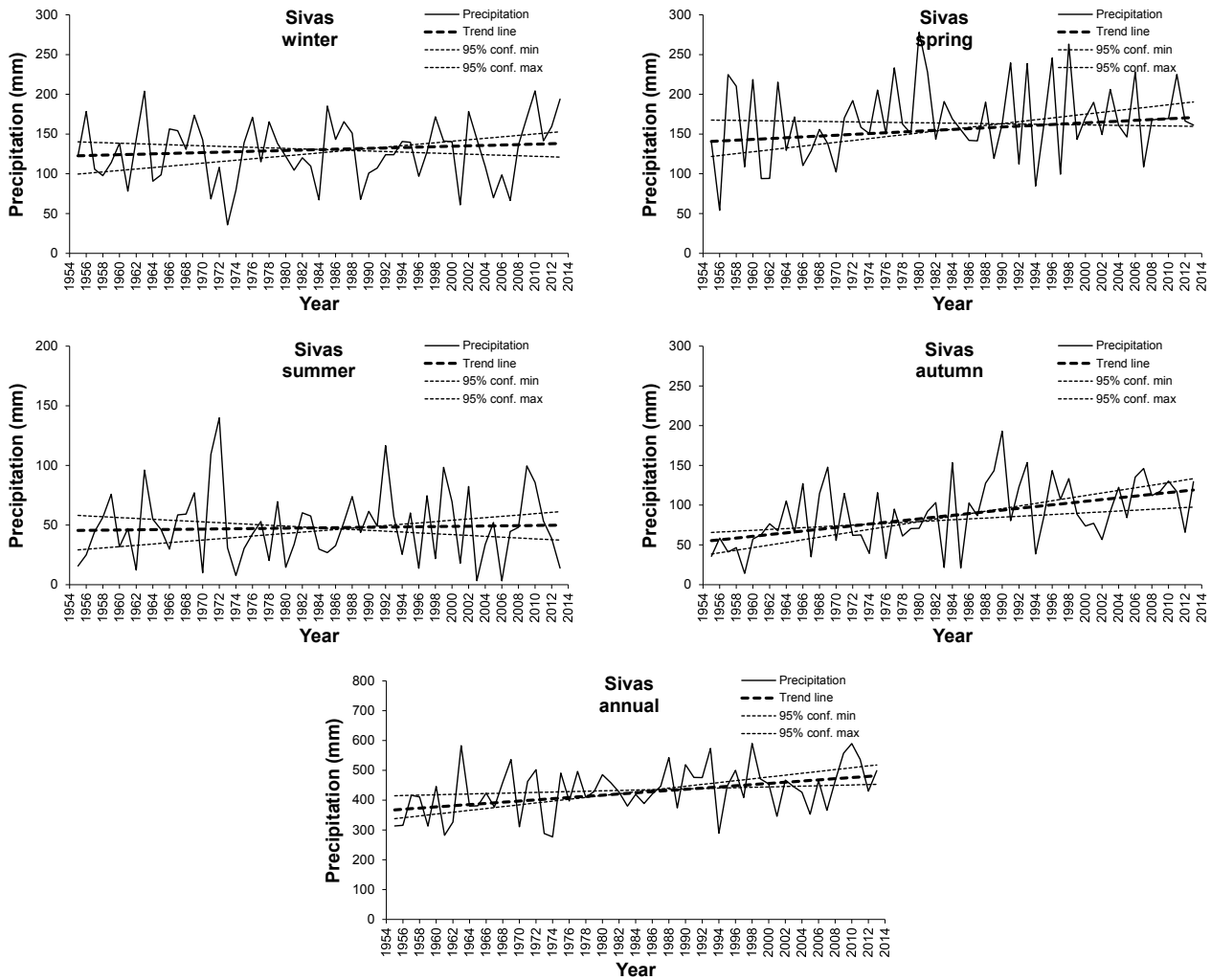


Fig. 2. Seasonal and annual precipitation totals, trend line and its lower and upper limits at the 95% confidence level at the station of Sivas (1955–2013).

These findings are in agreement with other studies partly dealing with precipitation trends in the wider area (Feidas and Lalas 2001; Türkeş et al., 2007; Feidas et al., 2007; Karabulut and Cosun 2009; Philandras et al., 2011; Şimşek et al., 2013; Çiçek and Duman 2015).

3.2 Relation of circulation indices with precipitation in Turkey

Table 5 presents the Pearson correlation coefficients between the five circulation indices (NAOI, MOI, MCI, EMPI and NCPI) and the seasonal and annual precipitation percentages, spatially averaged over Turkey.

The important influence of the NAO on the winter precipitation in Turkey is highlighted by the highest and

statistically significant negative correlation coefficient ($r = -0.45$), with the percentage of the explained winter precipitation variance being up to 20%. A smaller proportion of the winter precipitation variability can be also explained by the NCPI (15%) and EMPI (10%). The MCI plays the most important role in the summer and autumn precipitation accounting for 22% ($r = -0.47$) and 14% ($r = -0.37$) of the precipitation variance, respectively. Only a small proportion of the spring precipitation variance (14%) is explained by the EMPI. No significant correlation has been found between the annual precipitation and any of the atmospheric circulation indices. Figure 7 presents the best correlation between seasonal precipitation in Turkey and atmospheric circulation indices.

The previous results suggest the important role of the NAOI and MCI on the winter and summer precipitation

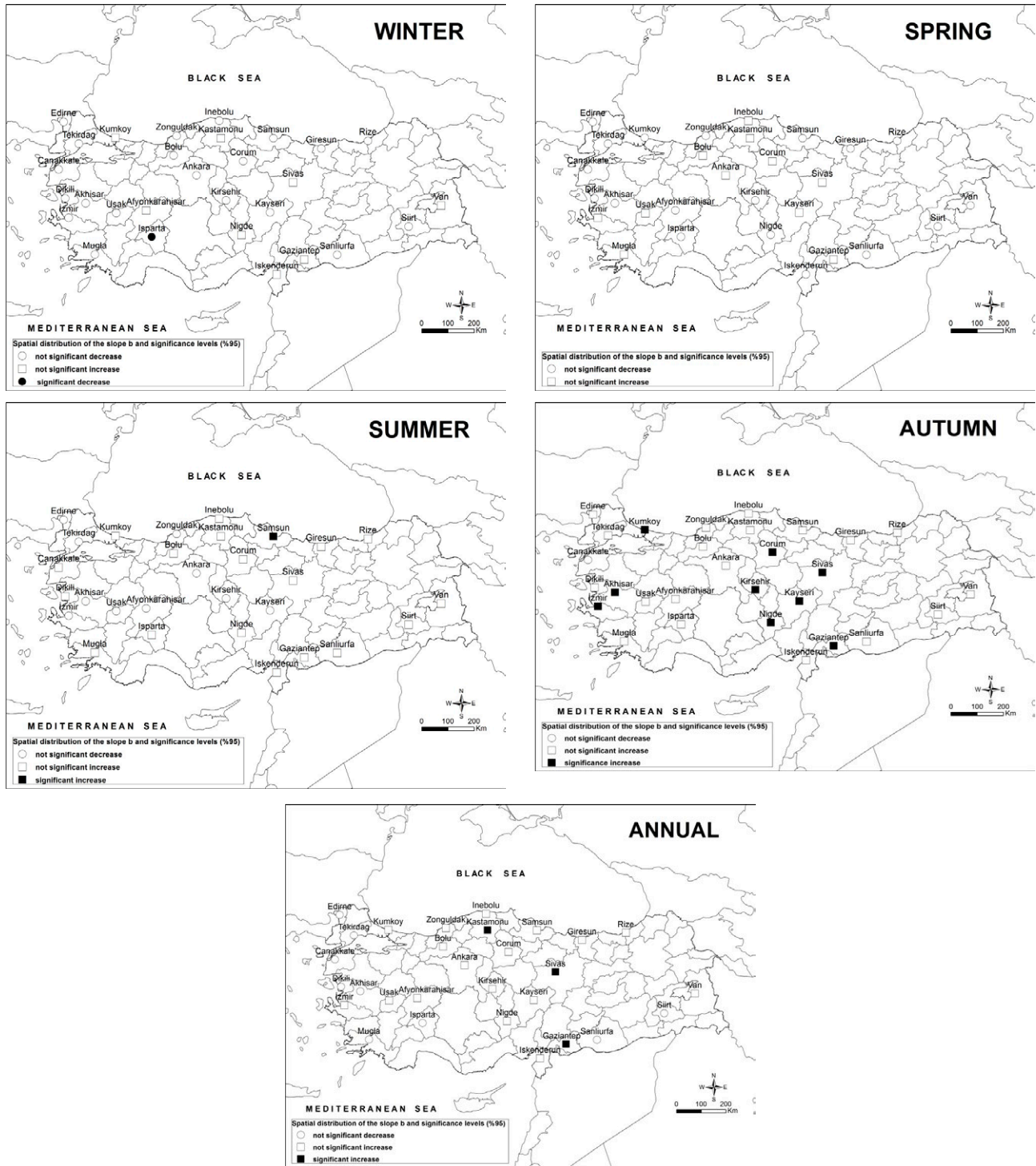


Fig. 3. Spatial distribution of the of the sign and statistical significance slope b values of the trend line for the seasonal and annual precipitation series (period 1955-2013). Squares indicate positive values and circles denote negative slope values. The filled symbols indicate a 95% confidence level.

on Turkey, respectively, which is consistent with the results of other studies (Feidas et al., 2007; Türkes and Erlat, 2003; 2005; López-Moreno et al., 2011; Cullen et al., 2002)

who found that the NAO extends into the Middle East and Turkey. Autumn and spring precipitation is weakly linked with the regional oscillation modes of EMP and MC.

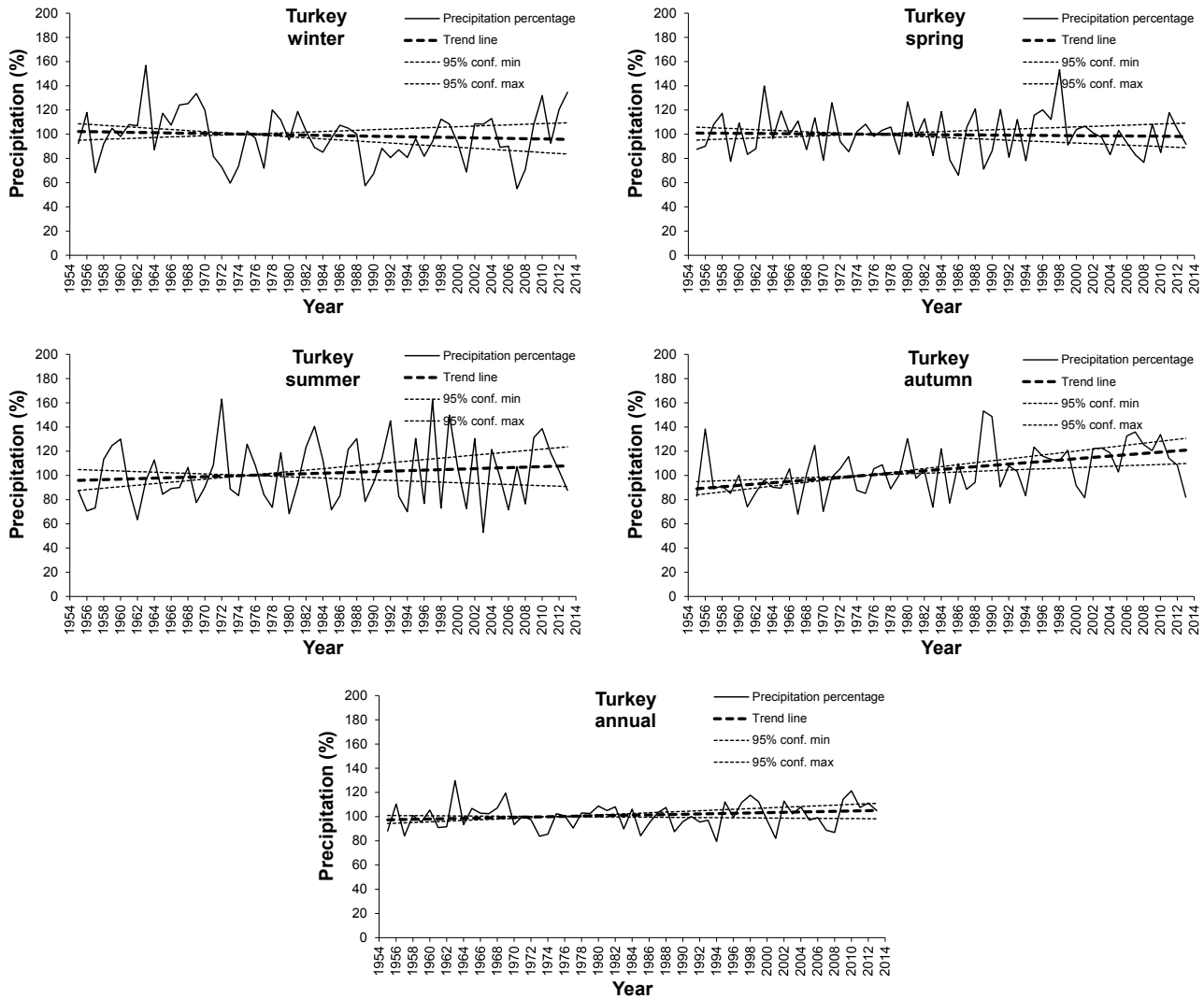


Fig. 4. Seasonal and annual precipitation averaged over Turkey, trend line and its lower and upper limits at the 95% confidence level (1955 – 2013). Precipitation observations are expressed as percentages of the normal for the 1961–1990 period.

The relationship between precipitation variability over Turkey and circulation indices (NAOI and MCI) can be physically explained as follows. In winters, positive (negative) values of the NAOI result from a strong (weak) meridional surface pressure gradient inducing northerly (easterly) airflow that forces cold and dry (warm and wet) continental (maritime) air into the Mediterranean region.

Positive (negative) MCI values in winters are induced by a centre of strong positive (negative) sea level pressure anomalies over north-eastern Atlantic and the western Mediterranean combined with a center of negative (positive) surface pressure anomalies covering the eastern and south-eastern Mediterranean. These coupled pressure patterns build a strong meridional pressure gradient

which brings cold and dry (warm and humid) northeasterly (southwesterly) airflow over the Mediterranean basin (Feidas 2017).

Precipitation trends may be explained by the temporal changes of the large-scale and regional scale atmospheric circulation patterns, mainly for autumn and winter. In particular, autumn precipitation in Turkey was found to be driven mainly by the Mediterranean Circulation (MC) atmospheric teleconnection. The trend analysis showed a statistically significant decreasing trend for the autumn MCI, which is in agreement with the corresponding rising trend in autumn precipitation over Turkey. This shift from positive to negative values of the MCI indicates a weakening of the meridional surface

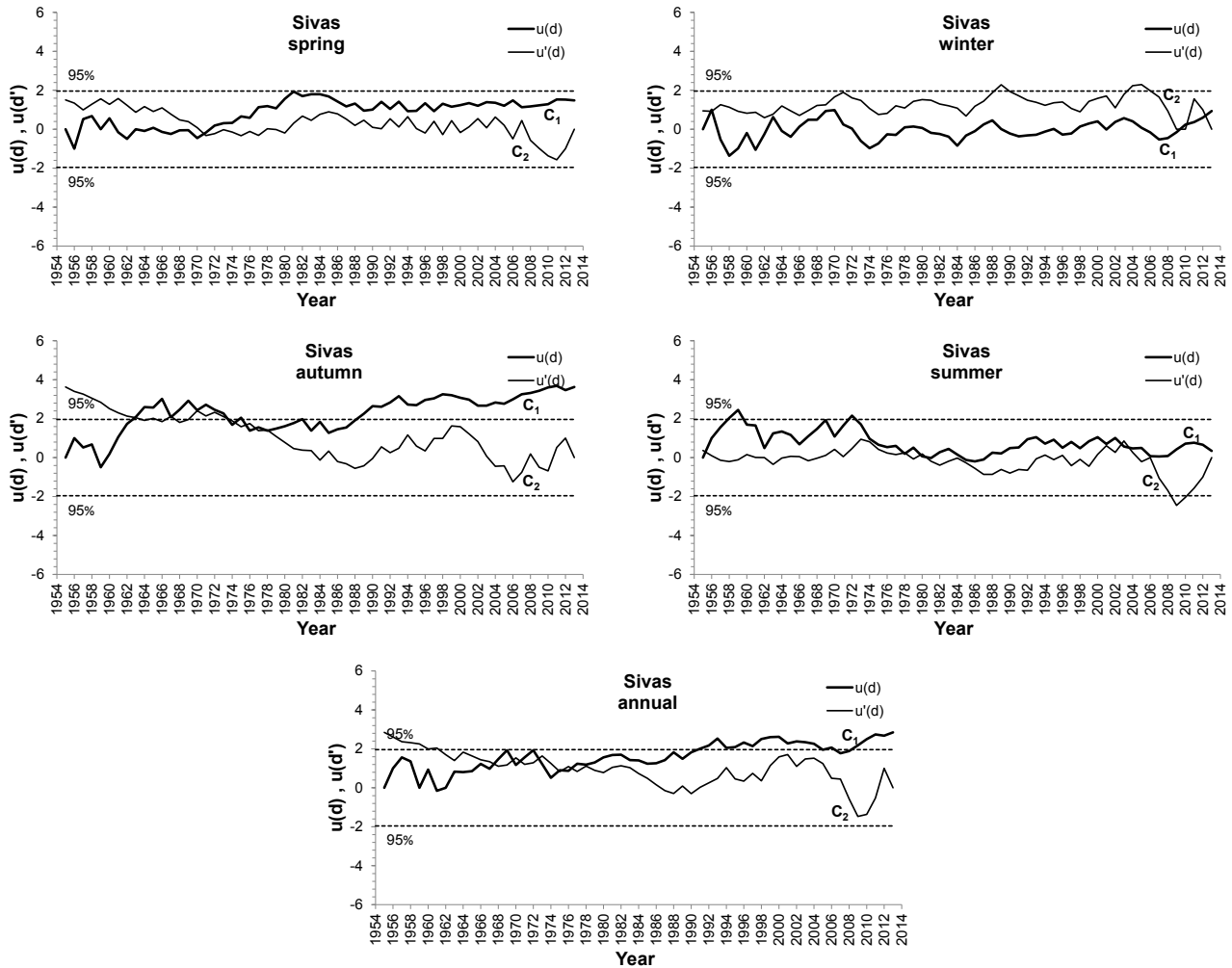


Fig. 5. Plot of the series of the Mann-Kendall statistics $u(d)$ (curve C_1) and $u'(d)$ (curve C_2), for seasonal and annual precipitation at the station of Sivas.

pressure gradient in autumn inducing easterly airflow that forces warm and wet maritime air into the Turkey from the Mediterranean region.

In winter, however, the NAO plays a crucial role in precipitation variability in Turkey as the centers of action of the NAO shift to the south. The observed slight, but not statistically significant, decreasing winter precipitation trend in Turkey is linked mainly to a rising trend in the hemispheric circulation modes of NAO which induces significantly cooler and drier conditions in Turkey.

Application of the Mann-Kendall rank statistics on the time series of the circulation indices NAOI and MCI indicated an upward trend in NAOI starting in 1971 and a downward trend in MCI initiating in 1984. These results match quite well with the starting years of changes in the winter and autumn precipitation time series, respectively.

The previous findings support the assumption that the Mediterranean Circulation and the North Atlantic Oscillation in pressure patterns can be considered a climatic forcing factor for Turkey.

4. CONCLUSIONS

Trends of seasonal and annual precipitation in Turkey were analyzed for the period 1955–2013, using two statistical tests. The trend analysis revealed the presence of variations and trends in Turkey. The link between precipitation variability in Turkey and atmospheric circulation patterns was also investigated using five atmospheric circulation indices.

On an individual station level, a distinct increasing trend ranging from 8.6%/decade to 14.7%/decade for the

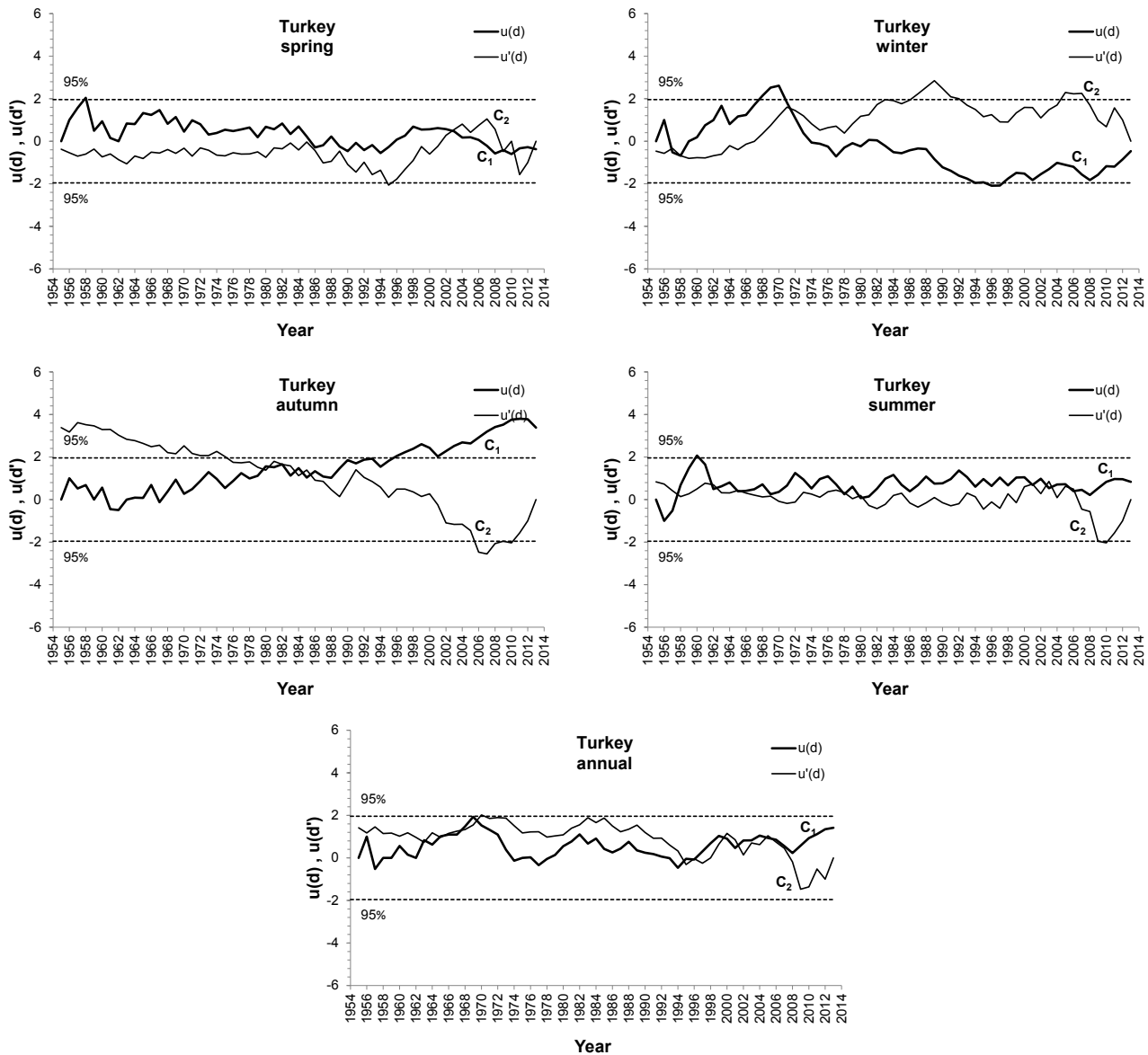


Fig. 6. Same as Figure 5 but for seasonal and annual precipitation averaged over Turkey.

whole period 1955-2013 is evident only in autumn precipitation series, which, however, is statistically significant only in a few stations (9 out of the 29 stations) located mainly in central Anatolia. Half of the 29 stations showed an upward trend starting from early 1960s to early 1980s. Although only one significant downward trend was detected in winter series for the whole period 1955-2013, the investigation of the initiation years of a trend showed a downward trend starting during the period 1970-1980 in almost one third of the stations. Only three stations were found to have small but statistically significant (upward) trends in the annual time series in the range 3.8 - 4.9%

but there is not any clear signal in the starting year of the trends.

At the national scale, only autumn precipitation exhibits a clear significant upward trend of 5.5%/decade for the entire period 1955-2013. No clear significant trend was detected in the other seasons. Based on the investigation of abrupt precipitation changes, Turkey shows a distinct significant upward trend in autumn precipitation starting in 1984, whereas winter presents a downward trend initiating in 1971, which, however, seems to start reversing after 1996.

From a climatic point of view, changes in precipitation trends are the result of respective changes in atmospheric

Tab. 4. The starting year of the upward or downward trend for seasonal and annual precipitation, for the period 1955–2013, based on the Mann-Kendall test.

Stations	Winter	Spring	Summer	Autumn	Annual
Iskenderun	*	1965-	1968+	1977+	*
Kumkoy	*	*	1965+	2001+ (2011-)	1968+
Mugla	1980-	*	1955+	1968+	*
Izmir	*	*	*	1975+	*
Dikili	1974-	*	*	*	1964-
Gaziantep	*	*	*	1980+	1962+
Sanliurfa	1983-	*	*	*	*
Siirt	*	*	*	1960+	*
Isparta	1977-	*	*	*	1972-
Afyonkarahisar	*	*	*	*	*
Usak	*	*	*	1970+	*
Akhisar	1970-	*	*	1975+	*
Nigde	*	*	*	1997+	*
Kayseri	*	*	*	1961+	*
Ankara	*	*	*	*	*
Kirsehir	1978-	*	*	1968+	*
Corum	*	*	*	1964+	1960+
Sivas	*	*	*	1963+	1968+
Van	*	*	*	*	*
Canakkale	1971-	*	*	*	1963-
Edirne	1971-	*	*	*	1961-
Tekirdag	1963+ (1971-)	*	*	*	1957-
Bolu	*	*	*	1975+	*
Kastamonu	*	*	*	1968+	1962+
Zonguldak	1965-	*	*	1983+	*
Inebolu	*	*	*	*	*
Samsun	1960-	*	1989+	*	*
Giresun	*	*	*	*	*
Rize	*	*	*	1995+	*
Turkey	1971-	*	*	1984+	*

* No abrupt change found at the 95% level of confidence

+ Increasing trend

- Decreasing trend

() Year of a not statistically significant new abrupt change in a trend.

circulation. For example, the upward trend in autumn precipitation starting in 1984 and the downward trend in winter precipitation initiating in 1971, match quite well with the starting years of changes in the MCI and NAOI time series, respectively.

Analysis of the five circulation indices points out the strong link of precipitation regime in Turkey with variations in atmospheric circulation patterns. Precipitation variability in Turkey may be the result of variability of some coupled atmospheric circulation patterns (mainly

Tab. 5. Correlation coefficients of circulation indices with seasonal and annual precipitation in Turkey (95% level of confidence is indicated with boldface characters).

	Winter	Spring	Summer	Autumn	Annual
NAOI	-0.45	-0.18	-0.04	-0.09	-0.22
MOI	-0.24	0.06	-0.05	-0.30	-0.21
MCI	0.16	-0.01	-0.47	-0.37	-0.24
EMPI	0.32	0.38	0.10	-0.06	0.00
NCPI	-0.39	0.22	0.16	-0.08	-0.14

the NAO and MC). More precisely, NAOI is the most suitable circulation index for explaining annual precipitation variability in Turkey. In addition, the MCI captures a large proportion of the precipitation variability in summer. Autumn and spring precipitation have a weak relationship with the regional oscillation modes of EMP and MC.

The link between precipitation variability in Turkey and atmospheric circulation patterns can also account for the observed precipitation trends over Turkey. In particular, the significant rising trend in autumn precipitation can be explained by the respective decreasing trend in the autumn MCI. The negative values of the MCI enhanced frequency of the northwest or northeast continental, dry and cold mid-tropospheric airflow advected from northern Europe leads to a lack of precipitation over Turkey.

This enhanced frequency of negative MCI values in autumn indicates a weakening of the meridional surface pressure gradient that induces an increased frequency of easterly maritime, warm and wet airflow advected from the Mediterranean Sea into the Turkey leading to an increase of precipitation over Turkey.

The observed slight but not statistically significant downward winter precipitation trend in Turkey is linked mainly to a rising trend in the hemispheric circulation modes of NAO. The enhanced frequency of positive NAOI values results in significantly cooler and drier conditions in Turkey as the increased frequency of northerly airflow brings continental, cold and dry air into the eastern Mediterranean region.

The findings of this study is in agreement with previous studies on the precipitation trends in the region (Türkeş and Erlat 2003; Türkeş et al., 2007; Feidas et al., 2007; Karabulut et al., 2008; Karabulut and Cosun 2009; Türkeş et al., 2009; Philandras et al., 2011). The important role of NAO and MCI in the precipitation regime of Greece and Turkey during winter has been also pointed out in the studies of Feidas et al., (2007) and Türkeş and Erlat (2003).

One major difference of our findings to previous studies covering similar periods (Toros, 2012; Efe et al., 2015; Sensoy et al., 2013) is that no statistically significant trend

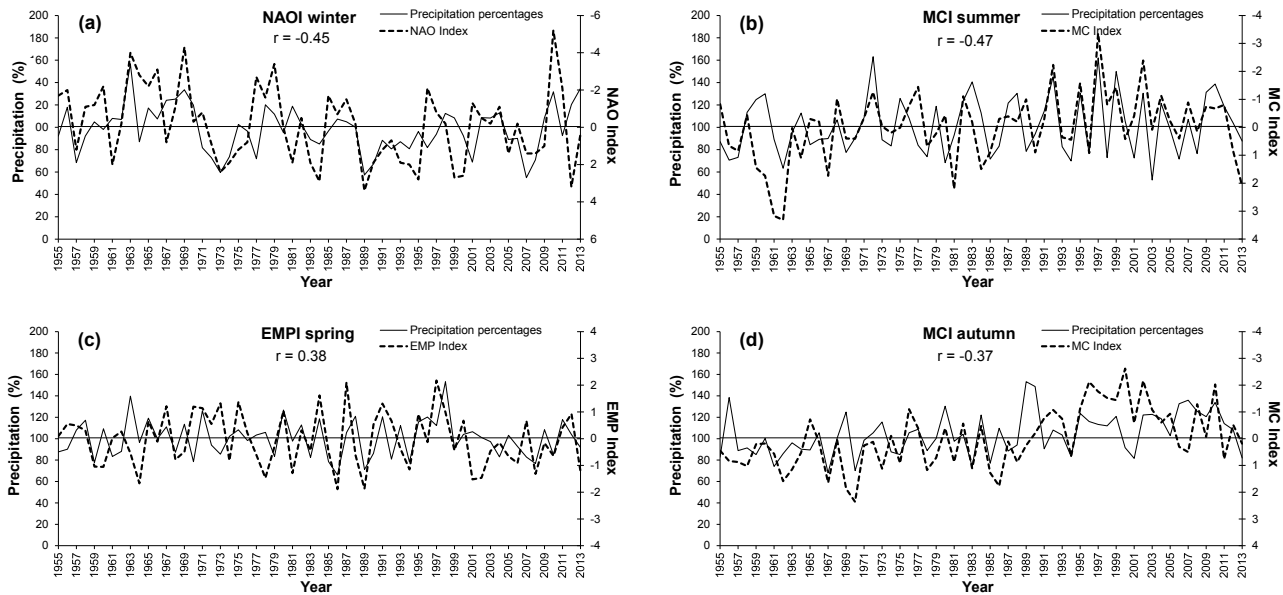


Fig. 7. Plots of the variability of seasonal precipitation in Turkey and seasonal circulation indices presenting the best correlation.

was found in our study in the annual and winter precipitation over Turkey for the examined period 1955-2013. In our study, only 3 out of the 29 stations were found to present a significant increasing trend in annual precipitation. It should be pointed out, however, that trend analysis results depend strongly on the time period of the time series and the statistical test used to detect the trend and its significance. Moreover, trends found in the study of Efe et al. (2015), were assessed and categorized differently. Another difference with these studies is that no significant correlation has been found between the annual precipitation and any of the atmospheric circulation indices in our study.

ACKNOWLEDGEMENTS

This study has been prepared in Aristotle University of Thessaloniki, School of Geology, Department of Meteorology and Climatology in Greece, under the supervision of Professor Haralambos Feidas, in the frame of Kahramanmaraş Sutcu Imam University Foreign Relations Office Erasmus Internship Mobility 2015.

REFERENCES

Alexandrov V., Schneider M., Koleva E., Moisselin J.M. 2004. Climate variability and change in Bulgaria during the 20th century. *Theor. Appl. Climatol.* **79**, 133–149.

- Bachmann N. 2007. The North Atlantic Oscillation (NAO). Term paper Writing for MSc Biogeochemistry and Pollutant. Dynamics ETH Zurich.
- Brunetti M., Maugeri M., Nanni T. 2002. Atmospheric circulation and precipitation in Italy for the last 50 years. *Int J Climatol*, **22**, 1455-1471.
- Buishand T.A. 1982. Some Methods for Testing the Homogeneity of Rainfall Records. *J Hydrol* **58**: 11–27
- Burhanuddin S.N.Z.A., Deni S.M.D., Ramli N.M. 2017. Revised normal ratio methods for imputation of missing rainfall data. *Advanced Science Letters*, **23** (11): 10981-10985.
- Clegg L.X., Hankey B.F., Tiwari R., Feuer E.J., Edwards B.K. 2009. Estimating average annual per cent change in trend analysis. *Stat Med.* 2009 Dec **20**; **28**(29): 3670–3682. Published online 2009 Oct 23. doi: 10.1002/sim.3733
- Çiçek I. and Duman N. 2015. Seasonal and Annual Precipitation Trends in Turkey. *Carpathian Journal of Earth and Environmental Sciences*, **10** (2): 77–84.
- Colacino M and Conte M. 1993. Greenhouse effect and pressure patterns in the Mediterranean basin. *Il Nuovo Cimento C* **16**: 67-76.
- Conte M., Giuffrida S., Tedesco S. 1989. The Mediterranean oscillation: impact on precipitation and hydrology in Italy. Proc. Conference on Climate and Water, vol. 1, *Academy of Finland*, **9**, 121–137.
- Criado-Aldeanueva F. and Soto-Navarro F.J. 2013. The Mediterranean Oscillation Teleconnection Index: Station-Based versus Principal Component Paradigms.

- Advances in Meteorology* 2013, Article ID 738501, 10 pages, doi.org/10.1155/2013/738501
- Cullen H.M. and de Menocal P.B. 2000. North Atlantic influence on Tigris-Euphrates streamflow. *Int J Climatol*, **20**, 853–863.
- Cullen H.M., Kaplan A., Arkin P.A., de Menocal P.B. 2002. Impact of the North Atlantic Oscillation on Middle Eastern climate and streamflow. *Climatic Change*, **55**, 315–338.
- Douguedroit A. 1998. Que peut-on dire d'une oscillation Méditerranéenne ? In *Climate and Environmental Change*. Alcoforado MJ (ed.). Evora: 135-136.
- Efe B., Toros H., Deniz A. 2015. Türkiye için Sıcaklık ve Yağışın Eğilim İncelemesi. 7. Atmosfer Bilimleri Sempozyumu. İstanbul (in Turkish).
- Erlat E. 2002. Türkiye'de Yağış Anomalileri ve Kuzey Atlantik Salınımı ile İlişkisi Klimatoloji Çalıştayı. (11-13 Nisan 2002), 193-210 (in Turkish).
- Feidas H. and Lalas D. 2001. Climatic Changes in Mediterranean and Greece: A Critical Review. 7th International Conference on Environmental Science and Technology Ermoupolis, Syros island, Greece – Sept. 2001.
- Feidas H., Nouloupoulou C.H., Makrogiannis T., Borsenta E. 2007. Trend Analysis of Precipitation Time Series In Greece And Their Relationship With Circulation Using Surface And Satellite Data: 1955–2001. *Theor Appl Climatol* **87**, 155–177. doi 10.1007/s00704-006-0200-5
- Feidas H. 2017. Trend analysis of air temperature time series in Greece and their relationship with circulation using surface and satellite data: recent trends and an update to 2013. *Theor Appl Climatol* **129** (3-4), 1383-1406.
- Giorgi F. and Lionello P. 2008. Climate change projections for the Mediterranean region. *Global Planet Change*, **63**, 90-104.
- Goossens C. and Berger A. 1986. Annual and Seasonal Climatic Variations over the Northern Hemisphere and Europe during the Last Century. *Ann Geophys B*: 385–400.
- Greatbach J.R. 2000. The North Atlantic Oscillation. *Stochastic Environment Research and Risk Assessment*, **14**, 213–242.
- Hatzaki M., Flocas H.A., Asimakopoulos D.N., Maheras P. 2007. The eastern Mediterranean teleconnection pattern: identification and definition. *Int J Climatol* **27**, 727-737.
- Irvem A. and Ozbuldu M. 2019. Evaluation of Satellite and Reanalysis Precipitation Products Using GIS for All Basins in Turkey. *Advances in Meteorology*, 1-12. 10.1155/2019/4820136
- IPCC 2007. The Physical Science Basis”, Contribution of Working Group I to the Fourth Assessment Report of the Intergovernmental Panel on Climate Change, 2007. Solomon, S., D. Qin, M. Manning, Z. Chen, M. Marquis, K.B. Averyt, M. Tignor and H.L. Miller (eds.), Cambridge University Press, Cambridge, United Kingdom and New York, NY, USA.
- IPCC 2014. Climate Change 2014: Synthesis Report. Contribution of Working Groups I, II and III to the Fifth Assessment Report of the Intergovernmental Panel on Climate Change [Core Writing Team, R.K. Pachauri and L.A. Meyer (eds.)]. IPCC, Geneva, Switzerland.
- Kadioglu M. 1993. Türkiye'de iklim değişikliği ve olası etkileri. *Çevre Koruma (Environmental Protection)*. İstanbul, **47**, 3637 (in Turkish).
- Kadioglu M. 2000. Regional variability of seasonal precipitation over Turkey. *Int J Climatol* **20**, 1743–1760.
- Karabork M.C., Kahya E., Karaca M. 2002. Kuzey Atlantik Salınımı ve Türkiye Uzerine Olası Etkileri. Klimatoloji Çalıştayı, (11-13 Nisan 2002), EU, İzmir. (in Turkish)
- Karabulut M. and Cosun F. 2009. Kahramanmaraş İlinde Yağışların Trend Analizi. *Journal of Coğrafi Bilimler*, **7** (1): 65-83 (in Turkish).
- Karabulut M., Gürbüz M., Korkmaz H. 2008. Precipitation and Temperature Trend Analyses in Samsun, *J.Int. Environmental Application & Science*, **3**(5): 399-408.
- Karakoç A. and Tagil S. 2014. İzmir ve Ankara'da Yağış Paterni ile Kuzey Atlantik Salınımı (NAO) Arasındaki İlişki. *Uluslararası Sosyal Araştırmalar Dergisi*, **7** (30): 148-157 (in Turkish).
- Krichak S.O. and Alpert P. 2005. Signatures of the NAO in the atmospheric circulation during wet winter months over the Mediterranean region. *Theor Appl Climatol*, **82**, 27–39.
- Kutiel H., Maheras P., Guika S. 1996. Circulation and extreme rainfall conditions in the eastern Mediterranean during the last century. *Int J Climatol* **16**, 73-92.
- Kutiel H., Benaroch Y 2002. North Sea Caspian Pattern (NCP) - an upper level atmospheric teleconnection affecting the eastern Mediterranean: Identification and definition. *Theor Appl Climatol*, **71**, 17-28.
- Levene H. 1960. Robust tests for equality of variances. In: Olkin I (ed) Contributions to probability and statistics: essays in honor of Harold Hotelling. Stanford, CA: Stanford University Press, pp 278–292.
- López-Moreno J.I., Vicente-Serrano S.M., Morán-Tejeda E., Lorenzo-Lacruz J., Kenawy A., Beniston M. 2011. Effects of the North Atlantic Oscillation (NAO) on Combined Temperature and Precipitation Winter Modes in the Mediterranean Mountains: Observed

- Relationships and Projections for the 21st Century. *Global and Planetary Change*, 77, 62-76.
- Maheras P, Kutiel H 1999. Spatial and Temporal Variations in the Temperature Regime in the Mediterranean and their Relationship with Circulation During the Last Century. *Int J Climatol* 19, 745-764.
- Maheras P., Xoplaki E., Kutiel H. 1999. Wet and dry monthly anomalies across the Mediterranean basin and their relationship with circulation, 1860-1990. *Theor Appl Climatol* 64, 189-199.
- MEB 1941. Birinci Coğrafya Kongresi 6-21 Haziran 1941 Raporlar, Müzakereler, Kararlar. Ankara (in Turkish).
- Mitchell J.M., Dzerdzeevski B., Flohn H., Hofmery W. 1966. Climatic change. WMO Tech Note 79. WMO No. 195. TP-100, Geneva, 79.
- Norrrant C., Douguédroit A. 2006. Monthly and daily precipitation trends in the Mediterranean (1950–2000). *Theoretical Applied Climatology*, 83 (1-4), 89-106.
- Ozfidaner M. 2007. Türkiye Yagis Verilerinin Trend Analizi ve Nehir Akimlari Uzerine Etkisi. Cukurova University, Science Institute, Agricultural Structures and Irrigation Department Master Thesis, Adana (in Turkish).
- Palutikof J.P., Trigo R.M., Adcock S.T. 1996. Scenarios of future rainfall over the Mediterranean: is the region drying?, in: Proceedings of Mediterranean Desertification, Research Results and Policy Implications, Crete, Greece.
- Partal T. and Kahya E. 2006. Trend analysis in Turkish precipitation data. *Hydrological Processes*, 20 (9): 2011-2026. doi: 10.1002/hyp.5993
- Peterson T.C., Easterling D.R., Karl T.R., Groisman P., Nicholls N., Plummer N., Torok S., Auer I., B€ohm R., Gullet D., Vincent L., Heino R., Tuomenvirta H., Mestre O., Szentimrey T., Salinger J., Førland E.J., Hansen-Bauer I., Alexandersson H., Jones P., Parker D. 1998. Homogeneity adjustments of in situ atmospheric climate data: a review. *Int J Climatol* 18, 126–135.
- Philandras C.M., Nastos P.T., Kapsomenakis K., Douvis K.C., Tselioudis G., Zerefos C.S. 2011. Long Term Precipitation Trends And Variability With In The Mediterranean Region, *Nat. Hazards Earth Syst. Sci.*, 11, 3235–3250.
- Piervitali E., Colasino M., Conte M. 1997. Signals of climatic change in the Central-Western Mediterranean basin, *Theor. Appl. Climatol.*, 58, 211–219.
- Piervitali E., Colasino M., Conte M. 1999. Rainfall over the central-western Mediterranean basin in the period 1951-1995. Part II: precipitation scenarios. *Il Nuovo Cimento C* 22: 649-661.
- Rogers J.C. and van Loon H. 1979. The seesaw in winter temperatures between Greenland and northern Europe. Part II: some oceanic and atmospheric effects in middle and high latitudes. *Mon Wea Rev* 107: 509-519.
- Sariş F., Hannah M.D., Eastwood J.W. 2010. Changes in Precipitation and River Flow in Northeast Turkey: Associations with the North Atlantic Oscillation. Sixth World Friend Conference, (October, 2010), Fez, Morocco.
- Schönwiese C.D. and Rapp J. 1997. Climate Trend Atlas of Europe Based on Observations 1891-1990. Kluwer, Dordrecht.
- Sen, P.K. 1968. Estimates of the regression coefficient based on Kendall's tau. *Journal of the American Statistical Association* 63, 1379-1389.
- Sensoy S., Türkoglu N., Akçakaya A., Ekici M., Ulupınar Y., Demircan M., Atay H., Tüvan A., Demirbaş H. 2013. 1960 -2010 yılları arası Türkiye iklim indisi trendleri. 6. Atmosferik Bilimler Sempozyumu, 24-26 Nisan 2013, İTÜ, İstanbul (in Turkish).
- Singh V.P. 1992. Elementary hydrology. New Jersey: Prentice-Hall, 973.
- Sneyers R. 1990. On the statistical analysis of series of observations. Tech. Note 143, WMO No. 415, Geneva, 192.
- Şimşek O., Gümüş V., Soydan N.G., Yenigün K., Kavşut M.E., Topçu E. 2013. Hatay ilinde bazı meteorolojik verilerin gidiş analizi. *SDU International Journal of Technological Science*, 5 (2): 132-144 (in Turkish).
- Tayanç M., Im U., Doğruel M., Karaca M. 2009. Climate change in Turkey for the last half century, *Climatic Change*, 94, 483–502.
- Tomozoiu R., Stefan S., Busuioc A. 2005. Winter precipitation variability and large-scale circulation patterns in Romania. *Theor. Appl. Climatol.* 81, 193–201.
- Toros H. 2012. Spatio-temporal precipitation change assessments over Turkey. *International Journal of Climatology*, 32 (9): 1310-1325.
- Toros H., Deniz A., Karan H. 1994. Bati Anadolu yagislarinin istatistiksel olarak incelenmesi. I. Ulusal Hidrometeoroloji Sempozyumu, Istanbul Teknik Universitesi, Istanbul, 185-198 (in Turkish).
- Trigo R., Xoplaki E., Zorita E., Luterbacher J., Krichak S.O., Alpert P., Jacobeit J., Saenz J., Fernandez J., Rouco F.G., Herrera R.G., Rodo X., Brunetti M., Nanni T., Maugeri M., Türkeş M., Gimeno L., Ribera P., Brunet M., Trigo I.F., Crepon M., Mariotti A. 2002. Relations between Variability in the Mediterranean Region and Mid-latitude Variability. *Mediterranean Climate Variability*, Chapter 3: 79-226.
- Türkeş M. 1996. Spatial and temporal analysis of annual rainfall variations in Turkey. *Int. J. Climatol*, 16, 1057–1076.

- Türkeş M. 1998. Influence of Geopotential Heights, Cyclone Frequency and Southern Oscillation on Rainfall Variations in Turkey. *International Journal of Climatology*, **18**, 649-680.
- Türkeş M, Erlat E 2003. Precipitation Changes and Variability in Turkey Linked to the North Atlantic Oscillation During the Period 1930-2000. *International Journal of Climatology*, **23**, 1771-1796.
- Türkeş M. and Erlat E. 2005. Climatological Responses of Winter Precipitation in Turkey to Variability of the North Atlantic Oscillation during the Period 1930-2001. *Theoretical and Applied Climatology*, **81**, 45-69.
- Türkeş M. and Erlat E. 2006. Influences of the North Atlantic Oscillation on Precipitation Variability and Changes in Turkey, *Nuovo Cimento Della Societa Italiana Di Fisica C-Geophysics and Space Physics*, **29**, 117-135.
- Türkeş M., Koç T., Sariş F. 2007. Türkiye'nin Yağış Toplamı ve Yoğunluğu Dizilerindeki Değişikliklerin ve Eğilimlerin Zamansal ve Alansal Çözümlemesi. *Cografî Bilimler Dergisi*, **3**, 57-73 (in Turkish).
- Türkeş M., Koç T., Sariş F. 2009. Spatiotemporal variability of precipitation total series over Turkey. *Int. J. Climatol.* **29**, 1056-1074.
- Turp M.T. 2006. Statistical Relationship between the North Atlantic Oscillation and the Climate of Turkey. B.S., Physics, Yıldız Technical University, İstanbul.
- Visbeck M., Hurrell W.J., Polvani L., Cullen M.H. 2000. The North Atlantic Oscillation: Past, Present and Future. Proceedings at the 12th Annual Symposium on Frontiers of Science. **98**, 12876-12877.
- Von Neumann J. 1941. Distribution of the ratio of the mean square successive difference to the variance. *Annals of Mathematical Statistics* **13**, 367-395.
- Walker G.T. 1924. Correlations in seasonal variations of weather. IX. Memoirs Indian Meteorology Department **24**, 275-332.
- Walker G.T. and Bliss E. 1932. World weather V. Memoirs of the Royal Meteorological Society **4**, 53-84.
- Xoplaki E. 2002. Climate Variability Over the Mediterranean, PhD Dissertation, University Of Bern. Switzerland.
- Xoplaki E., Luterbacher J., Burkard R., Patrikas I., Maheras P. 2000. Connection between the large scale 500 hPa geopotential height fields and precipitation over Greece during wintertime. *Climate Research* **14**, 129-126.



Citation: B. Pouzeshimiya, S.R. Fani (2020) Epidemiology and Aerobiology of *Pseudoperonospora cubensis* in northwest Iran. *Italian Journal of Agrometeorology* (2): 109-116. doi: 10.13128/ijam-850

Received: November 22, 2020

Accepted: May 23, 2020

Published: January 25, 2021

Copyright: © 2020 B. Pouzeshimiya, S.R. Fani. This is an open access, peer-reviewed article published by Firenze University Press (<http://www.fupress.com/ijam>) and distributed under the terms of the Creative Commons Attribution License, which permits unrestricted use, distribution, and reproduction in any medium, provided the original author and source are credited.

Data Availability Statement: All relevant data are within the paper and its Supporting Information files.

Competing Interests: The Author(s) declare(s) no conflict of interest.

Epidemiology and Aerobiology of *Pseudoperonospora cubensis* in northwest Iran

BEHNAM POUZESHIMIYAB^{1,*}, SEYED REZA FANI²

¹ Department of Plant Pathology, Marand Branch, Islamic Azad University, Marand, Iran

² Plant Protection Research Department, Yazd Agricultural and Natural Resources Research and Education Center, AREEO, Yazd, Iran

*Corresponding author. E-mail: pouzeshi2@marandiau.ac.ir; rezafani52@gmail.com

Abstract. This study was aimed at evaluating climatic variables and concentrations of airborne sporangia of *Pseudoperonospora cubensis*, the causal agent of cucumber downy mildew and its relation with the severity of the disease. Monitoring was conducted in a cucumber field located in Marand, Iran during 2014-2015. The aerial concentration of sporangia was evaluated by a whirling arm trap and the weather parameters were monitored using a local meteorological station. Statistical analysis indicated a significant correlation between disease severity and some climatic factors ($P \leq 0.05$). The results showed that evaluation of airborne sporangia and the use of forecasting models could reduce the risk of disease in the northwest of Iran. The factorial analysis of the climate variables resulted in the development of two factors, average humidity and rain, that could be used as predictor variables in linear regression models for the downy mildew.

Key words. Cucumber, downy mildew, meteorological variables, sporangia dispersal.

INTRODUCTION

Cucumber downy mildew (CDM), caused by *Pseudoperonospora cubensis* [(Berk. & M.A. Curtis) Rostovzev], is a wide spread and devastating disease of cucurbit crops, including cucumber, squash, pumpkin, melon in the open field and in greenhouse productions (Lebeda and Cohen, 2011). Disease occurrence may lead to tremendous yield losses (up to 100%) in all production areas (Call *et al.*, 2012, Cohen, 2015).

Disease epidemics are driven by the production of asexually derived sporangia. Environmental and ecological conditions significantly contribute to the progression of downy mildew disease as sporangia are mainly produced during warm (20–25°C) and humid (>85% RH) nights (low light intensity). Sporangia bearing structures (sporangiophores) can be seen arising from stomatal openings and are reliant on wind for dispersal of attached sporangia. Upon contact with susceptible host tissue, sporangia release zoospores which require sufficient leaf wetness/access to free water to swim to and successfully penetrate stomata. Post penetration, intercellular mycelium is produced and the disease cycle continues (Lebeda and Cohen, 2011).

Because of the favorable climatic conditions in Iran, cucurbits can be grown year-round in open fields or greenhouses. This production system ensures continuous host availability and eliminates the need for lengthy overwintering strategies for the obligate biotrophic pathogen. The unrestricted ability of the pathogen to produce inoculum and cause disease is presenting farmers with year-round challenges in disease management. Disease prediction models based on the aerodynamics of pathogen multiplication are urgently needed to mitigate costly chemical spraying during critical disease periods and to develop regional integrated pest management programs (Ojiambo *et al.*, 2011).

However, some effective factors in the development of the disease by the dispersion of airborne sporangia have not been evaluated for use in the CDM forecasting system (Ojiambo *et al.*, 2011).

CDM disease severity is directly related to production and release of sporangia by the pathogen. A disease outbreak can be evaluated with consideration of these two parameters (Neufeld *et al.*, 2013). Combining the inoculum data with weather data assists disease prediction models to assess the risk of infection more accurately (West *et al.*, 2008). This risk assessment allows growers to foresee possible disease outbreaks and adjust fungicide applications accordingly (Gent *et al.*, 2013; Gent *et al.*, 2009; Granke and Hausbeck 2011; Granke *et al.*, 2014). Knowledge of temporal changes in *P. cubensis* populations during a single growing season can promote effective management strategies.

The aim of this study was to evaluate and relate climatic variables and concentrations of airborne sporangia of *P. cubensis* to CDM disease severity.

2. MATERIAL AND METHODS

2.1. Experimental plots and Meteorological measurements

The plots were maintained according to the standard production practices for cucumber (*Cucumis sativus*) production in Iran.

The population of *P. cubensis* sporangia were observed in cucumber fields in two regions of Marand during the growing seasons of April–October 2014 and 2015. In each region, the plot was planted with the same cultivar (Superstar, Semo, Czech). The cultivation area of each plot was 2 hectares. The fields were naturally infected and no fungicides were applied during the study.

The weather parameters were evaluated daily using a local meteorological station 1.5 m above the soil level less than 10 m outside the experimental plot. The temperature, relative humidity, rainfall, precipitation, wind speed and radiation were recorded. The wind speed was measured

approximately 2 m above the ground. Data was recorded every 3 min to 15 min by the weather station.

2.2. Monitoring sites and aerobiological studies

The monitoring was done at two regions of Arbatan, a village 10 km west of Marand, located in northwest of Iran (38°10'29"N, 46°56'14"E or 38.174722°, 46.937222°). The spore trapping was carried out 24 hours a day from April 8 to October 9 in 2014 and 2015.

On each assessment day, the aerial concentration of *P. cubensis* sporangia, C (sporangia m⁻³), was monitored above the cucumber canopy, using whirling arm trap (Burkard trap, Hirst-type U.K). The spore trap was installed 0.5 m above the canopy of the plants. The sporangia were trapped on sticky-coated tape (adhesive tape) mounted on the leading edge of the rotating arms. The tape strips were made sticky with a petroleum silicone grease coating. After use, tapes were mounted on microscope slides (sampler). A rain-shield was mounted above the coated-tape (Lacey and West, 2006). The tape strips were exposed to the air at 8 am until 6 pm daily for 117 days in 2014 and 132 days in 2015. After exposure, strips were transferred to the laboratory for identification and enumeration of sporangia. The sporangia were identified and quantified using a microscope equipped with a 100X lens (Nikon Optiphot II, Japan). Concentrations of the sporangia were expressed as the number of spores per cubic meter of air. The first sporangia were trapped on April 29, 2014 and April 21, 2015. Sampling was conducted every three days until October 20, 2014 and October 19, 2015.

2.3. Evaluation of disease severity

To evaluate CDM disease severity, 10 plants were selected randomly in each 20 × 10 m² plot. Foliar disease severity was determined using the 0 to 9 index developed by Thomas *et al.* (1987) with some modification (Table 1). The following design was used to evaluate the disease severity for each plant or plot:

$$DS = [\sum (n_i \times v_i) / N \times V] \times 100$$

Where DS: disease severity, n_i: number of leaves with the same score, v_i: disease score from 0-9 for each leaf, N: total number of evaluated leaves, and V: highest disease score (9).

The disease severity was recorded 3 days after the last sampling date to assess the number of sporangia, and was carried out from May 2 to October 23 (39 times) and from April 24 to October 22 (42 times) for 2014 and 2015 respectively.

Tab. 1. The pattern used for the disease severity scaling of cucumber downy mildew.

Symptoms description	Score
No symptom	0
Visual spots without sporangium formation (incompatible)	3
Visual spots with a few sporangium (compatible)	5
Visual spots with scattered sporangium (5×10^3 spores per square cm of spot)	7
Spots covered the leaf surface (highly compatible) with a lot of sporangium (5×10^4 spores per square cm of spot)	9

2.4. Statistical analyses

All data obtained from the meteorological station and the number of sporangia registered during the seasons, as well as data on pathogenicity expressed as mean \pm standard deviation, were analyzed using SPSS ver. 20 (SPSS Inc., Chicago IL). Paired sample t-tests for meteorological data, sporangium number and severity of disease were employed as the statistical tests, with the level of significance set at $p < 0.05$. The sum of the spores was calculated. A paired sample T-test (paired by the collection dates for the same site) was used to compare the mean sporangial concentrations collected in the growing seasons 2014-2015.

Pearson's correlation coefficients (r) analysis was carried out in order to assay the effect of meteorological factors, the maximum, minimum and mean temperatures ($^{\circ}\text{C}$), the mean relative humidity (%) and rainfall (mm) on concentrations of sporangia and disease severity. The level of significance was set at ≤ 0.05 and ≤ 0.01 . SPSS software was used to model and determine the mathematical relationship of the population of captured spores with climatic factors. The three-day sum of the captured spores was related to the weather data three days before (total rainfall, maximum and minimum temperature average, maximum and minimum relative humidity and total sunny hours in three days).

Regression statistical analysis was performed for the relationship between climatic factors and disease severity. A stepwise regression analysis was conducted on weather parameters and sporangia and disease severity data collected daily starting April 8 and ending October 9 in 2014 and 2015. Additionally, linear model analyses were conducted using in-season climate variables as predictors.

3. RESULTS

3.1. Disease severity and dynamism of sporangia

Symptoms of disease were first observed on April 29, 2014 and April 21, 2015 with a severity of 1.03 and 0.5%,

respectively (Table 2). 10 leaves per plant were evaluated. The concentration of airborne sporangia differed significantly ($P < 0.05$) among months (May until October) and between years. Although based on the value of the Pearson's correlation coefficients (r), it has been shown that the dynamics of sporangia in the air in these monitoring years are similar in some respects (Table 3).

In the beginning of April 2014 and 2015, the daily concentration of *P. cubensis* sporangia increased slowly (Figure 1). In mid-May a rapid increase of daily sporangia density occurred. The highest spore density was observed on May 29, 2014 ($3025 \text{ sporangia}^{-3}$) and May 27, 2015 ($4528 \text{ sporangia}^{-3}$). After five weeks, the concentration of spores rapidly decreased (Table 2). On September 17, 2014 and September 1, 2015, the concentration of *P. cubensis* sporangia again increased and reached the highest value on August 1, 2014 and September 22, 2015 (Figure 1).

A three day average spore count peaks were recorded on May 26 and May 30 2014 and 2015 (Figure 1). The six days before these dates (time point to start infection), the average relative humidity of 59 and 54.5 %, maximum temperatures of 22.4 and 21.8 $^{\circ}\text{C}$, minimum temperatures 11.2 and 11.2 $^{\circ}\text{C}$, sun sum 8.6 and 6.6 h, wind speed of 17008 and 15005 m/s and rainfall 0.6 and 0.1 mm were recorded for 2014 and 2015 respectively (Table 2). The second period of high sporangia concentration occurred on Oct. 5 and Sep. 22 for 2014 and 2015 respectively, which could have been influenced by many features (Figure 1).

The diseases severity in the years 2014 and 2015 years were very similar, and a comparison between the two years showed almost similar climatic conditions in creating maximum spore (Table 2).

A series of Paired-samples t-tests conducted to compare all meteorological variables showed that was significantly associated with the number of sporangia during the years 2014- 2015. Similarly, there was a significant difference between the severity of the disease and the sporangia during the 2-year study period (Table 3).

In both years of study (2015-2014), the lowest and highest concentrations of sporangia at 0.5 m above the canopy were in the range of 198-310 sporangium^{-3} with a disease severity of 0.5-1.03% and 3025- 4528 sporangium^{-3} with a disease severity of 35%. (Complete data were not presented due to a large number of tables, but figure 1 shows the extent to which these numbers are somewhat consistent with the sporangia graph and the severity of the disease).

The Pearson's correlation coefficient showed no significant correlation between the spore concentration in the sampler and the climatic factors. In contrast, there was a significant relationship between the climatic factors (except total sunshine, wind speed and rain) and the disease

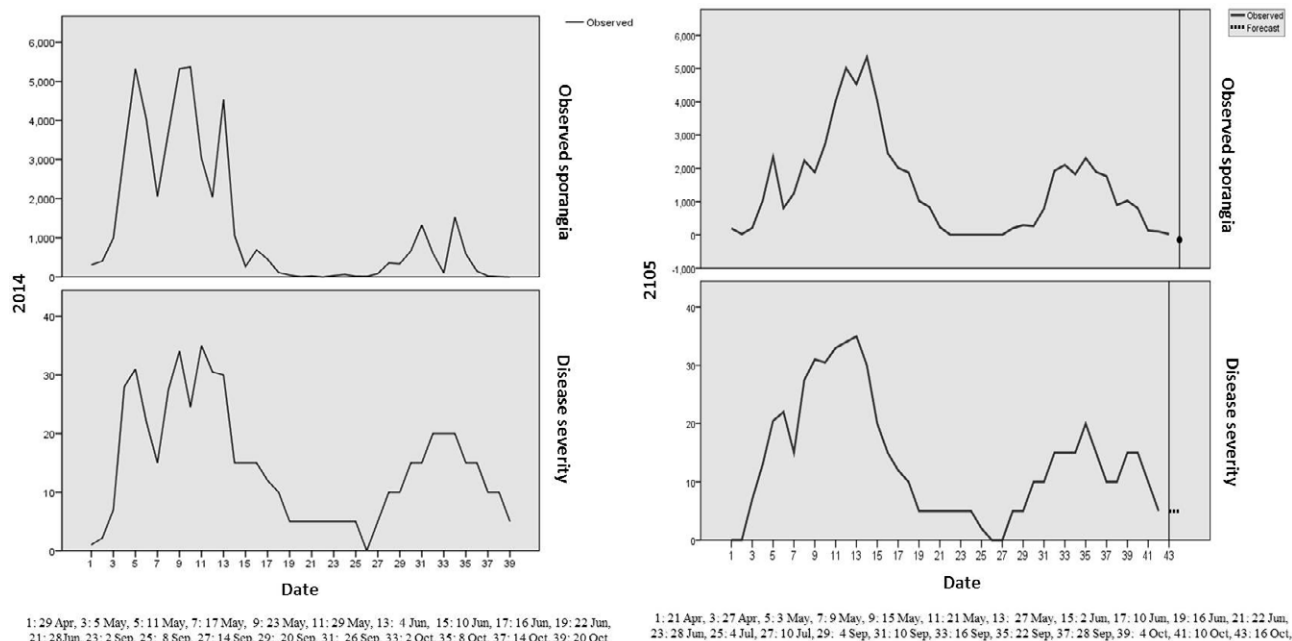


Fig. 1. Diurnal pattern of aerial concentration of *Pseudoperonospora cubensis* sporangia (m^3) above a cucumber canopy during downy mildew epidemics at Marand, North West, Iran. Curves are fitted by locally weighted regression to illustrate daily trends. Data are shown for disease assessment periods that represent the range of disease severity levels observed during 2014-2015.

Tab. 2. Standing crop of *Pseudoperonospora cubensis* sporangia escape and meteorological variables for the assessment periods in during the 2-year (2014-2015) study period.

	Date	Severity % ^a	No. of spores	RH ^b . max. (%)	RH. min. (%)	RH. av.(%)	T ^c . min. (°C)	T. max. (°C)	Sun(h)	Wind speed (m/s)	Rainfall (mm)
The first symptom	29 Apr. 2014	1.03	310	61	20	41	11	22.2	8.50	21009	0
	21 Apr. 2015	0.5	198	48	26	37	12.2	17.2	6.7	21027	0
Minimum disease severity	12 Sep. 2014	0.4	48	33	5	19	22.8	33.6	13.3	15009	0
	10 Jul. 2015	0.1	.00	35	12.00	23.5	25.8	37.6	12.7	16006	0
Maximum disease severity	20 May 2014	35	3025	71	47	59	11.2	22.4	8.6	17008	0.6
	24 May 2015	35	4528	74	35	54.5	11.2	21.8	6.6	15005	0.1

^a Disease severity was assessed visually as the percentage of leaf area infected on each date when sporangia were collected.

^b RH min, max and ave; maximum, minimum and average daily relative humidity

^c T. max. and min.; maximum and minimum daily temperature

severity. In both years, the same result has been achieved. (Table 4).

Based on the correlation results, the prediction of capacity of the climate parameters and combination of several parameters were evaluated. The sporangia density was calculated every three days for obtaining time-series models and to forecast the *P. cubensis* airborne sporangia on the cucumber plot (Figure 1). Figure 1 illustrates the observation and prediction of the *P. cubensis* sporangia by the adjusted model for each cucumber crop cycle. The

lines indicate the number of observed spores and the severity of the disease. Only in 2015, as shown in Figure 1, prediction time was determined based on the number of spores and the severity of the disease. In the figure, the sporangia dynamism are marked with the line and severity of the disease marked by dots.

The regression analysis of weather variables and disease severity data from April 8 to October 9 in 2014 and 2015 showed that linear regression was significant at $P < 0.01$. (Table 5).

Tab. 3. Paired-samples t-test to compare all meteorological variables and sporangia *Pseudoperonospora cubensis* and disease severity for the assessment periods in during the 2-year (2014-2015) study period.

		Paired Samples Test							t	df	Sig. (2-tailed)
		Paired Differences					95% Confidence Interval of the Difference				
		Year	Mean	Std. Deviation	Std. Error Mean	Lower		Upper			
Pair 1	Sporangium – RH ^a max.	2014	1191.22	1705.60	273.12	638.32	1744.11	4.36	38	.000	
		2015	1347.85	1450.95	221.26	901.31	1794.38	6.09	42	.000	
Pair 2	Sporangium – RH min.	2014	1218.99	1706.41	273.25	665.83	1772.15	4.46	38	.000	
		2015	1377.04	1454.43	221.79	929.48	1824.65	6.21	42	.000	
Pair 3	Sporangium – RH av.	2014	1205.11	1706.01	273.17	652.08	1758.13	4.41	38	.000	
		2015	1362.44	1452.68	221.53	915.37	1809.51	6.15	42	.000	
Pair 4	Sporangium – T ^b min.	2014	1237.92	1711.46	274.05	683.13	1792.72	4.58	38	.000	
		2015	1387.89	1455.26	221.92	940.02	1835.75	6.25	42	.000	
Pair 5	Sporangium – T max.	2014	1228.50	1710.96	273.97	673.86	1783.13	4.48	38	.000	
		2015	1379.28	1454.78	221.85	931.56	1826.99	6.22	42	.000	
Pair 6	Sporangium – SS ^c	2014	1243.21	1710.67	273.93	688.67	1797.751	4.54	38	.000	
		2015	1394.87	1453.85	221.71	947.44	1842.305	6.29	42	.000	
Pair 7	Sporangium - Wind	2014	-16317.72	9379.97	1501.99	-19358.36	-13277.09	-10.86	38	.000	
		2015	-16020.27	11045.71	1684.45	-19419.63	-12620.89	-9.51	42	.000	
Pair 8	Sporangium - Rain	2014	1251.39	1710.31	273.86	696.97	1805.80	4.56	38	.000	
		2015	1402.75	1454.19	221.76	955.22	1850.28	6.33	42	.000	
Pair 9	Sporangium – Disease severity	2014	1238.15	1701.99	272.53	686.43	1789.87	4.54	38	.000	
		2015	-1424.01	1446.51	223.20	-1874.76	-973.22	-6.38	41	.000	

^a Relative humidity, ^b Temperature, ^c Sunshine sum.

The statistical significance of regression equations was checked by F-test and the analysis of variance (ANOVA) for models was summarized in Table 6. Based on the 2014 model, with an increase in 1 sporangia unit and 1 mm of rainfall, the severity of the disease will increase by 0.72 (0.005 + 0.715). However, in the 2015 model, the same amount of sporangia unit and rainfall will increase the severity of the disease by 0.393 (0.006 + 0.195 + 0.192). A regression model was showing correlation between sporangium and severity (Figure 2).

4. DISCUSSION

Determination of environmental factors that affect the pathogenic contamination and sporulation allows the time of fungicide application to control the disease (Yang *et al.*, 2007).

This study showed *P. cubensis* sporangia to be present in the atmosphere throughout the two years, with their concentrations becoming higher during the mid and last stages of the crop growth. The number of sporangia in the

air decreases with warming and decreasing moisture in the summer.

The concentrations of the sporangia in the atmosphere were very low at the time of the crop emergence, as the growth and expansion of the plant's green areas prevent the rapid accumulation of inoculum. The sporangia often spread again on aging or dying leaves so that spore concentrations often peak in the mid-stage, when the leaves are drying out (Figure 1).

The current study found a significant positive correlation between climate factors and spore concentration. With the rise in the mean, maximum and minimum temperatures, the spore density in the air increases, this makes *P. cubensis* a temperature-dependent pathogen. In Marand (the site of the study), the most sporangia in the atmosphere were found when the minimum temperatures were over 11.2 °C and maximum temperatures fell between 21.8 and 22.4 °C. *P. cubensis* sporangia belong to parasitic species that germinate within the optimum temperatures of 10–20 °C (Cohen, 1977).

Maximum relative humidity during the study years (2014-2015) was 71-74%. Favorable conditions for the re-

Tab. 4. Pearson's correlation coefficients (r) between for the overall meteorological variables and sporangia *Pseudoperonospora cubensis* and disease severity in during the 2-year (2014-2015) study period.

2014 ¹ , 2015 ²		Sporangium	RH max.	RH min.	RH av.	T min.	T max.	SSS	Wind	Rain	Severity
Sporangium ¹	Pearson Correlation	1	.263	.227	.258	-.255	-.134	-.179	-.205	-.048	.828**
	Sig. (2-tailed)		.105	.165	.113	.117	.416	.275	.210	.771	.000
	N	39	39	39	39	39	39	39	39	39	39
Severity ¹	Pearson Correlation	.828**	.403*	.348*	.396*	-.329*	-.181	-.291	-.124	.211	1
	Sig. (2-tailed)	.000	.011	.030	.013	.041	.271	.073	.451	.198	
	N	39	39	39	39	39	39	39	39	39	39
Sporangium ²	Pearson Correlation	1	.179	-.053	.102	-.253	-.157	.011	-.130	-.038	.860**
	Sig. (2-tailed)		.252	.736	.514	.102	.313	.944	.405	.810	.000
	N	43	43	43	43	43	43	43	43	43	42
Severity ²	Pearson Correlation	.860**	.454**	.236	.409**	-.447**	-.376*	-.161	.05	.217	1
	Sig. (2-tailed)	.000	.003	.132	.007	.003	.016	.308	.977	.168	
	N	42	42	42	42	42	42	42	42	42	42

Tab. 5. Results of the analysis of variance (ANOVA) for the disease severity of cucumber downy mildew and weather variables.

Model		Sum of Squares	DF ^a	Mean Square	F	Sig.
2014	Regression	2761.558	2	1380.779	53.691	.000 ^b
	Residual	925.819	36	25.717		
	Total	3687.377	38			
2015	Regression	3510.438	3	1170.146	69.205	.000 ^c
	Residual	642.520	38	16.908		
	Total	4152.958	41			

^a Degrees of freedom; ^b Predictors: (Constant), Sporangium, Rain; ^c Predictors: Sporangium, RH av., Rain.

Tab. 6. The regression models analysis of weather variables and disease severity of cucumber downy mildew during 2014 and 2015.

Model		Unstandardized Coefficients		Standardized Coefficients	t	Sig.
		B	Std. Error	Beta		
2014	Constant	7.493	1.053		7.115	.000
	Sporangium	.005	.000	.840	10.051	.000
	Rain	.715	.238	.251	3.002	.005
2015	Sporangium	.006	.000	.833	12.879	.000
	RHav	.195	.059	.237	3.319	.002
	Rain	.192	.093	.147	2.075	.045

production and dissemination of the pathogen are warm temperatures (20–25°C) and high humidity (>85% RH) (Lebeda and Cohen, 2011), which are available during the growing season in many parts of East Azarbaijan, Iran.

The highest concentrations of *P. cubensis* sporangia in this study were recorded under these conditions.

The temperature and moisture conditions for the dispersal of *P. cubensis* sporangia in cucumber were observed. They were similar to those reported Neufeld *et al.*, (2013) and Naegele *et al.*, (2016).

Given the correlation between the climatic conditions and the spore levels, the observed pattern was similar during the two study periods. Aerobiological studies serve as an essential means of predicting the disease risk as they greatly contribute to the determination of the levels of inoculum (Neufeld *et al.* 2013).

Many aerobiological studies on the dispersion of plant pathogen have used daily measurements of the standing crop of spores on the study site as the measure of inoculum source strength (Aylor and Taylor, 1983; Aylor *et al.*, 2001, 2011; Andrade *et al.*, 2009). However, it is possible to base the disease management decisions on the assumed or actual identification of inoculum. In both regression models were presented, there was the correlation between percentage of disease severity and sporangia. This suggested the models could well predict disease severity of cucumber downy mildew. Linear logistic models are generally used in aerobiological studies to predict spore concentrations (Rodríguez-Rajo *et al.*, 2010).

The replication of this study by considering the relation of sporangia, rain and average humidity with the epidemic development could promote the development and/or improvement of the forecasters of cucumber downy mildew (CDM) disease in the East Azarbaijan.

This study was primarily aimed at generating data as a foundation for improving the CDM forecasting system that functions as a decision-making tool for controlling downy mildew. It more specifically focused on the data

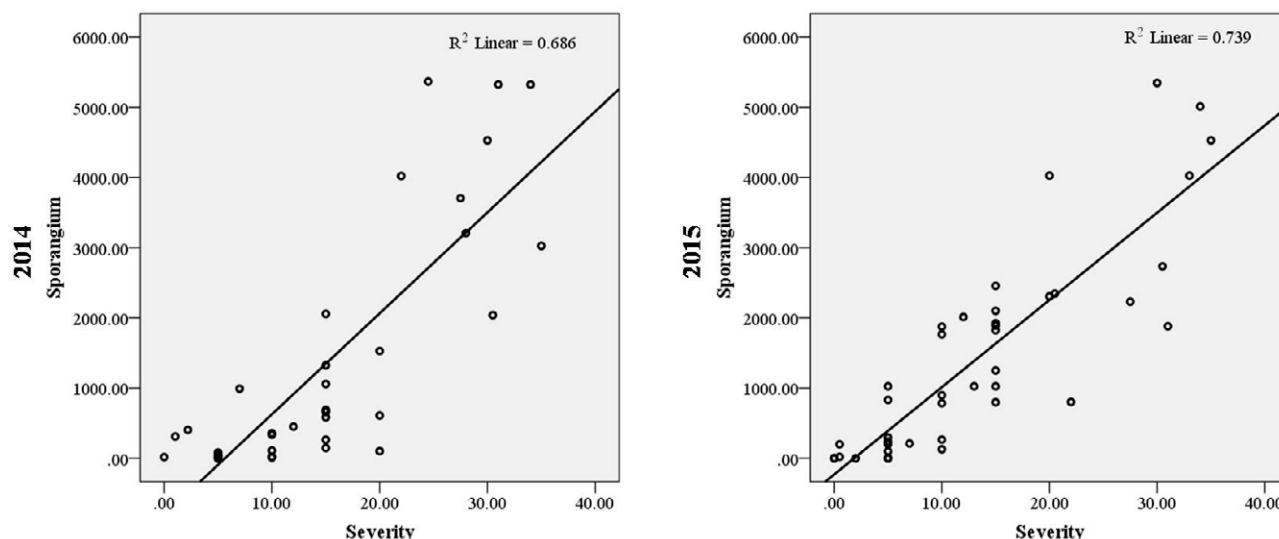


Fig. 2. Relationship between disease severity and sporangia due to downy mildew of cucumber during 2014 and 2015 in Iran- Marand.

that can be applied to adapt the aerial concentrations of sporangia and sporangia escape to the weather parameter along the projected pathways of sporangia transport and deposition for the risk prediction (Ojiambo *et al.*, 2011). This forecasting system has reportedly led to a reduction of fungicide applications used by growers.

In Iran, farmers often use plastic houses, glass houses and net houses to grow cucurbits. They are confronted with the devastating attacks of downy mildew, especially on cucumber in winter, and are forced to frequent use fungicide applications (Fani *et al.*, 2014, Pouzeshimiab and Fani, 2016). The relatively higher temperatures and humidity of these glass-covered houses in winter provides favorable conditions for the development of downy mildew, enabling the produced sporangia to stay inside and spread more infection.

ACKNOWLEDGEMENT

This Research was financially supported by the. Marand Branch, Islamic Azad University, Marand, Iran.

REFERENCES

- Andrade D., Pan Z., Dannevik W., Zidek J., 2009. Modeling soybean rust spore escape from infected canopies: model description and preliminary results. *Journal of Applied Meteorology and Climatology*, 48: 789–803.
- Aylor D.E., Fry W.E., Mayton H., Andrade-Piedra J.L., 2001. Quantifying the rate of release and escape of *Phytophthora infestans* sporangia from a potato canopy. *Phytopathology*, 91: 1189–1196.
- Aylor D.E., Schmale III D.G., Shields E.J., Newcomb M., Nappo C.J., 2011. Tracking the potato late blight pathogen in the atmosphere using unmanned aerial vehicles and Lagrangian modelling. *Agricultural and Forest Meteorology*, 151: 251–260.
- Aylor D.E., Taylor G.S., 1983. Escape of *Peronospora tabacina* spores from a field of disease tobacco plants. *Phytopathology*, 73: 525–529.
- Call A.D., Criswell A.D., Wehner T.C., Klosinska U., Kozik E.U., 2012. Screening Cucumber for Resistance to Downy Mildew Caused by *Pseudoperonospora cubensis* (Berk. and Curt.) Rostov. *Crop Science*, 52: 577–592.
- Cohen Y., 2015. The Novel Oomycide Oxathiapiprolin Inhibits All Stages in the Asexual Life Cycle of *Pseudoperonospora cubensis* - Causal Agent of Cucurbit Downy Mildew. *PLoS One*, 10(10), e0140015.
- Cohen Y., Eyal H., 1977. Growth and differentiation of sporangia and sporangiophores of *Pseudoperonospora cubensis* on cucumber cotyledons under various combinations of light and temperature. *Physiological Plant Pathology*, 10: 93–103
- Cohen Y., Perl M., Rotem J., 1971. The effect of darkness and moisture on sporulation of *Pseudoperonospora cubensis* in cucumbers. *Phytopathology*, 61: 594–595.
- Fani S.R., Moradi M., Esmailzadeh-Hosseini S.A., Dashtekian K., Sarpeleh A., 2014. Efficacy of Cyazofamid fungicide in the control of downy mildew of greenhouse cucumber. *Pesticides Plant Protection*

- Science, 1: 103-114.
- Gent D.H., Mahaffee W.F., McRoberts N., Pfender W.F., 2013. The use and role of predictive systems in disease management. *Annual Review of Phytopathology*, 51: 267–289.
- Gent D.H., Nelson M.E., Farnsworth J.L., Grove G.G., 2009. PCR detection of *Pseudoperonospora humuli* in air samples from hop yards. *Plant Pathology*, 58: 1081–1091
- Granke L.L., Hausbeck M.K., 2011. Dynamics of *Pseudoperonospora cubensis* sporangia in commercial cucurbit fields in Michigan. *Plant Disease*, 95: 1392–1400
- Granke L.L., Morrice J.J., Hausbeck M.K., 2014. Relationships between airborne *Pseudoperonospora cubensis* sporangia, environmental conditions, and cucumber downy mildew severity. *Plant Disease*, 98: 674–681
- Kanetis L., Holmes G.J., Ojiambo P.S., 2010. Survival of *Pseudoperonospora cubensis* sporangia exposed to solar radiation. *Plant Pathology*, 59: 313–323.
- Lacey M.E., West J.S. 2006. *The Air Spora: A manual for catching and identifying airborne biological particles*. Dordrecht, Springer, 163 pp.
- Lebeda A., Cohen Y., 2011. Cucurbit downy mildew (*Pseudoperonospora cubensis*) biology, ecology, epidemiology, host-pathogen interaction and control. *European Journal of Plant Pathology*, 129: 157–192.
- Neufeld K.N., Ojiambo P.S., 2012. Interactive effects of temperature and leaf wetness duration on sporangia germination and infection of cucurbit hosts by *Pseudoperonospora cubensis*. *Plant Disease*, 96: 345–353.
- Neufeld K.N., Isardb S.A., Ojiambo P.S., 2013. Relationship between disease severity and escape of *Pseudoperonospora cubensis* sporangia from a cucumber canopy during downy mildew epidemics. *Plant Pathology*, 62: 1366–1377.
- Naegele R.P., Quesada-Ocampo L.M., Kurjan J.D., Saude C., Hausbeck M.K., 2016. Regional and Temporal Population Structure of *Pseudoperonospora cubensis* in Michigan and Ontario. *Phytopathology*, 106: 372-379.
- Ojiambo P., Kanetis L., Holmes G., 2009. Forecasting long distance movement of *Pseudoperonospora cubensis* and the Cucurbit ipmPIPE. *Phytopathology*, 99: 171.
- Ojiambo P.S., Holmes G.J., 2011. Spatiotemporal spread of cucurbit downy mildew in the eastern United States. *Phytopathology*, 101: 451–461.
- Pouzeshimiyab B., Fani S.R., 2016. Evaluation of some current fungicides against downy mildew caused by *Pseudoperonospora cubensis* Rostovzev. on greenhouse cucumber. *Research Plant Pathology Journal*, 4: 1-12.
- Rodríguez-Rajo F.J., Jato V., Fernández-González M., Aira M.J., 2010. The use of aerobiological methods for forecasting *Botrytis* spore concentrations in a vineyard. *Grana*, 49: 56–65.
- Thomas C., Indaba T., Cohen Y., 1987. Physiological and specialization in *Pseudoperonospora cubensis*. *Phytopathology*, 77: 1621-1624.
- West J.S., Atkins S.D., Emberlin J., Fitt B.D.L., 2008. PCR to predict risk of airborne disease. *Trends in Microbiology*, 16: 380–387.
- Yang X., Li M., Zhang Z., Hou Y., 2007. Early warning model for cucumber downy mildew in unheated greenhouses. *New Zealand Journal of Agriculture Research*, 50: 1261–1268.



Citation: H. Piri Sahragard, M. Ajourlo, P. Karami (2020) Predicting impacts of future climate change on the distribution and ecological dimension of *Amygdalus scoparia* Spach. *Italian Journal of Agrometeorology* (2): 117-130. doi: 10.13128/ijam-845

Received: January 27, 2020

Accepted: May 17, 2020

Published: January 25, 2021

Copyright: © 2020 H. Piri Sahragard, M. Ajourlo, P. Karami. This is an open access, peer-reviewed article published by Firenze University Press (<http://www.fupress.com/ijam>) and distributed under the terms of the Creative Commons Attribution License, which permits unrestricted use, distribution, and reproduction in any medium, provided the original author and source are credited.

Data Availability Statement: All relevant data are within the paper and its Supporting Information files.

Competing Interests: The Author(s) declare(s) no conflict of interest.

Predicting impacts of future climate change on the distribution and ecological dimension of *Amygdalus scoparia* Spach

HOSSEIN PIRI SAHRAGARD^{1,*}, MAJID AJORLO², PEYMAN KARAMI³

¹ Assistant Professor, Rangeland and Watershed Management Department, Faculty of Soil and Water, University of Zabol, Zabol, Iran

² Associate Professor, Rangeland and Watershed Management Department, Faculty of Soil and Water, University of Zabol, Zabol, Iran

³ PhD candidate, Department of Environmental Sciences, Faculty of Natural Resources and Environment Sciences, Malayer University, Malayer, Iran

*Corresponding author. E-mail: hopyry@uoz.ac.ir

Abstract. This study aimed to predict the potential distribution of *Amygdalus scoparia* and the changes in its ecological dimension under climate change scenarios using MaxEnt model in Iran. Species presence data, current climate data and different scenarios of CCM4 in 2050 and 2070 were used. Fars Province boundary and whole area of Iran were considered as the modeling boundary and projection boundary, respectively. The predictive power of the model was within acceptable levels (AUC = 0.88). The Bio3, Bio15 and Bio4 variables had the greatest impact on predicting the potential distribution of *A. scoparia*. The highest percentage of potential niche of *A. scoparia* will occur in 2070 under RCP4.5 scenario (24.62%) in Fars Province. In Iran, however, the highest (22.57%) and lowest (16.77%) potential niche of *A. scoparia* belong to current and RCP8.5 scenarios in 2050. *Amygdalus scoparia* lacks specialization in Fars Province, but the breadth of its ecological niche will be decreased in future and its distribution will be limited in main mountain ranges, i.e., the Alborz in northern and the Zagros in western Iran.

Keywords. Climate Change, Potential Distribution, *Amygdalus scoparia*, MaxEnt, Ecological Niche.

1. INTRODUCTION

Wild almond (*Amygdalus scoparia*) is a distinct and well-known xerophyte species in mountainous areas of Irano-Turanian floristic region. Large areas of its stands are distributed over dry and hot mountains of central, eastern and western Iran, Turkey, Afghanistan, Turkmenistan, and western Pakistan (Mozaffarian, 2004). It is an upright broom-like shrub up to 3-4 m tall with non-angled branches. The trunks of well developed individuals can be as thick as an arm. In some localities, *A. scoparia* is the dominant element in the arid forest ecosystems. It occurs most commonly above 1200 m altitude. The most elevated

stands reach 2700 m (Browicz and Zohary, 1996). *A. scoparia* as a lithophyte plant grows on loose conglomerates and limestone cliffs, loose volcanic rocks, crevices in rock slopes and in clay and sandy soils in arid and semi-arid mountainous regions where soils are very poorly developed. It is highly drought tolerant and play valuable role in soil conservation, slopes stabilization and surface runoff reduction in arid mountainous areas (Tavakoli Neko *et al.*, 2012; Abbasi, 2017). Furthermore, it is a pioneer species that colonizes sites lacking developed soil and provide favorable conditions for establishment of other species through providing microclimate and coping with unfavorable conditions in rock debris and stony slopes (Morshedi and Koravand, 2016).

A. scoparia plays pivotal role in the livelihood of local communities in arid mountainous regions of Iran. Local people and rural villagers use its fruits, gum and also bark and root for medicinal purposes. Furthermore, twigs are used for making traditional homewares and handicrafts. Wooden beams are used to build house and support roof. Branches and boughs are cut for wood fuel usage. Charcoal production is a major utilization of wild almond by locals (Browicz and Zohary, 1996).

Degradation of habitats by anthropogenic and natural factors such as overutilization, grafting of cultivated almond on the wild almond, insects and diseases outbreak, climate change, drought and fire are endangering factors in *A. scoparia* habitats (Golestaneh *et al.*, 2012). Despite the tremendous importance of this species for the livelihood and survival of local communities and arid mountain forests health and production, overuse during last decades was serious threats to survival and regeneration of *A. scoparia* and has imposed intolerable pressure on habitats (Haidarian Aghakhani *et al.*, 2017). Moreover, outbreak of pathogenic agents such as *Wilsonomyces carpophilus* and *Biscogniauxia mediterranea* have brought about various diseases such as dieback and decline, shot hole, canker and etc. on wild almond (Mirabdollahi *et al.*, 2019). Therefore, with regard to the outstanding ecological and economic attributes of this species in arid forests, it is necessary to provide favorable conditions for sustainable exploitation of current habitats and planning to expand its distribution in areas that are potentially suitable for establishment. This can be achieved through the study of the effects of destructive human and natural causes such as climate change on it to conserve and improve the economic, social and ecological values of *A. scoparia* forests.

Climate change is one of the main drivers of plant ecosystems distribution. Changes in plant species distribution within a specific ecosystem is also affected by climate change (Pacific *et al.*, 2015). Climate change can

greatly impact biodiversity in ecosystems (Sintayehu, 2018). However, the effects of climate change on arid and semi-arid ecosystems are more severe than humid and semi-humid ecosystems (Grime *et al.*, 2008). Since displacement or alteration of species geographical distribution is one of the ways for resistance to climate change, understanding the impact of climate change on species potential distribution and mitigating its deleterious effects on biodiversity is necessary for management decisions (Pressey *et al.*, 2007). Plant species respond to climate change in a variety of ways such as adaptation, displacement in various directions and movement to higher elevation and latitude to find suitable climates. Local, regional, or global extinction is another response of plants to climate change (Parmesan and Hanley, 2015). Factors such as the genetic diversity of plant species, the ability to adapt to the magnitude of climate change, and the availability of space for species movement to other micro-climates can influence plant species responses to climate change (Loarie *et al.*, 2009). Because of these differences, plant species are not equally susceptible to climate change (Walther, 2010).

Recent conditions of climate change have taken the plants, particularly the rare ones, to the brink of extinction (Deb *et al.*, 2017). There is increasing evidence that species are changing their distribution as a result of environmental warming, particularly in montane ecosystems and that organisms living at high altitudes are particularly at risk because of their restricted climatic niches and specific adaptations (Bennett *et al.*, 2019). It has been reported that average air temperature will rise between 1.69 and 6.88 °C in Iran by 2100 and climate is getting warm across the country especially in spring and summer (Zarenistanak *et al.*, 2014). The effect of rising temperature on reducing current and potential distribution range of species has been reported in several studies (Vessella and Schirone, 2013; Al-Qaddi *et al.*, 2016; Tarkesh and Jetschke, 2016). For example, climate change has been reported as a major factor in the decline of desirable habitat of *Ferula xylorhachis* in northeastern Iran (Mazangi *et al.*, 2016). In a study by Sangoony *et al.* (2016) the optimal habitat size of *Bromus tomentellus* decreased by more than 51% in scenario 2080. Haidarian Aghakhani *et al.* (2017) reported a decrease of 43% and 59% in the area of *A. scoparia* habitat in Central Zagros Mountain, in Chaharmahal-e Bakhtiari Province, western Iran under RCP4.5 and RCP8.5 scenarios by 2050. Moreover, among the studies conducted from 2014 to 2018 on 37 species in Iran, about 81% of the studies indicated a decrease in the habitat size and distribution area of species due to climate change that reptiles followed by plants has shown highest declining rate (Yousefi *et al.*, 2019). Therefore, understanding the

potential impacts of climate change on species distribution to ameliorate its destructive effects on biodiversity is essential (Pressey *et al.*, 2007). Consequently, predicting the potential distributions of endangered species in future climates can provide useful insights into their responses to climate change.

The use of species distribution models (SDMs) to predict the impact of climate change on species distribution and ecological dimension has become common and an important tool for assessing the potential impacts of climate change on plant communities (Sinclair *et al.*, 2010). The SDMs correlate the climatic conditions associated with the species habitat to the observed presence areas of each species, which is consistent with Hutchinson's (1957) definition of species' environmental niche (Bellard *et al.*, 2016). In other words, ecological niche models try to simulate the climatic nesting of a species using environmental variables and mathematical algorithms and present it geographically on a map (Mckennedy *et al.*, 2007). The predictions made by these models provide the basis for conservation planning decisions, so these models are useful for important decisions in ecological issues (Guisan and Zimmermann, 2000; Upson *et al.*, 2016). In addition, General Circulation Models (GCM) have been developed as reliable and powerful tools to enhance understanding of climate change impacts and improve the ability to predict future climate patterns (Potta, 2004). The RCPs (Representative Concentration Pathways) are climate change scenarios that have been developed based on various input variables such as the amount of greenhouse gas emissions due to population growth and the economy of different countries, the level of used technologies, land use changes and environmental policies to be used in GCM models. The RCPs reflect the trends of different concentrations of greenhouse gases including carbon dioxide, vapor, nitrogen oxides, methane and ozone (Pachauri *et al.*, 2014).

Due to the value of *A. scoparia* forest in Iran, various studies have been carried out to recognize its ecological needs, to model its distribution and to predict the impact of climate change on its distribution in different parts of Iran (Salarian *et al.*, 2008; Goodarzi *et al.*, 2012; Tavakoli Neko *et al.*, 2012; Piri Sahragard *et al.*, 2017; Haidarian Aghakhani *et al.*, 2017). However, there is little information on how the size and extent of *A. scoparia* forests vary in facing of climate change. Therefore, this study aimed to predict the current potential distribution and the changes of potential ecological niche of *A. scoparia* under the climate change scenarios using MaxEnt model in Iran. Based on the literature review, this study is the first of its kind that models current and future distribution of *A. scoparia* under different climate scenarios across Iran.

2. MATERIALS AND METHODS

2.1 Study and projection areas

In this study, Fars Province boundary and whole area of Iran were considered as the modeling boundary and projection boundary, respectively (Fig. 1). Fars Province is located in southern part of the Zagros Mountains and in Irano-Turanian floristic region. The climate of Fars Province is semi-arid with average annual temperature and rainfall of 18 °C and 307 mm, respectively (Arvin and Shojaeezadeh, 2014). The average air temperature in the southern and northern parts of Iran ranges from 25 to 40 and 10 to 20 °C, respectively. Although there is considerable variation in temperature and precipitation across the country, the average annual precipitation is about 240 mm (Alizadeh, 2010).

2.2 Recording presence points of *A. scoparia*

First, pure habitats of *A. scoparia* were identified in Fars Province. Then, geographical coordinates of 200 presence points of *A. scoparia* were recorded using the GPS in 2017-2019 period. The presence points were identified by locating quadrats along four sampling lines (sample lines were perpendicular to each other) (Fig. 1). The distance between sample lines was 1000 m according to habitat conditions and vegetation changes. In order to avoid spatial autocorrelation, the presence points were considered one kilometer apart. So that, only one presence point was recorded in each 1 Km² network (Shrestha *et al.*, 2018). Quadrat size was determined 25 m² by the minimal area method according to species characteristics (Piri Sahragard *et al.*, 2017).

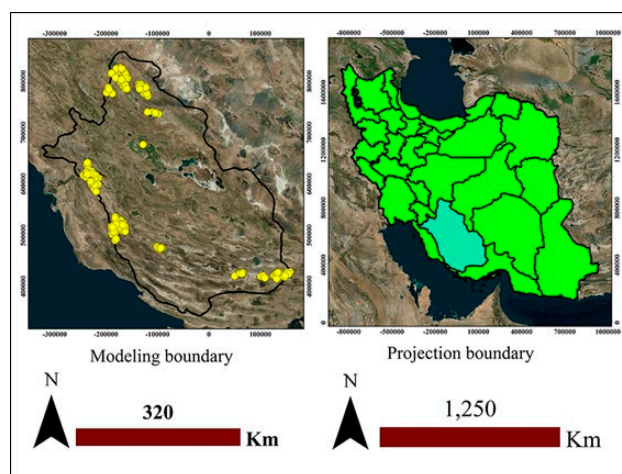


Fig. 1. Fars Province with the presence points of *Amygdalus scoparia* (left) and whole area of Iran (right).

2.3 Climate variables

The CCM4 model available in the Worldclim climate database was used for modeling of climate change (Hijmans *et al.*, 2005). In this model, there are four climate change scenarios from optimistic to pessimistic for 2050 and 2070. These scenarios include RCP2.5, RCP4.5, RCP6 and RCP8.5. Current climate data were used to estimate the current distribution area of *A. scoparia*. This information was obtained from the interpolation of the geographical position of all meteorological stations in 1950-2000 period. Before entering the input variables into the model, the correlation between them was calculated and the variables with high correlation (higher than 0.85) were not entered into the model. Table 1 shows climate variables used in the study along with their range of changes and measurement units. Due to the necessity of the variables being identical in all modeling scenarios, the same scenarios were used to generalize the modeling results.

2.4 Modeling current and future potential distribution and analyzing the importance of variables

Modeling the potential distribution of *A. scoparia* under current conditions and climatic scenarios of RCP2.6; RCP4.5; RCP6 and RCP 8.5 was performed for 2050 and 2070 using the MaxEnt model (Phillips *et al.*, 2006). In this study, 70% of the data were considered for training and 30% for test. The maximum iteration of the model run was assumed 1000 to achieve proper convergence. Model validation was performed using the area under the curve (AUC) of ROC function. The Jackknife test was used to determine the importance of environmental variables. This

Tab. 1. Variables, units and range of change in Fars Province.

Variable	Title	Range of change	Unit
Bio3	Isothermality (BIO2/BIO7)	32-43	Dimensionless
Bio4	Temperature Seasonality (Standard Deviation)	5784-9017	Degrees Celsius
Bio13	Precipitation of Wettest Month	27-86	Millimeters
Bio14	Precipitation of Driest Month	0-2	Millimeters
Bio15	Precipitation Seasonality (Coefficient of Variation)	79-126	Fraction
Bio17	Precipitation of Driest Quarter	0-17	Millimeters
Bio19	Precipitation of Coldest Quarter	66-201	Millimeters

method has acceptable accuracy for assessing the importance of variables (Verbyla and Litvaitis, 1989).

2.5 Selecting the threshold limit of species presence

The TSS statistic was used to determine the optimum threshold for presence of the species and to identify the point of distinction based on sensitivity (SE) and specificity (SP) values in R 3.1.1 software; then prediction map of presence-absence of species was prepared. The TSS statistic is one of the appropriate statistic to determine the optimum threshold of presence. Independency of the model sensitivity to species prevalence is main reason for choosing this method (Allouche *et al.*, 2006). For this purpose, 10,000 background absence points and presence points as well as the predicted value for these points were used. After applying the optimum threshold limit on species distribution map, calculations of changes in potential niche area of species were performed using ArcGIS 10.2 software. Assessment of threshold value for separation of presence and absence data including Correct classification, Misclassification, Sensitivity, Specificity, False positive rate and False negative rate was performed in SPSS 20 software.

2.6 Quantifying the dimensions of ecological niche

Statistical values of habitat overlap showing the extent of overlap between ecological niches as well as breadth of niches representing specialist and generalist were calculated in ENMtools 1.3 software. Overlap analysis of ecological niches was performed using two indices of Schoener's D (Schoener, 1968) and Hellinger's I (Warren *et al.*, 2008). Habitat overlap indices range from 0 to 1 (Mirshamsi, 2013) whose high values mean complete overlap and low values mean less overlap of ecological niches. Breadth index of ecological niche was measured with Levin's B1 and B2 (uncertainty) indices (Levin, 1968). The values for these indices also fluctuate between 0 and 1, with values close to zero meaning specialist and values close to 1 meaning generalist (Vorsino *et al.*, 2013).

3. RESULTS

3.1 Evaluating accuracy of the prediction models

As noted, the AUC was used to evaluate the accuracy of the prediction models. The AUC which is derived from the ROC diagram is a quantitative indicator for showing the performance and predictive power of the model. Vertical axis indicates the sensitivity (true positive) and the horizontal axis shows the specificity (false positive) in the

AUC curve. According to Swets (1988) classification (Appendix 1), the AUC values indicated acceptable accuracy of prediction models in training and test phases in this study (AUC = 0.88).

3.2 Analyzing the significance of climatic variables and response curves

Investigating the importance of variables using the Jackknife test showed that Bio3, Bio15 and Bio4 variables had the most effects on habitat distribution of *A. scoparia* (Fig. 2). The Bio19 had the least effect on the prediction model of species distribution. Interpretation of the response curves of *A. scoparia* to each of these variables showed that by increasing the value of Bio3 variable the suitability of the habitat is decreased and consequently the probability of species presence decrease. Accordingly, the highest rate of habitat suitability and thus the highest probability of occurrence for this species is in areas with isothermal value between 31 and 34. On the other hand, by increasing the Bio15 variable (seasonal precipitation coefficient) up to 85, the habitat suitability can increase and thus the probability of species presence increase. However, by increasing the value of this variable to over 85, habitat suitability and species probability decrease (Appendix 2). Investigating of the species response curve to change in Bio4 variable (seasonal temperature variations) also indicates that by increasing the value of this variable up to 6500 will increase habitat suitability and increase the probability of species presence. But a further increase in this value can reduce habitat suitability and thus reduce the likelihood of species presence probability.

3.3 Prediction map of potential and current distribution of species in Fars Province and Iran

Prediction map for potential distribution of *A. scoparia* in current scenario is presented in Fig. 3. On this map blue color states high probability and brown color

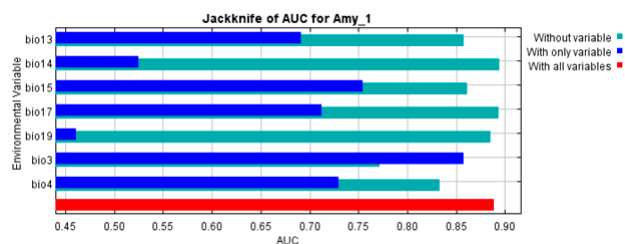


Fig. 2. Jackknife test results to determine the importance of environmental variables in *Amygdalus scoparia* habitats.

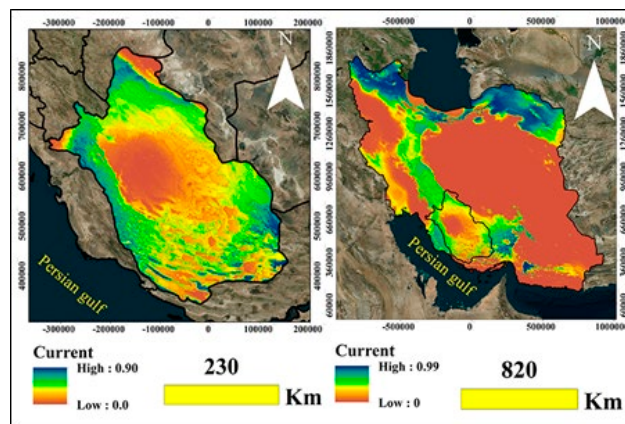


Fig. 3. Prediction map for potential distribution of *Amygdalus scoparia* in current scenario in Fars Province and Iran.

presents low probability. Accordingly, the most favorable areas for species presence in Fars Province are in the western, southeastern, and northern regions of the province (left map). Studying the potential distribution range of *A. scoparia* in Iran showed that the species has the ability to grow in northwest, north, northeast and along the Zagros Mountains to the north of Bandar Abbas City in southern Iran. In general, the northern parts of the country are more favorable for the establishment of the species, and the potential distribution of the species in this area is higher than in other parts of the country.

Examination of potential distribution changes of *A. scoparia* under climate scenarios of 2050 and 2070 showed that in central parts of Fars Province which are not suitable for the species at current scenario will have the potential for species presence in 2050 under RCP4.5 and RCP8.5 scenarios. In the case of RCP 8.5 scenario occurrence, parts of south-east, south and south-west of Fars Province that have high potential for species presence in RCP2.6 and RCP4.5 scenarios will face a decline in suitability and thus a decrease in potential for the species distribution. The 2070 map shows that under the RCP2.6, RCP6 and RCP8.5 scenarios, the central area of Fars Province is still unsuitable for species distribution. In the RCP4.5 scenario, large portions of the province will have potential for species presence, which is similar to the results for the RCP4.5 scenario in 2050 (Fig. 4). Modeling the potential distribution range of the species in Iran also showed that in 2050 under the RCP4.5 and RCP6 scenarios some parts of the south and south of the country will have potential for species presence. As temperatures rise in 2050 and move toward a pessimistic scenario, the range of species distribution will be reduced and the potential distribution of species will be limited to the western and north-western parts of the country. In 2070, by moving from an

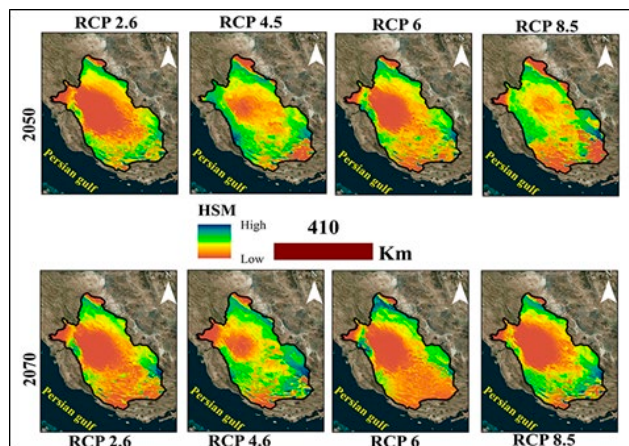


Fig. 4. Potential distribution of *Amygdalus scoparia* in different scenarios of 2050 and 2070 in Fars Province.

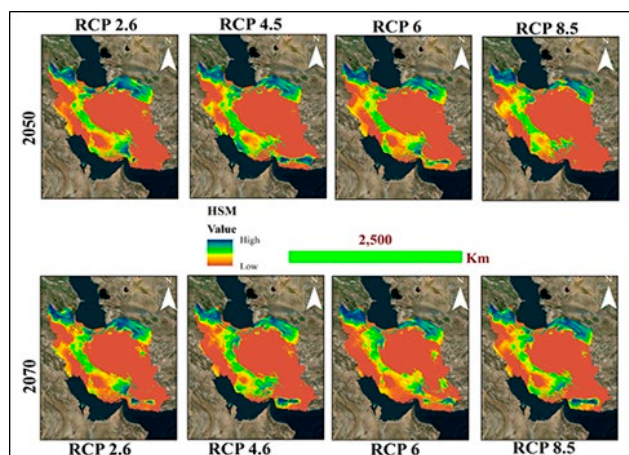


Fig. 5. Potential distribution of *Amygdalus scoparia* in different scenarios of 2050 and 2070 in Iran.

optimistic scenario to a pessimistic scenario the potential distribution range of the species will extend to eastern and southeastern regions of the country in addition to the western and northern parts (Fig. 5).

3.4 Dimensions of ecological niche of species

The results of investigating of niche breadth index in different scenarios showed that the highest niche breadth in Fars Province was at RCP4.5 scenario. This increase in niche width is line with the increase in the potential distribution of species (Fig. 6). The lowest niche breadth in Fars Province was related to the RCP6 scenario in 2070 (Table 2). In this scenario, large areas in the center of the province lack the potential for species presence, which has reduced the ecological niche breadth of the species. The

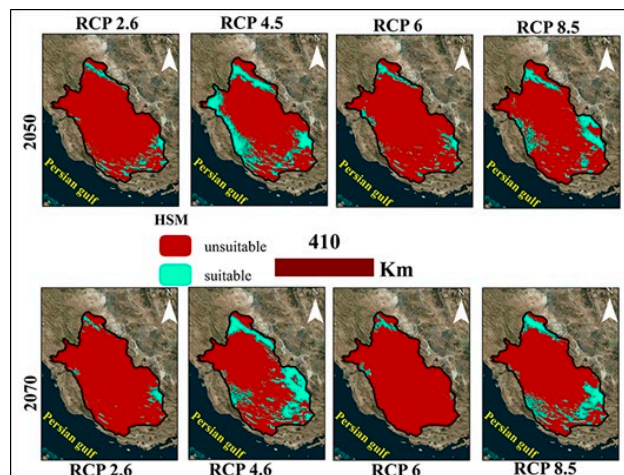


Fig. 6. Prediction binary map of potential climatic niche of *Amygdalus scoparia* under different scenarios in Fars Province.

Tab. 2. Breadth changes of *Amygdalus scoparia* niche based on relevant metrics used in climatic scenarios.

Scenario, Year	Fars Province		Iran	
	B1	B2	B1	B2
Rcp2.6, 2050	0.57	0.96	0.32	0.93
Rcp2.6, 2070	0.55	0.96	0.34	0.93
Rcp4.5, 2050	0.75	0.98	0.37	0.94
Rcp4.5, 2070	0.74	0.98	0.35	0.93
Rcp6, 2050	0.61	0.97	0.35	0.93
Rcp6, 2070	0.54	0.96	0.35	0.94
Rcp8.5, 2050	0.70	0.98	0.31	0.92
Rcp8.5, 2070	0.60	0.96	0.36	0.93
Current	0.71	0.98	0.35	0.93

results of the potential distribution range of the species in Iran showed that the highest and lowest extent of niches belong to the RCP4.5 and RCP8.5 scenarios, respectively, in 2050. This is in consistent with the potential distribution maps of the species in 2050.

The overlap rates of *A. scoparia* ecological niche based on I and D indices in Fars Province and Iran are presented in Tables 3-6. In Fars Province, the highest rate of niche overlap was 0.86 which calculated between RCP6, 2050 and RCP2.6, 2070 scenarios. The overlap value for the mentioned scenarios was 0.98 based on I index. The lowest value of niche overlap in Fars Province was calculated 0.63 for the scenarios of RCP8.5, 2050 and RCP2.6, 2050 (Appendix 3). The overlap value of these two scenarios was 0.84 based on I index (Appendix 4).

In Iran, over 50% overlap among all the scenarios was observed. The highest overlap of niches currently was with the RCP2.6 scenarios for 2050 and 2070. The lowest

Tab. 3. Overlap of ecological niches of *Amygdalus scoparia* based on D index in Iran.

Species	2.62050	2.62070	4.52050	4.52070	6.2050	6.2070	8.52050	8.52070	Current
2.62050	1	0.85	0.77	0.75	0.84	0.72	0.71	0.78	0.86
2.62070	x	1	0.80	0.79	0.87	0.78	0.75	0.81	0.85
4.52050	x	x	1	0.78	0.82	0.72	0.74	0.81	0.85
4.52070	x	x	x	1	0.82	0.77	0.76	0.84	0.77
6.2050	x	x	x	x	1	0.77	0.77	0.83	0.85
6.2070	x	x	x	x	x	1	0.72	0.77	0.72
8.52050	x	x	x	x	x	x	1	0.74	0.74
8.52070	x	x	x	x	x	x	x	1	0.77
Current	x	x	x	x	x	x	x	x	1

Tab. 4. Overlap of ecological niches of *Amygdalus scoparia* based on I index in Iran.

Species	2.62050	2.62070	4.52050	4.52070	6.2050	6.2070	8.52050	8.52070	Current
2.62050	1	0.95	0.91	0.89	0.94	0.87	0.87	0.91	0.96
2.62070	x	1	0.93	0.93	0.96	0.91	0.90	0.94	0.95
4.52050	x	x	1	0.91	0.94	0.87	0.90	0.92	0.96
4.52070	x	x	x	1	0.94	0.91	0.91	0.95	0.90
6.2050	x	x	x	x	1	0.90	0.91	0.95	0.95
6.2070	x	x	x	x	x	1	0.86	0.92	0.87
8.52050	x	x	x	x	x	x	1	0.89	0.90
8.52070	x	x	x	x	x	x	x	1	0.91
Current	x	x	x	x	x	x	x	x	1

overlap with an index value of 0.71 was found between the RCP2.6, 2050 and RCP8.5, 2050 scenarios (Tables 3 and 4). According to the results of I index, the highest overlap of ecological nests was 0.96 which related to the RCP2.62070, RCP6 2050, RCP4.52050 and current scenarios. According to this index, the lowest value of overlap between the different scenarios was 0.87 (Appendix 5).

3.5 Selecting the optimal threshold and evaluating the accuracy of prediction models

The appropriate threshold value was calculated 0.51 based on TSS statistic. Then, the accuracy of the classification of presence and absence data was evaluated with regard to threshold value by the statistic presented in Tab. 5. This indicates that resulting threshold had suitable discriminatory ability to distinguish presence and absence of species in the classification of species presence and absence. Because by considering optimum threshold of 0.51, the model’s ability to detect species presence and absence was greater than 0.80. In other words, the prediction model was able to correctly predict 85% of species presence (Sensitivity = 0.85). Species absence was predicted with an

Tab. 5. Statistic of evaluating the accuracy of prediction model after applying threshold value.

Statistic	Value	Lower bound (95%)	Upper bound (95%)
Correct classification	0.83	0.82	0.83
Misclassification	0.16	0.16	0.17
Sensitivity	0.85	0.79	0.89
Specificity	0.83	0.82	0.83
False positive rate	0.17	0.16	0.17
False negative rate	0.15	0.10	0.19

accuracy of 0.83 (Specificity = 0.83). In total, 83% of the used points were classified correctly. Misclassification of the presence and absence points was 16%.

3.6 Final maps of species potential distribution in different climatic scenarios

In Fars Province, large portions of the province were identified unsuitable by applying threshold limit derived from the RCP2.6 scenario in 2050. In this scenario, a lim-

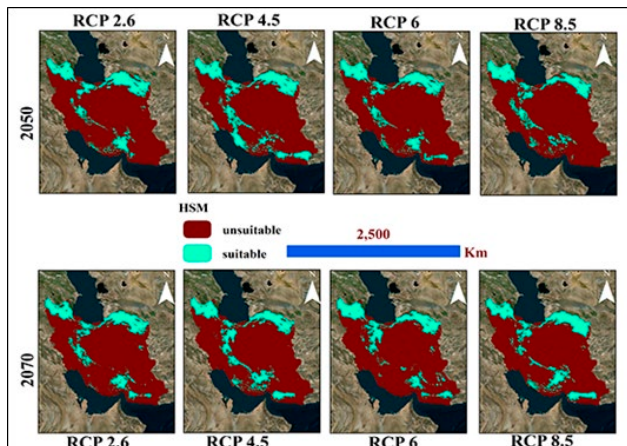


Fig. 7. Prediction binary map of potential climatic niche of *Amygdalus scoparia* under different scenarios in Iran.

ited portion (4.41%) of the province will have the potential to accept the species (4.41%). The highest area (23.33%) of the province that have the potential to accept the species in 2050 belongs to the RCP4.5 scenario. The results of the applying scenarios in 2070 also largely coincided with 2050. The largest area of the species potential habitat in 2070 will be under the RCP4.5 scenario (24.62%) in the province (Fig. 6). In whole country of Iran, the highest extent (22.57%) of habitat occupation will occur in 2050 under the RCP4.5 scenario. In 2050, in addition to northern parts of Iran, the south and southwestern parts of the country around Khuzestan Province will potentially have a species presence. But in later scenarios, the potential distribution of the species will be reduced. The lowest extent of potential distribution in 2050 will occur under the RCP8.5 scenario (16.77%) (Fig. 7).

Table 6 shows the changes in the area of desirable habitats under species occupation in different scenarios along with the occupancy rate. In the scale of Iran, the largest area that can be potentially occupied by species is related to the current scenario (22.5%). The lowest potential occupation will occur in the RCP8.5 scenario in 2050 in Iran.

4. DISCUSSION

Climatic variables are the most important controller of species distribution (Guisan and Zimmermann, 2000) in terrestrial ecosystems. They have a direct influence on the behavior and physiology of plants. Temperature is the most important driver among the climatic factors in species distribution, in particular. They can largely affect the plants, as they cannot evade adverse climatic conditions by sheltering or migrating (Hirzel and Le Lay, 2008). In

Tab. 6. Changes in the area of desirable habitats of *Amygdalus scoparia* under different scenarios in Fars Province and Iran.

Scenario	Area in Fars Province (Km ²)	% of occupation	Area in Iran (Km ²)	% of occupation
2.62050	10374.50	8.44	297702.01	18.34
2.62070	5423.58	4.41	298744.30	18.44
4.52050	28652.21	23.33	365594.15	22.57
4.52070	30234.71	24.62	323839.93	19.99
62050	10138.52	8.25	302383.39	18.67
62070	2986.27	2.43	300007.54	18.52
8.52050	18756.17	15.27	271112.44	16.73
8.52070	21316.22	17.36	331563.08	20.47
Current	21266.31	17.32	365303.01	22.55

other words, the spatial distribution of each plant species depends on its range of tolerance to climatic factors, ecological niche, and its biological interactions (Pearman et al., 2008). A decrease in the area of a species habitat due to climate change is one of the factors that can affect species survival in ecosystem (Lavergne et al., 2006; Becerra-López et al., 2017). In fact, due to the species' need for moisture and temperature, climate change can affect the geographical range of species distribution. In this study, the potential impacts of climate change on the potential distribution of *A. scoparia* and its ecological dimensions in Fars Province and Iran were investigated using the MaxEnt model for the first time.

Model accuracy evaluation with the AUC statistic indicated acceptable performance of the prediction model (AUC = 0.88). It has been reported that the value of AUC statistic in the MaxEnt model is mostly affected by the extent of ecological niche of plant species. The prediction performance of the MaxEnt model is excellent for species with small ecological niches (Zare Chahouki and Piri Sahragard, 2016). As discussed before, *A. scoparia* has tiny ecological niche. Numerous studies have reported that the MaxEnt is a suitable method for modeling plant species distribution due to its special features such as high prediction performance with low sample size (Pearson, 2007), lack of over-fitting (when wrong prediction of absence is zero and there are no in overestimation error or error in presence prediction) (Williams, 1995; Tibshirani, 1996), being generative and productive and ease of use by experts and users (Phillips et al., 2006). Because of these capabilities, the successful application of this method in modeling species geographical distribution, tolerance of species to environmental variables, conservation of species niche, identifying areas for conservation priority and logical estimation of species niche even with low sample

size have been reported (Suárez-Mota et al., 2016; Antún- ez et al., 2018).

The largest potential habitats of *A. scoparia* are located in the eastern, southeastern, western and northern parts in Fars Province at the present time. Large parts of Iran including northwest, north and north-east are potentially capable to support the species. It has the ability to settle in these areas provided other conditions to be favorable. Overall, the northern parts of Iran are more favorable for the establishment of the species especially in terms of climatic conditions. This part of the country is more likely to be occupied by *A. scoparia* than other parts. Currently, total area of *A. scoparia* habitats in Fars Province and Iran is 21266.31 km² (17.32% of the province total area) and 365303.01 km² (22.55% of the country total area), respectively.

Analysis of relative importance of *A. scoparia* habitat's variables showed that the Bio3, Bio4 and Bio15 variables had the most influence on species distribution and habitat suitability determination. These variables can provide useful information on the habitat distribution of this species; whereas the Bio19 variable had the least effect in this respect. Therefore, model run only with this variable is not useful for estimating the distribution of the species under study. The most suitable habitat and thus high probability of species presence are in areas where the Bio3 variable (isothermal) is about 31 to 34 °C, Bio15 variable (seasonal rainfall) with coefficient of variation between 80 and 90; and the Bio4 variable (seasonal temperature) with standard deviation between 6000 and 7000. Any increase in the values of these variables to higher amount will result in lower habitat suitability and thus lower probability of species presence in these areas. Annual temperature and rainfall have been reported as important variables affecting the occurrence of *A. scoparia*. This species is more likely to occur in areas with temperatures of 24 to 26 °C and annual rainfall of 400 to 600 mm (Haiydariyan Aghakhani *et al.*, 2017). In total, isothermal, seasonal rainfall and seasonal temperature variables accounted for a significant percentage of changes in species distribution, and have the highest contribution in determining habitat suitability for *A. scoparia*.

The use of overlap and ecological niche breadth indices provides complete insight into the status of plant species (Wan et al., 2017). In the modeling process, the use of niche measurement indices enables researchers to judge about the ecological niche of a species based on the input variables to the model (Suárez-Mota et al., 2015). If the species ecological niche is large, it can be considered equivalent to the suitable conditions based on the variables used. The value represented by the metrics used indicates the degree of overlap that has been happened with regard to the variables used in modeling. Considering the climatic

variables used in Fars Province based on niche breadth criteria, the highest niche breadth was in the RCP4.5 scenario in 2050, which is consistent with the findings from the distribution area. The highest niche size of the species was in the RCP4.5 scenario of 2070, which is justified by findings for distribution area. The highest niche overlap of species was observed between RCP2.6 in 2070 and RCP6 in 2050 according to D and I indices in Fars Province. Because 86% of habitats in these period are considered as common. In Fars Province, ecological niches overlap was greater than 50% in most of the studied scenarios. This indicates that with the change in temperature in different scenarios, the occupation of the new area will be accompanied by including of the old areas. On the scale of Iran, results indicated the same situation. Consequently, most climate nests of *A. scoparia* will be located in areas that has been previously occupied by other scenarios in future climate change scenarios.

Modeling of current and future potential distribution of *A. scoparia* showed that some parts at the center of Fars Province that do not currently occupied by the species will have potential suitability under the RCP4.5 and RCP8.5 scenarios in 2050. By 2070, a large proportion of the province will have a potential for species presence (24.62%) in the RCP4.5 scenario in 2050. Due to the limited range of climatic factors affecting the habitat suitability of the species resulting narrow niches of *A. scoparia*, high fluctuations of the effective climatic variables can lead to loss of potential habitat suitability. It has been reported that failure to adapt to the prevailing environmental conditions in an area and thus having limited habitat can ultimately lead to species extinction (Pressey, 2007). It should be noted that fluctuations in climate variables can even affect the suitability of habitats where species are currently available.

Although the generation of binary maps from continuous probabilistic maps has been criticized due to some limitations in evaluating the accuracy of probabilities predicted by the model (Vaughan and Ormerod, 2005; Freeman and Moisen, 2008), these maps can be used to evaluate the predictive validity of the model as well as in practical projects (Jimenez-Valverde and Lobo, 2007). According to the binary maps of suitability, the highest habitat area for occupation of species will be occurred under the RCP4.5 scenario in 2050 and 2070 in Fars Province (23.33 and 24.62% of the province total area), respectively. In the scale of Iran, the highest and lowest areas that potentially can be occupied by species was allocated to the current and the RCP8.5 scenarios, in 2050, respectively. In other words, the species have the largest potential habitats in current climatic conditions. The current potential distribution range of the species is limited to the northeast, northwest and western regions (around the Zagros Mountains) in Iran. Results of

species distribution changes in 2050 showed that under the RCP2.6 scenario the extent of habitat of the species will expand to the south of the country due to favorable climatic conditions, and species distribution range will decrease by moving to pessimistic scenarios. With the use of pessimistic climate scenarios, the areas in the southeastern part of the country will have high potential for species distribution due to favorable climatic conditions by 2070. Our results revealed that the trend of potential niche changes in *A. scoparia* will not be linear with the change in scenarios of temperature rise. Consistent with the findings of this study, the expansion of potential areas for species establishment under the influence of RCP and RCP8.5 climate scenarios in the western Himalayas has been reported by Thapa *et al.* (2018). In fact, with increasing temperature and stress to plants, their ability to survive in drier, warmer and minimum conditions of its favorable distribution range will decrease (Allen and Breshears, 1998). Therefore, organizing strategies for the conservation and restoration of forest ecosystems under short and long terms neither guarantee species survival nor distribution (Antúnez *et al.*, 2018). Given the adverse ecosystem conditions in arid forests of the Fars Province and the unique habitat conditions of *A. scoparia*, these issues should be considered by planners and authorities in the conservation, exploitation, and development programs.

In general, it seems that the central regions of Fars Province are not suitable for the presence of species due to lower altitude and consequently higher temperatures even under different climatic scenarios. In eastern, southeastern, western and northern parts of Fars Province suitable climatic conditions and other environmental factors such as elevation, physiographic and soil characteristics meet the ecological needs of the species, thus have more potential for species establishment. It has been reported that climate change can affect the spatial distribution of species through expansion of suitable potential habitats toward highlands (Thuiller, 2007; Bellard *et al.*, 2013). In addition to climate change, other factors such as infrastructure development, human intervention and land use change can also lead to species migration to higher altitudes (Shrestha *et al.*, 2018). In the case of *A. scoparia*, the results of previous studies indicate that in addition to climatic factors, altitude, physiographic characteristics, soil physical characteristics such as sand percentage and type of geological formation are the most important factors in limiting the presence of *A. scoparia* (Salarian *et al.*, 2008; Tavakoli Neko *et al.*, 2012). For example, the highest probability of *A. scoparia* presence in different parts of Iran is at an altitude of 1500 to 2150 m above msl and the presence of species outside this elevation range is severely restricted (Tavakoli Neko *et al.*, 2012).

5. CONCLUSIONS

Local authorities have started a rehabilitation and conservation program to recover degraded habitats and relicts of *A. scoparia* stands in Fars Province, Iran. They aim to extend the area of current habitats to larger size. Understanding potential impact of climate change on current and potential distribution areas of *A. scoparia* is major requirements to implement rehabilitation and conservation practices in the habitats. The findings of this research provide significant implications for the understanding of how and to what extent the spatial distribution of *A. scoparia* affected by the variations of environmental and climatic variables.

Our study showed that most of the potential habitats of *A. scoparia* in Fars Province and Iran belong to current scenario. However, in some areas potential habitat expansion or contraction will occur in future climate scenarios in both Fars Province and Iran. The relationship between temperature rise in climate scenarios and the spread of species ecological niches is not linear. Clearly, an increase in the area of potential habitats with favorable climatic conditions will expand habitats of this species in the future. Following the expansion of *A. scoparia* habitats in Fars Province and Iran in future, sustainable forest ecosystems in these areas will be provided in addition to reduction in soil erosion and land degradation. However, it should be noted that the presence of a plant species in an area is resultant of numerous environmental variables including soil, geological formations, land use, ecological demands of the species and etc. Therefore, these variables along with climatic variables must be considered in identification of potential desirable areas for the establishment of the species.

Various actions must be undertaken by the local authorities to promote the conservation of *A. scoparia* in Fars Province as well as Iran. Enhancing the position of local communities and utilizer groups in conservation of habitats, creating alternative livelihoods for utilizer groups to provide sustainable income for them and reduce their forest dependency, development of ecotourism in wild almond forest in order to introduce the importance of such species to the people, introducing modern utilization methods to the utilizer groups, manual seeding of wild almond seeds in degraded habitats to enhance its natural regeneration, and finally prohibit of grafting domestic almond on the rootstocks and twigs of wild almonds by farmers and utilizers are some actions that we recommend to be implemented by the local authorities.

ACKNOWLEDGMENTS

This research was supported by the University of Zabol, Iran through project UOZ-PR-97-8. Authors would

like to express their gratitude to Vice-chancellery for Research and Technology, University of Zabol for funding this project.

REFERENCES

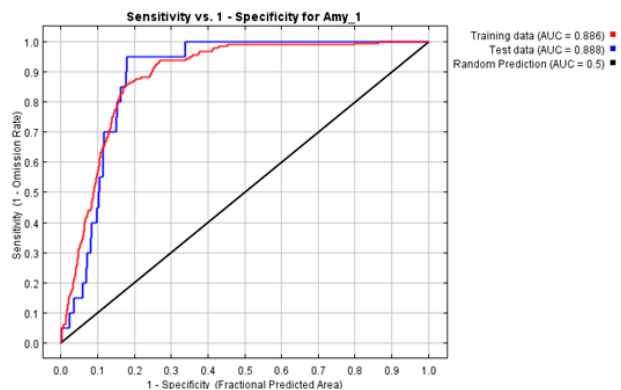
- Abbasi S., 2017. Persian gum: a novel natural hydrocolloid. *Nutrition and Food Sciences Research*, 4, 1–2.
- Alizadeh A., 2010. *Principals of applied hydrology*. 29th edition, University of Imam Reza Press, Iran, 912p.
- Allen C.D., Breshears D.D., 1998. Drought-induced shift of a forest-woodland ecotone: rapid landscape response to climate variation. *Proceedings of the National Academy of Sciences of the United States of America*, 95, 14839–14842.
- Allouche O., Tsoar A., Kadmon R., 2006. Assessing the accuracy of species distribution models: prevalence, kappa and the true skill statistic (TSS). *Journal of Applied Ecology*, 43, 1223–1232.
- Al-Qaddi N., Vessella F., Stephan J., Al-Eisawi D., Schirone B., 2016. Current and future suitability areas of kermes oak (*Quercus coccifera* L.) in the Levant under climate change. *Regional Environmental Change*, 17, 143–156.
- Antúnez P., Suárez-Mota M.E., Valenzuela-Encinas, C., Ruiz-Aquino F., 2018. The potential distribution of tree species in three periods of time under a climate change scenario. *Forests*, 9, 628.
- Arvin A., Shojaezadeh K., 2014. Assessment of climate tourism in Shiraz city using physiologic equivalence temperature and predicted mean vote indexes. *Journal of Physical Geography*, 7, 87–98.
- Becerra-López J.L., Bautista A. R., Méndez U.R., Pavón N.P., Rojas G.S., 2017. Effect of climate change on halophytic grasslands loss and its impact in the viability of *Gopherus flavomarginatus*. *Nature Conservation*, 21, 39–55.
- Bellard C., Cassey P., Blackburn T.M., 2016. Alien species as a driver of recent extinctions. *Biology Letters*, 12, 20150623.
- Bellard C., Thuiller W., Leroy B., Genovesi P., Bakkenes M., Courchamp F., (2013). Will climate change promote future invasions? *Global Change Biology*, 19, 3740–3748.
- Bennett M., Marquet P.A., Sillero-Zubiri C., Marino J., 2019. Shifts in habitat suitability and the conservation status of the Endangered Andean cat *Leopardus jacobita* under climate change scenarios. *Oryx*, 53(2), 356–367.
- Browicz K., Zohary D., 1996. The genus *Amygdalus* L. (Rosaceae): Species relationships, distribution and evolution under domestication. *Genetic Resources and Crop Evolution*, 43, 229–247.
- Deb C.R., Jamir N.S., Kikon Z.P., 2017. Distribution prediction model of a rare Orchid species (*Vanda bicolor* Griff.) using small sample size. *American Journal of Plant Sciences*, 8 (06), 1388.
- Freeman E.A., Moisen G.G., 2008. A comparison of the performance of threshold criteria for binary classification in terms of predicted prevalence and kappa. *Ecological Modelling*, 217, 48–58.
- Golestaneh S.R., Karampour F., Farrar N., 2012. Introduction of the destructive agents affecting wild almond *Amygdalus scoparia* forests in Koh-Siah Dashti area in Bushehr Province. *Forest and Range Protection Research*, 10, 153–164.
- Goodarzi Gh.R., Sagheb-Talebi Kh., Ahmadloo F., 2012. The study of effective factors on Almond (*Amygdalus scoparia* Spach.) distribution in Markazi Province. *Iranian Journal of Forest*, 4, 209–220.
- Grime J.P., Fridley J.D., Askew A.P., Thompson K., Hodgson J.G., Bennett R., 2008. Long-term resistance to simulated climate change in an infertile grassland. *Proceedings of the National Academy of Sciences*, 105, 10028–10032.
- Guisan A., Zimmermann N.E., 2000. Predictive habitat distribution models in ecology. *Ecological Modelling*, 135, 147–186.
- Haidarian Aghakhani M., Tamartash R., Jafarian Z., Tarkesh Esfahani M., Tatian M.R., 2017. Forecasts of climate change effects on *Amygdalus scoparia* potential distribution by using ensemble modeling in Central Zagros. *Journal of RS & GIS for Natural Resources*, 8, 1–14. (In Persian).
- Hijmans R.J., Cameron S. E., Parra J.L., Jones P.G., Jarvis A., 2005. Very high resolution interpolated climate surfaces for global land areas. *International Journal of Climatology*, 25, 1965–1978.
- Hirzel A.H., Le Lay G., 2008. Habitat suitability modeling and niche theory. *Journal of Applied Ecology*, 45, 1372–1381.
- Hutchinson G.E., 1957. Population studies – animal ecology and demography – concluding remarks. *Cold Spring Harbor Symposia on Quantitative Biology*, 22, 415–427.
- Jimenez-Valverde A., Lobo J.M., 2007. Threshold criteria for conversion of probability of species presence to either-or presence-absence. *Acta Oecologica*, 31, 361–369.
- Lavergne S., Molina J., Debussche M., 2006. Fingerprints of environmental change on the rare Mediterranean flora: a 115-year study. *Global Change Biology*, 12, 1466–1478.

- Levin R., 1968. Evolution in Changing Environments: Some Theoretical Explorations, Monographs in Population Biology. Princeton University Press, USA, 120 pp.
- Loarie S.R., Duffy P.B., Hamilton H., Asner G.P., Field C.B., Ackerly D.D., 2009. The velocity of climate change. *Nature*, 462 (7276), 1052±5.
- McKenney D.W., Pedlar J.H., Lawrence K., Campbell K., Hutchinson M.F., 2007. Potential impacts of climate change on the distribution of North American trees. *BioScience*, 57, 939–948.
- Mazangi A., Ejtehadi H., Mirshamsi O., Ghassemzade, F., Hosseinian yousefkhani S.S., 2016. Effects of climate change on the distribution of endemic *Ferula xylorhachis* Rech.f. (Apiaceae: Scandiceae) in Iran: predictions from ecological niche models, *Russ. Journal of Ecology*, 47(4), 349–354.
- Mirabdollahi Shamsi M., Akbarinia M., Mirabolfathy M., Manzari Sh., Ahmadikhah A., 2019. Dieback and decline of wild almond (*Amygdalus scoparia* Spach) in the Harat protected forest of Yazd Province, Iran. *Forest Pathology*, DOI: 10.1111/efp.12538
- Mirshamsi O., 2013. Ecological niche modeling of two scorpion species *Mesobuthus eupeus* (C. L. Koch, 1839) and *M. Phillipsii* (Pocock, 1889) from the Iranian Plateau and Zagros region (Arachnida: Scorpi-ones). *Euscorpius*, 15, 1–10.
- Morshedi J., Koravand E., 2016. Site selection for *Amygdalus scoparia* implant using GIS techniques and AHP methods In Mordghafar Watershed, Izeh Township. *Wetland Ecobiology*, 7 (4), 69-86.
- Mozaffarian V., 2004. Trees and shrubs of Iran. Contemporary culture publications, Iran, 671 pp.
- Pachauri R.K., Allen M.R., Barros V., Broome J., Cramer W., Christ R., Church J., Clarke L., Dahe Q., Dasgupta P., 2014. Climate change 2014: synthesis Report. Contribution of working groups I, II and III to the fifth assessment report of the intergovernmental panel on climate change, IPCC, 153 pp.
- Parmesan C., Hanley M.E., 2015. Plants and climate change: complexities and surprises. *Annals of Botany*, 116, 849±64.
- Pearman P.B., Guisan A., Broennimann O., Randin C.F., 2008. Niche dynamics in space and time. *Trends in Ecology and Evolution*, 23, 149–158.
- Phillips S., Robert P., Anderso C., Robert E., 2006. Maximum entropy modeling of species geographic distribution. *Ecological Modeling*, 190, 231–259.
- Piri Sahragard H., Zare Chahouki M. A., Ajorlo M., Nohtani M., 2017. Predictive habitat distribution modeling of *Amygdalus scoparia* Spach in Moshakieh rangelands of Qom Province. *Journal of Forestry and Wood Products*, 69, 725–734.
- Potta S., 2004. Application of Stochastic Downscaling Techniques to Global Climate Model Data for Regional Climate Prediction, MSc Thesis, Louisiana State University, 153 pp.
- Pressey R.L., Cabeza M., Watts M.E., Cowling R.M., Wilson K.A., 2007. Conservation planning in a changing world. *Trends in Ecology and Evolution*, 22, 583–592.
- Sangoony H., Vahabi M., Tarkesh M., Soltani S., 2016. Range shift of *Bromus tomentellus* Boiss as a reaction to climate change in Central Zagros, Iran. *Applied Ecology and Environment Research*, 14, 85-100.
- Salarian A., Mataji A., Iranmanesh Y., 2008. Study of habitat requirement of *Amygdalous scoparia* species in Zagros forests. (Case study: Kareh bas habitat of Chahar Mahal and Bakhtiari Province. *Iranian Journal of Forest and Poplar Research*, 4, 528–542.
- Schoener T.W., 1968. Anolis lizards of Bimini: resource partitioning in a complex fauna. *Ecology*, 49,704–726.
- Shrestha U.B., Sharma K.P., Devkota A., Siwakoti M., Shrestha B.B., 2018. Potential impact of climate change on the distribution of six invasive alien plants in Nepal. *Ecological Indicators*, 95, 99–107.
- Sinclair S., White M., Newell G., 2010. How useful are species distribution models for managing biodiversity under future climates? *Ecology and Society*, 15, 8 [online].
- Sintayehu D.W., 2018. Impact of climate change on biodiversity and associated key ecosystem services in Africa: a systematic review. *Ecosystem Health and Sustainability*, 4, 225–239.
- Suárez-Mota M.E., Ortiz E., Villaseñor J.L., Espinosa-García F.J., 2016. Ecological niche modeling of invasive plant species according to invasion status and management needs: The case of *Chromolaena odorata* (Asteraceae) in South Africa. *Polish Journal of Ecology*, 64, 369–383.
- Suárez-Mota M.E., Villaseñor J.L., López-Mata L., 2015. Ecological niche similarity between congeneric Mexican plant species. *Plant Ecology and Evolution*, 148, 318–328.
- Swets J.A., 1988. Measuring the accuracy of diagnostic systems. *Science*, 240, 1285–1293.
- Tarkesh M., Jetschke G., 2016. Investigation of current and future potential distribution of *Astragalus gossypinus* in Central Iran using species distribution modeling. *Arabian Journal of Geosciences*, 9(1), 1-11.
- Tavakoli Neko H., Pourmeydani A., Adnani S.M., Sagheb-Talebi Kh., 2012. Impact of some important ecological factors on presence of mountain Almond (*Amygdalus scoparia* Spach.) in Qom Province, Iran. *Iranian Journal of Forest and Poplar Research*, 19, 523–542.

- Thapa S., Chitale V., Joshi-Rijal S., Bisht N., Shrestha B.B., 2018. Understanding the dynamics in distribution of invasive alien plant species under predicted climate change in Western Himalaya. *PLoS One*, 13, e0195752.
- Thuiller W., 2007. Biodiversity: climate change and the ecologist. *Nature*, 448, 550–552.
- Upton R., Williams J.J., Wilkinson T.P., Clubbe C.P., Maclean I.M.D., McAdam J.H., Moat J.F., 2016. Potential impacts of climate change on native plant distributions in the Falkland islands. *PLoS ONE*, 11(11): e0167026.
- Verbyla D.L., Litvaitis J.A., 1989. Resampling methods for evaluation of classification accuracy of wildlife habitat models. *Environmental Management*, 13, 783–787.
- Vessella F., Schirone B., 2013 Predicting potential distribution of *Quercus suber* in Italy based on ecological niche models: Conservation insights and reforestation involvements. *Forest Ecology and Management*, 304, 150–161.
- Vorsino A.E., King C.B., Haines W.P., Rubinoff D., 2013. Modeling the Habitat Retreat of the Rediscovered Endemic Hawaiian Moth *Omiodes continuatalis* Wallengren (Lepidoptera: Crambidae). *PLoS ONE*, 8, e51885.
- Walther G.R., 2010. Community and ecosystem responses to recent climate change. *Philosophical Transactions of the Royal Society B: Biological Sciences*, 365, 2019–2024.
- Wan J.Z., Wang C.J., Tan J.F., Yu F.H., 2017. Climatic niche divergence and habitat suitability of eight alien invasive weeds in China under climate change. *Ecology and evolution*, 7, 1541–1552.
- Yousefi M., Kafash A., Valizadegan N., Ilanloo S.S., Rajabizadeh M., Malekoutikhah S., Yousefkhani S.Sh., Ashrafi S., 2019. Climate Change is a Major Problem for Biodiversity Conservation: A Systematic Review of Recent Studies in Iran. *Contemporary Problems of Ecology*, 12(4), 394–403.
- Zare Chahouki M.A., Piri Sahragard H., 2016. MaxEnt modelling for distribution of plant species habitats of rangelands (Iran). *Polish Journal of Ecology*, 64, 453–467.
- Zarenistanak M., Dhorde A. G., Kripalani R.H., 2014. Temperature analysis over southwest Iran: trends and projections. *Theoretical and Applied Climatology*, 116(1), 103–117.

Appendix 1. Classification of the Area under the Curve of the ROC curve (Swets, 1988)

Coefficient class	Range
Poor	0.50-0.70
Acceptable	0.70-0.90
Good	0.90-1.00



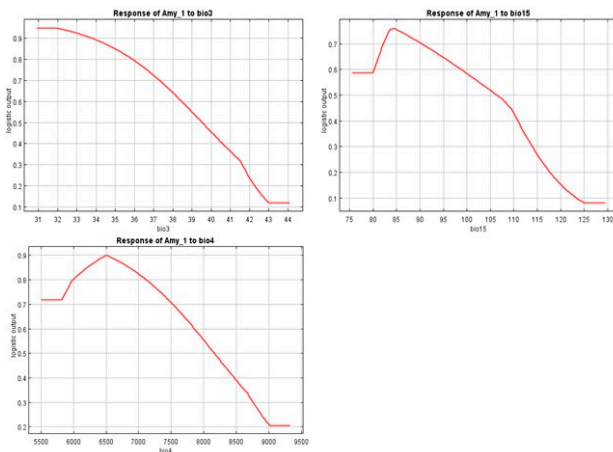
Appendix 2. The value of the AUC for the ROC curve for training and test data in maximum entropy prediction model.

Appendix 3. Overlap of ecological niches of *Amygdalus scoparia* based on D index in Fars Province.

Species	2.62050	2.62070	4.52050	4.52070	6.2050	6.2070	8.52050	8.52070	Current
2.62050	1	0.78	0.72	0.74	0.80	0.73	0.63	0.83	0.74
2.62070	x	1	0.72	0.75	0.86	0.82	0.69	0.77	0.74
4.52050	x	x	1	0.81	0.76	0.68	0.78	0.75	0.81
4.52070	x	x	x	1	0.79	0.70	0.79	0.77	0.77
6.2050	x	x	x	x	1	0.80	0.72	0.81	0.78
6.2070	x	x	x	x	x	1	0.65	0.71	0.72
8.52050	x	x	x	x	x	x	1	0.66	0.72
8.52070	x	x	x	x	x	x	x	1	0.74
Current	x	x	x	x	x	x	x	x	1

Appendix 4. Overlap of ecological niches of *Amygdalus scoparia* based on I index in Fars Province.

Species	2.62050	2.62070	4.52050	4.52070	6.2050	6.2070	8.52050	8.52070	Current
2.62050	1	0.96	0.90	0.92	0.96	0.94	0.84	0.97	0.93
2.62070	x	1.00	0.93	0.95	0.98	0.97	0.90	0.96	0.94
4.52050	x	x	1.00	0.95	0.94	0.91	0.95	0.92	0.96
4.52070	x	x	x	1.00	0.95	0.92	0.94	0.93	0.94
6.2050	x	x	x	x	1.00	0.96	0.90	0.97	0.95
6.2070	x	x	x	x	x	1.00	0.87	0.94	0.93
8.52050	x	x	x	x	x	x	1.00	0.86	0.91
8.52070	x	x	x	x	x	x	x	1.00	0.93
Current	x	x	x	x	x	x	x	x	1.00



Appendix 5. Response curves of their most important variables in the habitat of *A. scoparia*.

Finito di stampare da
Logo s.r.l. - Borgoricco (PD) - Italia

RIGOROUS PEER REVIEW

Each submission to IJAm is subject to a rigorous quality control and peer-review evaluation process before receiving a decision. The initial in-house quality control check deals with issues such as competing interests; ethical requirements for studies involving human participants or animals; financial disclosures; full compliance with IJAm's data availability policy, etc. Submissions may be returned to authors for queries, and will not be seen by our Editorial Board or peer reviewers until they pass this quality control check. Each paper is subjected to critical evaluation and review by Field Editors with specific expertise in the different areas of interest and by the members of the international Editorial Board.

OPEN ACCESS POLICY

The Italian Journal of Agrometeorology provides immediate open access to its content. Our publisher, Firenze University Press at the University of Florence, complies with the Budapest Open Access Initiative definition of Open Access: By "open access", we mean the free availability on the public internet, the permission for all users to read, download, copy, distribute, print, search, or link to the full text of the articles, crawl them for indexing, pass them as data to software, or use them for any other lawful purpose, without financial, legal, or technical barriers other than those inseparable from gaining access to the internet itself. The only constraint on reproduction and distribution, and the only role for copyright in this domain is to guarantee the original authors with control over the integrity of their work and the right to be properly acknowledged and cited. We support a greater global exchange of knowledge by making the research published in our journal open to the public and reusable under the terms of a Creative Commons Attribution 4.0 International Public License (CC-BY-4.0). Furthermore, we encourage authors to post their pre-publication manuscript in institutional repositories or on their websites prior to and during the submission process and to post the Publisher's final formatted PDF version after publication without embargo. These practices benefit authors with productive exchanges as well as earlier and greater citation of published work.

COPYRIGHT NOTICE

Authors who publish with IJAm agree to the following terms:

Authors retain the copyright and grant the journal right of first publication with the work simultaneously licensed under a Creative Commons Attribution 4.0 International Public License (CC-BY-4.0) that allows others to share the work with an acknowledgment of the work's authorship and initial publication in IJAm. Authors are able to enter into separate, additional contractual arrangements for the non-exclusive distribution of the journal's published version of the work (e.g., post it to an institutional repository or publish it in a book), with an acknowledgment of its initial publication in this journal.

Authors are allowed and encouraged to post their work online (e.g., in institutional repositories or on their website) prior to and during the submission process, as it can lead to productive exchanges, as well as earlier and greater citation of published work (See The Effect of Open Access).

PUBLICATION FEES

Unlike many open-access journals, the Italian Journal of Agrometeorology does not charge any publication fee.

WAIVER INFORMATION

Fee waivers do not apply at Firenze University Press because our funding does not rely on author charges.

PUBLICATION ETHICS

Responsibilities of IJAm's editors, reviewers, and authors concerning publication ethics and publication malpractice are described in IJAm's Guidelines on Publication Ethics.

CORRECTIONS AND RETRACTIONS

In accordance with the generally accepted standards of scholarly publishing, IJAm does not alter articles after publication: "Articles that have been published should remain extant, exact and unaltered to the maximum extent possible". In cases of serious errors or (suspected) misconduct IJAm publishes corrections and retractions (expressions of concern).

Corrections

In cases of serious errors that affect or significantly impair the reader's understanding or evaluation of the article, IJAm publishes a correction note that is linked to the published article. The published article will be left unchanged.

Retractions

In accordance with the "Retraction Guidelines" by the Committee on Publication Ethics (COPE) IJAm will retract a published article if:

- there is clear evidence that the findings are unreliable, either as a result of misconduct (e.g. data fabrication) or honest error (e.g. miscalculation)
- the findings have previously been published elsewhere without proper crossreferencing, permission or justification (i.e. cases of redundant publication)
- it turns out to be an act of plagiarism
- it reports unethical research.
- An article is retracted by publishing a retraction notice that is linked to or replaces the retracted article. IJAm will make any effort to clearly identify a retracted article as such.

If an investigation is underway that might result in the retraction of an article IJAm may choose to alert readers by publishing an expression of concern.

ARCHIVING

IJAm and Firenze University Press are experimenting a National legal deposition and long-term digital preservation service.

SUBMITTING TO IJAm

Submissions to IJAm are made using FUP website. Registration and access are available at: <https://riviste.fupress.net/index.php/IJAm/submission>
For more information about the journal and guidance on how to submit, please see <https://riviste.fupress.net/index.php/IJAm/index>

Principal Contact

Simone Orlandini, University of Florence
simone.orlandini@unifi.it

Support Contact

Alessandro Pierno, Firenze University Press
alessandro.pierno@unifi.it

GUIDE FOR AUTHORS

1. Manuscript should refer to original researches, not yet published except in strictly preliminary form.
2. Articles of original researches findings are published in Italian Journal of Agrometeorology (IJAm), subsequent to critical review and approval by the Editorial Board. External referees could be engaged for

particular topics.

3. Three types of paper can be submitted: original paper, review, technical note. Manuscript must be written in English. All pages and lines of the manuscript should be numbered.

4. First Name, Last Name, position, affiliation, mail address, telephone and fax number of all the Co-Authors are required. Corresponding Authors should be clearly identified.

5. The abstract should be no longer than 12 typed lines.

6. Full stop, not comma, must be used as decimal mark (e.g. 4.33 and not 4,33).

7. Figures, tables, graphs, photos and relative captions should be attached in separate files. All images must be vector or at least 300 effective ppi/dpi to ensure quality reproduction.

8. Captions should be written as: Fig. x – Caption title, Tab. x – Caption title. Images should be referred to in the text as (Fig. x), (Tab. x).

9. Proof of the paper (formatted according to the Journal style) will be sent to the Corresponding Author for proof reading just one time. Corrections can be made only to typographical errors.

10. All the references in the text must be reported in the "References" section and vice-versa. In the text, only the Author(s) last name must be present, without the name or the first letter of the name (e.g. "Rossi, 2003" and not "Federico Rossi, 2003" or "F. Rossi, 2003"). If two authors are present, refer to them as: "Bianchi and Rossi, 2003" in the text (do not use "&" between the surnames). If more than two Authors are present, refer to them as: "Bianchi et al., 2003" in the text.

For journals, references must be in the following form:

Bianchi R., Colombo B., Ferretti N., 2003. Title. Journal name, number: pages.

For books:

Bianchi R., Colombo B., Ferretti N., 2003. Book title. Publisher, publishing location, total number of pages pp.

Manuscripts "in press" can be cited.

BECOME A REVIEWER

Peer review is an integral part of the scholarly publishing process. By registering as a reviewer, you are supporting the academic community by providing constructive feedback on new research, helping to ensure both the quality and integrity of published work in your field. Once registered, you may be asked to undertake reviews of scholarly articles that match your research interests. Reviewers always have the option to decline an invitation to review and we take care not to overburden our reviewers with excessive requests.

You must login before you can become a reviewer.

If you don't want to be a reviewer anymore, you can change your roles by editing your profile.

COMPETING INTERESTS

You should not accept a review assignment if you have a potential competing interest, including the following:

- Prior or current collaborations with the author(s)
- You are a direct competitor
- You may have a known history of antipathy with the author(s)
- You might profit financially from the work

Please inform the editors or journal staff and recuse yourself if you feel that you are unable to offer an impartial review.

When submitting your review, you must indicate whether or not you have any competing interests.



Italian Journal of Agrometeorology

Rivista Italiana di Agrometeorologia

n. 2 – 2020

Table of contents

Alice Crespi, Anna Borghi, Arianna Facchi, Claudio Gandolfi, Maurizio Maugeri Spatio-temporal variability and trends of drought indices over Lombardy plain (northern Italy) from meteorological station records (1951–2017)	3
Elahe Hojjati, Ghorban Mahtabi, Farshid Taran, Ozgur Kisi Estimating evaporation from reservoirs using energy budget and empirical methods: Alavian dam reservoir, NW Iran	19
Sarah Khajeh Hosseini, Farzad Fanoodi, Sayed Ali Tabatabaei, Rostam Yazdani Biouki, Jafar Masoud Sinaki Drought stress response of hyssop (<i>Hyssopus officinalis</i> L.) as influenced via the antitranspirants and osmolytes materials	35
Rossana Monica Ferrara, Nicola Martinelli, Gianfranco Rana CO ₂ and H ₂ O fluxes due to green manuring under Mediterranean conditions	45
Abdelkader Laaboudi, Abdeldjalil Slama Using Neuro-fuzzy and linear models to estimate reference Evapotranspiration in South region of Algeria (A comparative study)	55
Özlem Baydaroğlu Yeşilköy, Kasım Koçak, Levent Şaylan Prediction of commonly used drought indices using support vector regression powered by chaotic approach	65
Ibrahim Mubarak, Mussaddak Janat Quinoa response to different transplanting dates and nitrogen fertilization levels in an arid environment	77
Muhammet Topuz, Haralambos Feidas, Murat Karabulut Trend analysis of precipitation data in Turkey and relations to atmospheric circulation: (1955-2013)	91
Behnam Pouzeshimiyab, Seyed Reza Fani Epidemiology and Aerobiology of <i>Pseudoperonospora cubensis</i> in northwest Iran	109
Hossein Piri Sahragard, Majid Ajorlo, Peyman Karami Predicting impacts of future climate change on the distribution and ecological dimension of <i>Amygdalus scoparia</i> Spach	117